



Ana Filipa Soares Pires

Master of Bioengineering and Nanosystems

**Liposomes encapsulating catechins:
a biophysical approach for skin cancer therapy**

Thesis submitted in partial fulfillment
of the requirements for the degree of

Doctor of Philosophy in
**Radiation Biology and Biophysics:
Biophysics**

Adviser: Maria de Fátima Guerreiro da Silva Campos Raposo,
Associate Professor with Habilitation,
Universidade Nova de Lisboa

Examination Committee

Chair: Paulo Manuel Assis Loureiro Limão Vieira
Rapporteurs: Ana Margarida Madeira Viegas de Barros Timmons
Cecília Ribeiro da Cruz Calado
Member: Quirina Alexandra Tavares Ferreira

 **FACULDADE DE
CIÊNCIAS E TECNOLOGIA
UNIVERSIDADE NOVA DE LISBOA**

July, 2019

Liposomes encapsulating catechins: a biophysical approach for skin cancer therapy

Copyright © Ana Filipa Soares Pires, Faculty of Sciences and Technology, NOVA University Lisbon.

The Faculty of Sciences and Technology and the NOVA University Lisbon have the right, perpetual and without geographical boundaries, to file and publish this dissertation through printed copies reproduced on paper or on digital form, or by any other means known or that may be invented, and to disseminate through scientific repositories and admit its copying and distribution for non-commercial, educational or research purposes, as long as credit is given to the author and editor.

'Ó mar salgado, quanto do teu sal
São lágrimas de Portugal!
Por te cruzarmos, quantas mães choraram,
Quantos filhos em vão rezaram!
Quantas noivas ficaram por casar
Para que fosses nosso, ó mar!
Valeu a pena? Tudo vale a pena
Se a alma não é pequena.
Quem quer passar além do Bojador
Tem que passar além da dor.
Deus ao mar o perigo e o abismo deu,
Mas nele é que espelhou o céu.'

Fernando Pessoa

ACKNOWLEDGEMENTS

During this journey, I have been lucky enough to meet and work with good people that made me grow as a person and helped me to improve and develop new science skills. So, I would like to convey my regards and express my gratitude to all of them.

First and foremost, I would like to sincerely express my gratitude to my supervisor Prof. Dr. Maria Raposo, for her guidance, encouragement throughout these 4 years, for believing in my ideas and for the incredible opportunities to attend conferences and training schools abroad, which were crucial to my growth as a scientist. I'll never forget the amazing trips we did together, her kindness, comprehension and, specially, the crucial conversations and advices that she gave me in the final stage of my PhD.

Also, I want to express my gratitude to Prof. Dr. Osvaldo N. Oliveira Jr. for giving me the chance to work in the Group of Polymers 'Prof. Bernhard Gross' at the Instituto de Física de São Carlos (Universidade de São Paulo), for your warm reception, generosity and for the valuable discussions and comments provided during reviewing my manuscripts.

I would like to acknowledge Prof. Dr. Miguel Machuqueiro, always smiling and ready to help me better understand the 'molecular dynamics simulations world'. I always learned something new from our discussions and I am thankful for his effort in proof reading and revising our manuscript.

I also like to thank Prof. Dr. Jorge Silva for the possibility to carry out the cell studies in his laboratory facilities, providing everything I needed at my disposal. He also gave valuable guidelines in planning experiments.

Also, I would like to acknowledge Prof. Dr. Paulo Limão-Vieira who, as a coordinator of the Radiation Biology and Biophysics Doctoral Training Programme, always quickly solved a lot of bureaucracy and, of course, for giving me the opportunity to pursue my PhD.

To Dr. Rodrigo de Almeida and António de Granada-Flor from the Centro de Química e Bioquímica of FCUL/UNL, for helping me with the fluorescence measurements.

I want to thank Prof. Dr. Paulo Ribeiro for reading drafts and, especially, by his good mood shared in the work environment. I thank Prof. Dr. Susana Sério and Dr. Paula Chicau for providing the facilities to carry out UV-Vis and DLS measurements, respectively.

My sincere thanks also goes to Dr. Vananélia Geraldo, who was always so helpful and provided me a friendly and knowledgeable assistance throughout Langmuir monolayer experiments.

I also wish to acknowledge Prof. Dr. Alexandre Marletta, Prof. Dr. Andrea Antunes, Prof. Dr. Gabriela A. Silva, Prof. Dr. Ana Botelho do Rego, Prof. Dr. Demeter Tzeli, Dr. Søren Vrønning Hoffmann, Dr. N. C. Jones, Dr. Ana Ferraria and Dr. Diogo Bitoque for collaboration on several developed projects.

To my colleagues of RABBIT, Telma Santos, Alexandra Loupas e Telma Silva, who accompanied me throughout these years, thanks for their friendship, support and for all the amazing moments we shared. To my friend Alessandra Barbosa thanks for the warm hospitality and for the marvelous time I had with you on my visit to Curitiba.

Thank you my sweet friend Mónica Mendes for your unceasing help, tremendous support and for advice me in different aspects of my life. Thanks for being such a good friend that always was there for me no matter how far away we were from each other in distance or in time.

To the Department of Physics of NOVA University of Lisbon and CEFITEC through UID/FIS/00068/2019 and PTDC/FIS-NAN/0909/2014. To the financial support from the Portuguese National Funding Agency FCT-MCTES through PD/BD/106036/2015 scholarship. This work was also supported by Radiation Biology and Biophysics Doctoral Training Programme (RaBBiT, PD/00193/2012); UID/Multi/04378/2013 (UCIBIO).

I thank the secretariat assistant Mrs. Ana Cruz from CEFITEC, who is ethical and exceptionally caring, her professionalism and supportive words when times were tough for me.

I also thank my fellow labmates in for all the fun we have had in the last years. Particularly, I want to thank my sweet friend Jeniffer Santos who taught me and gave me support in cellular experiments and for the joy that she brought to our laboratory. To my dear friend Filipe Bernardo, who was always so helpful and saved me multiple times from some serious informatics issues. To Gonçalo Magalhães-Mota, for the incredible and enjoyable adventures that we lived together, which were important to rest my mind outside of my research.

Thank you my dearest Ana Gracinda Pires and Adérito Pires, for being some of the most supportive, reliable and most kind hearted people I know.

To my adorable and protective brother João, a person that always picks me up when I am fall, a person that doesn't realize that teaches me life's important lessons. Thanks for being the best brother, you will always be my little buddy.

I extend the utmost appreciation to my sweet mom and dad, I have no words to acknowledge your love and support. You have been there, day after day, believing in me and I am so much of what I learned from you.

ABSTRACT

Every year, a large number of skin cancer cases caused by a prolonged ultraviolet radiation exposure, are diagnosed around the world. Epigallocatechin-3-gallate (EGCG) derived from green tea leaves, display protective effect against oxidative stress which reduce the risk of contracting skin cancer. However, frequently, the antioxidant and anti-inflammatory activities of EGCG in are compromised because this molecule is extremely unstable and rapidly degraded in physiological conditions. Considering these issues, the main goal of this thesis was developed a stable liposomal nanocarrier for topical/transdermal delivery of EGCG, firstly, to increase its bioavailability and, secondly, to offer an desirable skin protection against harmful effects of UV radiation. Primarily, the molecular mechanisms between EGCG and different phospholipids were studied using Langmuir experiments, revealing the affinity and localization of EGCG on each lipidic membrane, which according to the results depends on the molecular organization of lipidic monolayer (functional groups anchored at headgroup) and of the degree of protonation of EGCG. EGCG establishes electrostatic and hydrogen-bonding interactions with zwitterionic (DMPC, DPPC) and anionic (DPPG and DPPS) phospholipids, which condense the monolayers and alter the membrane's potential and compressibility. Regarding the irradiation experiments, the results indicated that EGCG efficiently slows down the oxidant events in monolayers and in lipid bilayers, which were produced by blue and ultraviolet radiation exposure, respectively. Lastly, the nanofibers meshes containing EGCG-loaded liposomes are biocompatible, support human fibroblasts adhesion and scavenge the oxidant species generated by UV radiation, which guarantees a higher cell survival.

Keywords: skin cancer; oxidative stress; EGCG; liposomes; wound healing

RESUMO

A cada ano, um grande número de casos de cancro da pele, causados por uma prolongada exposição à radiação ultravioleta, são diagnosticados em todo o mundo. A Epigallocatequina-3-galato (EGCG) extraída do chá verde, tem um efeito protector contra o stress oxidativo, o que reduz o risco de desenvolver cancro da pele. Contudo, as actividades antioxidantes e anti-inflamatórias da EGCG ficam comprometidas, uma vez que esta é extremamente instável e rapidamente degradada em condições fisiológicas. Assim, o principal objectivo desta tese foi desenvolver um nanotransportador lipossómico estável para entregar a EGCG via tópica/transdermal na pele, de forma a aumentar a biodisponibilidade e proteger adequadamente a pele dos efeitos nocivos da radiação UV. Inicialmente, os mecanismos moleculares entre a EGCG e diferentes fosfolípidos foram estudados usando experiências de Langmuir, revelando a afinidade e a localização da EGCG em cada monocamada. De acordo com os dados, esta depende da organização molecular da monocamada lipídica (grupos funcionais ancorados na cabeça do lípido) e do grau de protonação da EGCG. A EGCG estabelece interações electrostáticas e pontes de hidrogénio com os fosfolípidos neutros (DMPC, DPPC) e negativos (DPPG e DPPS), condensa e altera o potencial e a compressibilidade das monocamadas. Segundo os ensaios de irradiação, a EGCG retarda eficientemente os eventos oxidantes tanto nas monocamadas como nas bicamadas lipídicas. Por fim, concluiu-se que as nanofibras que contêm liposomas com a EGCG encapsulada são biocompatíveis, permitem a adesão de fibroblastos humanos e eliminam as espécies oxidantes geradas pela radiação UV, o que garante uma maior sobrevivência celular.

Palavras-chave: cancro da pele; stress oxidativo; EGCG; liposomas; cicatrização de feridas

CONTENTS

List of Figures	xviii
List of Tables	xxii
Acronyms	xxiii
Symbols	xxvii
1 General Introduction	1
2 Interactions of Flavonoids and DNA	5
2.1 Introduction	6
2.2 Polyphenolic Molecules	7
2.3 Interactions of Flavonoids within cellular environment	8
2.4 Flavonoids and epigenetic environment	13
2.5 Flavonoids: agents for epigenetics pharmacotherapy	21
2.6 Conclusion	24
2.7 Acknowledgements	27
References	28
3 EGCG–delivery nanoplatforms to maximize skin protection against harmful radiation	47
3.1 Introduction	48
3.2 Radiation-induced lipid peroxidation	49
3.3 Antioxidant action of catechins	51
3.4 <i>In vivo</i> bioavailability of catechins	53
3.5 Liposomal-based EGCG delivery systems	54
3.6 Challenges in Dermal/Transdermal EGCG Delivery	56
References	58
4 Experimental Concepts & Methodology	71
4.1 Langmuir Monolayer studies	71

4.2	Liposomes studies	78
	References	84
5	Effect of blue light on the stability of lipid molecules in the presence of EGCG	87
5.1	Introduction	88
5.2	Experimental Details	89
5.3	Results and Discussion	90
5.4	Conclusions	100
5.5	Acknowledgements	101
	References	101
6	The impact of blue light in tumorigenic and nontumorigenic monolayers containing EGCG	109
6.1	Introduction	110
6.2	Experimental	111
6.3	Results	112
6.4	Conclusion	125
6.5	Acknowledgements	125
	References	126
7	On the role of EGCG in protecting phospholipid molecules against UV irradiation	131
7.1	Introduction	132
7.2	Experimental details	133
7.3	Results and discussion	136
7.4	Conclusion	146
7.5	Acknowledgments	147
	References	147
8	Evaluation of EGCG loading capacity in DMPC membranes	155
8.1	Introduction	156
8.2	Experimental	158
8.3	Results and discussion	162
8.4	Conclusion	172
8.5	Acknowledgements	173
	References	173
9	Cell-based Results	185

9.1 Introduction	186
9.2 Methodology	187
9.3 Conclusion	206
9.4 Acknowledgments	207
References	207
10 Concluding Remarks	217
Apêndices	223
A Effect of blue light on the stability of lipid molecules in the presence of EGCG	223
B The impact of blue light in tumorigenic and nontumorigenic monolayers containing EGCG	227
C On the role of EGCG in protecting phospholipid molecules against UV irradiation	231
D Evaluation of EGCG loading capacity in DMPC membranes	233

LIST OF FIGURES

2.1	Chemical structures of the main subclasses of flavonoids.	9
2.2	Gene activation status determined by DNA methylation and histone modifications.	18
3.1	Exogenous and endogenous sources of ROS formation involved in cell damage.	49
3.2	By-products of water radiolysis due to ionizing radiation.	50
3.3	Structure of the different catechins present in green tea. Image adapted from [34].	52
3.4	Physicochemical parameters that regulate drug permeation across skin. Image adapted from [103].	56
4.1	The Langmuir monolayers at the air-water interface were formed in a KSV NIMA Langmuir trough.	72
4.2	Surface pressure - area isotherm of DPPC monolayer and schematic gaseous (G), liquid-expanded (LE) and condensed (LC) phase behavior of the monolayer during compression.	74
4.3	Lipid monolayer spread at air-buffer subphase exposed to blue LED irradiation for 1h.	77
4.4	Preparation of liposomes using the dry-film hydration method.	79
4.5	Structure of membrane phospholipids studied throughout this thesis.	79
5.1	Surface Pressure for DPPG monolayers with different contents of EGCG at the water interface.	92
5.2	PM-IRRAS spectra of DPPG monolayers with different EGCG percentages in aqueous solutions at a surface pressure of 30 mN/m.	95
5.3	Irradiation with blue light of pure DPPG (A) and DPPG+13 mol% EGCG (B) monolayers isotherms.	97
5.4	PM-IRRAS spectra of DPPG (A, C, E) and DPPG+13%EGCG (B, D, F) monolayers, before and after blue light irradiation.	99

6.1	Surface pressure isotherms registered for DPPC (A) and DPPS (B) monolayers containing different EGCG molar fractions.	114
6.2	PM-IRRAS spectra for neat DPPC, mixed EGCG/DPPC, neat DPPS and mixed EGCG/DPPS monolayer in the lipid alkyl chains (A-D) and carbonyl (E-H) region, before and after blue light irradiation.	116
6.3	PM-IRRAS spectra for neat DPPC, mixed EGCG/DPPC, neat DPPS and mixed EGCG/DPPS monolayer in the phosphate (A-D) and choline (E-H) region, before and after blue light irradiation.	117
6.4	Illustrative model for DPPC monolayer (A) and EGCG interaction with a DPPC monolayer (B). EGCG intercalates among DPPC molecules at the air/water interface establishing H-bonding between the OH groups of EGCG and P=O and C=O groups of DPPC (green circle), in addition to ion pairing interactions between the charged oxygen groups of EGCG and the quaternary N ⁺ of DPPC (orange circle). From the differences in the ordering of acyl chains, it seems that EGCG can insert into the hydrophobic region of the lipids. C. Illustrative model for DPPS monolayer. D. Illustrative model for EGCG interaction with a closely packed DPPS monolayer. The tighter packing of the DPPS monolayer prevents EGCG penetration to the hydrophobic lipid chains. EGCG binds onto the DPPS surface at the interface through H-bonding between the OH groups of EGCG and P=O and C=O groups of DPPS (green circle), in addition to the electrostatic interactions between the charged oxygen groups of EGCG and the protonated amine NH ₃ ⁺ of DPPS (orange circle).	119
6.5	BAM micrographs of DPPC and DPPC+10% EGCG monolayers at several surface pressures before and after blue light irradiation.	124
6.6	BAM micrographs of DPPS and DPPS+10% EGCG monolayers obtained at several surface pressures before and after blue light irradiation.	124
7.1	Absorption spectra of EGCG (a,b), DPPG liposomes (c,d) and DPPG + EGCG liposomes (e,f)	137
7.2	Absorption spectra of DPPG liposomes and DPPG + EGCG liposomes before and after irradiation.	139
7.3	a) Synchronous and b) asynchronous 2D correlation maps in the wavelength region between 190 and 300 nm of aqueous solutions of EGCG, vesicle suspension of DPPG and DPPG + EGCG.	141

7.4	FTIR spectra for cast films of EGCG, DPPG and DPPG + EGCG before and after UV irradiation.	144
8.1	Schematic chemical structure of Epigallocatechin-3-gallate (EGCG). .	157
8.2	Initial (A) and final (B) conformations of the EGCG membrane insertion process	163
8.3	Area per lipid (A_l) values of DMPC calculated in the presence of different amounts of EGCG (A).	165
8.4	Lipid tails order in the presence of different molar ratios of EGCG. . .	167
8.5	Surface potential at different A_l values for the different EGCG molar fractions in DMPC monolayers (A).	169
9.1	Dose-dependent cytotoxic effects of EGCG in Vero cells.	193
9.2	SEM images showing the morphology of PCL+GEL nanofibers containing liposomal formulations.	196
9.3	ATR-FTIR spectra of the PCL/gelatin nanofibers before (a) and after (b) GTA crosslinking process.	198
9.4	Release profiles of EGCG from each type of PCL/gelatin membranes.	199
9.5	Results of the cytotoxicity test using extracts of the PCL / gelatin nanofibers containing different liposomal formulations.	200
9.6	SEM micrographs of HFFF2 cells seeded over PCL/gelatin membranes containing liposomal formulations with EGCG, EGCG + T80 and EGCG + T80 + PEG.	201
9.7	Cell viability of HFFF2 cells cultured on PCL/gelatin nanofibers containing different liposomal formulations after 4, 24 and 72 h of oxidative stress induced by 50 μM H_2O_2 treatment.	202
9.8	Assessment of ROS formation in HFFF2 cells following incubation with 50 μM H_2O_2 (30min) based on the fluorescence intensity of DCFDA dye.	203
9.9	Fluorescence images of HFFF2 cells seeded on unloaded PCL/gelatin (A), PCL/EGCG (B), PCL/EGCG/T80 (C) and PCL/EGCG/PEG (D) membranes.	204
9.10	Cell viability of HFFF2 cells cultured on PCL/gelatin nanofibers containing different liposomal formulations after oxidative stress induced by UVC light exposure at a dose of 2 or 8 J/cm^2	205
A.1	Surface Pressure for DPPG monolayers with different contents of EGCG at water interface.	224

A.2	Compression-decompression cycles of DPPG+13% EGCG monolayer irradiated with blue light over 1h at a surface pressure of 30 mN/m.	225
B.1	PM-IRRAS spectra for neat DPPC (A) and mixed EGCG/DPPC monolayer (B) monolayer in the CH_2 methylene deformation region before and after blue light irradiation.	228
B.2	Surface pressure-area isotherms for neat DPPC (A) and DPPC containing EGCG (B) monolayers before and after blue light irradiation.	229
B.3	Surface pressure-area isotherms for neat DPPS (A) and DPPS containing EGCG (B) monolayers before and after blue light irradiation.	230
C.1	EGCG seems to protect the phosphate and carbonyl groups of DPPG phospholipids against UV irradiation.	232
D.1	A_1 values of DMPC head groups calculated in the presence of different amounts of EGCG and assuming that the catechin molecules are in the tails and not in the head group region.	233
D.2	Membrane thickness values in the presence of different EGCG molar fractions.	234
D.3	Deuterium order parameter (S_{CD}) values along the aliphatic chain for the different molar ratios of the EGCG/DMPC systems.	234
D.4	PM IRRAS measurements for different EGCG molar fractions in DMPC.	235
D.5	Top (left) and side-view (right) of DMPC headgroup bending in the presence of EGCG.	236

LIST OF TABLES

2.1	Protective mechanisms of flavonoids against death stimulus.	14
2.2a	Modulation of epigenome by bioactive compounds.	22
2.2b	Modulation of epigenome by bioactive compounds (continued).	23
2.3a	Targeting miRNAs by flavonoids.	25
2.3b	Targeting miRNAs by flavonoids (continued).	26
4.1	Chemical composition and transition temperature of each phospholipid used in thesis work.	78
6.1	Vibrational assignments and changes in band position of DPPC monolayer after blue light irradiation and interaction with EGCG.	120
6.2	Vibrational assignments and changes in band position of DPPS monolayer after blue light irradiation and interaction with EGCG.	123
7.1	Characteristic infrared absorptions of EGCG cast films prepared onto CaF ₂ solid supports.	143
7.2	Characteristic infrared absorptions of DPPG cast films prepared onto CaF ₂ solid supports.	145
9.1	Composition of liposomal formulations adsorbed on PCL / gelatin nanofibers.	194
9.2	Average nanofiber diameter before and after GTA vapor crosslinking.	195
9.3	VERO cells viability relative to the negative control after 1 and 3 days of culture with nanofibers-extracted media	200

ACRONYMS

AO	Acridine Orange
AR	Androgen Receptor
ATP	Adenosine Triphosphate
BAM	Brewster Angle Microscopy
BCCs	Basal Cell Carcinomas
BDE	Bond Dissociation Enthalpy
CDK1	Cyclin-dependent kinase 1
COMT	Catechol- <i>O</i> -methyltransferase
COX2	Cyclooxygenase 2
DCFDA	Dichlorofluorescein Diacetate
DLS	Dynamic Light Scattering
DMEM	Dulbecco's Modified Eagle Medium
DMPC	1,2-dimyristoyl- <i>sn</i> -glycero-3-phosphocholine
DNA	Deoxyribonucleic Acid
DNMT	DNA Methyltransferase
DPPC	1,2-dipalmitoyl- <i>sn</i> -glycero-3-phosphocholine
DPPG	1,2-dipalmitoyl- <i>sn</i> -glycero-3-[phospho- <i>rac</i> -(1-glycerol)] (sodium salt)
DPPS	1,2-dipalmitoyl- <i>sn</i> -glycero-3-phospho-L-serine (sodium salt)
DSC	Differential Scanning Calorimetry
EC	Epicatechin
ECG	Epicatechin-3-Gallate
EGC	Epigallocatechin

ACRONYMS

EGCG	Epigallocatechin-3-Gallate
EGF	Epidermal Growth Factor
EPR	Enhanced Permeability and Retention
ER	Estrogen Receptor
FASN	Fatty Acid Synthase gene
FBS	Fetal Bovine Serum
FDA	Food and Drug Administration
FTIR	Fourier-Transform Infrared
GSH	Glutathione
GST	Glutathione S-transferase
H3	Histone 3
HAT	Hydrogen Atom Transfer
HATs	Histone Acetyltransferases
HDACs	Histone Deacetylases
HFFF2	Human Fetal Foreskin Fibroblasts
HIF1	Hypoxia inducible factor-1
HNE	4-Hydroxynonenal
Keap 1	Kelch-like ECH-associated protein 1
LC	Liquid-Condensed state
LE	Liquid-Expanded state
LED	Light-Emitting Diode
LUVs	Large Unilamellar Vesicles
MD	Molecular Dynamics
MDA	Malonyldialdehyde
MGMT	O-6-methylguanine DNA methyltransferase
MLVs	Multilamellar Vesicles
MMP	Metalloproteinases
MWCNTs	Multi-walled Carbon Nanotubes

NFκB	Nuclear factor kappa B
NMR	Nuclear Magnetic Resonance
Nrf2	Nuclear factor-erythroid-2-related factor 2
NSCLC	Non-small Cell Lung Cancer
PAINS	Pan-Assay Interference Compounds
PBS	Phosphate-buffered Saline
PCA	Principal Component Analysis
PCL	Polycaprolactone
PCNA	Proliferating Cell Nuclear Antigen
PEG	Polyethylene Glycol
PM-IRRAS	Polarization modulated infrared reflection absorption spectroscopy
RES	Reticuloendothelial System
ROS	Reactive Oxygen Species
SAH	S-adenosyl-L-homocysteine
SAM	S-adenosyl-methionine
SC	Stratum Corneum
SD	Standard Deviation
SEM	Scanning Electron Microscopy
SET	Single Electron Transfer
SIRT-1	Sirtuin-1
SOD	Superoxide dismutase
SULTA1	Phenol Sulfotransferase
SUVs	Small Unilamellar Vesicles
UGTA1	Uridine Diphosphate Glucuronosyl-Transferase 1
UHFR1	E3 ubiquitin ligase
UV	Ultraviolet
UV-Vis	Ultraviolet and visible

ACRONYMS

VEGF Vascular Endothelial Growth Factor

SYMBOLS

θ	Angle
A_{LT}	Langmuir trough area
A_0	Minimum Area per Molecule
A_1	Molecular Area of Component 1 in monolayer
A_2	Molecular Area of Component 2 in monolayer
A	Absorbance
A_{ex}	Excess Area per Molecule
A_m	Area per molecule
b	Inter-particle distance
c	Concentration
$CatO^\bullet$	Phenoxy radical
$CatOH^{\bullet+}$	Stable radical cation
c_L	Speed of light
C_{lipid}	Total lipid concentration
C_n	EGCG concentration measured for the n^{th} time
$C = O$	Carbonyl group
C_s^{-1}	Surface Compressional Modulus
ρ_w	Material density
ρ_L	Subphase density
φ	Dihedral angle
m_n	Dihedral Multiplicity
D_T	Diffusion
ϵ_0	Vacuum permittivity

SYMBOLS

ε_a	Molar Absorption Coefficient
ΔE	Energy absorbed
C_{total}	Amount of EGCG in liposomes before dialysis
C_{encap}	Amount of EGCG in liposomes after dialysis
ε	Effective dielectric constant
ν	Frequency
F	Net force
g	Gravitational acceleration
ΔG	Excess Gibbs Free Energy
G	Corrector factor for detector sensitivity
h	Depth
H^\bullet	Hydrogen radical
H_2O_2	Hydrogen Peroxide
h_p	Planck's constant
I	Transmitted light intensity
I_0	Incident Light Intensity
ξ_n	Improper Dihedral Angle
I	Fluorescence Emission
k_B	Boltzmann Constant
k	Constant force
K_p	Liposome/water Partition Coefficient
l	Optical Path Length
L	Length
R^\bullet	Lipid radical
M	Molecular mass
μ_1	Dipole moment of lipid headgroup
μ_2	Dipole moment of lipid hydrophobic tails

μ_3	Dipole moment of water molecules at interface
M_t	Total EGCG content incorporated in each membrane
μ_n	Intrinsic dipole moment of molecule
N_A	Avogadro number
n_L	Number of moles of EGCG in lipid bilayer
n_W	Number of moles of EGCG in water
OH^\bullet	Hydroxyl radical
δ_n	Phase angle
π	Surface Pressure
$P = O$	Phosphate group
Ψ_0	Counter-ions in subphase
q	Partial Charge
Q	Quantity of released EGCG
$\Delta R/R$	Differential Reflectivity
$\langle r \rangle$	Fluorescence Anisotropy
R_H	Hydrodynamic Radius of Particle
RH	Lipid hydroperoxide
R_p	Perpendicular Reflectance
R_s	Parallel Reflectance
σ	Finite distance where the net electric potential is zero
$O_2^{\bullet-}$	Superoxide radical
t_h	Thickness
T	Temperature
γ	Surface tension
t	time
V	Volume

SYMBOLS

ΔV Surface Potential

η Viscosity

V_L Volume of liposomes in dialysis bag

V_W Volume of liposomes in water

V_0 Total volume of the release medium

*

w Width

λ Wavelength

X_1 Mole fraction of Component 1 in monolayer

X_2 Mole fraction of Component 2 in monolayer

GENERAL INTRODUCTION

Currently, cancer still is a serious health problem globally, despite the tremendous technological advances in the field of diagnosis imaging, immunotherapy, epigenetics and nanotheranostics. Cancer is basically a disease that arises from genetic mutations that greatly increase the rate of cell division. Only a small percentage of these genetic defects are caused by inherited faulty genes, being the great majority (90-95 %) due to unhealthy lifestyle and exposure to environmental contaminants. The major cancer risk factors involve a deficient plant-based diet, sedentarism, smoking habits and a long-term exposure to ionizing radiation (such as gamma radiation, X-ray and ultraviolet (UV)).

Definitively, there is a causal relationship between the exposure to UV radiation from sunlight and skin cancer, having the Caucasian population and people living in equatorial regions (greater UV exposure) a higher propensity to get this type of cancer. Furthermore, the ongoing threats to the ozone layer will eventually contribute to increasing incidence of skin cancer, since UV rays of shorter wavelength (UVC rays) will easily start travelling across the 'perturbed' atmosphere and, consequently, will reach the Earth's surface. Several studies shown that the exposure to UV radiation suddenly increases the production of reactive oxygen species (ROS), which change the chemical structure of deoxyribonucleic acid (DNA), start off lipid peroxidation phenomenon and often cause unrepaired abnormalities in the cellular metabolism. Other worrisome recent studies, showed that these harmful oxidant species are also produced by the short-wavelength visible light (blue light) emitted by smartphones and laptops.

In past few decades, a variety of natural molecules like catechins-derived from

green tea leaves, have been extensively studied considering the anti-inflammatory, antioxidant and free radical scavenging properties, that alleviate side-effects stemming from radiation exposure and regulate some steps of the carcinogenesis process. Despite the clear health benefits, the molecular interactions that regulate the partitioning of catechins into cellular membranes, the precise location of catechins within lipid bilayer and their effect on the dynamics and structural organization of membrane remains an issue controversial and unclear in the literature.

Another crucial issue towards the clinical use of catechins is given by the long-term stability of these molecules in bloodstream. Regrettably, most of the time, catechins are hydrolyzed and oxidized by a vast array of enzymes along their journey through the systemic circulation, hence resulting in a small number of catechins therapeutically active and capable of targeting tumor tissues.

At present, several nanotechnology-based drug delivery systems (such as liposomes) hold tremendous potential to enhance the therapeutic effect of catechins, since these systems improve the *in vivo* stability of catechins and precisely regulate their deliver rate to the target tissue.

Considering this, the main goals of the thesis are to understand catechin-lipid interactions at molecular level and how radiation disturb them and, ultimately, develop a stable catechin-loaded liposome that, after topical administration, prevents the oxidative skin damage induced by UV radiation and accelerates the healing of skin lesions.

The thesis is divided into six major parts. The first is devoted to the state of the art focused on two promising different strategies to use catechins in cancer treatment. The first strategy explores the action of flavonoids on epigenetic mechanisms to control gene expression in cancer cells (Chapter 2). The second strategy mostly lies on the antioxidant activity of catechins that balances the production and elimination of ROS and so, it can prevent UV-induced damage. More precisely, the peroxidative damage of lipids caused by UV radiation is discussed in detail. Additionally, current state of liposome-based delivery systems that improve the pharmacokinetic behavior of catechins, as well as, the challenges for their use in dermal applications, were also revised (Chapter 3).

In the second part, the basic fundamentals of instrumental techniques used to prepare mixed catechin-lipid monolayer/bilayer systems as well as to identify molecular details of catechin-lipid interactions and the underlying mechanisms by which catechin decreases the membrane sensitivity to blue or UV radiation damage were described. Moreover, the production process of the nanofibers incorporating catechin-loaded liposomes and, the cell lines used to assess the

biocompatibility and the *in vitro* pharmacologic effects of these nanofibers against oxidative stress induced either by UVC radiation and H₂O₂ exposure, are also explained.

In the third part, experimental results relating to the anionic and zwitterionic lipid/EGCG monolayers, spread in air/water or air/buffer subphases and exposed to blue irradiation, are shown and discussed in the context of the surface behavior and the structural changes (Chapter 5 and 6, respectively). These experiments explain the role of lipid headgroup composition (size, charge) and also the effect of subphase pH, on the miscibility and molecular interactions between catechin and lipid monolayers.

The fourth section addresses the antioxidant potential of catechin by exposing liposomal systems to UV radiation (Chapter 7) and explores the maximum catechin loading capacity of the liposomes without compromising the integrity of the vesicles (Chapter 8). The fifth section concerns the *in vitro* studies performed to test the efficiency and the antioxidant activity of the EGCG-carrying liposomes immobilized onto nanofibers mats for promoting skin healing (Chapter 9).

The sixth and final part presents the main conclusions of the thesis and discusses future challenges in the field of liposomes to improve the administration of natural antioxidants to the skin.

INTERACTIONS OF FLAVONOIDS AND DNA

Dietary polyphenols working as epigenetics modulators: impact on cancer prevention¹

Abstract

Carcinogenesis is one of the most fearsome diseases on the whole society, given the alarming increase of new diagnosed cases every day around the globe. Malignant cellular transformation can be due to the disruption and changes of epigenetic mechanisms, including DNA methylation patterns, chromatin and histone remodeling and microRNA expression. These epigenetics abnormalities, in addition with genetics defects promote the cancer initiation as well its propagation. Polyphenols (catechins, resveratrol, genistein, curcumin) are molecules present in fruit and vegetables that can reverse adverse epigenetic markers in cells, modulating intracellular signaling pathways that regulate cell proliferation and migration to other tissues (metastasis). In this review we discuss in detail, the role and potential use of flavonoids, as epigallocatechin-3-gallate, major catechin present in green tea, on the epigenetic regulation of genes opening new approaches to cancer chemoprevention. A critical review about the impact of changes in lifestyle and diet supplementation with natural phytochemicals on cancer statistics was done. This review highlights the new advances in understanding the anticancer activity of flavonoids based on its ability to damage DNA in cancer cells.

¹This chapter is based on the following publication:

Pires, F., Magalhães-Mota, G. and Raposo, M. Dietary polyphenols working as epigenetics modulators: impact on cancer prevention. *Advances in Medicine and Biology*, 2018, 127:10, Nova Science Publishers.

2.1 Introduction

People of a modern urban society are exposed to high levels of stress and do not have any time to practice sports or to prepare meals, choosing a rapid solution when its time to eat. Unfortunately, in the majority of cases, this rapid solution is related with the practice of bad dietary habits (consumption of fast food and sweetened drinks). The harmful and hazardous consumption of a wrong decision has long-term consequences, evidenced by the alarming increase of the number of cases of colorectal, pancreas, kidney and breast cancers worldwide.

Most of cancer cases (90%) emerge from the regular exposition to risk factors (cigarette smoking, alcohol, radiation, diet, infectious agents) and from somatic mutations. Endogenous processes as the upregulation of oncogenes, radiation-induced DNA lesions and the overproduction of inflammatory cytokines disrupt the cellular homeostasis, leading to an abnormal growth of cells with a malignant phenotype. Cancer cells have an uncontrolled rate of growth and they easily proliferate and spread to other surrounded and distant tissues, due to their sustained angiogenesis and elevated resistance against growth inhibitors [1, 2]. According with cancer statistics around 1 million of new cancer cases, per year, will be recorded in United States in 2020, of which germline mutations contributed with a low percentage for these cancer statistics [3].

A centuries ago, Hippocrates, "Father of Modern Medicine", said "Everyone has a doctor in him or her; we just have to help it in its work. Our food should be our medicine". Vegetables and fruits are rich in polyphenols. Polyphenols boosts the immune system, modulate the activity of enzymes and cell receptors and they are strong antioxidants that scavenge the reactive oxygen species (ROS), reducing in this way the risk of chronic diseases (cardiovascular, stroke, cancer, diabetes, obesity and arthritis) [4, 5].

Nutrition, stress and toxins are factors that govern epigenomes lifetime. In simplified terms, according to Rigges, epigenetics is a phenomenon that refers to mitotically and/or meiotically heritable changes in gene expression that does not involve DNA sequence [6].

Typical hallmarks of cancer cells are their irregularities at level of DNA methylation status, expression pattern of a gene, regulation of miRNA expression accompanied by variations in histone organization. In view of all this, epigenomes can work as biomarkers to detect cancer cells, since "healthy" and cancer cells have, for example, unequal DNA methylation status. From a clinical point of view, new therapeutic approaches have been explored based on epigenetics machinery, considering the efficacy of epigenetic players to control the cell, organ and tissue

function, by turning genes on ("expressed") and off ("silenced") at specific time and locations. In cancer thematic, several studies discussed in detail in the next section, proved that epigenetic regulation of gene expression by histone modifications or by DNA methylation triggers environmental and intrinsic signals that suppresses tumorigenesis.

Recently, nutraceuticals compounds (catechins, curcumin, genistein, resveratrol, anthocyanins) have been assessed as modulators to reverse the adverse epigenetic marks in cancer cells in order to sensitize cancer cells to drugs or to blockage cancer progression and metastasis. In addition, considering the fact that epigenetic defects are more easily reverse than genetic changes, researchers have also been focused on the development of epi-drugs based on bioactive dietary components as epigallocatechin-3-gallate (EGCG) to be used in therapy against cancer, reviewed in the coming section.

In this review, we focused on the largest family of polyphenolic compounds (flavonoids class), reviewing the large number of published articles with recent findings and research in the field, in order to discuss in detail how the failure in the proper regulation of epigenetic mechanisms promotes carcinogenesis and how this health problem can be ameliorate by regular intake of flavonoids. We also discuss the clinical potential of phytochemical based-epigenetic pharmacology as an efficient strategy for cancer treatment.

2.2 Polyphenolic Molecules

A polyphenolic molecule has several phenolic rings in its structure. Each polyphenol is grouped in a subclasse according with the number of phenol rings, the structural elements that connects the various rings to each other and the type of functional group linked to rings. The main subclasses of polyphenols are flavonoids and non-flavonoids (stilbenes, polyphenolic acids and lignans).

Flavonoid structure has two aromatic rings (A and B) linked by an oxygen containing heterocycle (C). Flavonoids can be grouped in subclasses considering the number of hydroxyl groups attached to phenol rings as well the glycosylation and alkylation patterns. Some of the best-known flavonoids subclasses, illustrated in Figure 2.1, include flavonols (quercetin, kaempferol), flavones (apigenin, luteolin), flavan-3-ol (catechins), flavanones (naringenin), isoflavonoids (genistein) and anthocyanins. For instance, flavonols (quercetin) are distinguished from flavanols (catechins) by their binding mode between C2 and C3 and by the linkage of a specific group on C4 position. Flavanols establish a single bond between C2

and C3 and have a methylene resonance on C4 position, in contrast with flavonols which form a double bond and has a carbonyl group attached.

The efficacy of a flavonoid to interact with cell membranes is strongly influenced by the structural aspects of flavonoid backbone as the degree of hydroxylation, the binding mode between C2 and C3 or, simply, the linkage of a specific group on Cx position [7, 8, 9, 10, 11]. For instance, catechins, or flavanol-3-ols, are antioxidant molecules present in great amount in tea leaves, that regulate some intracellular signalling pathways showing significant anticancer effects in a time and concentration dependent-manner. A typical bag of green tea contains the following catechins: (-)-epicatechin (EC), (-)-epigallocatechin (EGC), defined as flavanol monomers, (-)-epicatechin 3-gallate (ECG), (-)-epigallocatechin 3-gallate (EGCG), which are known as flavanol gallates. This division into flavanol monomers and flavanol gallates considers the presence/absence of the gallate group into position 3 of C ring and the presence of different side groups into position 3 and 5' of C and B rings, respectively. Several studies reported that the cellular uptake of gallate catechins (ECG/EGCG) is higher than EC/EGC. In fact, the presence of the ester bond connecting gallic acid and C3 renders a non-polar cis-type EGCG with a higher topological surface area that binds to the surface of a lipid bilayer through hydrogen-bonding, without change structural conformation. However, several studies highlights the fact that the precise molecular mechanisms underlying the action mode of catechin remain puzzling, like in other studies that involved other flavonoids [12, 13].

2.3 Interactions of Flavonoids within cellular environment

2.3.1 Flavonoids and DNA bases

Studies of the interaction between polyphenols and biological molecules (DNA, proteins, lipids, enzymes) are crucial to understand the processes that occur in cells in the presence of polyphenol molecules. However, the number of papers focused on the analyses of the interactions DNA bases - polyphenol molecules is reduced, even known that the outcomes from this type of experiments are significant, bringing clear and important conclusions for this thematic. Some interesting simple results are described below.

2.3. INTERACTIONS OF FLAVONOIDS WITHIN CELLULAR ENVIRONMENT

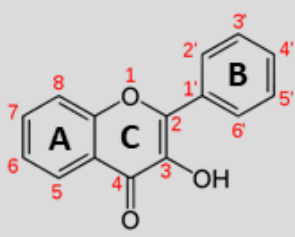
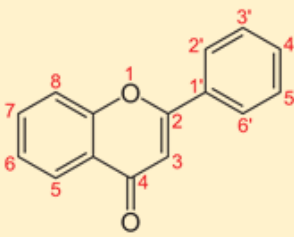
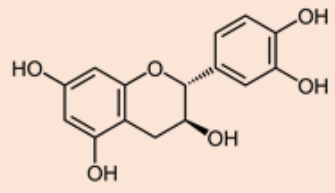
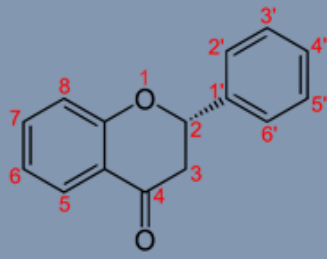
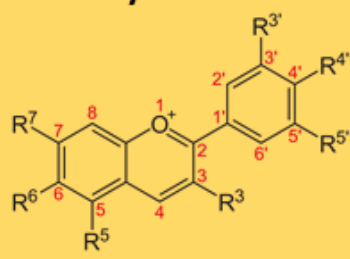
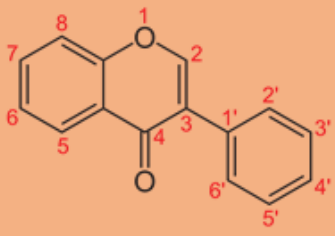
Main classes of Flavonoids (Dietary Phytochemicals)		
<p>Flavonols</p> 	<p>Flavones</p> 	<p>Flavanols</p> 
<p>Molecules: quercetin, fisetin, kaempferol</p> <p>Sources: capers, onions, asparagus, lettuce, berries, spinach, kale, oregano</p>	<p>Molecules: apigenin, luteolin</p> <p>Sources: parsley, rosemary, chamomile, red wine, celery seed</p>	<p>Molecules: catechin, EC, EGCG</p> <p>Sources: teas, cocoa, red wine, apples, blackberries, dark chocolate, pears</p>
<p>Flavanones</p> 	<p>Anthocyanins</p> 	<p>Isoflavone</p> 
<p>Molecules: hesperitin, butin, naringenin</p> <p>Sources: tomatoes, mint, citrus fruit</p>	<p>Molecules: cyanidin, malvidin</p> <p>Sources: red wine, aubergines, cabbage, beans, onions, radishes</p>	<p>Molecules: genistein, daidzein</p> <p>Sources: soya, leguminous plants</p>

Figure 2.1: Chemical structures of the main subclasses of flavonoids.

Recently, Ensafi et al developed a new electrochemical biosensor to demonstrate the effect of Acridine Orange (AO) on DNA damage and to check the inhibitor effect of flavonols antioxidants as myricetin, fisetin and kaempferol on DNA damage [14]. In fact, AO presents high affinity to nucleic acid and stretch the double helical structure of DNA, contributing for the reductions of the intensities of guanine and adenine oxidation signals after the interaction of AO molecules with DNA. In presence of the myricetin, fisetin and kaempferol molecules the DNA damage was reduced being the anti-damaging effects of kaempferol and fisetin better than of myricetin. Theoretical calculations demonstrated that best conformers of flavonol molecules are docked in binding sites of DNA molecule [14]. Already previously, a study of the interaction of DNA with the textile dyes Disperse Orange 1 (DO1) and Disperse Red 1(DR1) have shown significant changes in the characteristic oxidation peaks of the guanine and adenine moieties of immobilized dsDNA while when flavonoids as myricetin and apigenin are added the oxidation peaks are reduced, allowing to conclude that these flavonoids were able to protect adenine and guanine from interaction with those dyes [15]. The interaction of DNA and the flavonoid–transition metal complex (Cu(II)–naringin complex) was demonstrated using square wave voltammetry (SWV) electrochemical method which demonstrates changes in the oxidation peak of the guanine and adenine bases in presence of naringin complex, while the variations of the spectroscopic characteristics of DNA and Cu(II)–naringin complex in aqueous medium demonstrated that the predominant interaction mode may be by intercalation being the guanine site the most adequate for the interaction [16]. Recently, Bhattacharjee et al. used double stranded (duplex) DNA and guanine-rich sequences, which have the propensity to fold into a four stranded DNA structure known as a G-quadruplex (G4), to study the interactions of two polyphenols (fisetin and naringenin) with DNA. Experimental and theoretical results demonstrate the differential binding ability of the two flavonoids with G4 and duplex DNA. Naringenin have shown stronger binding affinity to duplex rather than G4 DNA, while fisetin had shown the opposite behavior. The C-ring planarity of the flavonoid structure appears to be a crucial factor for preferential DNA recognition of flavonoids [17].

2.3.2 Flavonoids and DNA damage

Carcinogenesis is a complex and multistep process which is categorized in the following stages: initiation, promotion and progression [18]. The extensive DNA damage caused by the exposure to cytotoxic or genotoxic agents (ionizing and

2.3. INTERACTIONS OF FLAVONOIDS WITHIN CELLULAR ENVIRONMENT

ultraviolet radiation, environmental agents, therapeutic agents and ROS) attacks the nitrogen bases and sugar-phosphate backbone of DNA, causing single and double-stranded DNA breaks [19, 20, 21, 22, 23]. These exogenous and endogenous lesions disrupt and/or impair the DNA replication and transcription, affecting the genetic stability critical for cell function. Genome instability together with defective DNA repair mechanisms and high frequency of mutations, leads to cellular transformation, decrease cellular defenses and triggers aberrant inflammatory signalling associated with initiation and progression of cancer [24, 25, 26].

Two different strategies are underlying the use of flavonoids in cancer therapy: the first one is see the flavonoids as **killers of cancer cells** and, the second one, is see the **flavonoids as biological soldiers** that fight progression and metastasis of cancer cells. Scientific reports demonstrated that flavonoids induce apoptosis in cancer cells in order to destroy them [27, 28] and protect "healthy" cells against radiation-induced DNA damage working as scavengers of ROS and enhancers of DNA repair genes. Under suitable physiological conditions, cellular organelles produces ROS to mediate phagocytosis, apoptosis and cell signalling to maintain cell homeostasis. Oppositely, under pathological conditions, serious defects in scavenging system leads to a high accumulation of ROS, a situation which increases the oxidation rate of biomolecules and worsens inflammation and cancer.

Physiologically, apoptosis is a cellular process extremely sensible to death stimulus as DNA damage, UV radiation, oxidative stress, chemotherapeutic agents and oncogenic stress. Apoptosis is a normal, well regulated and essential process of cellular suicide coordinated by caspases to maintain the tissue homeostasis, surveillance and host defense mechanisms. Apoptosis can be intrinsic and extrinsically induced by mitochondrial and death receptor-mediated pathways, respectively. Death receptors are plasma membrane receptors which suffer oligomerization upon binding of a specific ligand, resulting in the recruitment of specialized adaptor proteins and in the activation of caspase cascades to trigger cell suicide [29, 30, 31, 32, 33]. Failure in proper apoptosis mechanism, coming from epigenetic events as downregulation of caspase expression, specific inhibition of caspase activity either by cysteine nitrosylation or by overexpression of caspase inhibitors (survinin), promotes tumorigenesis.

Flavonoids induces apoptosis in cancer cells via inhibiting fatty acid synthase (FASN) activity, increasing DNA fragmentation, regulating the caspase-3 and p53 transcript expression or by increasing intracellular ROS level. In many different types of human cancer cells, apigenin showed anti-proliferative and anti-invasiveness properties by targeting the PI3K/Akt signaling pathway along

with downregulation of gene expression of matrix metalloproteinases-9, glycogen synthase kinase-3 β and HEF1 [34, 35]. Butin protects lung fibroblast cells against hydrogen peroxide-induced apoptosis by reducing DNA fragmentation and caspase-3 activity. Moreover, this molecule reduces intracellular ROS level by restoring the antioxidant enzymes level, named SOD and catalase [36].

Inflammation is another natural biological response of the host surveillance mechanisms against harmful stimuli. Several studies points out an association between the persistence of an inflammatory process and a higher tendency to develop cancer [2, 37]. Nuclear factor kappa B (NFkB) is one among the many intracellular signalling pathways which comes into operation as soon as inflammatory and immune responses occurs, controlling the expression of various genes involved, for example, in the interruption of apoptotic biochemical cascades as well in the steps of initiation and progression of carcinogenesis. The conversion of a latent form to a biologically active form of NFkB is triggered by the release of pro-inflammatory cytokines (TNF- α , IL-6, IL-8, IL-1b and IL-1a) from immune or adjacent stromal cells. The activation of epidermal growth factor (EGF) receptor, the production of cyclooxygenase 2 (COX-2), the I κ B phosphorylation, the elevation of intracellular calcium levels and the oxidative stress, are also activators of NFkB [38, 39, 40, 41, 42]. Defects in NFkB signalling pathway up-regulates the expression of anti-apoptotic genes and down-regulates apoptotic genes, keeping the cell proliferation rate and guaranteeing resilience against apoptosis. Moreover, the permanent activation of NFkB confers resistance to tumor cells to the action of chemotherapeutic agents via inactivation of caspases.

Considering all this, researchers have been studying different classes of drugs (immunomodulatory drugs, nonsteroidal anti-inflammatory drugs and newly developed selective IKK inhibitors) to control NFkB activation, since this signalling pathway is an attractive target for anti-cancer therapy [43, 44, 45, 46, 47, 48]. A detailed study of reports on the anti-inflammatory and apoptotic responses of different subclass of flavonoids against death stimulus, covering publication searches between 2010 and 2017, is presented in Table2.1.

The modulation of a particular signalling pathway by a flavonoid is strongly dose dependent. High concentrations of quercetin (100 μ M) inactivates NFkB activity in intestinal epithelial cells and human hepatoma cells [49, 50], whereas a concentration of 40 μ M increased the translocation of NFkB to the nucleus of HT29 and HCT15 human colonic cancer cell lines [51]. In addition, another interesting point reported in this study is the fact that quercetin only induced apoptosis in HT29 cells via partial inactivation of COX-2, increasing the intercellular ROS level and caused cell cycle arrest at G1 check point. HCT15 cells

proved to be insensible to quercetin-induced apoptosis since these cells did not expressed *cox-2* RNA transcript, maintaining unaltered the antioxidant status and a lower intracellular ROS level.

2.4 Flavonoids and epigenetic environment

2.4.1 Flavonoids action in DNA methylation

Epigenetic modifications as DNA methylation associated with histone modifications alters the chromatin architecture controlling in this way the functioning of genome and the signalling pathways that control the cell cycle and apoptosis.

DNA methylation is the most studied epigenetic modification since DNA is stable comparative to proteins and mRNA. DNA methyltransferases (DNMT1, DNMT3a and DNMT3b) are the enzymes responsible to chemically bind a methyl group in DNA sequence, specifically, in the region in which a cytosine and guanine nucleotides are separated by only one phosphate (CpG site), using S-adenosyl-methionine (SAM) as a substrate [52]. CpG islands has a great amount of GC ($\approx 55\%$), in the majority of cases, in unmethylated state. DNA methylation pathway is maintained by DNMT3a and DNMT3b during development and by DNMT1 during cell division (mitosis) [53]. Even so, this process can be disturbed by single nucleotide mutations resulting from, for example, the coupling of 5-methylcytosine deaminase as well the failure of the thymine DNA glycosylase to correct them [54].

According with Cheng et al.[55], DNMT has a catalytic core structure similar to the catechol-*O*-methyltransferase (COMT), belonging both enzymes to the same family: SAM-dependent methyltransferases. COMT is an enzyme present in mammalian tissues (liver, kidney, small intestine) that catalyzes *O*-methylation of catechol-structure molecules (catecholamines, catechins, flavonoids). Catechins and their metabolites are substrates for the COMT-mediated methylation, yielding significant amounts of the demethylated SAM (S-adenosyl-L-homocysteine, SAH), a potent noncompetitive inhibitor of DNMTs [56, 57, 58, 59]. COMT methylates the D-ring of EGCG *in vitro* and *in vivo* forming 4-MeEGCG and 4'-4-DiMeEGCG, which compromises EGCG bioavailability in bloodstream and, consequently, its therapeutic action [60, 61, 62]. Having in mind, that the presence of gallate group (D-ring) in EGCG plays an inhibitory effect on COMT-activity, is expect that EGCG also inhibit DNMT by binding to certain catalytic site [55, 63].

CHAPTER 2. INTERACTIONS OF FLAVONOIDS AND DNA

Table 2.1: Protective mechanisms of flavonoids against death stimulus.

Bioactive Compound	Cell Line	Death Stimulus	Biological Action
Apigenin	HaCaT skin keratinocytes [64]	UVB radiation	DNA protection via: ↑ NER genes expression ↓ CPDs ↓ ROS generation ↓ NFκB and MAPK
	T-24 human bladder cancer cells [65]	Tumorigenesis	Inhibition cancer cell proliferation via: Induction of cell cycle arrest: ↑ p53 phosphorylation ↓ Cyclin A, Cyclin B1, Cyclin E, CDK2, Cdc2, and Cdc25C Induction of Apoptosis: ↑ cytochrome c release ↑ proapoptotic proteins level (Bax, Bad, and Bak) ↑ cysteine proteases (caspase-3, -7, and -9) ↑ ROS
Butin	V79-4 lung fibroblast cells [66]	H ₂ O ₂	Decrease oxidative damage via: ↓ H ₂ O ₂ -induced 8-OHdG level ↑ OGG1 mRNA and protein levels ↑ Phosphorylation of Akt
Cyanidin	SH-SY5Y neuroblastoma cell [67]	Aggregated Aβ	Protection against neuronal injury via: ↓ ROS ↓ SOD and GSH-Px expression ↓ intracellular [Ca ²⁺] ↓ HO-1, NQO1, and Bcl-2 protein level
EGCG	C57 BL/6 male mice [68]	Gamma Radiation	DNA repair via: ↓ HDAC activity ↑ Chromatin opening
	HaCaT human epidermal keratinocyte cells [69]	X-rays radiation	Radioreistance to HaCaT via: ↓ intracellular ROS ↑ anti-apoptotic protein Bcl-2 ↓ pro-apoptotic protein Bax ↓ γ-H2AX foci number ↓ DSBs ↑ SOD2 and HO-1 expression
Genistein	NHDF and KEL dermal fibroblast cells [70]	UV radiation	Photoprotection of cell by decreasing concentration of free radicals
	Pheochromocytoma (PC12) cells [71]	Aggregated amyloid beta Aβ	Cell survival via: ↓ Cytochrome c and Smac release ↓ caspase-3 activity ↓ phosphorylation of JNK
	Albino Sprague-Dawley rats [72]	AlCl ₃	Protection against neuronal injury via: ↑ GSH and SOD ↓ AChE activity ↓ TNF-α, NF-κβ subunit P65 and COX-2 expression ↑ ER-β mRNA expression
Quercetin	CF1 mice [73]	Azoxymethane	Decrease precancerous lesions
	Rat primary hippocampal neurons [74]	Aggregated Aβ H ₂ O ₂	Protection against neuronal injury via: ↓ ROS Restoring of the mitochondrial morphology and potential ↓ superoxide anion
	Kidney and bladder tissues of Sprague-Dawley rats [75]	X-rays radiation	Attenuation of irradiation-induced oxidative damage via: ↓ TNF- α levels ↓ 8-OH dG levels ↓ caspase-3 ↓ MPO ↓ ROM-mediated recruitment of neutrophils ↓ pro-inflammatory mediators release ↓ radiation-induced tissue destruction

According with Zhu *et al.*, EGCG is much stronger inhibitor of DNMT1 compared to other catechins (epicatechin and catechin), forming complexes EGCG-DNMT1 through a reaction energetically more favorable in the presence of magnesium ions. Computer modelling showed that D-ring of EGCG (gallate group) is able to form hydrogen bonds with Glu1265 residue at the catalytic core site of DNMT1 [76]. Natural products working as inhibitors of DNMTs, in particular DNMT1, guarantees the re-expression of silenced-genes in daughter cells since the hypermethylation status was reversed. The therapeutic potential of EGCG in early studies was assessed in cancer cells. It was shown that treatment of colon cancer cells with EGCG downregulates the expression of DNMT3b by inhibition of E3 ubiquitin ligase (UHRF1) which plays a critical role in cancer progression by gene silencing and DNMTs recruitment [77, 78]. The reduction in DNMT expression induced by EGCG inhibited promoter methylation of retinoid X receptor alpha (RXR α), disrupting cancer cell proliferation and promoting cell cycle arrest in CIMP+ colon cancer cells and in colon tumors of Apc^{Min/+} mice [79].

In fact, changes in DNA methylation pattern status trigger different biological actions. For example, hypermethylation causes the inactivation of tumor suppressor genes (p16INK4a, APC, and BRCA1) involved in different cancer type [80, 81, 82], while hypomethylation disturbs chromosomal stability, increases the mutations events resulting in cancer development and progression [83, 84]. The accumulation of epigenetic changes in multiple genes and in underlying intracellular signalling pathways (apoptosis, inflammation), alters the cellular metabolism, as for example, the acceleration of glucose metabolism in cancer cells. The DNA methylation pattern is strongly influenced by oxidative stress. The overproduction of ROS overloads the intracellular detoxification system, damaging the biomolecules (DNA, cell membranes) and affecting the transduction pathways, promoting apoptosis, inflammation, necrosis and other diseases [85].

The binding of the Nuclear factor-erythroid-2-related factor 2 (Nrf2) to the cytosolic protein Kelch-like ECH-associated protein 1 (Keap 1) is the major intracellular mechanism against oxidative stress. The dissociation of Nrf2-Keap1 complex, promoted by the oxidation or covalent modifications on the thiols of the cysteine residues of Keap1, leads to Nrf2 translocation to cell nucleus, where activates antioxidant and phase II detoxifying enzyme genes. A deficient gene and protein expression of Nrf2, often coming from the hypermethylation of the first five CpG residues in Nrf2 promoter, being one of the classical hallmarks of prostate carcinogenesis [86]. An impairment in Nrf2-Keap1 pathway compromises cellular defence mechanisms against oxidative and electrophilic stress due

to the deregulation of expression of many cytoprotective genes that encodes detoxifying proteins such as superoxide dismutase (SOD), glutathione S-transferase (GST), glutathione peroxidase, catalase, among others, leading to an inevitable tumor development and chemoresistance [87, 88, 89, 90].

The action of the flavonoids lie in their antioxidant and scavenger power together with their ability to target some transcription factors (NF κ B, estrogen receptor (ER), hypoxia inducible factor-1 (HIF-1)) involved in the regulation of anti-inflammatory and antitumor processes [91, 92, 93]. There is a substantial body of evidence that bioactive drugs, reviewed in Table 2.2a, influence the status of epigenetic machinery namely, microRNA expression, DNA methylation and chromatin dynamics in gene and cell line specific, in an exposure time-dependent manner. In malignant melanocytes, EGCG prevented metastasis and cancer growth, after directly binds to Gln54, Ile72, Cys73, Gly55, Asp57 and Lys96 residues in substrate-binding pocket of TRAF6, and after suppress the TRAF6 E3 ubiquitin ligase activity. Consequently, the IL-1 β -induced activation of the NF- κ B pathway was attenuated [94]. Some of the intermediary signalling pathways targeted by EGCG responsible for modulating the anti-tumour activities are Wnt/ β -Catenin, MAPK, AKT/STAT3 and p53 [95, 96, 97, 98].

In most of cases, the physiological concentrations used in *in vitro* experiments might be very difficult to obtain *in vivo*, considering the complex metabolic processes as well physical and biochemical barriers (gastrointestinal epithelium, stomach pH, liver first-pass metabolism, immune system mediated-clearance) that contributes to a poor absorption and a suboptimal drug delivery. However, some studies have demonstrated that lower concentrations of apigenin, easily achieved through dietary sources ($\sim 1.5\mu\text{M}$), are strong enough to exerts anti-inflammatory effects in different cell type via modulation of NF- κ B activity by different mechanisms [99]. Apigenin suppresses NF- κ B activity through blockage of pro-inflammatory cytokines and growth factors expression (IL-6, IL-8) and by controlling the p38MAPK phosphorylation level. Apigenin may compete with adenosine triphosphate (ATP) for binding to p38MAPK, considering the strong degree of similarity between the aglycone structure (ABC ring) of apigenin and the structure of the molecule ATP. The interference of apigenin in ATP binding and cleavage, prevents the activation of p38MAPK, acting as negative regulator of invasion and migration of tumor cells [100, 101, 102].

2.4.2 Flavonoids action in histone tail modifications

Histones are positively charged small proteins that governs DNA packing allowing the storage of approximately of 2 meters of DNA inside of the microscopic space of the human diploid cell nucleus. As a curiosity, "human body has 50 trillion cells corresponding to 100 trillion meters of DNA, meaning that each human has enough DNA to go from earth to the Sun and back more than 300 times" (Sun is 150 billion meters from Earth) [103].

Histones octamer (two copies of each H2A, H2B, H3, and H4) binds to DNA via electrostatic interactions (DNA is a negative-charged molecule due to the presence of phosphate groups), forming DNA-histone complexes called nucleosomes. Nucleosome, building block of chromatin, is connected to other nucleosome via linker DNA. H1 histones bind to a single nucleosome and to the linker DNA, exerting a chromatin-condensing action. During cell division, chromatin fibers fold upon themselves forming higher order chromosome structures[104, 105, 106, 107]. Figure 2.2 illustrates several intracellular reversible processes as acetylation, phosphorylation, ubiquitylation, glycosylation and sumoylation that can happens on aminoacid residues of histone tails (that are facing outside of nucleosome), which influences chromatin architecture and, consequently, gene expression. Chromatin in condensed state (Heterochromatin) hampers the binding of transcription factors and thereby occurs gene silencing. Of course, specific enzymes are crucial and work during these processes, being their intracellular concentration dependent of nutrients, energy level (ATP/ADP) and cellular metabolism (glycolysis, mitochondrial respiration rate, ROS/RNS production)[108, 109].

Acetylation phenomenon, catalyzed by enzymes of histone acetyltransferases (HATs), decreases the electrostatic interactions DNA-histones and loosens chromatin structure, which facilitates the binding of transcription factors and promotes gene expression.

Histone deacetylases (HDACs) catalyses histone deacetylation. HDACs (HDAC1, HDAC2, HDAC3) expression levels and activity are epigenetic shutters that repress genes and activate signalling pathways (Keap1/Nfr2, NFkB, HO-1, PGC-1 α , HIF-1 α) involved in the regulation of cellular responses to oxidative stress. Impairments in N-terminal tails of histones alters gene expression and compromise the functioning of signalling pathways mentioned before, resulting in many human pathologies which could be inherited in the next generations. Carcinogenesis can emerge from the imbalance between HATs and HDACs activity. Cancer cells have an uncontrolled cell division since cells miss cell cycle checkpoints(G1,

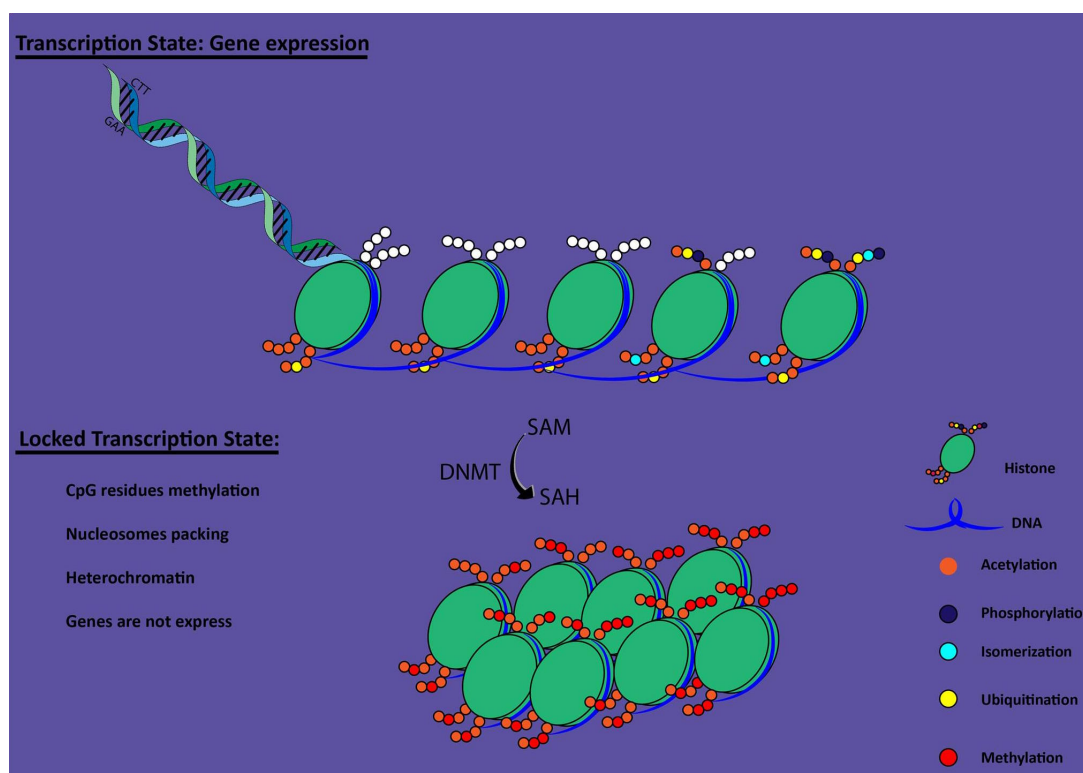


Figure 2.2: **Gene activation status determined by DNA methylation and histone modifications.** Histone tails contains residues that are susceptible to translational covalent modifications as ubiquitylation, isomerization, phosphorylation, sumoylation, methylation and acetylation. When CpG sites are methylated, a process catalyzed by DNMT, occurs histone modifications which trigger the activation or repression of gene depending upon which residue is modified and the degree of methylation. The recruitment of DNMT turns chromatin more condensed, preventing the access of transcription factors to DNA and, consequently, gene expression.

S, G2, M) due to repression of genes involved in inhibition of cyclins and cyclin-dependent kinases *p21* or in induction of apoptosis (*BAX*). HDACs inhibitors (vorinostat, romidepsin, belinostat and panobinostat) are a new class of FDA-approved anticancer drugs which suppress the overexpression of the HDAC enzymes and reactivates the expression of *p21* in malignant tumors, controlling cell proliferation rate and blocking angiogenesis and inflammation. Unfortunately, the dampening of angiogenesis and inflammation decrease drug delivery and therapeutic response in solid tumors, which compromises the use of HDACs inhibitors in cancer clinic. In view of all this, researchers studied the potential of several nutraceuticals for modifying histones by themselves or by synergism with HDACs inhibitors, as a suitable way of combating cancer. In a recent study, the ability of 131 different natural products to regulate HDACs activity was assessed, resulting in eighteen new bioactive compounds working as HDAC inhibitors, able

to increased the lysine acetylation in rat cardiac cells, showing potential to be used for treatment of heart failure. [110, 111].

Apigenin prevented the uncontrolled growth rate of breast cancer cells via suppression of cyclins (cyclin A, cyclin B, and CDK1) and through the induction of H3 acetylation which, consequently, leads to the activation of *p21* promoter. As a consequence, *p21* binds to PCNA (proliferating cell nuclear antigen) inhibiting the progression of the cells into M phase of the cell cycle [112]. In another study, apigenin inhibited prostate cancer cells progression through the regulation of the MAPK and PI3K/Akt signaling pathways, inducing G0/G1 cell cycle arrest [113].

Yoon and co-workers showed that different catechins (EGCG, EGC and EC) induced cell death and prevent growth of androgen-sensitive (LNCaP) human prostate cancer cell line, in a concentration- dependent manner. Androgen receptor (AR) is an essential hormone nuclear receptor for normal prostate development. Mutations and post-transcriptional modifications (acetylation and phosphorylation) on AR receptor have been related with acceleration of prostate cancer progression. EGCG decreased HAT activity (p300) and, thus the acetylation level of AR and histone H3, delaying in this way the prostate cancer progression [114]. Modification of histone acetylation by EGCG was also observed in human cervical cancer cells. EGCG decreased enzymatic activity of DNMT3b and HDAC1 in HeLa cells in a time-dependent manner. Docking studies suggested that gallate moiety of EGCG interacts with binding pocket of DNMT3b, in particular, with residues Arg 832, Arg 731, Arg 733 and Asn 652 [115]. Synergistic effects of a combination of EGCG and trichostatin A (HDACs inhibitor) in ER α negative MDA-MB-231 breast cancer cells was reported. Researchers found that EGCG reactivated ER α expression through alterations in histone acetylation and methylation status [116]. In lung cancer cells, the protein level of HDAC4, -5, and -6 were decreased, due to the synergism coming from the combination of EGCG with retinoids (Am80). Furthermore, the combination EGCG+Am80 also promoted acetylation of lysine 382 in *p53* (a non-histone protein), enhancing the *p21* gene expression and thus the apoptosis in cancer cells [117].

Medical conditions as hyperglycemia (HG) is a risk factor to develop cancer, besides additional problems as cardiovascular disease, kidney failure and blindness. The deacetylation of NF κ B-p65 at lysine 310 and histone 3 (H3) at lysine 9 position resulting from the sirtuin-1 (SIRT-1) activation induced by resveratrol, decreased the cardiac oxidative stress and normalized the mRNA expression of genes (TNF- α , IL-6, COX-2, Bax, NOX1 and NOX4), which are overexpressed in a diabetic heart [118]. In another study, the combination treatment with fisetin

and luteolin induced the SIRT-1 activation, increase the FOXO3a expression, decreased the activity of histone acetyltransferase, promoted the deacetylation of the p65 subunit of NF- κ B and modulated the release of proinflammatory molecules in human monocytes under HG conditions, showing their potential to be used as a therapeutic agent for the treatment of diabetes [119].

2.4.3 Flavonoids action in miRNAs expression

A bulk of literature has suggested that an abnormal expression of MicroRNAs (miRNAs) is one of the hallmarks of cancer, leading to an overproduction of oncogenes and inhibition of tumor suppressor genes [120]. miRNAs are shorter non-coding sequences of RNAs, which binds to Argonaute protein family leading to mRNA cleavage and posttranscriptional gene silencing. The analysis of miRNA signatures is a specific and sensitive tool that improves the capability for an early detection of cancer, based on the differences in miRNA expression in cancer and cancer-free patients. Recently, effort had been made to improve diagnostic method, through non-invasive procedure as the quantification of the miRNA expression (miR-10b, miR-1 and miR-30a) in bronchoalveolar lavage, sputum and plasma of lung cancer patients instead of tissue/biopsy samples [121].

An interesting fact about miRNAs is that they can work as epigenetics modulators, but themselves can be regulated through epigenetic modifications. DNA methylation status and histone modifications are key regulators of miRNAs expression since a substantial portion of miRNAs are present near of CpG islands. For instance, in the epithelial tissue of patients with colorectal cancer, the miRNAs (*hsa-miR-9*, *hsa-miR-124*, *hsa-miR-129*, *hsa-miR-137*, *hsa-miR-149*) are down-regulated. All of these miRNAs are localized on CpG island, being the DNA hypermethylation and histone acetylation the phenomena responsible for the decrease of miRNAs expression [122].

Flavonoids induce changes in miRNA profile, illustrated in Table 2.3a, as happens in DNA and histones to trigger anti-cancer effect. *In vitro* study shown that the exposure of oral cancer cells to a 5 μ M of luteolin for 6 hours, was an efficient treatment to decrease the rate of angiogenesis and cell proliferation. Furthermore, a significant decrease in histone acetylation ((H3K9 and H3K14) and significant global changes in miRNAs expression was observed. Luteolin decreased the expression of oncogenes (miR-135a) and increased the expression of tumor suppressor genes (miR-195/215, let7c) [123]. Another *in vitro* study revealed that luteolin suppressed survival, proliferation and migration of MDA-MB-231 breast cancer cells by triggering a decrease in Notch-1 signalling by

regulating mRNAs expression. Luteolin increased the expression of miR-34a, miR-139-5p, miR-246, miR-181a, miR-224 and decrease miR-155 in order to inhibit Notch pathway. Suppressing effect of luteolin in Notch signalling caused downregulation of growth factors (VEGF) and metalloproteinases (MMP-2, MMP-9), which are involved in angiogenesis that sustains cancer survival and migration [124]. In addition, luteolin also activate ERK and p38 signalling pathways to promote the nuclear translocation of mitochondrial protein (AIF) to induce breast cancer cell death [125].

Zarghami et al. encapsulated chrysin, a flavone found in bee pollen, in PLGA-PEG nanoparticles to improve its bioavailability and efficacy to prevent proliferation of gastric cancer cell line, through regulation of miRNAs expression. The dysregulation of miRNA-9 is a fingertip identified in many different types of cancers, including breast, colon, gastric, lung and neck. The nanoencapsulation form of chrysin increased the expression of miR-9, Let7-a, miR-22, miR-34a and miR-126 on human gastric cancer cells compared to free chrysin. The restoration of tumor suppressor genes (miR-22, miR-34a and miR-126) expression reduced gastric tumor growth through induction of apoptosis [126, 127].

2.5 Flavonoids: agents for epigenetics pharmacotherapy

As aforementioned, drug's journey to cancer site is hampered by physical (vascular architecture, porosity, natural filtration systems) or chemical constraints (pH, temperature, oxygen, enzymes and immune systems attack), that decrease drug concentration in bloodstream (bioavailability) and that impair its interaction with cell membrane as well as its deliver to target specific tissues.

Epigenetic drugs approved by Food and Drug Administration (FDA) modulate the DNA methylation and histone acetylation status, acting as inhibitors of DNMTs (azacitidine and decitabine) and of HDACs (vorinostat, romidespin, trichostatin and belinostat), respectively [128]. However, clinical trials alerts to toxicity, low efficacy in solid tumors and side-effects associated to several epigenetic drugs.

Table 2.2a: Modulation of epigenome by bioactive compounds.

Bioactive Compound	Cancer type	Cell Line	Epigenetic modifications	Cellular Consequences
Apigenin	Breast [112]	MDA-MB-231	↓ Cyclin A, cyclin B, and cyclin-dependent kinase-1 (CDK1) expression ↑ Acetylation of histone H3 in the p21 ^{WAF1/CIP1} promoter region	Inhibition of cell proliferation G2/M phase cell cycle arrest
Apigenin (10 μM)	Breast [102]	HCA	↓ IL-1A-stimulated IL-6 secretion ↓ IP10/CXCL10 ↓ NF-κB activity ↓ IRAK1/IRAK4/p38MAPK phosphorylation	↓ Cell proliferation rate Supress SASP to stimulate breast cancer cell proliferation
22 EGCG	Esophageal [63, 129, 130]	ECa109 cells (50-200mg/L)	↑ p16 gene demethylation ↑ p16 mRNA expression ↑ protein expression	G1 phase cell cycle arrest Inhibition of proliferation and malignant transformation Induction of apoptosis
		KYSE510 (50 μmol/L for 6d)	Inhibition of O-6-methylguanine- DNA methyltransferase (MGMT) Reactivation of methylation-silenced genes (p16 ^{INK4a} , RARβ, MGMT, and hMLH1) Reactivation RARβ mRNA Inhibition of promoter cytosine (CpG islands) hypermethylation	↑ Protein expression ↑ Tumor cell apoptosis
EGCG + AM80 (synthetic retinoid)	Lung [117]	PC-9	↑ Alteration of acetylation status of nonhistone proteins (p53 and α-tubulin) ↓ HDAC4, -5 and -6 protein expression through posttranscriptional regulation ↑ GADD153, DR5 and p21 ^{waf1} gene expression	↑ Apoptosis
EGCG (20 μM) + SFN from broccoli sprouts (10 μM)	Breast [131]	ERα(-) MDA-MB-231	Partial reactivation of ERα re-expression Reduction gene expression of HDAC1 at mRNA level Decrease enzymatic activities of HDACs and DNMTs	Inhibition of cancer cell proliferation Re-sensitization of cancer cells to hormonal therapy

Table 2.2b: Modulation of epigenome by bioactive compounds (continued).

Bioactive Compound	Cancer type	Cell Line	Epigenetic modifications	Cellular Consequences
FN1 (Curcumin Analog) (50-250 nM)	Prostate [132]	TRAMP-C1	<p>↑ Nfr2 mRNA ↑ HO-1 mRNA ↑ NQO1, UGT1A1 protein expression ↓ Keap1 expression ↓ DNMT1, DNMT3a, DNMT3b ↓ HDAC4</p>	Inhibition of cancer growth ↓ Colony formation
Genistein 23	Prostate [133]	Prostate Specimens (30 mg capsules daily for 3-6 weeks)	Demethylation of ADCY4 promoter Expression of NOTCH3 and JAG1 mRNAs Promotion of PTEN activity and inhibition of MYC activity	↓ Cell proliferation ↓ Cell survival
		LNCaP, LAPC-4 and PC-3 (0.5-10 μmol/L)	Reversion of ER-β promoter hypermethylation Induction of phosphorylation, nuclear translocation and transcriptional activity ER-β	↑ Apoptosis
	Lung [134]	NSCLC A549	Reversion of Keap1 promoter hypermethylation Inhibition of NQO1 protein expression Inhibition of Nrf2 translocation to the nucleus Inhibition of synthesis of GSH	↑ Radiosensitivity ↑ ROS Level ↑ Radiation-induced apoptosis
Quercetin (10 μM)	Colon [51]	HCT15 HT29	<p>↑ Caspase 3 ↑ Cytosolic cytochrome c ↓ pAkt, pGSK-3β and cyclin D1 expression ↑ COX-2 ↑ TNF-α miRNA ↓ GSH</p>	Apoptosis of HCT15 and HT29 colon cancer cell Chromatin cleavage Breakdown of chromosomal DNA Increase of intracellular ROS level
Resveratrol	— [118]	H9C2	<p>Deacetylates NFκB-p65 at Lys 310 and histone 3 (H3) at Lys 9 ↓ mRNA expression TNF-α, IL-6, COX-2, Bax, NOX1 and NOX4 ↓ NADPH oxidase expression ↑ SIRT-1 activity</p>	↓ Cardiac oxidative stress

A recent study showed that the combination of EGCG and sulforaphane (SFN), present in broccoli sprouts, is a green natural strategy that epigenetically modulates the activation of tumor-related gene expression in a similar way to synthetic epigenetic drugs, but without toxicity signs. In this particular study, EGCG (amount corresponding to half a cup of green tea) acts on DNA methylation and SFN on histone acetylation status. The combination EGCG + SFN is strong enough to reactivate the expression of ER α in MDA-MB-231 breast cancer cells, re-sensitizing them to hormonal therapy both *in vitro* as *in vivo* [131].

Another major problem of the available chemotherapeutic anticancer drugs is their poor selectivity to cancer cells, being toxic to surrounded "healthy" cells. Genistein, a natural isoflavone present in soybeans, promotes radiation-induced apoptosis in non-small cell lung cancer (NSCLC A549 cells) but exerts radioprotective effect on normal lung fibroblast (MRC-5 cells), confirming its selectivity. In fact, genistein act as epigenetic modulator, inducing the demethylation of Keap1 promoter which blocked the Nrf2 translocation to nucleus of NSCLC A549 cells, compromising the gene expression involved in Nrf2-dependent antioxidant system. NSCLC A549 cells have an impaired Nrf2-dependent antioxidant system, suffering apoptosis induced by ROS coming from the exposure to X-rays. In "healthy" cells, genistein did not alters gene promoter region status, maintaining functional and active the production of antioxidant enzymes (GSH) needed to protect cells against oxidative stress-induced by X rays [134].

2.6 Conclusion

A healthy balanced diet is the best weapon to fight cancer and other chronic diseases. The daily consumption of natural compounds, coming from various sources available on earth, offers health-benefits coming from their anti-oxidant, anti-inflammatory and anti-cancer properties. The main advantages of flavonoids is that they can be used over longer periods of time since they have very low toxicity. Flavonoids are promising therapeutic drugs for fighting multistage diseases as cancer, since they regulate the expression of tumor suppressor genes (upregulation) and of oncogenes (downregulation). These nutraceuticals also have the ability to modulate some intracellular pathways, namely, the pathways involved in the activation of apoptosis and cell cycle arrest, thus preventing cancer cell survival and migration.

Table 2.3a: Targeting miRNAs by flavonoids.

Bioactive Compound	Cancer type	Up-regulated miRNA transcript	Down-regulated miRNA transcript	Biological Action
Chrysin	Gastric Cancer [127, 135, 136]	miR-9,Let-7a,miR-34a,miR-22,miR-126	miR-18a, miR-21 and miR-221	Induction of apoptosis
25 EGCG	Hepatocellular cancer [137]	Let-7a, Let-7b, Let-7c, Let-7d, miR-16, miR18, miR-20a, miR25, miR-92, miR93, miR221, miR-320, miR377	miR-467bn,miR-487b,miR-197,miR-805,miR-374n, let-7 f, miR-350,miR-24-1n,miR-137,miR-335-3p,miR-222, miR-26b,miR-30c-1n,miR-98,miR-30c,miR-30bn,miR-32, miR-674n,miR-532-5p,let-7g,miR-192,miR-302d,miR-30b, miR-802,let-7e,miR-322,miR-720,miR-146b,miR-340-3p, miR-185,miR-425,miR-10a,miR-126-5p,miR-101a,miR-30en, miR-141,miR-33,miR-29an,miR-199b,miR-450a-5p,miR-21, miR-23a,miR-101b,miR-148a,miR-193,miR-23b,miR-107, miR-140,miR-551b,miR-466c-5p,miR-106a,miR-590-3p, miR-875-3p,miR-224,miR-292-5p,miR-678,miR-469,miR-463n, miR-32,miR-674n,miR-532-5p,let-7g,miR-192,miR-302d, miR-30b,miR-802,let-7e,miR-322,miR-720,miR-146b,miR-340-3p, miR-185,miR-425,miR-10a,miR-126-5p,miR-101a,miR-30en, miR-141,miR-33,miR-29an,miR-199b,miR-450a-5p,miR-21,miR-23a, miR-101b,miR-148a,miR-193,miR-23b,miR-107,miR-140,miR-551b, miR-466c-5p,miR-106a,miR-590-3p,miR-875-3p,miR-224,miR-292-5p, miR-678,miR-469,miR-463n,miR-574-3p,miR-201,miR-290-3p, miR-181a,miR-302a,miR-429,miR-133a,miR-190b,miR-710,miR-135b, miR-296-5p,miR-191n,miR-188-5p,miR-298,miR-181a-1n,miR-466 g, miR-26bn,miR-466 f-3p,miR-29bn,miR-1224,miR-291b-5p,miR-324-5p, miR-486,miR-128,miR-450b-3p,miR-135an,miR-294,miR-671-5p, miR-878-3p,miR-801,miR-370,miR-1,miR-494,miR-133b	Induction of apoptosis
	Colorectal cancer [138]	miR-34a, miR-145, miR-200c		Inhibition of self-renewal
	Neuroblastoma [139, 140]	miR-7-1, miR-34a, miR-99a	miR-92, miR-93, miR-106b	Inhibition of self-renewal
	Lung cancer [141, 142, 143]	miR-210, mmu-miR-2137, mmu-miR-449a, mmu-miR-144, mmu-miR-486, mmu-miR-3107, mmu-miR-5130, mmu-miR-2861 mmu-miR-763, mmu-miR-3473a, hsa-miR-98-5p	mmu-miR-696, mmu-miR-449c-5p,mmu-miR-7a-5p, mmu-miR-205-5p mmu-miR-450a-2-3p, mmu-miR-1199-3p, mmu-miR-374c-5p mmu-miR-218-5p , mmu-let-7b-3p	Inhibition cell proliferation Chemotherapy sensitivity
	Breast cancer [144]	miR-16		Inhibition cell proliferation
Nasopharyngeal cancer [145]	hsa-miR-454,hsa-miR-1202, hsa-miR-1207-5p hsa-miR-205-3p hsa-miR-1225-5p, hsa-miR-1246,hsa-miR-1915, hsa-miR-1973 hsa-miR-210, hsa-miR-2861,hsa-miR-29b-1-5p, hsa-miR-3162 hsa-miR-3196, hsa-miR-34a,hsa-miR-3656, hsa-miR-3665,hsa-miR-4281 hsa-miR-1268, hsa-miR-1290 hsa-miR-186, hsa-miR-193b hsa-miR-21, hsa-miR-219-5p hsa-miR-22, hsa-miR-22-5p hsa-miR-29a,hsa-miR-365 hsa-miR-4299, hsa-miR-494, hsa-miR-572,hsa-miR-574-5p, hsa-miR-7	hsa-miR-205-3p	Induction of apoptosis Inhibition of cell proliferation Inhibition of angiogenesis	

Table 2.3b: Targeting miRNAs by flavonoids (continued).

Bioactive Compound	Cancer type	Up-regulated miRNA transcript	Down-regulated miRNA transcript	Biological Action
Curcumin	Lymphoma [146, 147]	miR-22, miR-15a, miR-16		↓ Bcl-2 expression Inhibition tumor progression
	Pancreatic Cancer [148, 149]	miR-200, miR-22	miR-21, miR-199	Inhibition tumor progression
	Prostate Cancer [150, 151]	miR-205	miR-21, miR-141, miR-183	↑ Proteins expression Inhibition tumor progression
Genistein	Breast Cancer [152, 153]	miR-23b	miR-155	Induction of apoptosis Inhibition cell survival Inhibition cell proliferation
26 Luteolin	Head and neck [123]	hsa-miR-1308, hsa-miR-98, hsa-miR-193b, hsa-miR-26b, hsa-miR-31, hsa-miR-378, hsa-miR-221, hsa-let-7c, hsa-miR-222, hsa-miR-195, hsa-miR-658, hsa-miR-484, hsa-miR-223, hsa-miR-484, hsa-miR-144	hsa-miR-122, hsa-miR-576-5p, hsa-miR-609, hsa-miR-147b, hsa-miR-634, hsa-miR-1284, hsa-miR-15b, hsa-miR-191, hsa-miR-517a, hsa-miR-664, hsa-miR-522, hsa-miR-933, hsa-miR-377, hsa-let7b	Inhibition of cell proliferation Inhibition of angiogenesis
Morin	Prostate Cancer [154]		miR-155, miR-143, miR-146b	Induction of apoptosis Chemosensitivity Decrease tumor size GATA3 expression
Proanthocyanidin	Glioblastoma [155]	miR-30e		↑ Induction of apoptosis
Resveratrol	Pancreatic cancer [156, 157]	miR-663	miR-21, miR-155, miR-27a	↑ Induction of apoptosis
	Prostate cancer [158, 159, 160, 161]	miR-328, miR-149, miR-639 miR-939, miR-572, miR-150	miR-17, miR-21, miR-7 miR-197, miR-129, Let-7c, miR-659	↓ Cell proliferation ↓ Metastasis ↑ Tumor suppressor genes ↓ Oncogenes

A wide array of evidence suggest that flavonoids are epigenetic modulators, which alter the DNMT and HDACs enzymes activity, turning on or off specific genes-involved in carcinogenesis, in a concentration and time dependent manner. Besides their multitargeting capacity, flavonoids also minimizes the side-effects of radiotherapy and chemotherapy. In addition, flavonoids boosts the effectiveness of chemotherapy by increasing the chemotherapeutic sensitivity of cancer cells. Despite these promising findings, a huge obstacle to be solved before implementation of flavonoids in clinic is the improvement of stability, routes of administration, organ specificity and efficiency delivery to target cancer cells. Of course, a plenty of different drug delivery approaches as liposomes, hydrogels, nanoparticles, cyclodextrins, have already be designed and tested in recent years, proving be suitable vehicles that improve flavonoid's stability, half-life and that facilitate its accumulation at the site of action. Furthermore, another concern in the field of cancer epigenetics, is the maintenance of the epigenetic changes over time. Any flavonoid or synthetic drug should maintain epigenetic modifications in order to preserve cellular identity, cellular processes and to permanently delete the abnormal cancer epigenome.

Clearly, new combinatorial pharmacological formulations based on the synergism of natural compounds and hormonal drugs capable of modulating the epigenome, paves the way to cancer prevention and treatment. Future studies focus on to better elucidate the molecular mechanisms underlying flavonoids action *in vitro* and *in vivo* using proper animal models for each cancer can provided valuable information to design successful strategies to treat solid tumors.

2.7 Acknowledgements

The authors acknowledge the financial support from FEDER, through Programa Operacional Factores de Competitividade—COMPETE and Fundação para a Ciência e a Tecnologia—FCT, by the project PTDC/FIS-NAN/0909/2014 and for the Portuguese research Grant No. PEst-OE/FIS/UI0068/2011 and UID/FIS/00068 / 2013. Filipa Pires acknowledges the fellowship PD/BD/106036/2015 from RABBIT Doctoral Programme (Portugal).

Post-scriptum: Currently, the protective effect of different EGCG concentrations on calf thymus DNA against UV radiation is being addressed in our laboratory, for understanding the binding mechanism and the pharmacological behavior of EGCG responsible to enhance the susceptibility or resistance of DNA against oxidative stress, respectively. Afterwards, the idea is to assess the implications

of the same EGCG concentrations on certain epigenetic targets (non-coding RNA and DNA-associated proteins). Nonetheless, considering the fact that the therapeutic potential of this epigenetic-based strategy will be strongly dependent of the *in vivo* EGCG concentration, this thesis work mostly focused on developing liposome-encapsulated EGCG formulations that will stabilize and protect EGCG from degradation and therefore, will guarantee an adequate and effective deliver of EGCG in specific locations such as the cell nucleus.

References

- [1] A. Mantovani, P. Allavena, A. Sica, and F. Balkwill. "Cancer-related inflammation." In: *Nature* 454.7203 (2008), p. 436.
- [2] S. I. Grivennikov, F. R. Greten, and M. Karin. "Immunity, inflammation, and cancer." In: *Cell* 140.6 (2010), pp. 883–899.
- [3] H. K. Weir, T. D. Thompson, A. Soman, B. Møller, and S. Leadbetter. "The past, present, and future of cancer incidence in the United States: 1975 through 2020." In: *Cancer* 121.11 (2015), pp. 1827–1837.
- [4] E. Middleton, C. Kandaswami, and T. C. Theoharides. "The effects of plant flavonoids on mammalian cells: implications for inflammation, heart disease, and cancer." In: *Pharmacological reviews* 52.4 (2000), pp. 673–751.
- [5] R. H. Liu. "Potential synergy of phytochemicals in cancer prevention: mechanism of action." In: *The Journal of nutrition* 134.12 (2004), 3479S–3485S.
- [6] V. Russo, R. Matiensen, and A. Riggs. *Epigenetic Mechanisms of gene regulation*. Cold Spring Harbor Laboratory Press. 1996.
- [7] A Hässig, W. Linag, H Schwabl, and K Stampfli. "Flavonoids and tannins: plant-based antioxidants with vitamin character." In: *Medical Hypotheses* 52.5 (1999), pp. 479–481.
- [8] B. H. Havsteen. "The biochemistry and medical significance of the flavonoids." In: *Pharmacology & therapeutics* 96.2 (2002), pp. 67–202.
- [9] L. Marzocchella, M. Fantini, M. Benvenuto, L. Masuelli, I. Tresoldi, A. Modesti, and R. Bei. "Dietary flavonoids: molecular mechanisms of action as anti-inflammatory agents." In: *Recent patents on inflammation & allergy drug discovery* 5.3 (2011), pp. 200–220.

- [10] M Monajjemi, M Khosravi, B Honarparvar, and F Mollaamin. "Substituent and solvent effects on the structural bioactivity and anticancer characteristic of catechin as a bioactive constituent of green tea." In: *International Journal of Quantum Chemistry* 111.12 (2011), pp. 2771–2777.
- [11] R. Tsao. "Chemistry and biochemistry of dietary polyphenols." In: *Nutrients* 2.12 (2010), pp. 1231–1246.
- [12] M. Shimizu, S. Adachi, M. Masuda, O. Kozawa, and H. Moriwaki. "Cancer chemoprevention with green tea catechins by targeting receptor tyrosine kinases." In: *Molecular nutrition & food research* 55.6 (2011), pp. 832–843.
- [13] M. Manohar, I. Fatima, R. Saxena, V. Chandra, P. L. Sankhwar, and A. Dwivedi. "(-)-Epigallocatechin-3-gallate induces apoptosis in human endometrial adenocarcinoma cells via ROS generation and p38 MAP kinase activation." In: *The Journal of nutritional biochemistry* 24.6 (2013), pp. 940–947.
- [14] A. A. Ensafi, E Heydari Soureshjani, M Jafari Asl, B Rezaei, J. B. Ghasemi, and E. Aghae. "Experimental and theoretical investigation effect of flavonols antioxidants on DNA damage." In: *Analytica chimica acta* 887 (2015), pp. 82–91.
- [15] C. V. Uliana, G. S. Garbellini, and H. Yamanaka. "Electrochemical investigations on the capacity of flavonoids to protect DNA against damage caused by textile disperse dyes." In: *Sensors and Actuators B: Chemical* 192 (2014), pp. 188–195.
- [16] L. D. Mello, R. M. Pereira, A. C. Sawaya, M. N. Eberlin, and L. T. Kubota. "Electrochemical and spectroscopic characterization of the interaction between DNA and Cu (II)–naringin complex." In: *Journal of pharmaceutical and biomedical analysis* 45.5 (2007), pp. 706–713.
- [17] S. Bhattacharjee, S. Chakraborty, P. K. Sengupta, and S. Bhowmik. "Exploring the Interactions of the Dietary Plant Flavonoids Fisetin and Naringenin with G-Quadruplex and Duplex DNA, Showing Contrasting Binding Behavior: Spectroscopic and Molecular Modeling Approaches." In: *The Journal of Physical Chemistry B* 120.34 (2016), pp. 8942–8952.
- [18] J. E. Trosko. "Evolution of energy metabolism, stem cells and cancer stem cells: how the Warburg and Barker hypothesis might be linked." In: *BMC proceedings*. Vol. 7. 2. BioMed Central. 2013, K8.

- [19] P. J. Gomes, A. M. G. da Silva, P. A. Ribeiro, O. N. Oliveira, and M. Raposo. "Radiation damage on Langmuir monolayers of the anionic 1,2-dipalmitoyl-sn-glycero-3-[phospho-rac-(1-glycerol)](sodium salt)(DPPG) phospholipid at the air-DNA solution interface." In: *Materials Science and Engineering: C* 58 (2016), pp. 576–579.
- [20] P. J. Gomes, P. A. Ribeiro, D. Shaw, N. J. Mason, and M. Raposo. "UV degradation of deoxyribonucleic acid." In: *Polymer Degradation and Stability* 94.12 (2009), pp. 2134–2141.
- [21] P. J. Gomes, M. Coelho, M. Dionísio, P. António Ribeiro, and M. Raposo. "Probing radiation damage by alternated current conductivity as a method to characterize electron hopping conduction in DNA molecules." In: *Applied Physics Letters* 101.12 (2012), p. 123702.
- [22] M. Raposo, M. Coelho, P. J. Gomes, P. Vieira, P. A. Ribeiro, N. J. Mason, C. A. Hunniford, and R. W. McCullough. "DNA damage induced by carbon ions (C3+) beam accessed by independent component analysis of infrared spectra." In: *International journal of radiation biology* 90.5 (2014), pp. 344–350.
- [23] P. Gomes, A. Ferraria, A. Botelho do Rego, S. Hoffmann, P. Ribeiro, and M. Raposo. "Energy thresholds of DNA damage induced by UV radiation: An XPS study." In: *The Journal of Physical Chemistry B* 119.17 (2015), pp. 5404–5411.
- [24] A. Tubbs and A. Nussenzweig. "Endogenous DNA damage as a source of genomic instability in cancer." In: *Cell* 168.4 (2017), pp. 644–656.
- [25] D. C. van Gent and R. Kanaar. "Exploiting DNA repair defects for novel cancer therapies." In: *Molecular biology of the cell* 27.14 (2016), pp. 2145–2148.
- [26] J. Puc, A. K. Aggarwal, and M. G. Rosenfeld. "Physiological functions of programmed DNA breaks in signal-induced transcription." In: *Nature Reviews Molecular Cell Biology* (2017).
- [27] K. Brusselmans, R. Vrolix, G. Verhoeven, and J. V. Swinnen. "Induction of cancer cell apoptosis by flavonoids is associated with their ability to inhibit fatty acid synthase activity." In: *Journal of Biological Chemistry* 280.7 (2005), pp. 5636–5645.
- [28] S. Ramos. "Effects of dietary flavonoids on apoptotic pathways related to cancer chemoprevention." In: *The Journal of nutritional biochemistry* 18.7 (2007), pp. 427–442.

- [29] W. C. Earnshaw, L. M. Martins, and S. H. Kaufmann. "Mammalian caspases: structure, activation, substrates, and functions during apoptosis." In: *Annual review of biochemistry* 68.1 (1999), pp. 383–424.
- [30] S. Fulda and K.-M. Debatin. "Extrinsic versus intrinsic apoptosis pathways in anticancer chemotherapy." In: *Oncogene* 25.34 (2006), p. 4798.
- [31] S. K. Rupinder, A. K. Gurpreet, and S. Manjeet. "Cell suicide and caspases." In: *Vascular pharmacology* 46.6 (2007), pp. 383–393.
- [32] C. Wang and R. J. Youle. "The role of mitochondria in apoptosis." In: *Annual review of genetics* 43 (2009), pp. 95–118.
- [33] P. E. Czabotar, G. Lessene, A. Strasser, and J. M. Adams. "Control of apoptosis by the BCL-2 protein family: implications for physiology and therapy." In: *Nature reviews. Molecular cell biology* 15.1 (2014), p. 49.
- [34] Z. Zhou, M. Tang, Y. Liu, Z. Zhang, R. Lu, and J. Lu. "Apigenin inhibits cell proliferation, migration, and invasion by targeting Akt in the A549 human lung cancer cell line." In: *Anti-cancer drugs* 28.4 (2017), pp. 446–456.
- [35] G. Zhao, X. Han, W. Cheng, J. Ni, Y. Zhang, J. Lin, and Z. Song. "Apigenin inhibits proliferation and invasion, and induces apoptosis and cell cycle arrest in human melanoma cells." In: *Oncology Reports* 37.4 (2017), pp. 2277–2285.
- [36] R. Zhang, S. Chae, K. A. Kang, M. J. Piao, D. O. Ko, Z. H. Wang, D. B. Park, J. W. Park, H. J. You, and J. W. Hyun. "Protective effect of butin against hydrogen peroxide-induced apoptosis by scavenging reactive oxygen species and activating antioxidant enzymes." In: *Molecular and cellular biochemistry* 318.1-2 (2008), pp. 33–42.
- [37] L. M. Coussens and Z. Werb. "Inflammation and cancer." In: *Nature* 420.6917 (2002), p. 860.
- [38] K. B. Harikumar, B. Sung, S. T. Tharakan, M. K. Pandey, B. Joy, S. Guha, S. Krishnan, and B. B. Aggarwal. "Sesamin manifests chemopreventive effects through the suppression of NF- κ B-regulated cell survival, proliferation, invasion, and angiogenic gene products." In: *Molecular Cancer Research* 8.5 (2010), pp. 751–761.

- [39] R. J. MacLeod. “Extracellular calcium-sensing receptor/PTH knockout mice colons have increased Wnt/[beta]-catenin signaling, reduced non-canonical Wnt signaling, and increased susceptibility to azoxymethane-induced aberrant crypt foci.” In: *Laboratory Investigation* 93.5 (2013), pp. 520–527.
- [40] J. Wang, Y.-T. Liu, L. Xiao, L. Zhu, Q. Wang, and T. Yan. “Anti-inflammatory effects of apigenin in lipopolysaccharide-induced inflammatory acute lung injury by suppressing COX-2 and NF- κ B pathway.” In: *Inflammation* 37.6 (2014), pp. 2085–2090.
- [41] J. W. Bradford and A. S. Baldwin. “IKK/nuclear factor- κ B and oncogenesis: roles in tumor-initiating cells and in the tumor microenvironment.” In: *Adv Cancer Res* 121.121 (2014), pp. 125–145.
- [42] J. C. Tobon-Velasco, E. Cuevas, and M. A. Torres-Ramos. “Receptor for AGEs (RAGE) as mediator of NF- κ B pathway activation in neuroinflammation and oxidative stress.” In: *CNS & Neurological Disorders-Drug Targets (Formerly Current Drug Targets-CNS & Neurological Disorders)* 13.9 (2014), pp. 1615–1626.
- [43] F. R. Greten, C. K. Weber, T. F. Greten, G. Schneider, M. Wagner, G. Adler, and R. M. Schmid. “Stat3 and NF- κ B activation prevents apoptosis in pancreatic carcinogenesis.” In: *Gastroenterology* 123.6 (2002), pp. 2052–2063.
- [44] L.-W. Chong, Y.-C. Hsu, Y.-T. Chiu, K.-C. Yang, and Y.-T. Huang. “Anti-fibrotic effects of thalidomide on hepatic stellate cells and dimethylnitrosamine-intoxicated rats.” In: *Journal of biomedical science* 13.3 (2006), pp. 403–418.
- [45] R. R. Ruela de Sousa, K. C. S. Queiroz, A. C. S. Souza, S. A. Gurgueira, A. C. Augusto, M. A. Miranda, M. P. Peppelenbosch, C. V. Ferreira, and H. Aoyama. “Phosphoprotein levels, MAPK activities and NF κ B expression are affected by fisetin.” In: *Journal of enzyme inhibition and medicinal chemistry* 22.4 (2007), pp. 439–444.
- [46] V. Rubio, A. I. García-Pérez, A. Herráez, C. Ordóñez, G. Herranz, M. C. Tejedor, and J. C. Diez. “Nrf2 and NF κ B involvement in the antioxidant action of esculetin or quercetin in human leukemia NB4 cells.” In: *Free Radical Biology and Medicine* 108 (2017), S25.

- [47] M. Zeinali, S. A. Rezaee, and H. Hosseinzadeh. "An overview on immunoregulatory and anti – inflammatory properties of chrysin and flavonoids substances." In: *Biomedicine & Pharmacotherapy* 92 (2017), pp. 998–1009.
- [48] V. Y. Shin and A. Kwong. "Prostaglandin and Its Receptors: Potential Targets for Gastrointestinal Inflammation and Cancer." In: *Therapeutic Targets for Inflammation and Cancer: Novel Therapies for Digestive Diseases*. World Scientific, 2017, pp. 295–308.
- [49] A. B. Granado-Serrano, M. A. Martín, L. Bravo, L. Goya, and S. Ramos. "Quercetin modulates NF – κ B and AP – 1/JNK pathways to induce cell death in human hepatoma cells." In: *Nutrition and cancer* 62.3 (2010), pp. 390–401.
- [50] J Ke, X Long, Y Liu, Y. Zhang, J Li, W Fang, and Q. Meng. "Role of NF- κ B in TNF- α -induced COX-2 Expression in Synovial Fibroblasts from Human TMJ." In: *Journal of dental research* 86.4 (2007), pp. 363–367.
- [51] S. B. Raja, V. Rajendiran, N. K. Kasinathan, P Amrithalakshmi, S. Venkatabalasubramanian, M. R. Murali, H. Devaraj, and S. N. Devaraj. "Differential cytotoxic activity of Quercetin on colonic cancer cells depends on ROS generation through COX-2 expression." In: *Food and Chemical Toxicology* 106 (2017), pp. 92–106.
- [52] G. Egger, G. Liang, A. Aparicio, and P. A. Jones. "Epigenetics in human disease and prospects for epigenetic therapy." In: *Nature* 429.6990 (2004), p. 457.
- [53] T. Yokochi and K. D. Robertson. "Preferential methylation of unmethylated DNA by mammalian de novo DNA methyltransferase Dnmt3a." In: *Journal of Biological Chemistry* 277.14 (2002), pp. 11735–11745.
- [54] J. A. Law and S. E. Jacobsen. "Establishing, maintaining and modifying DNA methylation patterns in plants and animals." In: *Nature reviews. Genetics* 11.3 (2010), p. 204.
- [55] X. Cheng. "Structure and function of DNA methyltransferases." In: *Annual review of biophysics and biomolecular structure* 24.1 (1995), pp. 293–318.
- [56] B. T. Zhu, E. L. Ezell, and J. G. Liehr. "Catechol – O – methyltransferase – catalyzed rapid O – methylation of mutagenic flavonoids. Metabolic inactivation as a possible reason for their lack of carcinogenicity in vivo." In: *Journal of Biological Chemistry* 269.1 (1994), pp. 292–299.

- [57] B. T. Zhu, U. K. Patel, M. X. Cai, and A. H. Conney. "O – Methylation of tea polyphenols catalyzed by human placental cytosolic catechol – O – methyltransferase." In: *Drug Metabolism and Disposition* 28.9 (2000), pp. 1024–1030.
- [58] M. Nagai, A. H. Conney, and B. T. Zhu. "Strong inhibitory effects of common tea catechins and bioflavonoids on the O-methylation of catechol estrogens catalyzed by human liver cytosolic catechol–O–methyltransferase." In: *Drug metabolism and disposition* 32.5 (2004), pp. 497–504.
- [59] D. Chen, C. Y. Wang, J. D. Lambert, N. Ai, W. J. Welsh, and C. S. Yang. "Inhibition of human liver catechol – O – methyltransferase by tea catechins and their metabolites: structure – activity relationship and molecular – modeling studies." In: *Biochemical pharmacology* 69.10 (2005), pp. 1523–1531.
- [60] H. Lu, X. Meng, and C. S. Yang. "Enzymology of methylation of tea catechins and inhibition of catechol– O – methyltransferase by (–) – epigallocatechin gallate." In: *Drug metabolism and disposition* 31.5 (2003), pp. 572–579.
- [61] K. Landis-Piowar, D. Chen, T. H. Chan, and Q. P. Dou. "Inhibition of catechol – O – methyltransferase activity in human breast cancer cells enhances the biological effect of the green tea polyphenol (–) – EGCG." In: *Oncology reports* 24.2 (2010), pp. 563–569.
- [62] X. Meng, S. Sang, N. Zhu, H. Lu, S. Sheng, M.-J. Lee, C.-T. Ho, and C. S. Yang. "Identification and characterization of methylated and ring-fission metabolites of tea catechins formed in humans, mice, and rats." In: *Chemical research in toxicology* 15.8 (2002), pp. 1042–1050.
- [63] M. Z. Fang, Y. Wang, N. Ai, Z. Hou, Y. Sun, H. Lu, W. Welsh, and C. S. Yang. "Tea polyphenol (–)-epigallocatechin-3-gallate inhibits DNA methyltransferase and reactivates methylation-silenced genes in cancer cell lines." In: *Cancer research* 63.22 (2003), pp. 7563–7570.
- [64] S. Das, J. Das, A. Paul, A. Samadder, and A. R. Khuda-Bukhsh. "Apigenin, a bioactive flavonoid from *Lycopodium clavatum*, stimulates nucleotide excision repair genes to protect skin keratinocytes from ultraviolet B-induced reactive oxygen species and DNA damage." In: *Journal of acupuncture and meridian studies* 6.5 (2013), pp. 252–262.

- [65] M.-D. Shi, C.-K. Shiao, Y.-C. Lee, and Y.-W. Shih. "Apigenin, a dietary flavonoid, inhibits proliferation of human bladder cancer T – 24 cells via blocking cell cycle progression and inducing apoptosis." In: *Cancer cell international* 15.1 (2015), p. 33.
- [66] K. A. Kang, J. H. Lee, S. Chae, R. Zhang, M. J. Piao, H. S. Kim, H. J. You, and J. W. Hyun. "Butin decreases oxidative stress-induced 8-hydroxy-2'-deoxyguanosine levels via activation of oxoguanine glycosylase 1." In: *Chemico-biological interactions* 181.3 (2009), pp. 338–342.
- [67] L.-s. Meng, B. Li, D.-n. Li, Y.-h. Wang, Y. Lin, X.-j. Meng, X.-y. Sun, and N. Liu. "Cyanidin –3 – O – glucoside attenuates amyloid – beta (1–40) – induced oxidative stress and apoptosis in SH – SY5Y cells through a Nrf2 mechanism." In: *Journal of Functional Foods* 38 (2017), pp. 474–485.
- [68] M. Tiwari, B. Dixit, S. Parvez, and P. K. Agrawala. "EGCG, a tea polyphenol, as a potential mitigator of hematopoietic radiation injury in mice." In: *Biomedicine & Pharmacotherapy* 88 (2017), pp. 203–209.
- [69] W. Zhu, J. Xu, Y. Ge, H. Cao, X. Ge, J. Luo, J. Xue, H. Yang, S. Zhang, and J. Cao. "Epigallocatechin-3-gallate (EGCG) protects skin cells from ionizing radiation via heme oxygenase-1 (HO-1) overexpression." In: *Journal of radiation research* 55.6 (2014), pp. 1056–1065.
- [70] M. Jurzak, P. Ramos, and B. Pilawa. "The influence of genistein on free radicals in normal dermal fibroblasts and keloid fibroblasts examined by EPR spectroscopy." In: *Medicinal Chemistry Research* 26.6 (2017), pp. 1297–1305.
- [71] F. You, Q. Li, G. Jin, Y. Zheng, J. Chen, and H. Yang. "Genistein protects against A β 25–35 induced apoptosis of PC12 cells through JNK signaling and modulation of Bcl-2 family messengers." In: *BMC neuroscience* 18.1 (2017), p. 12.
- [72] M. Wahby, D. Mohammed, A. Newairy, H. Abdou, and A Zaky. "Aluminum – induced molecular neurodegeneration: The protective role of genistein and chickpea extract." In: *Food and Chemical Toxicology* (2017).
- [73] K. Yang, S. A. Lamprecht, Y. Liu, H. Shinozaki, K. Fan, D. Leung, H. Newmark, V. E. Steele, G. J. Kelloff, and M. Lipkin. "Chemoprevention studies of the flavonoids quercetin and rutin in normal and azoxymethane – treated mouse colon." In: *Carcinogenesis* 21.9 (2000), pp. 1655–1660.

- [74] J. A. Godoy, C. B. Lindsay, R. A. Quintanilla, F. J. Carvajal, W. Cerpa, and N. C. Inestrosa. "Quercetin exerts differential neuroprotective effects against H₂O₂ and A β aggregates in hippocampal neurons: the role of mitochondria." In: *Molecular neurobiology* (2016), pp. 1–13.
- [75] H Özyurt, Ö Çevik, Z Özgen, A. Özden, S Çadırcı, M. Elmas, F Ercan, M. Gören, and G Şener. "Quercetin protects radiation-induced DNA damage and apoptosis in kidney and bladder tissues of rats." In: *Free radical research* 48.10 (2014), pp. 1247–1255.
- [76] W. J. Lee, J.-Y. Shim, and B. T. Zhu. "Mechanisms for the inhibition of DNA methyltransferases by tea catechins and bioflavonoids." In: *Molecular pharmacology* 68.4 (2005), pp. 1018–1030.
- [77] V. R. Moseley, J. Morris, R. W. Knackstedt, and M. J. Wargovich. "Green tea polyphenol epigallocatechin 3-gallate, contributes to the degradation of DNMT3A and HDAC3 in HCT 116 human colon cancer cells." In: *Anti-cancer research* 33.12 (2013), pp. 5325–5333.
- [78] Y. Jenkins, V. Markovtsov, W. Lang, P. Sharma, D. Pearsall, J. Warner, C. Franci, B. Huang, J. Huang, G. C. Yam, et al. "Critical role of the ubiquitin ligase activity of UHRF1, a nuclear RING finger protein, in tumor cell growth." In: *Molecular biology of the cell* 16.12 (2005), pp. 5621–5629.
- [79] J. Morris, V. R. Moseley, A. B. Cabang, K. Coleman, W. Wei, E. Garrett-Mayer, and M. J. Wargovich. "Reduction in promotor methylation utilizing EGCG (epigallocatechin-3-gallate) restores RXR α expression in human colon cancer cells." In: *Oncotarget* 7.23 (2016), p. 35313.
- [80] J. Silva, J. M. Silva, G. Domínguez, J. M. García, B. Cantos, R. Rodríguez, F. J. Larrondo, M. Provencio, P. Espana, and F. Bonilla. "Concomitant expression of p16INK4a and p14ARF in primary breast cancer and analysis of inactivation mechanisms." In: *The Journal of pathology* 199.3 (2003), pp. 289–297.
- [81] Z Jin, G Tamura, T Tsuchiya, K Sakata, M Kashiwaba, M Osakabe, and T Motoyama. "Adenomatous polyposis coli (APC) gene promoter hypermethylation in primary breast cancers." In: *British Journal of Cancer* 85.1 (2001), p. 69.
- [82] V. Birgisdottir, O. A. Stefansson, S. K. Bodvarsdottir, H. Hilmarsdottir, J. G. Jonasson, and J. E. Eyfjord. "Epigenetic silencing and deletion of the BRCA1 gene in sporadic breast cancer." In: *Breast cancer research* 8.4 (2006), R38.

- [83] M. Esteller and J. G. Herman. "Cancer as an epigenetic disease: DNA methylation and chromatin alterations in human tumours." In: *The Journal of pathology* 196.1 (2002), pp. 1–7.
- [84] K. D. Robertson. "DNA methylation and human disease." In: *Nature reviews. Genetics* 6.8 (2005), p. 597.
- [85] N. Chia, L. Wang, X. Lu, M.-C. Senut, C. A. Brenner, and D. M. Ruden. "Hypothesis: environmental regulation of 5-hydroxymethylcytosine by oxidative stress." In: *Epigenetics* 6.7 (2011), pp. 853–856.
- [86] Z.-Y. Su, T. O. Khor, L. Shu, J. H. Lee, C. L.-L. Saw, T.-Y. Wu, Y. Huang, N. Suh, C. S. Yang, A. H. Conney, et al. "Epigenetic reactivation of Nrf2 in murine prostate cancer TRAMP C1 cells by natural phytochemicals Z-ligustilide and Radix angelica sinensis via promoter CpG demethylation." In: *Chemical research in toxicology* 26.3 (2013), pp. 477–485.
- [87] T. Nguyen, P. Nioi, and C. B. Pickett. "The Nrf2-antioxidant response element signaling pathway and its activation by oxidative stress." In: *Journal of Biological Chemistry* 284.20 (2009), pp. 13291–13295.
- [88] H. J. Kim and N. D. Vaziri. "Contribution of impaired Nrf2-Keap1 pathway to oxidative stress and inflammation in chronic renal failure." In: *American Journal of Physiology-Renal Physiology* 298.3 (2010), F662–F671.
- [89] H. Motohashi and M. Yamamoto. "Nrf2–Keap1 defines a physiologically important stress response mechanism." In: *Trends in molecular medicine* 10.11 (2004), pp. 549–557.
- [90] K. Taguchi, H. Motohashi, and M. Yamamoto. "Molecular mechanisms of the Keap1–Nrf2 pathway in stress response and cancer evolution." In: *Genes to Cells* 16.2 (2011), pp. 123–140.
- [91] M. A. Parasramka, E. Ho, D. E. Williams, and R. H. Dashwood. "MicroRNAs, diet, and cancer: new mechanistic insights on the epigenetic actions of phytochemicals." In: *Molecular carcinogenesis* 51.3 (2012), pp. 213–230.
- [92] S. M. Meeran, A. Ahmed, and T. O. Tollefsbol. "Epigenetic targets of bioactive dietary components for cancer prevention and therapy." In: *Clinical epigenetics* 1.3 (2010), p. 101.
- [93] W. V. Berghe. "Epigenetic impact of dietary polyphenols in cancer chemoprevention: lifelong remodeling of our epigenomes." In: *Pharmacological research* 65.6 (2012), pp. 565–576.

- [94] J. Zhang, Z. Lei, Z. Huang, X. Zhang, Y. Zhou, Z. Luo, W. Zeng, J. Su, C. Peng, and X. Chen. “Epigallocatechin-3-gallate (EGCG) suppresses melanoma cell growth and metastasis by targeting TRAF6 activity.” In: *Oncotarget* 7.48 (2016), p. 79557.
- [95] Y. Chen, X.-Q. Wang, Q. Zhang, J.-Y. Zhu, Y. Li, C.-F. Xie, X.-T. Li, J.-S. Wu, S.-S. Geng, C.-Y. Zhong, et al. “(-)- Epigallocatechin- 3 – Gallate Inhibits Colorectal Cancer Stem Cells by Suppressing Wnt/ β – Catenin Pathway.” In: *Nutrients* 9.6 (2017), p. 572.
- [96] O.-Y. Hong, E.-M. Noh, H.-Y. Jang, Y.-R. Lee, B. K. Lee, S. H. Jung, J.-S. Kim, and H. J. Youn. “Epigallocatechin gallate inhibits the growth of MDA – MB – 231 breast cancer cells via inactivation of the β –catenin signaling pathway.” In: *Oncology Letters* 14.1 (2017), pp. 441–446.
- [97] C.-H. Yuan, C.-T. Horng, C.-F. Lee, N.-N. Chiang, F.-J. Tsai, C.-C. Lu, J.-H. Chiang, Y.-M. Hsu, J.-S. Yang, and F.-A. Chen. “Epigallocatechin gallate sensitizes cisplatin-resistant oral cancer CAR cell apoptosis and autophagy through stimulating AKT/STAT3 pathway and suppressing multidrug resistance 1 signaling.” In: *Environmental toxicology* 32.3 (2017), pp. 845–855.
- [98] J. Zhu, Y. Jiang, X. Yang, S. Wang, C. Xie, X. Li, Y. Li, Y. Chen, X. Wang, Y. Meng, et al. “Wnt/ β -catenin pathway mediates (-)-Epigallocatechin-3-gallate (EGCG) inhibition of lung cancer stem cells.” In: *Biochemical and biophysical research communications* 482.1 (2017), pp. 15–21.
- [99] A. Gradolatto, J.-P. Basly, R. Berges, C. Teyssier, M.-C. Chagnon, M.-H. Siess, and M.-C. Canivenc-Lavier. “Pharmacokinetics and metabolism of apigenin in female and male rats after a single oral administration.” In: *Drug metabolism and disposition* 33.1 (2005), pp. 49–54.
- [100] H. K. Koul, M. Pal, and S. Koul. “Role of p38 MAP kinase signal transduction in solid tumors.” In: *Genes & cancer* 4.9-10 (2013), pp. 342–359.
- [101] M. Funakoshi-Tago, K. Nakamura, K. Tago, T. Mashino, and T. Kasahara. “Anti-inflammatory activity of structurally related flavonoids, Apigenin, Luteolin and Fisetin.” In: *International immunopharmacology* 11.9 (2011), pp. 1150–1159.
- [102] K. M. Perrott, C. D. Wiley, P.-Y. Desprez, and J. Campisi. “Apigenin suppresses the senescence-associated secretory phenotype and paracrine effects on breast cancer cells.” In: *GeroScience* 39.2 (2017), pp. 161–173.

- [103] C. L. Woodcock and R. P. Ghosh. “Chromatin higher-order structure and dynamics.” In: *Cold Spring Harbor perspectives in biology* 2.5 (2010), a000596.
- [104] K. Luger, A. W. Mader, R. K. Richmond, D. F. Sargent, and T. J. Richmond. “Crystal structure of the nucleosome core particle at 2.8 angstrom resolution.” In: *Nature* 389.6648 (1997), p. 251.
- [105] M. Bustin, F. Catez, and J.-H. Lim. “The dynamics of histone H1 function in chromatin.” In: *Molecular cell* 17.5 (2005), pp. 617–620.
- [106] H. J. Szerlong and J. C. Hansen. “Nucleosome distribution and linker DNA: connecting nuclear function to dynamic chromatin structure This paper is one of a selection of papers published in a Special Issue entitled 31st Annual International Asilomar Chromatin and Chromosomes Conference, and has undergone the Journal’s usual peer review process.” In: *Biochemistry and Cell Biology* 89.1 (2010), pp. 24–34.
- [107] B.-R. Zhou, H. Feng, H. Kato, L. Dai, Y. Yang, Y. Zhou, and Y. Bai. “Structural insights into the histone H1-nucleosome complex.” In: *Proceedings of the National Academy of Sciences* 110.48 (2013), pp. 19390–19395.
- [108] R. Teperino, K. Schoonjans, and J. Auwerx. “Histone methyl transferases and demethylases; can they link metabolism and transcription?” In: *Cell metabolism* 12.4 (2010), pp. 321–327.
- [109] U. E. Martinez-Outschoorn, M. Prisco, A. Ertel, A. Tsirigos, Z. Lin, S. Pavlides, C. Wang, N. Flomenberg, E. S. Knudsen, A. Howell, et al. “Ketones and lactate increase cancer cell “stemness,” driving recurrence, metastasis and poor clinical outcome in breast cancer: achieving personalized medicine via Metabolo-Genomics.” In: *Cell cycle* 10.8 (2011), pp. 1271–1286.
- [110] L. D. Godoy, J. E. Lucas, A. J. Bender, S. S. Romanick, and B. S. Ferguson. “Targeting the epigenome: Screening bioactive compounds that regulate histone deacetylase activity.” In: *Molecular nutrition & food research* 61.4 (2017).
- [111] L. W. Evans, S. S. Romanick, and B. S. Ferguson. “Natural product inhibitors of acetyl-lysine erasers in the prevention and treatment of heart failure.” In: *Functional Foods in Health and Disease* 7.8 (2017), pp. 577–603.

- [112] T.-H. Tseng, M.-H. Chien, W.-L. Lin, Y.-C. Wen, J.-M. Chow, C.-K. Chen, T.-C. Kuo, and W.-J. Lee. "Inhibition of MDA – MB – 231 breast cancer cell proliferation and tumor growth by apigenin through induction of G2/M arrest and histone H3 acetylation-mediated p21WAF1/CIP1 expression." In: *Environmental toxicology* 32.2 (2017), pp. 434–444.
- [113] S. Shukla and S. Gupta. "Apigenin – induced cell cycle arrest is mediated by modulation of MAPK, PI3K – Akt, and loss of cyclin D1 associated retinoblastoma dephosphorylation in human prostate cancer cells." In: *Cell cycle* 6.9 (2007), pp. 1102–1114.
- [114] Y.-H. Lee, J. Kwak, H.-K. Choi, K.-C. Choi, S. Kim, J. Lee, W. Jun, H.-J. Park, and H.-G. Yoon. "EGCG suppresses prostate cancer cell growth modulating acetylation of androgen receptor by anti-histone acetyltransferase activity." In: *International journal of molecular medicine* 30.1 (2012), pp. 69–74.
- [115] M. A. Khan, A. Hussain, M. K. Sundaram, U. Alalami, D. Gunasekera, L. Ramesh, A. Hamza, and U. Quraishi. "(-)-Epigallocatechin-3-gallate reverses the expression of various tumor-suppressor genes by inhibiting DNA methyltransferases and histone deacetylases in human cervical cancer cells." In: *Oncology reports* 33.4 (2015), pp. 1976–1984.
- [116] Y. Li, Y.-Y. Yuan, S. M. Meeran, and T. O. Tollefsbol. "Synergistic epigenetic reactivation of estrogen receptor- α (ER α) by combined green tea polyphenol and histone deacetylase inhibitor in ER α -negative breast cancer cells." In: *Molecular cancer* 9.1 (2010), p. 274.
- [117] Y. Oya, A. Mondal, A. Rawangkan, S. Umsumarng, K. Iida, T. Watanabe, M. Kanno, K. Suzuki, Z. Li, H. Kagechika, et al. "Down-regulation of histone deacetylase 4, 5 and 6 as a mechanism of synergistic enhancement of apoptosis in human lung cancer cells treated with the combination of a synthetic retinoid, Am80 and green tea catechin." In: *The Journal of nutritional biochemistry* 42 (2017), pp. 7–16.
- [118] P. K. Bagul, N. Deepthi, R. Sultana, and S. K. Banerjee. "Resveratrol ameliorates cardiac oxidative stress in diabetes through deacetylation of NF κ B-p65 and histone 3." In: *The Journal of nutritional biochemistry* 26.11 (2015), pp. 1298–1307.
- [119] A. Kim and J.-M. Yun. "Combination Treatments with Luteolin and Fisetin Enhance Anti-Inflammatory Effects in High Glucose-Treated THP-1 Cells

- Through Histone Acetyltransferase/Histone Deacetylase Regulation.” In: *Journal of Medicinal Food* 20.8 (2017), pp. 782–789.
- [120] K. B. Reddy. “MicroRNA (miRNA) in cancer.” In: *Cancer cell international* 15.1 (2015), p. 38.
- [121] R. Sheervalilou, A. M. Khamaneh, A. Sharifi, M. Nazemiyeh, A. Taghizadieh, K. Ansarin, and N. Zarghami. “Using miR-10b, miR-1 and miR-30a expression profiles of bronchoalveolar lavage and sputum for early detection of non-small cell lung cancer.” In: *Biomedicine & Pharmacotherapy* 88 (2017), pp. 1173–1182.
- [122] E. Bandres, X. Agirre, N. Bitarte, N. Ramirez, R. Zarate, J. Roman-Gomez, F. Prosper, and J. Garcia-Foncillas. “Epigenetic regulation of microRNA expression in colorectal cancer.” In: *International journal of cancer* 125.11 (2009), pp. 2737–2743.
- [123] R. B. Selvi, A. Swaminathan, S. Chatterjee, M. K. Shanmugam, F. Li, G. B. Ramakrishnan, K. S. Siveen, A. Chinnathambi, M. E. Zayed, S. A. Alharbi, et al. “Inhibition of p300 lysine acetyltransferase activity by luteolin reduces tumor growth in head and neck squamous cell carcinoma (HNSCC) xenograft mouse model.” In: *Oncotarget* 6.41 (2015), p. 43806.
- [124] D.-W. Sun, H.-D. Zhang, L. Mao, C.-F. Mao, W. Chen, M. Cui, R. Ma, H.-X. Cao, C.-W. Jing, Z. Wang, et al. “Luteolin inhibits breast cancer development and progression in vitro and in vivo by suppressing notch signaling and regulating miRNAs.” In: *Cellular Physiology and Biochemistry* 37.5 (2015), pp. 1693–1711.
- [125] M. J. Kim, J. S. Woo, C. H. Kwon, J. H. Kim, Y. K. Kim, and K. H. Kim. “Luteolin induces apoptotic cell death through AIF nuclear translocation mediated by activation of ERK and p38 in human breast cancer cell lines.” In: *Cell biology international* 36.4 (2012), pp. 339–344.
- [126] F. Mohammadian, A. Abhari, H. Dariushnejad, A. Nikanfar, Y. Pilehvar-Soltanahmadi, and N. Zarghami. “Effects of chrysin – PLGA – PEG nanoparticles on proliferation and gene expression of miRNAs in gastric cancer cell line.” In: *Iranian journal of cancer prevention* 9.4 (2016).
- [127] F. Mohammadian, Y. Pilehvar-Soltanahmadi, F. Zarghami, A. Akbarzadeh, and N. Zarghami. “Upregulation of miR-9 and Let-7a by nanoencapsulated chrysin in gastric cancer cells.” In: *Artificial cells, nanomedicine, and biotechnology* 45.6 (2017), pp. 1201–1206.

- [128] N. J.-M. Raynal, E. M. Da Costa, J. T. Lee, V. Gharibyan, S. Ahmed, H. Zhang, T. Sato, G. G. Malouf, and J.-P. J. Issa. “Repositioning FDA-approved drugs in combination with epigenetic drugs to reprogram colon cancer epigenome.” In: *Molecular cancer therapeutics* 16.2 (2017), pp. 397–407.
- [129] J. Meng, Q. Tong, X. Liu, Z. Yu, J. Zhang, and B. Gao. “Epigallocatechin-3-gallate inhibits growth and induces apoptosis in esophageal cancer cells through the demethylation and reactivation of the p16 gene.” In: *Oncology Letters* 14.1 (2017), pp. 1152–1156.
- [130] M. Fang, D. Chen, and C. S. Yang. “Dietary polyphenols may affect DNA methylation.” In: *The Journal of nutrition* 137.1 (2007), 223S–228S.
- [131] Y. Li, S. M. Meeran, and T. O. Tollefsbol. “Combinatorial bioactive botanicals re-sensitize tamoxifen treatment in ER-negative breast cancer via epigenetic reactivation of ER α expression.” In: *Scientific Reports* 7 (2017).
- [132] W. Li, D. Pung, Z.-Y. Su, Y. Guo, C. Zhang, A. Y. Yang, X. Zheng, Z.-Y. Du, K. Zhang, and A.-N. Kong. “Epigenetics Reactivation of Nrf2 in Prostate TRAMP C1 Cells by Curcumin Analogue FN1.” In: *Chemical research in toxicology* 29.4 (2016), pp. 694–703.
- [133] B. Bilir, N. V. Sharma, J. Lee, B. Hammarstrom, A. Svindland, O. Kucuk, and C. S. Moreno. “Effects of genistein supplementation on genome-wide DNA methylation and gene expression in patients with localized prostate cancer.” In: *International Journal of Oncology* 51.1 (2017), pp. 223–234.
- [134] X. Liu, C. Sun, B. Liu, X. Jin, P. Li, X. Zheng, T. Zhao, F. Li, and Q. Li. “Genistein mediates the selective radiosensitizing effect in NSCLC A549 cells via inhibiting methylation of the keap1 gene promoter region.” In: *Oncotarget* 7.19 (2016), p. 27267.
- [135] F. Mohammadian, A. Abhari, H. Dariushnejad, F. Zarghami, A. Nikanfar, Y. Pilehvar-Soltanahmadi, and N. Zarghami. “Upregulation of Mir-34a in AGS gastric cancer cells by a PLGA-PEG-PLGA chrysin nano formulation.” In: *Asian Pac J Cancer Prev* 16.18 (2015), pp. 8259–8263.
- [136] F. Mohammadian, Y. Pilehvar-Soltanahmadi, M. Mofarrah, M. Dastani-Habashi, and N. Zarghami. “Down regulation of miR-18a, miR-21 and miR-221 genes in gastric cancer cell line by chrysin – loaded PLGA – PEG nanoparticles.” In: *Artificial cells, nanomedicine, and biotechnology* 44.8 (2016), pp. 1972–1978.

- [137] W. P. Tsang and T. T. Kwok. “Epigallocatechin gallate up-regulation of miR-16 and induction of apoptosis in human cancer cells.” In: *The Journal of nutritional biochemistry* 21.2 (2010), pp. 140–146.
- [138] S. Toden, H.-M. Tran, O. A. Tovar-Camargo, Y. Okugawa, and A. Goel. “Epigallocatechin-3-gallate targets cancer stem-like cells and enhances 5-fluorouracil chemosensitivity in colorectal cancer.” In: *Oncotarget* 7.13 (2016), p. 16158.
- [139] M. Chakrabarti, M. Khandkar, N. L. Banik, and S. K. Ray. “Alterations in expression of specific microRNAs by combination of 4-HPR and EGCG inhibited growth of human malignant neuroblastoma cells.” In: *Brain research* 1454 (2012), pp. 1–13.
- [140] M. Chakrabarti, W. Ai, N. L. Banik, and S. K. Ray. “Overexpression of miR-7-1 increases efficacy of green tea polyphenols for induction of apoptosis in human malignant neuroblastoma SH-SY5Y and SK-N-DZ cells.” In: *Neurochemical research* 38.2 (2013), pp. 420–432.
- [141] H. Wang, S. Bian, and C. S. Yang. “Green tea polyphenol EGCG suppresses lung cancer cell growth through upregulating miR-210 expression caused by stabilizing HIF-1 α .” In: *Carcinogenesis* 32.12 (2011), pp. 1881–1889.
- [142] H. Zhou, J. X. Chen, C. S. Yang, M. Q. Yang, Y. Deng, and H. Wang. “Gene regulation mediated by microRNAs in response to green tea polyphenol EGCG in mouse lung cancer.” In: *BMC genomics* 15.11 (2014), S3.
- [143] D.-H. Zhou, X. Wang, and Q. Feng. “EGCG enhances the efficacy of cisplatin by downregulating hsa-miR-98-5p in NSCLC A549 cells.” In: *Nutrition and cancer* 66.4 (2014), pp. 636–644.
- [144] J.-Y. Jang, J.-K. Lee, Y.-K. Jeon, and C.-W. Kim. “Exosome derived from epigallocatechin gallate treated breast cancer cells suppresses tumor growth by inhibiting tumor-associated macrophage infiltration and M2 polarization.” In: *BMC cancer* 13.1 (2013), p. 421.
- [145] B.-B. Li, G.-L. Huang, H.-H. Li, X. Kong, Z.-W. He, et al. “Epigallocatechin-3-gallate Modulates MicroRNA Expression Profiles in Human Nasopharyngeal Carcinoma CNE2 Cells.” In: *Chinese medical journal* 130.1 (2017), p. 93.

- [146] N. A. Sibbesen, K. L. Kopp, I. V. Litvinov, L. Jønson, A. Willerslev-Olsen, S. Fredholm, D. L. Petersen, C. Nastasi, T. Krejsgaard, L. M. Lindahl, et al. “Jak3, STAT3, and STAT5 inhibit expression of miR-22, a novel tumor suppressor microRNA, in cutaneous T-Cell lymphoma.” In: *Oncotarget* 6.24 (2015), p. 20555.
- [147] J. Yang, Y. Cao, J. Sun, and Y. Zhang. “Curcumin reduces the expression of Bcl-2 by upregulating miR-15a and miR-16 in MCF-7 cells.” In: *Medical Oncology* 27.4 (2010), pp. 1114–1118.
- [148] S. Ali, A. Ahmad, S. Banerjee, S. Padhye, K. Dominiak, J. M. Schaffert, Z. Wang, P. A. Philip, and F. H. Sarkar. “Gemcitabine sensitivity can be induced in pancreatic cancer cells through modulation of miR-200 and miR-21 expression by curcumin or its analogue CDF.” In: *Cancer research* 70.9 (2010), pp. 3606–3617.
- [149] M. Sun, Z. Estrov, Y. Ji, K. R. Coombes, D. H. Harris, and R. Kurzrock. “Curcumin (diferuloylmethane) alters the expression profiles of microRNAs in human pancreatic cancer cells.” In: *Molecular cancer therapeutics* 7.3 (2008), pp. 464–473.
- [150] M. M. Yallapu, S. Khan, D. M. Maher, M. C. Ebeling, V. Sundram, N. Chauhan, A. Ganju, S. Balakrishna, B. K. Gupta, N. Zafar, et al. “Anti-cancer activity of curcumin loaded nanoparticles in prostate cancer.” In: *Biomaterials* 35.30 (2014), pp. 8635–8648.
- [151] M.-H. Teiten, A. Gaigneaux, S. Chateauvieux, A. M. Billing, S. Planchon, F. Fack, J. Renaut, F. Mack, C. P. Muller, M. Dicato, et al. “Identification of differentially expressed proteins in curcumin-treated prostate cancer cell lines.” In: *Omics: a journal of integrative biology* 16.6 (2012), pp. 289–300.
- [152] C. de la Parra, L. Castillo-Pichardo, A. Cruz-Collazo, L. Cubano, R. Redis, G. A. Calin, and S. Dharmawardhane. “Soy isoflavone genistein-mediated downregulation of miR-155 contributes to the anticancer effects of genistein.” In: *Nutrition and cancer* 68.1 (2016), pp. 154–164.
- [153] C. B. Avci, S. Y. Susluer, H. O. Caglar, T. Balci, D. Aygunes, Y. Dodurga, and C. Gunduz. “Genistein-induced mir-23b expression inhibits the growth of breast cancer cells.” In: *Contemporary Oncology* 19.1 (2015), p. 32.
- [154] B. Li, X. Jin, H. Meng, B. Hu, T. Zhang, J. Yu, S. Chen, X. Guo, W. Wang, W. Jiang, et al. “Morin promotes prostate cancer cells chemosensitivity to paclitaxel through miR-155/GATA3 axis.” In: *Oncotarget* 8.29 (2017), p. 47849.

- [155] M. Chakrabarti, D. J. Klionsky, and S. K. Ray. “miR-30e Blocks Autophagy and Acts Synergistically with Proanthocyanidin for Inhibition of AVEN and BIRC6 to Increase Apoptosis in Glioblastoma Stem Cells and Glioblastoma SNB19 Cells.” In: *PloS one* 11.7 (2016), e0158537.
- [156] P Liu, H Liang, Q Xia, P Li, H Kong, P Lei, S Wang, and Z Tu. “Resveratrol induces apoptosis of pancreatic cancers cells by inhibiting miR-21 regulation of BCL-2 expression.” In: *Clinical and Translational Oncology* 15.9 (2013), pp. 741–746.
- [157] E. Tili, J.-J. Michaille, B. Adair, H. Alder, E. Limagne, C. Taccioli, M. Ferracin, D. Delmas, N. Latruffe, and C. M. Croce. “Resveratrol decreases the levels of miR-155 by upregulating miR-663, a microRNA targeting JunB and JunD.” In: *Carcinogenesis* 31.9 (2010), pp. 1561–1566.
- [158] S. Sheth, S. Jajoo, T. Kaur, D. Mukherjea, K. Sheehan, L. P. Rybak, and V. Ramkumar. “Resveratrol reduces prostate cancer growth and metastasis by inhibiting the Akt/MicroRNA-21 pathway.” In: *PloS one* 7.12 (2012), e51655.
- [159] S. Dhar, A. Kumar, A. M. Rimando, X. Zhang, and A. S. Levenson. “Resveratrol and pterostilbene epigenetically restore PTEN expression by targeting oncomiRs of the miR-17 family in prostate cancer.” In: *Oncotarget* 6.29 (2015), p. 27214.
- [160] S. Dhar, C. Hicks, and A. S. Levenson. “Resveratrol and prostate cancer: promising role for microRNAs.” In: *Molecular nutrition & food research* 55.8 (2011), pp. 1219–1229.
- [161] W. Qin, K. Zhang, K. Clarke, T. Weiland, and E. R. Sauter. “Methylation and miRNA effects of resveratrol on mammary tumors vs. normal tissue.” In: *Nutrition and cancer* 66.2 (2014), pp. 270–277.

EGCG–DELIVERY NANOPPLATFORMS TO MAXIMIZE SKIN PROTECTION AGAINST HARMFUL RADIATION

Use of catechins in nanotech platforms to control the oxidative stress in cancer cells ¹

Abstract

Oxidative stress arises from an imbalance between oxidative species and antioxidant repair system response, leading to abnormalities in the cellular metabolism (DNA mutations and cancer). Following this reasoning, medical approaches providing large doses of dietary antioxidants should decrease the oxidative stress, and therefore the occurrence of diseases. So, in last decades, the research in flavonoids area increased owing to their anti-inflammatory and antioxidant properties. One of the most studied flavonoid subclass are the catechins found in fruits, chocolate, wine and tea. The potential of catechins for cancer therapy has been long recognised, but their low therapeutic effectiveness remains an issue. It appears that catechin action is compromised by their vulnerability to extreme environmental conditions (pH and temperature changes along gastrointestinal tract), that hinders their transport and uptake by intracellular targets. Recently, several nanotechnology-based delivery systems, such as liposomes, have been

¹This chapter is based on the publication in preparation for submission:
Pires, F., Oliveira Jr, O. N. and Raposo, M. Use of catechins in nanotech platforms to control the oxidative stress in cancer cells.

used to improve catechin's *in vivo* stability and pharmacokinetics. Although liposome carrying EGCG enhance bioavailability and showed higher antioxidant efficacy, their use in cosmetics industry can be compromised by their challenging issues in penetrate skin deeply.

3.1 Introduction

Cell plasma membrane is a complex and semipermeable barrier that surrounds and shields cell cytoplasm from external cytotoxic insults. This matrix is primarily composed by phospholipids arranged in a double-layered structure (phospholipid bilayer) with the hydrophilic headgroups pointing towards the aqueous environment and the hydrophobic tails oriented towards each other.[1] Also, plasma membrane contains lipid – anchored proteins, glycolipids and cholesterol that, together with phospholipids, regulate energy storage, cell signalling and as molecular transport (such as ions, water, drugs, sugars, amino acids) across the membrane, thus maintaining the integrity and the proper functioning of cell.

Hundreds of different lipids such as glycerophospholipids, sphingolipids and sterols (such as cholesterol) are present in all eukaryotic cell membranes. For example, erythrocytes cells anchor zwitterionic phospholipids as dipalmitoylphosphatidylcholine (DPPC) in the outer membrane leaflet and, anionic phospholipids as dipalmitoylphosphatidylserine (DPPS) in the inner membrane leaflet. [2] Additionally, DPPC, DPPS and anionic dipalmitoylphosphatidylglycerol (DPPG) phospholipids are present in great amounts in the mammalian lung surfactant which, together with proteins surfactant, confer resistance to respiratory pathogens and avoids respiratory infections.[3, 4] Besides saturated phospholipids, cell membranes also possess polyunsaturated lipids (lipids containing double bonds), which are extremely vulnerable to oxidative damage (discussed in further detail in the next section).

At physiological conditions, each organelle membrane of cell has a unique lipid distribution pattern that regulates membrane structure and mediates the drug trafficking across the membrane.[5, 6] The problem is that, sometimes, some pathological changes occur in cells due to certain perturbations in membrane lipid composition and organization, derived from the sensitivity of the plasma membrane to environmental factors. For instance, an abrupt change in the physiological level of ROS, which are routinely produced during cellular processes (cellular respiration and fatty acid β -oxidation), has important implications for

3.2. RADIATION-INDUCED LIPID PEROXIDATION

cell membrane integrity, fluidity, among others.[7, 8] Indeed, several studies reported that the imbalance between ROS production and elimination by antioxidant defence system, phenomenon known as oxidative stress, culminates in an overproduction of ROS that severely destabilize the lipid bilayer packing, breaks DNA chain, cause cellular dehydration and, depending on the severity of damage, culminate in cell death.[9, 10, 11] Apart from ROS generation by normal cellular metabolism, an exposure to heat, ionizing radiation and as to inflammatory and chemical toxins (cytokines and transient metals) have also been linked to the excessive increase in intracellular ROS levels (Figure 3.1).

Considering that one goal of this doctoral thesis is evaluate the antioxidant effect of catechin on phospholipids against radiation damage, the ROS-mediated lipid peroxidation phenomenon is discuss in more detail in the next section.

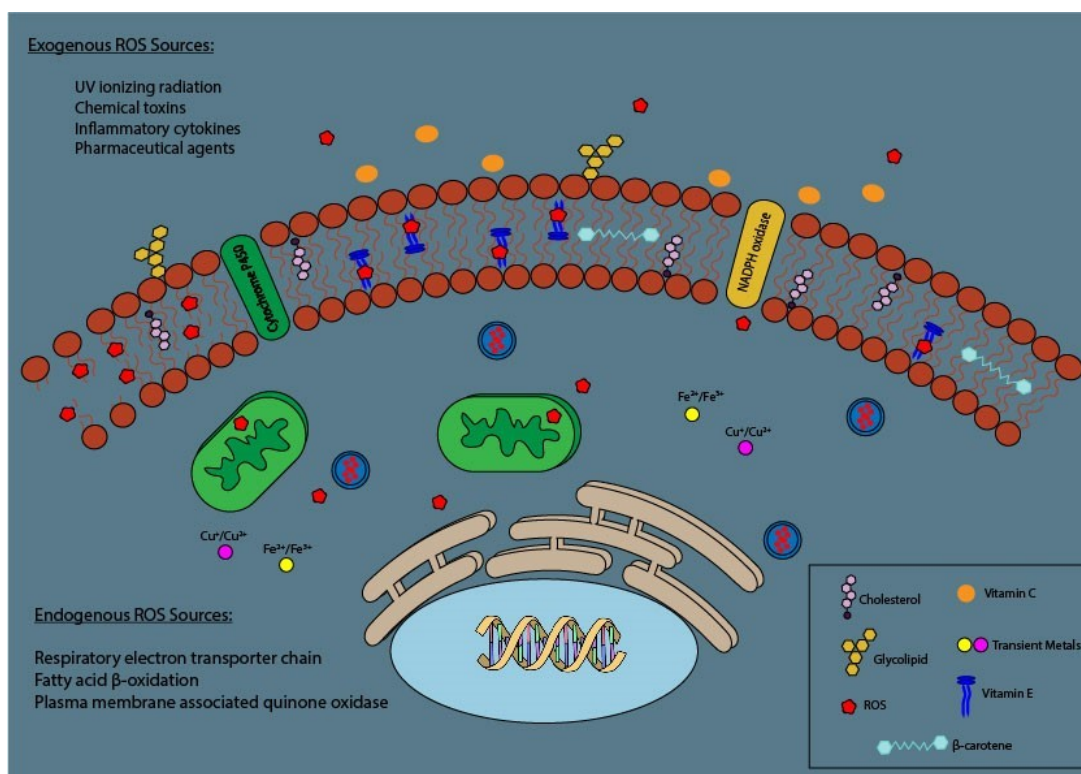


Figure 3.1: Exogenous and endogenous sources of ROS formation involved in cell damage.

3.2 Radiation-induced lipid peroxidation

In biological systems, radiation track can induce damage either by directly hitting the cell organelles or indirectly, through the generation of free radicals upon radiolysis of water. Since human cells are primarily composed of water ($\sim 70\%$), the

majority of cellular damage is due to the indirect action of radiation. When water molecules absorbed radiation they can be excited or become ionized, producing a significant number of free radicals (hydroxyl (OH^\bullet), hydrogen (H^\bullet) radicals, among others), molecular species (hydrogen peroxide) and secondary electrons (Figure 3.2).

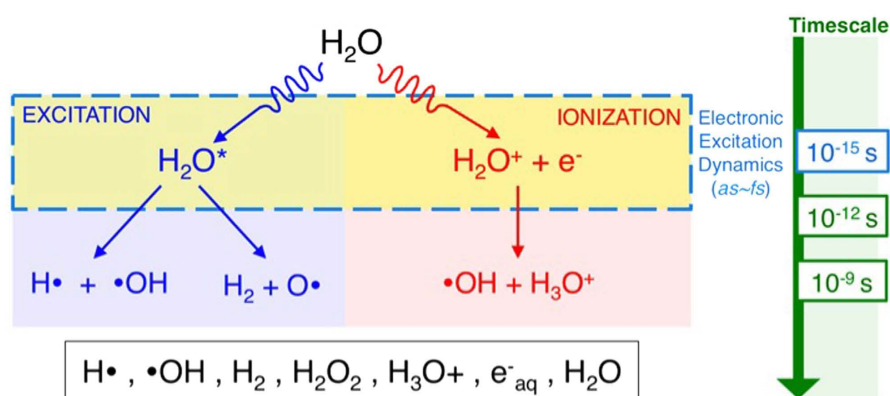


Figure 3.2: By-products of water radiolysis due to ionizing radiation. Image adapted from [12].

Most of the secondary electrons are stabilized and solvated through dipolar interactions with water molecules, however, part of them can react with H^+ forming H^\bullet radical. Free radicals are highly reactive species, because they carry unpaired electrons, that easily diffuse across cellular membranes and unspecifically attack biomolecules to attain stability. Moreover, these radicals can interact with molecular oxygen yielding ROS radicals such as peroxy and superoxide ($\text{O}_2^{\bullet-}$), which are far stronger oxidizing agents and thus, more troubling in biological system.[13, 14]

One of the major targets of hydroxyl and hydroperoxyl radicals is the lipid bilayer, where these species promote a cascade of oxidant events known as lipid peroxidation. Lipid peroxidation is a complex and repetitive process that rearranges the double bonds of unsaturated lipids, due to the hydrogen abstraction from a carbon that generates a carbon-centered lipid radical (initiation step). During propagation step, the carbon-centered lipid radical reacts with molecular oxygen yielding lipid peroxy radicals that attack neighboring polyunsaturated fatty acids and thus, give rise to new lipid radicals. A radical chain reaction ends up after an antioxidant molecule (like vitamin E) donate a hydrogen atom to the lipid peroxy radicals making that nonradical products, such as lipid hydroperoxides, are generated (termination step).[15, 16]

In addition to the lipid hydroperoxides, many secondary products such as aldehyde derivatives (malonyldialdehyde (MDA) and 4-hydroxynonenal (HNE))

are also formed via a cyclisation reaction during lipid peroxidation, which are also species extremely toxic to cellular organelles since they inhibit protein synthesis and enzyme activity [17, 18, 19, 20].

Besides the lipid peroxidation phenomena, the ROS species also decrease the saturation/unsaturation degree of the phospholipid acyl chains, cleavage the lipid headgroups, disrupt the lipid bilayer packing and change the mechanical properties of membranes by often converting a fluid-like membrane into rigid ones. [21, 22, 23, 24, 25].

Again, it is worth mentioning that, a sufficient amount of ROS in cells is required to activate some signalling pathways involved in normal cellular processes such as cell growth, differentiation, immune response, among others.[26, 27] Of course, the presence of an exacerbated amount of ROS in cell, is the driving force for upregulating the production of endogenous antioxidant molecules (glutathione peroxidase, superoxide dismutase, catalase) to reduce oxidative injury.[28, 29] Unfortunately, in some pathological conditions, the antioxidant defence system fails in counteracting the ROS toxicity, which compromises the survival of cell.

3.3 Antioxidant action of catechins

Over the past few decades, the synergistic action between dietary antioxidants and endogenous antioxidants has been explored as a promising strategy to decrease the human susceptibility to common ROS-mediated diseases such as neurodegenerative diseases and cancer.

As previously discussed in Chapter 2, a green tea bag contains a huge amount of different catechins, represented in Figure 3.3, that are believed to display *in vitro* and *in vivo* antioxidant and anticarcinogenic activities (for a review see [30] and references therein). As seen in Figure 3.3, each catechin subclass have distinct composition and number of functional side groups attached onto backbone that strongly influence the partitioning of catechin's into lipidic membrane and their chemical reactivity underlying the antioxidant activity.[31, 32, 33]

According to Quideau and co-workers[35], the catechins use two essential mechanisms for free radical scavenging: the hydrogen atom transfer (HAT) and the single electron transfer (SET), represented by equations 3.1 and 3.2, respectively. Focus on lipid radicals formed during lipid peroxidation, the hydroxyl groups of catechins (CatOH) dissociate and donate a hydrogen atom to lipid radical (R^\bullet), yielding species more stable and harmless such as lipid hydroperoxide

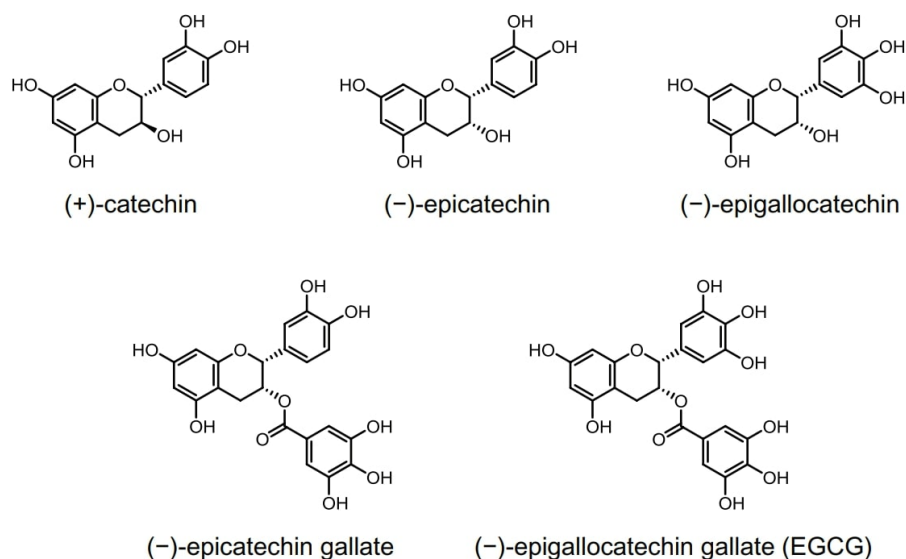


Figure 3.3: Structure of the different catechins present in green tea. Image adapted from [34].

(*RH*) and phenoxy radical (*CatO*[•]). Typically, the phenoxy radical is non-reactive, since the excited electron is delocalized and shared between aromatic rings, that provides stabilization. Clearly, the antioxidant efficiency of each type of catechin involving the HAT mechanism, is correlated with the bond dissociation enthalpy (BDE) of the phenolic O–H bond, meaning that catechins with lower BDE values are easily deprotonated and thus much more effective in radical scavenging.[36, 37]



With regard to SET mechanism, the ionization potential of each catechin is particularly important, since the mechanism involves an electron transfer reaction from the *CatOH* to the lipid radical, generating a stable radical cation *CatOH*^{•+} that is deprotonated after reacting with water. So, the reactive functional groups of catechins with lower ionization potential transfer an electron much more rapidly.[38]

In addition to these two radical scavenging mechanisms, catechins also reduce oxidative stress in an indirect way by upregulating the expression of the antioxidant enzymes (catalase, superoxide dismutase, glutathione peroxidase) via Nrf2 signalling pathway [39, 40, 41, 42], restoring appropriate vitamins C, E levels [43, 44] and blocking prooxidant enzymes (xanthine oxidase, lipoxygenase and

cyclooxygenase).[45, 46] Moreover, catechins have been found to chelate metal ions such as copper and iron, which frequently react with hydroperoxides to form the harmful hydroxyl radical via a Fenton-type reaction.[47, 48] In line with these findings, is expected that medical approaches relying on a large dose of dietary antioxidants should decrease the oxidative stress and therefore, the occurrence of diseases. However, there is an 'antioxidant paradox' since, unlike it was thought, a high dose of antioxidant are ineffective and brings deleterious effects. Despite the presence of phenolic hydroxyl groups increases the antioxidant/scavenging activity of catechins, it is also known that the oxidation of the catechol group on B-ring of catechins produces catechins by-products (quinones derivatives) that are toxic and cause adverse effects on biomolecules.[49, 50, 51] So, it is crucial address the mechanisms involved in catechin's autoxidation that reduce their *in vivo* stability. It is worth mentioning, though, that, some researchers have studied the prooxidant behavior of these ROS species arising from the autoxidation of catechins as a potential mechanism to attack the cellular DNA of cancer cells. [52, 53, 54] Nonetheless, in this doctoral thesis one intends to take advantage of the antioxidant activity of the most abundant catechin in green tea (epigallocatechin-3-gallate (EGCG)), instead of its prooxidant activity.

3.4 *In vivo* bioavailability of catechins

The use of catechins for pharmaceutical applications is mostly constrained due to the vulnerability and instability of these molecules to environmental factors (temperature, pH, radiation) that, consequently, influence the amount of unaltered catechins that reaches the systemic circulation to be distributed to target organs (bioavailability).[55, 56, 57, 58]

The *in vivo* bioavailability of catechins is relatively low because the phenolic hydroxyl groups are commonly oxidized and hydrolyzed by mouth, liver and small intestine esterases. For instance, the uridine diphosphate glucuronosyl-transferase (UGTA-1), catechol-*O*-methyltransferase (COMT) and phenol sulfotransferase (SULTA1) are hepatic esterases that glucuronate, methylate and sulfonate the hydroxyl groups of catechins, respectively.[59] Consequently, the loss of hydroxyl groups automatically impairs the HAT and SET mechanisms and thus, compromises the scavenging activity of catechins. Also, this extensive biotransformation and the alkaline milieu of the duodenum (pH ~ 8.5) increase the susceptibility of catechin to auto-oxidation and contribute to their poor absorption in the small intestine. [60, 61, 62, 63].

Therefore, new strategies are warranted for increasing *in vivo* bioavailability of catechins to further enhance their therapeutic action in target organs.

3.5 Liposomal-based EGCG delivery systems

Nanoencapsulation technology based on different formulations (solid nanoparticles, hydrogels, liposomes, among others) efficiently protect catechins from extreme and hazardous environmental conditions, greatly improve their stability and absorption and, successfully deliver them in specific cellular targets (for a review see [64] and references therein).

Here, one intends to focus mainly on the technological advances in the development of liposomal formulations to encapsulate EGCG.

Liposomes are sphere-shaped vesicles consisting in monolamellar or multilamellar phospholipids bilayers surrounding an aqueous nucleus, that spontaneously formed in aqueous solutions, known to efficiently entrap lipophilic molecules in the lipid bilayer and the hydrophilic ones into the aqueous nucleus. [65, 66] Since organization and distribution of phospholipids in liposomes is quite like the lipid fraction of natural cell membranes, these systems have been used as artificial models to evaluate, for instance, how a particular drug protects the membrane structure and dynamics against free radicals.[67, 68] Liposomes have been also used as nanocarriers in the pharmaceutical industry, since they offer advantages in terms of biocompatibility, biodegradability, payloading capacity and stability of entrapped drug. [69, 70, 71, 72] Also, it is possible to fine-tune the surface properties of liposomes to avoid their rapid clearance by the the mononuclear phagocyte system or reticuloendothelial system (RES) and increase their circulation time in the bloodstream, simply by coating the outer layer of liposome with hydrophilic polyethylene glycol (PEG) that shield them from destabilization (stealth liposomes).[73, 74]

Passive targeting and active targeting are the two mechanisms that mediate the *in vivo* liposome's accumulation in tumour site. In passive targeting, the drug-loaded nanocarrier accumulates in the tumour by the enhanced permeability and retention (EPR) effect, a phenomenon that does not occurs in healthy cells. EPR effect is reached when the liposomes survive to mononuclear phagocyte system and RES systems uptake, allowing their extravasation into tumour due to high permeability of blood vessels and poor lymphatic drainage.[75] In active targeting, the surface of liposomes is functionalized with a specific ligand that recognises and bind to a molecular receptor overexpressed only by cancer cells

(immunoliposomes) and thus, guarantee a site-specific accumulation of drug.[76, 77] Liposomes can be made by various methods, including film-hydration method (methodology used in this thesis and further discussed in Chapter 4), detergent depletion[78, 79], reverse-phase evaporation[80, 81], freeze-dried rehydration vesicles[82], high pressure homogenization[83, 84], supercritical fluidic technology[85, 86], among others. Regarding the vesicle size and number of lamellae, the resulting liposomes can be divided in: i) smaller unilamellar vesicles, SUVs (diameter 20–100 nm); ii) large unilamellar vesicles, LUVs (100–1000 nm in diameter) and multilamellar vesicles, MLVs (multiple number of membrane bilayers with diameter above 1 μm).[87] Some factors such as lipid composition, temperature, and pH strongly influence vesicle's characteristics (such as permeability and stability). Regarding the effect of temperature, each phospholipid has a characteristic phase transition temperature (T_m) that if raised, changes the flexibility of the hydrocarbon tails, meaning that the well-ordered and packed hydrocarbon tails of phospholipids (solid-gel phase) acquire a disordered conformation (liquid phase). Therefore, temperature is a key factor that strongly regulates the fluidity and permeability of liposomes.[88, 89] Several studies reported that the addition of cholesterol to liposomal formulation reduces the membrane permeability and avoids the premature release of entrapped drug.[90, 91, 92]

Liposome encapsulation solve the four major issues that affect the therapeutic efficacy of EGCG, which are the low water solubility, pH-dependent stability, poor bioavailability and inability to cross cell membrane. Fang et al. studied the encapsulation of EGCG in egg phosphatidylcholine:cholesterol:deoxycholic acid (4:1:0.25 wt%) liposomes and assessed its efficacy against basal cell carcinomas (BCCs). These liposomes efficiently entrapped EGCG ($\sim 99\%$) and, following injection in BCCs tumor region, they locally increased EGCG amount (by 20-fold compared to the free form) that was capable of inducing cell death.[93] Zou et al. demonstrated that tea polyphenol nanoliposomes improve the stability of the phenolic compounds in alkaline media and exhibit a sustained release rather than a burst release (typical of tea polyphenol solution), with minor compromise in the antioxidant and antibacterial activity.[94]

Cancer strategies based on synergistic effect of EGCG and anticancer drugs (such as 5-fluorouracil[95, 96], doxorubicin [97, 98], cisplatin [99, 100]) have gained increasing importance since the antioxidants ameliorates the toxicity and side-effects associated with anticancer drugs treatment and may also contribute to attenuation of carcinogenesis. Recently, Sugiyama et al. evaluated the anti-cancer activity of doxorubicin-loaded EGCG derivative-PEG-modified liposomes in B16F10 mouse melanoma cells. In this study, an monoamine-modified EGCG

CHAPTER 3. EGCG-DELIVERY NANOPLATFOMS TO MAXIMIZE SKIN PROTECTION AGAINST HARMFUL RADIATION

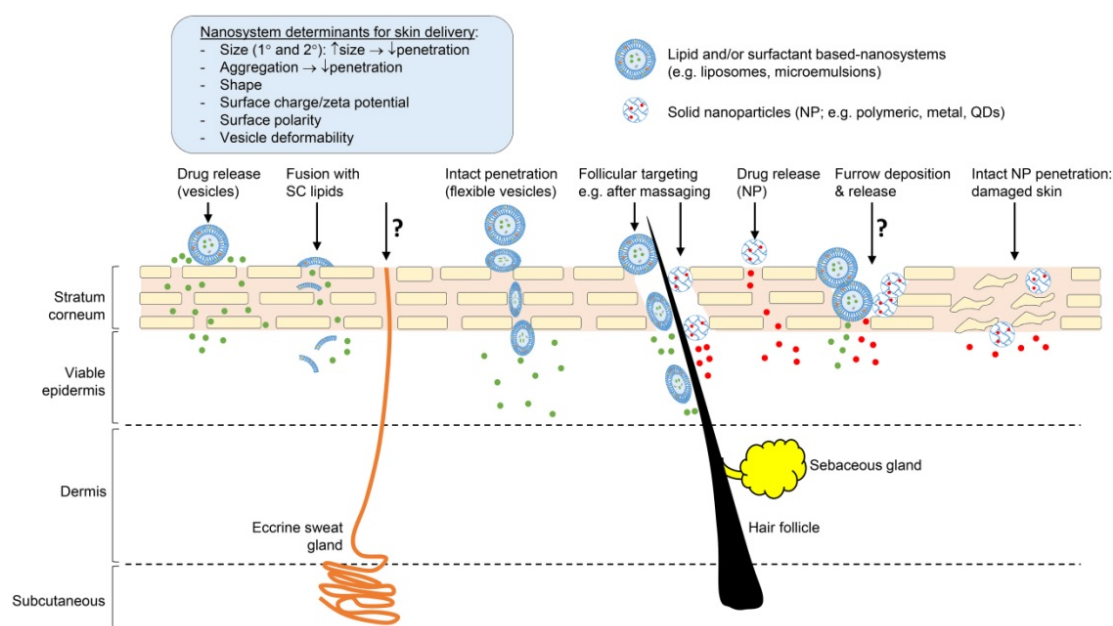


Figure 3.4: Physicochemical parameters that regulate drug permeation across skin. Image adapted from [103].

was synthesized for binding to 67-kDa laminin receptors overexpressed in cancer cells. These liposomes enhance the EGCG accumulation in tumor region, that in combination with doxorubicin, act synergistically to kill tumor cells by enhancing the activation of apoptotic activators such as caspase-8.[101]

In the last decades, several different liposomal formations have been designed to use in cosmetic preparations, especially in formulations that delays the skin aging and accelerates skin wound repair, however, as we can seen in the following section, drug permeation through skin is a major challenge in transdermal drug delivery.

3.6 Challenges in Dermal/Transdermal EGCG Delivery

The skin is an organ composed by three layers (epidermis, dermis, and subcutaneous tissue) that protects body from the external environment (mechanical injury, UV radiation, microorganisms), maintain water and electrolyte balance and regulates blood pressure and body temperature.[102] Typically, a drug can be topically (act on the surface of skin), dermally (drug act on dermal layer) or transdermally (drug cross dermal layer and enters in bloodstream) administered in skin, depending on lesion location and severity.

The Stratum Corneum (SC) is the outermost layer of the epidermis made of keratin, proteolytic enzymes and corneocytes embedded in a lipid matrix (ceramides, fatty acids, cholesterol), which is recognized as the major barrier that hinders the penetration of drug through the skin.[104, 105] A drug needs to have appropriate physicochemical features (such as a determined size, charge, shape) to overcome SC layer and achieve deep skin layers (Figure 3.4).[103] Some studies have shown that conventional liposomes efficiently deliver drugs in the upper layer of SC but hardly penetrates into deeper skin layers. However, attempts have been made to manipulate the depth of liposome penetration by adding, for instance, edge activators (sodium deoxycholate, Tween 80) in liposomal composition, to render liposomes more flexible and elastic.[106, 107, 108]

Avadhani et al. co-encapsulated hyaluronic acid and EGCG into soy phosphatidylcholine:sodium cholate liposomes by using by high-pressure homogenization technique. The liposomes incubated with human skin keratinocytes HaCaT cells and exposed to 60 J/m² of UV radiation, exhibited a high free radical-scavenging action since they lowered the production of by-products of lipid peroxidation (such as malondialdehyde) and decreased the activity of the matrix metalloproteinase in cells. Furthermore, the liposomes guaranteed a higher enhancement of skin permeation and deposition of EGCG ($38.90 \pm 1.16 \mu\text{g}/\text{cm}^2$) compared to that observed with EGCG aqueous solution ($3.94 \pm 0.18 \mu\text{g}/\text{cm}^2$).[109] In another study, the authors added Tween 20, a edge-activator, in EGCG-loaded liposome formulation to deliver EGCG in deep skin layers of HaCat cells. One important finding of this study was that as Tween 20 amount increases in liposomal formulation, the elasticity of vesicles increases but, the vesicle size and EGCG encapsulation efficiency decrease. Nonetheless, intact liposomes were able to cross the stratum corneum, following an osmotic transepidermal gradient, and promoted an EGCG sustained release in epidermal keratinocytes and dermal fibroblasts within 2 hours. [110]

Following the line of reasoning of this chapter, a liposomal carrier becomes a viable approach to improving EGCG stability and assuring a more efficient release in skin cells, that help protect them from oxidative stress induced by UV radiation. Hence, to demonstrate that, the developed EGCG-encapsulated liposomes will be immobilized in nanofibers and their potential to accelerate *in vivo* wound healing process will be determined in human fibroblasts cells following UVC exposure.

References

- [1] S. J. Singer and G. L. Nicolson. “The fluid mosaic model of the structure of cell membranes.” In: *Science* 175.4023 (1972), pp. 720–731.
- [2] J. Lopez Cascales, J García de la Torre, S. J. Marrink, and H. J. Berendsen. “Molecular dynamics simulation of a charged biological membrane.” In: *The Journal of chemical physics* 104.7 (1996), pp. 2713–2720.
- [3] J. A. Whitsett and T. E. Weaver. “Hydrophobic surfactant proteins in lung function and disease.” In: *New England Journal of Medicine* 347.26 (2002), pp. 2141–2148.
- [4] R. Veldhuizen, K. Nag, S. Orgeig, and F. Possmayer. “The role of lipids in pulmonary surfactant.” In: *Biochimica et Biophysica Acta (BBA)-Molecular Basis of Disease* 1408.2-3 (1998), pp. 90–108.
- [5] G. Van Meer, D. R. Voelker, and G. W. Feigenson. “Membrane lipids: where they are and how they behave.” In: *Nature reviews Molecular cell biology* 9.2 (2008), p. 112.
- [6] K. Simons and J. L. Sampaio. “Membrane organization and lipid rafts.” In: *Cold Spring Harbor perspectives in biology* 3.10 (2011), a004697.
- [7] A. L. Jackson and L. A. Loeb. “The contribution of endogenous sources of DNA damage to the multiple mutations in cancer.” In: *Mutation Research/-Fundamental and Molecular Mechanisms of Mutagenesis* 477.1-2 (2001), pp. 7–21.
- [8] C. R. Reczek and N. S. Chandel. “ROS-dependent signal transduction.” In: *Current opinion in cell biology* 33 (2015), pp. 8–13.
- [9] J. Ma, J.-L. Marignier, P. Pernot, C. Houée-Levin, A. Kumar, M. D. Sevilla, A. Adhikary, and M. Mostafavi. “Direct observation of the oxidation of DNA bases by phosphate radicals formed under radiation: a model of the backbone-to-base hole transfer.” In: *Physical Chemistry Chemical Physics* 20.21 (2018), pp. 14927–14937.
- [10] P. J. Gomes, A. M. G. da Silva, P. A. Ribeiro, O. N. Oliveira, and M. Raposo. “Radiation damage on Langmuir monolayers of the anionic 1,2-dipalmitoyl-sn-glycero-3-[phospho-rac-(1-glycerol)](sodium salt)(DPPG) phospholipid at the air-DNA solution interface.” In: *Materials Science and Engineering: C* 58 (2016), pp. 576–579.

- [11] H Nikjoo, D Emfietzoglou, T Liamsuwan, R Taleei, D. Liljequist, and S Uehara. "Radiation track, DNA damage and response—a review." In: *Reports on Progress in Physics* 79.11 (2016), p. 116601.
- [12] K. G. Reeves and Y. Kanai. "Electronic excitation dynamics in liquid water under proton irradiation." In: *Scientific Reports* 7.40379 (2017), pp. 1–8.
- [13] J. W. T. Spinks and R. J. Woods. In: *An introduction to radiation chemistry*. John Wiley and Sons, 1990.
- [14] E. I. Azzam, J.-P. Jay-Gerin, and D. Pain. "Ionizing radiation-induced metabolic oxidative stress and prolonged cell injury." In: *Cancer letters* 327.1-2 (2012), pp. 48–60.
- [15] H. Yin, L. Xu, and N. A. Porter. "Free radical lipid peroxidation: mechanisms and analysis." In: *Chemical reviews* 111.10 (2011), pp. 5944–5972.
- [16] A. Ayala, M. F. Muñoz, and S. Argüelles. "Lipid peroxidation: production, metabolism, and signaling mechanisms of malondialdehyde and 4-hydroxy-2-nonenal." In: *Oxidative medicine and cellular longevity* 2014 (2014), pp. 1–31.
- [17] H. Esterbauer and K. H. Cheeseman. "Determination of aldehydic lipid peroxidation products: malonaldehyde and 4-hydroxynonenal." In: *Methods in enzymology*. Vol. 186. Elsevier, 1990, pp. 407–421.
- [18] G. Barrera, S. Pizzimenti, M. Daga, C. Dianzani, A. Arcaro, G. P. Cetrangolo, G. Giordano, M. A. Cucci, M. Graf, and F. Gentile. "Lipid Peroxidation-Derived Aldehydes, 4-Hydroxynonenal and Malondialdehyde in Aging-Related Disorders." In: *Antioxidants* 7.8 (2018), pp. 1–17.
- [19] B. Sottero, D. Rossin, G. Poli, and F. Biasi. "Lipid oxidation products in the pathogenesis of inflammation-related gut diseases." In: *Current medicinal chemistry* 25.11 (2018), pp. 1311–1326.
- [20] E. Niki. "Lipid peroxidation: physiological levels and dual biological effects." In: *Free Radical Biology and Medicine* 47.5 (2009), pp. 469–484.
- [21] M. Choe, C. Jackson, and B. P. Yu. "Lipid peroxidation contributes to age-related membrane rigidity." In: *Free Radical Biology and Medicine* 18.6 (1995), pp. 977–984.
- [22] M.-K. Shih and M.-L. Hu. "Relative roles of metal ions and singlet oxygen in UVA-induced liposomal lipid peroxidation." In: *Journal of Inorganic Biochemistry* 77.3-4 (1999), pp. 225–230.

- [23] D. Marathe and K. Mishra. “Radiation-induced changes in permeability in unilamellar phospholipid liposomes.” In: *Radiation research* 157.6 (2002), pp. 685–692.
- [24] M Yusupov, K Wende, S Kupsch, E. Neyts, S Reuter, and A Bogaerts. “Effect of head group and lipid tail oxidation in the cell membrane revealed through integrated simulations and experiments.” In: *Scientific Reports* 7.5761 (2017), pp. 1–8.
- [25] O. Shadyro, I. Yurkova, and M. Kisel. “Radiation-induced peroxidation and fragmentation of lipids in a model membrane.” In: *International Journal of radiation biology* 78.3 (2002), pp. 211–217.
- [26] R. Mittler. “ROS are good.” In: *Trends in Plant Science* 22.1 (2017), pp. 11–19.
- [27] L. A. Sena and N. S. Chandel. “Physiological roles of mitochondrial reactive oxygen species.” In: *Molecular cell* 48.2 (2012), pp. 158–167.
- [28] M. Mari, A. Morales, A. Colell, C. García-Ruiz, and J. C. Fernández-Checa. “Mitochondrial glutathione, a key survival antioxidant.” In: *Antioxidants & Redox Signaling* 11.11 (2009), pp. 2685–2700.
- [29] J. M. Matés, C. Pérez-Gómez, and I. N. De Castro. “Antioxidant enzymes and human diseases.” In: *Clinical biochemistry* 32.8 (1999), pp. 595–603.
- [30] L. Xing, H. Zhang, R. Qi, R. Tsao, and Y. Mine. “Recent advances in the understanding of the health benefits and molecular mechanisms associated with green tea polyphenols.” In: *Journal of Agricultural and Food Chemistry* 67.4 (2019), pp. 1029–1043.
- [31] S. Antonczak. “Electronic description of four flavonoids revisited by DFT method.” In: *Journal of Molecular Structure: THEOCHEM* 856.1-3 (2008), pp. 38–45.
- [32] N. Hayashi and T. Ujihara. “Conformations of Flavan-3-ols in water: Analysis using density functional theory.” In: *Journal of natural products* 80.2 (2017), pp. 319–327.
- [33] P. Alov, I. Tsakovska, and I. Pajeva. “Computational studies of free radical-scavenging properties of phenolic compounds.” In: *Current topics in medicinal chemistry* 15.2 (2015), pp. 85–104.
- [34] N. Miyoshi, M Pervin, T Suzuki, K Unno, M Isemura, and M Nakamura. “Green tea catechins for well-being and therapy: Prospects and opportunities.” In: *Bot. Targets Ther* 5 (2015), pp. 85–96.

- [35] S. Quideau, D. Deffieux, C. Douat-Casassus, and L. Pouysegou. "Plant polyphenols: chemical properties, biological activities, and synthesis." In: *Angewandte Chemie* 50.3 (2011), pp. 586–621.
- [36] M. Leopoldini, N. Russo, and M. Toscano. "The molecular basis of working mechanism of natural polyphenolic antioxidants." In: *Food Chemistry* 125.2 (2011), pp. 288–306.
- [37] A. Pérez-González, A. M. Rebollar-Zepeda, J. R. León-Carmona, and A. Galano. "Reactivity indexes and OH bond dissociation energies of a large series of polyphenols: Implications for their free radical scavenging activity." In: *Journal of the Mexican Chemical Society* 56.3 (2012), pp. 241–249.
- [38] B. D. Craft, A. L. Kerrihard, R. Amarowicz, and R. B. Pegg. "Phenol-based antioxidants and the in vitro methods used for their assessment." In: *Comprehensive Reviews in Food Science and Food Safety* 11.2 (2012), pp. 148–173.
- [39] P. Saha and S. Das. "Elimination of deleterious effects of free radicals in murine skin carcinogenesis by black tea infusion, theaflavins & epigallocatechin gallate." In: *Asian Pac J Cancer Prev* 3.3 (2002), pp. 225–230.
- [40] J. Han, M. Wang, X. Jing, H. Shi, M. Ren, and H. Lou. "(-)-Epigallocatechin gallate protects against cerebral ischemia-induced oxidative stress via Nrf2/ARE signaling." In: *Neurochemical research* 39.7 (2014), pp. 1292–1299.
- [41] Y. Wang, B. Wang, F. Du, X. Su, G. Sun, G. Zhou, X. Bian, and N. Liu. "Epigallocatechin-3-Gallate Attenuates Oxidative Stress and Inflammation in Obstructive Nephropathy via NF- κ B and Nrf2/HO-1 Signalling Pathway Regulation." In: *Basic & clinical pharmacology & toxicology* 117.3 (2015), pp. 164–172.
- [42] H.-K. Na and Y.-J. Surh. "Modulation of Nrf2-mediated antioxidant and detoxifying enzyme induction by the green tea polyphenol EGCG." In: *Food and Chemical Toxicology* 46.4 (2008), pp. 1271–1278.
- [43] J. Intra and S.-M. Kuo. "Physiological levels of tea catechins increase cellular lipid antioxidant activity of vitamin C and vitamin E in human intestinal caco-2 cells." In: *Chemico-biological interactions* 169.2 (2007), pp. 91–99.

- [44] K. Mukai, S. Mitani, K. Ohara, and S.-I. Nagaoka. “Structure–activity relationship of the tocopherol-regeneration reaction by catechins.” In: *Free radical biology and medicine* 38.9 (2005), pp. 1243–1256.
- [45] J.-K. Lin, P.-C. Chen, C.-T. Ho, and S.-Y. Lin-Shiau. “Inhibition of xanthine oxidase and suppression of intracellular reactive oxygen species in HL-60 cells by theaflavin-3, 3'-digallate,(-)-epigallocatechin-3-gallate, and propyl gallate.” In: *Journal of Agricultural and Food Chemistry* 48.7 (2000), pp. 2736–2743.
- [46] J.-T. Hwang, J. Ha, I.-J. Park, S.-K. Lee, H. W. Baik, Y. M. Kim, and O. J. Park. “Apoptotic effect of EGCG in HT-29 colon cancer cells via AMPK signal pathway.” In: *Cancer letters* 247.1 (2007), pp. 115–121.
- [47] L. Mira, M Tereza Fernandez, M. Santos, R. Rocha, M Helena Florêncio, and K. R. Jennings. “Interactions of flavonoids with iron and copper ions: a mechanism for their antioxidant activity.” In: *Free radical research* 36.11 (2002), pp. 1199–1208.
- [48] S. López-Burillo, D.-X. Tan, J. C. Mayo, R. M. Sainz, L. C. Manchester, and R. J. Reiter. “Melatonin, xanthurenic acid, resveratrol, EGCG, vitamin C and α -lipoic acid differentially reduce oxidative DNA damage induced by Fenton reagents: a study of their individual and synergistic actions.” In: *Journal of pineal research* 34.4 (2003), pp. 269–277.
- [49] T. Nakayama, M. Ichiba, M. Kuwabara, K. Katsuko, and S. Kumazawa. “Mechanisms and structural specificity of hydrogen peroxide formation during oxidation of catechins.” In: *Food Science and Technology Research* 8.3 (2002), pp. 261–267.
- [50] T. Ishii, T. Mori, T. Tanaka, D. Mizuno, R. Yamaji, N.-T. Kumazawa Shigenori, and M. Akagawa. “Covalent modification of proteins by green tea polyphenol (–)-epigallocatechin-3-gallate through autoxidation.” In: *Free Radical Biology and Medicine* 45.10 (2008), pp. 1384–1394.
- [51] T. Ishii, T. Mori, T. Ichikawa, M. Kaku, K. Kusaka, Y. Uekusa, M. Akagawa, Y. Aihara, T. Furuta, T. Wakimoto, et al. “Structural characteristics of green tea catechins for formation of protein carbonyl in human serum albumin.” In: *Bioorganic & medicinal chemistry* 18.14 (2010), pp. 4892–4896.
- [52] S Azam, N Hadi, N. U. Khan, and S. M. Hadi. “Prooxidant property of green tea polyphenols epicatechin and epigallocatechin-3-gallate: implications for anticancer properties.” In: *Toxicology in vitro* 18.5 (2004), pp. 555–561.

- [53] Z. Hou, S. Sang, H. You, M.-J. Lee, J. Hong, K.-V. Chin, and C. S. Yang. "Mechanism of action of (-)-epigallocatechin-3-gallate: Auto-oxidation-dependent inactivation of epidermal growth factor receptor and direct effects on growth inhibition in human esophageal cancer KYSE 150 cells." In: *Cancer research* 65.17 (2005), pp. 8049–8056.
- [54] R. Vittal, Z. E. Selvanayagam, Y. Sun, J. Hong, F. Liu, K.-V. Chin, and C. S. Yang. "Gene expression changes induced by green tea polyphenol (-)-epigallocatechin-3-gallate in human bronchial epithelial 21BES cells analyzed by DNA microarray." In: *Molecular Cancer Therapeutics* 3.9 (2004), pp. 1091–1099.
- [55] J. Hong, H. Lu, X. Meng, J.-H. Ryu, Y. Hara, and C. S. Yang. "Stability, cellular uptake, biotransformation, and efflux of tea polyphenol (-)-epigallocatechin-3-gallate in HT-29 human colon adenocarcinoma cells." In: *Cancer Research* 62.24 (2002), pp. 7241–7246.
- [56] S. Sang, M.-J. Lee, Z. Hou, C.-T. Ho, and C. S. Yang. "Stability of tea polyphenol (-)-epigallocatechin-3-gallate and formation of dimers and epimers under common experimental conditions." In: *Journal of Agricultural and Food Chemistry* 53.24 (2005), pp. 9478–9484.
- [57] R. Wang, W. Zhou, and X. Jiang. "Reaction kinetics of degradation and epimerization of epigallocatechin gallate (EGCG) in aqueous system over a wide temperature range." In: *Journal of Agricultural and Food Chemistry* 56.8 (2008), pp. 2694–2701.
- [58] S. Sang, I. Yang, B. Buckley, C.-T. Ho, and C. S. Yang. "Autoxidative quinone formation in vitro and metabolite formation in vivo from tea polyphenol (-)-epigallocatechin-3-gallate: studied by real-time mass spectrometry combined with tandem mass ion mapping." In: *Free Radical Biology and Medicine* 43.3 (2007), pp. 362–371.
- [59] C. H. Weinert, S. Wiese, H. M. Rawel, T. Esatbeyoglu, P. Winterhalter, T. Homann, and S. E. Kulling. "Methylation of catechins and procyanidins by rat and human catechol-O-methyltransferase: metabolite profiling and molecular modeling studies." In: *Drug Metabolism and Disposition* 40.2 (2012), pp. 353–359.
- [60] S. Roowi, A. Stalmach, W. Mullen, M. E. Lean, C. A. Edwards, and A. Crozier. "Green tea flavan-3-ols: colonic degradation and urinary excretion of catabolites by humans." In: *Journal of Agricultural and Food Chemistry* 58.2 (2009), pp. 1296–1304.

- [61] T. Ishii, T. Ichikawa, K. Minoda, K. Kusaka, S. Ito, Y. Suzuki, M. Akagawa, K. Mochizuki, T. Goda, and T. Nakayama. “Human serum albumin as an antioxidant in the oxidation of (-)-epigallocatechin gallate: participation of reversible covalent binding for interaction and stabilization.” In: *Bioscience, biotechnology, and biochemistry* 75.1 (2011), pp. 100–106.
- [62] M.-J. Lee, P. Maliakal, L. Chen, X. Meng, F. Y. Bondoc, S. Prabhu, G. Lambert, S. Mohr, and C. S. Yang. “Pharmacokinetics of tea catechins after ingestion of green tea and (-)-epigallocatechin-3-gallate by humans: formation of different metabolites and individual variability.” In: *Cancer Epidemiology and Prevention Biomarkers* 11.10 (2002), pp. 1025–1032.
- [63] H. Lu, X. Meng, and C. S. Yang. “Enzymology of methylation of tea catechins and inhibition of catechol–O–methyltransferase by (–)–epigallocatechin gallate.” In: *Drug metabolism and disposition* 31.5 (2003), pp. 572–579.
- [64] P. Puligundla, C. Mok, S. Ko, J. Liang, and N. Recharla. “Nanotechnological approaches to enhance the bioavailability and therapeutic efficacy of green tea polyphenols.” In: *Journal of functional Foods* 34 (2017), pp. 139–151.
- [65] A. Samad, Y Sultana, and M Aqil. “Liposomal drug delivery systems: an update review.” In: *Current drug delivery* 4.4 (2007), pp. 297–305.
- [66] R. D. Signorell, A. Papachristodoulou, J. Xiao, B. Arpagaus, T. Casalini, J. Grandjean, J. Thamm, F. Steiniger, P. Luciani, D. Brambilla, B. Werner, E. Martin, M. Weller, P. Roth, and J.-C. Leroux. “Preparation of PEGylated liposomes incorporating lipophilic lomeguatrib derivatives for the sensitization of chemo-resistant gliomas.” In: *International Journal of Pharmaceutics* 536.1 (2018), pp. 388–396.
- [67] N. P. Seeram and M. G. Nair. “Inhibition of lipid peroxidation and structure – activity – related studies of the dietary constituents anthocyanins, anthocyanidins, and catechins.” In: *Journal of Agricultural and Food Chemistry* 50.19 (2002), pp. 5308–5312.
- [68] S. V. Verstraeten, C. L. Keen, H. H. Schmitz, C. G. Fraga, and P. I. Oteiza. “Flavan – 3 – ols and procyanidins protect liposomes against lipid oxidation and disruption of the bilayer structure.” In: *Free Radical Biology and Medicine* 34.1 (2003), pp. 84–92.

- [69] D. Sharma, A. A. E. Ali, and L. R. Trivedi. "An Updated Review on: Liposomes as drug delivery system." In: *PharmaTutor* 6.2 (2018), pp. 50–62.
- [70] G. Amoabediny, F. Haghirsadat, Naderinezhad, E. Helder and Kharanaghi, J. Arough, and B. Zandieh-Doulabi. "Overview of preparation methods of polymeric and lipid – based (niosome, solid lipid, liposome) nanoparticles: A comprehensive review." In: *International Journal of Polymeric Materials and Polymeric Biomaterials* 67.6 (2018), pp. 383–400.
- [71] M. Rudokas, M. Najlah, M. A. Alhnan, and A. Elhissi. "Liposome delivery systems for inhalation: a critical review highlighting formulation issues and anticancer applications." In: *Medical Principles and Practice* 25.2 (2016), pp. 60–72.
- [72] A. Akbarzadeh, R. Rezaei-Sadabady, S. Davaran, S. W. Joo, N. Zarghami, Y. Hanifehpour, M. Samiei, M. Kouhi, and K. Nejati-Koshki. "Liposome: classification, preparation, and applications." In: *Nanoscale research letters* 8.102 (2013), pp. 1–9.
- [73] G. Pasut, D. Paolino, C. Celia, A. Mero, A. S. Joseph, J. Wolfram, D. Cosco, O. Schiavon, H. Shen, and M. Fresta. "Polyethylene glycol (PEG)-dendron phospholipids as innovative constructs for the preparation of super stealth liposomes for anticancer therapy." In: *Journal of controlled release* 199 (2015), pp. 106–113.
- [74] C. Zylberberg and S. Matosevic. "Pharmaceutical liposomal drug delivery: a review of new delivery systems and a look at the regulatory landscape." In: *Drug Delivery* 23.9 (2016), pp. 3319–3329.
- [75] J. Fang, H. Nakamura, and H. Maeda. "The EPR effect: unique features of tumor blood vessels for drug delivery, factors involved, and limitations and augmentation of the effect." In: *Advanced drug delivery reviews* 63.3 (2011), pp. 136–151.
- [76] S. H. Alavizadeh, F. Soltani, and M. Ramezani. "Recent advances in Immunoliposome-based Cancer therapy." In: *Current Pharmacology Reports* 2.3 (2016), pp. 129–141.
- [77] R. Petrilli, J. O Eloy, R. FV Lopez, and R. J Lee. "Cetuximab immunoliposomes enhance delivery of 5-FU to skin squamous carcinoma cells." In: *Anti-Cancer Agents in Medicinal Chemistry* 17.2 (2017), pp. 301–308.

- [78] J Brunner, P Skrabal, and H Hausser. "Single bilayer vesicles prepared without sonication physico-chemical properties." In: *Biochimica et Biophysica Acta (BBA)-Biomembranes* 455.2 (1976), pp. 322–331.
- [79] O. Zumbuehl and H. G. Weder. "Liposomes of controllable size in the range of 40 to 180 nm by defined dialysis of lipid/detergent mixed micelles." In: *Biochimica et Biophysica Acta (BBA)-Biomembranes* 640.1 (1981), pp. 252–262.
- [80] T. Imura, K. Otake, S. Hashimoto, T. Gotoh, M. Yuasa, S. Yokoyama, H. Sakai, J. F. Rathman, and M. Abe. "Preparation and physicochemical properties of various soybean lecithin liposomes using supercritical reverse phase evaporation method." In: *Colloids and Surfaces B: Biointerfaces* 27.2-3 (2003), pp. 133–140.
- [81] C. Pidgeon, S. McNeely, T. Schmidt, and J. E. Johnson. "Multilayered vesicles prepared by reverse-phase evaporation: liposome structure and optimum solute entrapment." In: *Biochemistry* 26.1 (1987), pp. 17–29.
- [82] T. Wang, Y. Deng, Y. Geng, Z. Gao, J. Zou, and Z. Wang. "Preparation of submicron unilamellar liposomes by freeze – drying double emulsions." In: *Biochimica et Biophysica Acta (BBA)-Biomembranes* 1758.2 (2006), pp. 222–231.
- [83] D. Carugo, E. Bottaro, J. Owen, E. Stride, and C. Nastruzzi. "Liposome production by microfluidics: potential and limiting factors." In: *Scientific Reports* 6.25876 (2016), pp. 1–15.
- [84] R. Barnadas-Rodriguez and M. Sabés. "Factors involved in the production of liposomes with a high-pressure homogenizer." In: *International Journal of Pharmaceutics* 213.1-2 (2001), pp. 175–186.
- [85] I. E. Santo, R. Campardelli, E. C. Albuquerque, S. A. V. De Melo, E. Reverchon, and G. Della Porta. "Liposomes size engineering by combination of ethanol injection and supercritical processing." In: *Journal of Pharmaceutical Sciences* 104.11 (2015), pp. 3842–3850.
- [86] I. E. Santo, R. Campardelli, E. C. Albuquerque, S. V. de Melo, G. Della Porta, and E. Reverchon. "Liposomes preparation using a supercritical fluid assisted continuous process." In: *Chemical Engineering Journal* 249 (2014), pp. 153–159.

- [87] A. Laouini, C. Jaafar-Maalej, I. Limayem-Blouza, S Sfar, C. Charcosset, and H. Fessi. "Preparation, characterization and applications of liposomes: state of the art." In: *Journal of colloid Science and Biotechnology* 1.2 (2012), pp. 147–168.
- [88] D Papahadjopoulos, K Jacobson, S Nir, and I Isac. "Phase transitions in phospholipid vesicles fluorescence polarization and permeability measurements concerning the effect of temperature and cholesterol." In: *Biochimica et Biophysica Acta (BBA) – Biomembranes* 311.3 (1973), pp. 330–348.
- [89] M. Norouzi, S. M. Boroujeni, N. Omidvarkordshouli, and M. Soleimani. "Advances in skin regeneration: application of electrospun scaffolds." In: *Advanced Healthcare Materials* 4.8 (2015), pp. 1114–1133.
- [90] C. Kirby, J. Clarke, and G. Gregoriadis. "Effect of the cholesterol content of small unilamellar liposomes on their stability in vivo and in vitro." In: *Biochemical Journal* 186.2 (1980), pp. 591–598.
- [91] J. Lopez-Pinto, M. Gonzalez-Rodriguez, and A. Rabasco. "Effect of cholesterol and ethanol on dermal delivery from DPPC liposomes." In: *International Journal of pharmaceuticals* 298.1 (2005), pp. 1–12.
- [92] S. Kaddah, N. Khreich, F. Kaddah, C. Charcosset, and H. Greige-Gerges. "Cholesterol modulates the liposome membrane fluidity and permeability for a hydrophilic molecule." In: *Food and chemical toxicology* 113 (2018), pp. 40–48.
- [93] J.-Y. Fang, W.-R. Lee, S.-C. Shen, and Y.-L. Huang. "Effect of liposome encapsulation of tea catechins on their accumulation in basal cell carcinomas." In: *Journal of dermatological science* 42.2 (2006), pp. 101–109.
- [94] L.-q. Zou, W. Liu, W.-l. Liu, R.-h. Liang, T. Li, C.-m. Liu, Y.-l. Cao, J. Niu, and Z. Liu. "Characterization and bioavailability of tea polyphenol nanoliposome prepared by combining an ethanol injection method with dynamic high-pressure microfluidization." In: *Journal of Agricultural and Food Chemistry* 62.4 (2014), pp. 934–941.
- [95] S. Toden, H.-M. Tran, O. A. Tovar-Camargo, Y. Okugawa, and A. Goel. "Epigallocatechin-3-gallate targets cancer stem-like cells and enhances 5-fluorouracil chemosensitivity in colorectal cancer." In: *Oncotarget* 7.13 (2016), p. 16158.
- [96] E. P.-F. López, F. G. García, and P. L. Jornet. "Combination of 5-Fluorouracil and polyphenol EGCG exerts suppressive effects on oral cancer cells exposed to radiation." In: *Archives of Oral Biology* 101 (2019), pp. 8–12.

- [97] L. Ray, P. Kumar, and K. C. Gupta. “The activity against Ehrlich’s ascites tumors of doxorubicin contained in self assembled, cell receptor targeted nanoparticle with simultaneous oral delivery of the green tea polyphenol epigallocatechin-3-gallate.” In: *Biomaterials* 34.12 (2013), pp. 3064–3076.
- [98] K. Liang, J. E. Chung, S. J. Gao, N. Yongvongsoontorn, and M. Kurisawa. “Highly Augmented Drug Loading and Stability of Micellar Nanocomplexes Composed of Doxorubicin and Poly (ethylene glycol)–Green Tea Catechin Conjugate for Cancer Therapy.” In: *Advanced Materials* 30.14 (2018), pp. 1706963–1706971.
- [99] F. Hu, F. Wei, Y. Wang, B. Wu, Y. Fang, and B. Xiong. “EGCG synergizes the therapeutic effect of cisplatin and oxaliplatin through autophagic pathway in human colorectal cancer cells.” In: *Journal of Pharmacological Sciences* 128.1 (2015), pp. 27–34.
- [100] C. Mayr, A. Wagner, D. Neureiter, M. Pichler, M. Jakab, R. Illig, F. Berr, and T. Kiesslich. “The green tea catechin epigallocatechin gallate induces cell cycle arrest and shows potential synergism with cisplatin in biliary tract cancer cells.” In: *BMC Complementary and Alternative Medicine* 15.194 (2015), pp. 1–7.
- [101] I. Sugiyama, K. Kaihatsu, Y. Soma, N. Kato, and Y. Sadzuka. “Dual-effect liposomes with increased antitumor effects against 67-kDa laminin receptor-overexpressing tumor cells.” In: *International Journal of pharmaceuticals* 541.1-2 (2018), pp. 206–213.
- [102] B. Godin and E. Touitou. “Transdermal skin delivery: predictions for humans from in vivo, ex vivo and animal models.” In: *Advanced drug delivery reviews* 59.11 (2007), pp. 1152–1161.
- [103] M. Roberts, Y Mohammed, M. Pastore, S Namjoshi, S Yousef, A Alinaghi, I. Haridass, E Abd, V. Leite-Silva, H. Benson, and J. Grice. “Topical and cutaneous delivery using nanosystems.” In: *Journal of Controlled Release* 247 (2017), pp. 86–105.
- [104] G. K. Menon, G. W. Cleary, and M. E. Lane. “The structure and function of the stratum corneum.” In: *International Journal of pharmaceuticals* 435.1 (2012), pp. 3–9.
- [105] E. Proksch, J. M. Brandner, and J.-M. Jensen. “The skin: an indispensable barrier.” In: *Experimental dermatology* 17.12 (2008), pp. 1063–1072.

- [106] D. K. Mishra, V. Pandey, R. Maheshwari, P. Ghode, and R. K. Tekade. "Cutaneous and Transdermal Drug Delivery: Techniques and Delivery Systems." In: *Basic Fundamentals of Drug Delivery*. 15. Academic Press, 2019, pp. 595–650.
- [107] E Touitou, N Dayan, L Bergelson, B. Godin, and M Eliaz. "Ethosomes – novel vesicular carriers for enhanced delivery : characterization and skin penetration properties." In: *Journal of Controlled Release* 65.3 (2000), pp. 403–418.
- [108] G. Chen, D. Li, Y. Jin, W. Zhang, L. Teng, C. Bunt, and J. Wen. "Deformable liposomes by reverse-phase evaporation method for an enhanced skin delivery of (+)-catechin." In: *Drug Development and Industrial Pharmacy* 40.2 (2014), pp. 260–265.
- [109] K. S. Avadhani, J. Manikkath, M. Tiwari, M. Chandrasekhar, A. Godavarthi, S. M. Vidya, R. C. Hariharapura, G. Kalthur, N. Udupa, and S. Mutalik. "Skin delivery of epigallocatechin-3-gallate (EGCG) and hyaluronic acid loaded nano-transfersomes for antioxidant and anti-aging effects in UV radiation induced skin damage." In: *Drug Delivery* 24.1 (2017), pp. 61–74.
- [110] M. Marwah, Y. Perrie, R. K. S. Badhan, and D. Lowry. "Intracellular uptake of EGCG-loaded deformable controlled release liposomes for skin cancer." In: *Journal of liposome research* (2019), pp. 1–14.

EXPERIMENTAL CONCEPTS & METHODOLOGY

In this chapter the general concepts in Langmuir monolayers and liposomes structures are introduced, in particular, methods of preparation, applied molecular simulations and spectroscopic techniques used to characterize them. It is worth mentioning that the detailed description of procedures (details such as concentration, lipid composition, temperature, irradiation time, among others) only was done in each subsection of the Results section to avoid unnecessary repetition of information.

4.1 Langmuir Monolayer studies

4.1.1 Surface Pressure - Area Isotherms

The Langmuir monolayers, experimental models used in this work for mimicking half of a lipid bilayer membrane, are produced in an apparatus similar to that in Figure 4.1. Briefly, an appropriate concentration of the phospholipid molecules were dissolved in an appropriate organic solvent (chloroform, methanol) and spread, drop by drop using a microsyringe, on the water/buffer subphase between the barriers. The phospholipids are amphiphilic molecules which have the hydrophilic head (such as choline, carboxylic acid) immersed in the aqueous subphase and the hydrophobic fatty acid chains oriented into the air. Immediately after evaporation of the solvent, the two lateral symmetric barriers start to move, bringing the molecules closer to each other, and initiating the compression of the

monolayer. During monolayer compression, the variations in the surface pressure as a function of the area per molecule (A_m) on the subphase, at a given temperature, were monitored by the Wilhelmy plate method.[1] The A_m is calculated using the equation 4.1:

$$A_m = \frac{A_{LT} \times M}{c \times N_A \times V} \quad (4.1)$$

where the A_{LT} is the Langmuir trough area, M is the molecular mass, c is the concentration, N_A is the Avogadro number and V is the solution's volume spread.

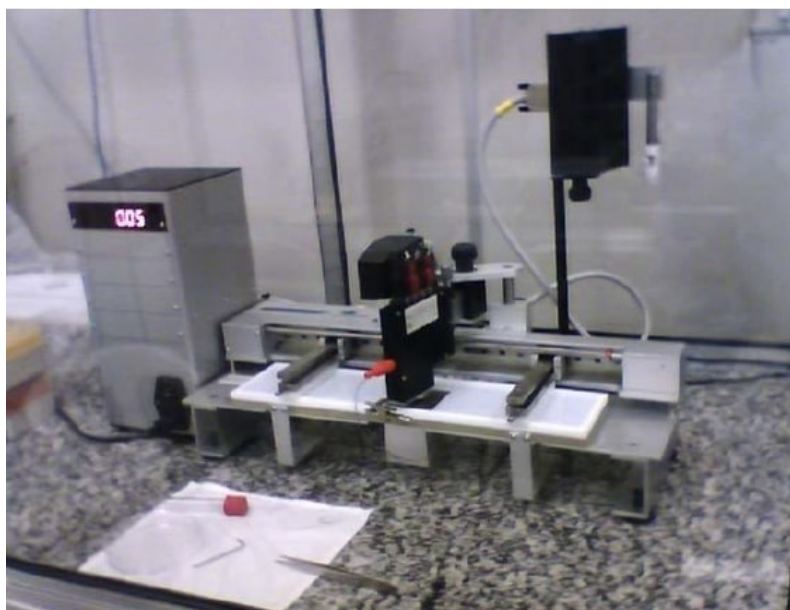


Figure 4.1: The Langmuir monolayers at the air-water interface were formed in a KSV NIMA Langmuir trough.

In these experiments, the Wilhelmy plate consists in a filter paper (10×20 mm) attached to a microbalance that was positioned perpendicular and partially immersed in water subphase to measure the surface pressure. The forces acting on the filter paper are the gravity and surface tension in a downward direction, and the buoyancy due to displaced water in an upward direction, that can be converted into surface tension (mN/m).

The net force downwards (F) in a rectangular plate (length (L) \times width (w) \times thickness (t_h), with a specific material density (ρ_W) immersed to depth of h in an aqueous subphase (density (ρ_L)) is obtained using the equation 4.2:

$$F = \rho_W g l w t + 2\gamma(t_h + w)\cos(\theta) - \rho_L g t_h w h \quad (4.2)$$

where γ is the surface tension of the liquid, g the acceleration of gravity and θ is the contact angle of the liquid on the solid plate ($\theta = 0$ if plate completely wetted). So, the surface pressure (π) is defined as the difference between the surface tension of water ($\gamma_0 = 73$ mN/m at 20 ° C) and the surface tension upon lipid monolayer formation at the interface (γ) as shown by equation 4.3:

$$\Pi = \gamma_0 - \gamma = \frac{\Delta F}{2(t+w)} = \frac{\Delta F}{2w} \quad (4.3)$$

if the thickness is small compared to the width of the plate ($t \ll w$).

This technique was used to explore the dynamical structural changes in lipid membrane that takes places upon mechanical compression and that arise after the addition of EGCG to the system (for further details about EGCG concentration used in each lipid monolayer studied, please see Results section). Commonly at high surface areas, the surface pressure remain unchanged since the monolayer is in a 'gaseous' state (G), meaning that the molecules have a long distance between them and thus they do not interact with each other. Upon compression, the surface pressure increases and the monolayer transits to a 'liquid-expanded' state (LE), where the molecules are closer with their hydrocarbon chains aligned in a more vertical position, although they still have a great number of gauche defects. As shown in Figure 4.2, on further compression, firstly a plateau in the isotherm corresponding to the LE and C coexistence appears and, subsequently, the surface pressure abruptly increases, indicating that the molecular interactions are maximized forming a closely packed monolayer with the lipid fatty acyl chains perfectly ordered at the water subphase (condensed state, LC). Moreover, at a certain threshold, the monolayer cannot be compressed further without become unstable and collapse, as this may form three-dimensional structures (such as aggregates), cause crack growth within monolayer and lost of material to the subphase.[2] The minimum area per molecule (A_0) at which the monolayer can be compressed without collapsing, is estimated by extrapolating the LC region of the isotherm to zero surface pressure on the molecular area axis (blue dashed line in Figure 4.2).

Furthermore, a qualitative estimation of the elastic properties of monolayer (surface compressional modulus, C_s^{-1}) can be obtained from the surface pressure—area isotherms by using Mohwald' equation[3] (4.4):

$$C_s^{-1} = -A_m \left(\frac{\partial \pi}{\partial A_m} \right)_T \quad (4.4)$$

Indeed, the stability, phase behavior and fluidity of a phospholipid monolayer

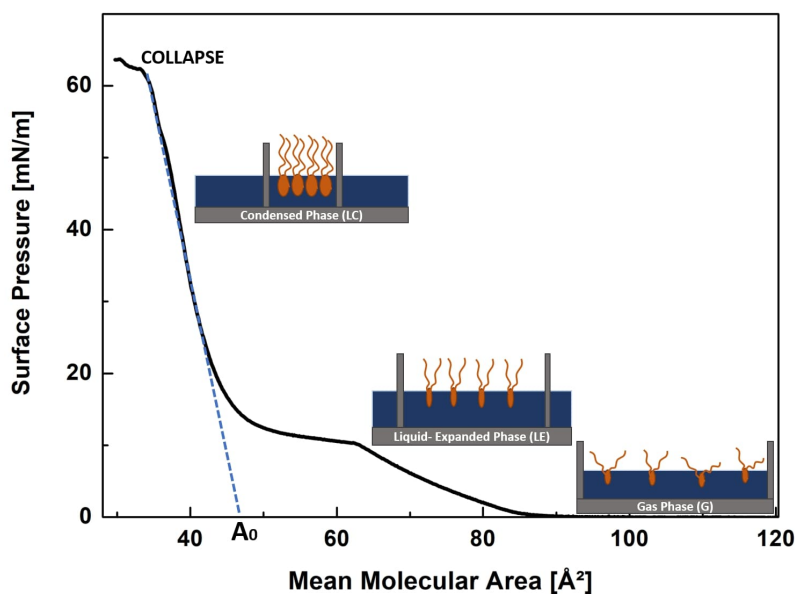


Figure 4.2: Surface pressure - area isotherm of DPPC monolayer and schematic gaseous (G), liquid-expanded (LE) and condensed (LC) phase behavior of the monolayer during compression.

can changes by the incorporation of a particular molecule. The stability and miscibility of these multicomponent monolayers are analyzed in terms of additivity rule and the excess Gibbs free energy of mixing (ΔG).[4] In theory, the area of a complete miscible or immiscible multicomponent monolayer is calculated based on the additive rule (equation 4.5):

$$A_{id} = A_1X_1 + A_2X_2 \quad (4.5)$$

where A_1 and A_2 are the molecular area of each individual component of the monolayer and the X_1 and X_2 the mole fraction of each component. Mostly, the experimental molecular area for a mixed system (A_{12}) deviates from the ideal area, due to the type of interactions established between the components in the monolayer. So, this deviation or excess area per molecule (A_{ex}) can be calculated doing the difference between the experimental determined and the ideal molecular area as showed in equation 4.6. Also, if the deviation is positive indicates repulsive interactions between the two components in the mixed monolayer, whereas a negative deviation shows attractive interactions.

$$A_{ex} = A_{12} - A_{id} \quad (4.6)$$

The ΔG for a mixed monolayer at a constant surface pressure is obtained from the following equation 4.7:

$$\Delta G = N_a \int_0^\pi A_{exc} d\pi \quad (4.7)$$

where N_A is the Avogadro number and π is the surface pressure. A negative and positive value of ΔG for the mixed monolayer means that the monolayer system is stable and unstable, respectively.

In the scope of thesis work, the surface-pressure area isotherms were used to monitor the adsorption and kinetic movement of EGCG at the air/water interface.

4.1.2 Surface Potential–Area Isotherms

The mechanism of interaction between EGCG and lipid monolayer was also determined by measuring the alterations in the monolayer surface potential. The monolayer surface potential (ΔV) is calculated by subtracting the potential of the monolayer covered subphase to that for the aqueous subphase (equation 4.8).

In the thesis work, the Kelvin vibrating capacitor technique was used to measure the potential difference (ΔV) between the vibrating plate (placed roughly 1-2 mm above the monolayer) and the reference electrode immersed into the water subphase.

$$\Delta V_{monolayer} = \Delta V_{monolayer+subphase} - \Delta V_{subphase} \quad (4.8)$$

A Langmuir monolayer at the air–water interface seems to obey the Helmholtz plate capacitor model (equation 4.9) that shows that is directly proportional to the intrinsic dipole moment of the molecule (μ_n) normal to the plane of the monolayer but, is inversely proportional to the A_m , vacuum permittivity (ϵ_0) and dielectric constant of the membrane interface (ϵ).

$$\Delta V = \frac{\mu_n}{A\epsilon_0\epsilon} \quad (4.9)$$

Further improvements in this model resulted when Demchach and Fort[5] proposed that for a non-ionised monolayer, the μ_n arises from the three independent dipole moment contributions, coming from the polar headgroups (μ_1), hydrophobic tails (μ_2) and the dipole reorientation of the water molecules at the interface (μ_3), having each region an effective dielectric constants (ϵ). Additionally, according to the Gouy–Chapman theory (equation 4.10), it should also be considered the contribution of the counter-ions in the subphase solution (Ψ_0) to ΔV , in those cases where the monolayer is partially ionised (for further details see [6] and references therein).

$$\Delta V = \frac{1}{A\varepsilon_0} \left[\frac{\mu_1}{\varepsilon_1} + \frac{\mu_2}{\varepsilon_2} + \frac{\mu_3}{\varepsilon_3} \right] + \Psi_0 \quad (4.10)$$

4.1.3 Polarization modulation-infrared reflection-adsorption spectroscopy

In the thesis work, the Polarization modulation-infrared reflection-adsorption spectroscopy (PM-IRRAS) was used to study the EGCG-induced conformational changes in lipid monolayer at molecular-level, such as the EGCG-induced alterations in the hydration status of lipid headgroups, lipid phase organization, hydrocarbon chains packing and also the dynamical changes in the hydrogen bonding networking. During PM-IRRAS measurements, the polarisation state of the infrared light that hits the monolayer at an incident angle of 80 °, is modulated into two components of radiation whom polarisation is oriented parallel (*p* polarisation) or perpendicular (*s* polarisation) to the plane of incidence, using a high frequency photoelastic modulator[7]. A portion of the light is reflected and the resulting differential reflectivity spectrum ($\Delta R/R$) correlates the parallel (R_s) and perpendicular (R_p) reflectances of the sample (equation 4.11).

$$\frac{\Delta R}{R} = \frac{(R_p - R_s)}{R_p + R_s} \quad (4.11)$$

Qualitatively, positive bands in the difference spectra indicate that the molecules have their dipole moment parallel to the interface (in-plane), whereas negative bands indicate that the dipoles are perpendicular to the water surface (out-of-plane).

Also, given that the polarisation state of incident light is modulated and that the reflection spectra of the lipid- forming surface is normalised to the reference (aqueous subphase) spectrum, the spectral interference of water vapor and carbon dioxide significantly decreases, which improves the 'in situ' PM-IRRAS spectra quality.

4.1.4 Brewster angle microscopy

The Brewster angle microscopy (BAM) was the technique used in this thesis to visualize the structural rearrangements in the monolayer that takes place due to EGCG-lipid interactions and those derived from blue radiation exposure. Shortly, the BAM technique assumes that when a *p*-polarised light enters at the air-water

interface at the Brewster angle (a particular angle of approximately 53°), no reflected light returns to the detector (BAM images appear dark). The BAM images are created considering the differences in the Brewster angle conditions arising from the presence of a monolayer on the water surface, that has a different refractive index from that of water subphase, and thus some light is reflected (BAM images became bright)[8, 9].

4.1.5 Blue LED irradiation setup

For assessment of antioxidant activity of EGCG against blue light-induced oxidative damage, the lipid monolayers were maintained under irradiation with blue LED (emission peak, 460 nm, with nominal light intensity of 77.1 mW/cm^2) positioned perpendicularly to the Langmuir trough through 25 cm above the surface illuminating the entire trough area for 1 h (Figure 4.3). After irradiation, surface-pressure area, PM-IRRAS and BAM measurements were carried out to monitor the structural changes in lipids promoted by irradiation. Control experiments were performed with the same setup but without the blue LED source. At least three replicates were performed to ensure reproducible results.

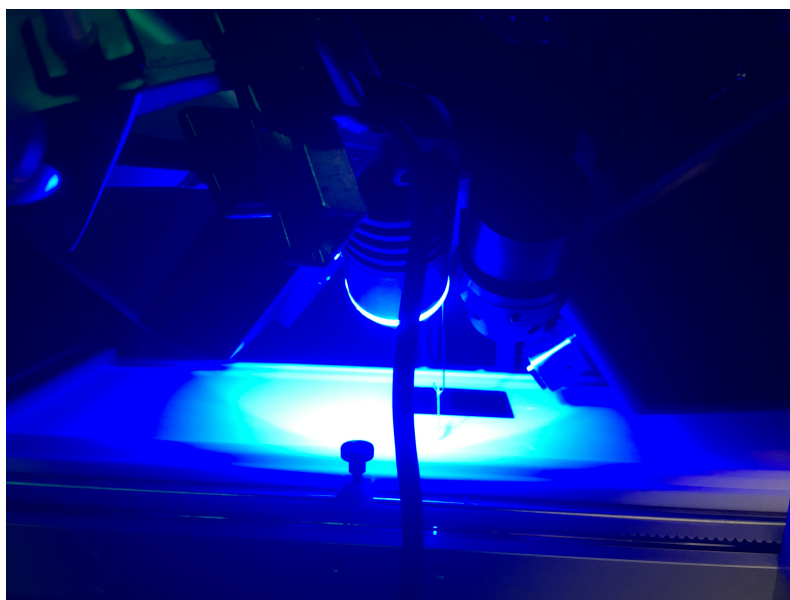


Figure 4.3: Lipid monolayer spread at air-buffer subphase exposed to blue LED irradiation for 1h.

4.2 Liposomes studies

4.2.1 Preparation of liposomes

During thesis work, the different liposomal suspensions (chemical composition and transition temperature of each phospholipid are given in Table 4.1) designed to carry and deliver EGCG, were prepared using the lipid thin-film hydration method developed by Alec Bangham and his colleagues (schematic illustration in Figure 4.4). Liposomes were made by dissolving the phospholipid in an chloroform/methanol solvent mixture into the round-bottomed flask. The solvent is evaporated under a gentle stream of nitrogen forming a dry film at the bottom of the flask. The residual traces of solvent were removed by putting the flask into an exsiccator at high vacuum for overnight. Thereafter, the dry film is hydrated by the addition of an appropriate aqueous medium for up 2 h under agitation, forming multiple concentric lipid bilayers (multilamellar vesicles). The structure of membrane phospholipids studied throughout this thesis is shown in Figure 4.5.

Table 4.1: Chemical composition and transition temperature of each phospholipid used in thesis work.

Phospholipid	Number of carbon	Headgroup Charge	Transition Temperature (°C)	Molecular Weight (g/mol)
DMPC	14:0	Neutral	24	678
DPPC	16:0	Neutral	41	734
DPPG	16:0	Anionic	41	745
DPPS	16:0	Anionic	54	736

The diameter of the multilamellar vesicles was reduced by using the probe sonication or extrusion (only used in DMPC liposomes, see further details in results section 8) techniques. Briefly, the tip sonicator is immersed into a liposomal suspension applying a high energy input that can causes local overheating, and so the liposomes-containing vessel must be immersed into an ice/water bath during the procedure. Moreover, the probe tip can also shed metal particles into the lipid suspension, evidencing a compromise between sonication time and liposomal vesicle size.

In the extrusion technique, the heterogeneous liposomal suspension is kept above the phase transition temperature and is forced to pass multiple times through a polycarbonate membrane filters with defined pore sizes, rendering unilamellar liposomes with a uniform size distribution.

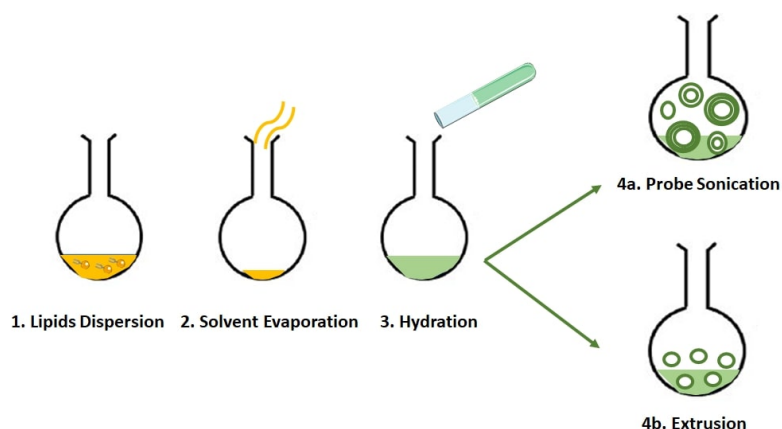


Figure 4.4: Preparation of liposomes using the dry-film hydration method.

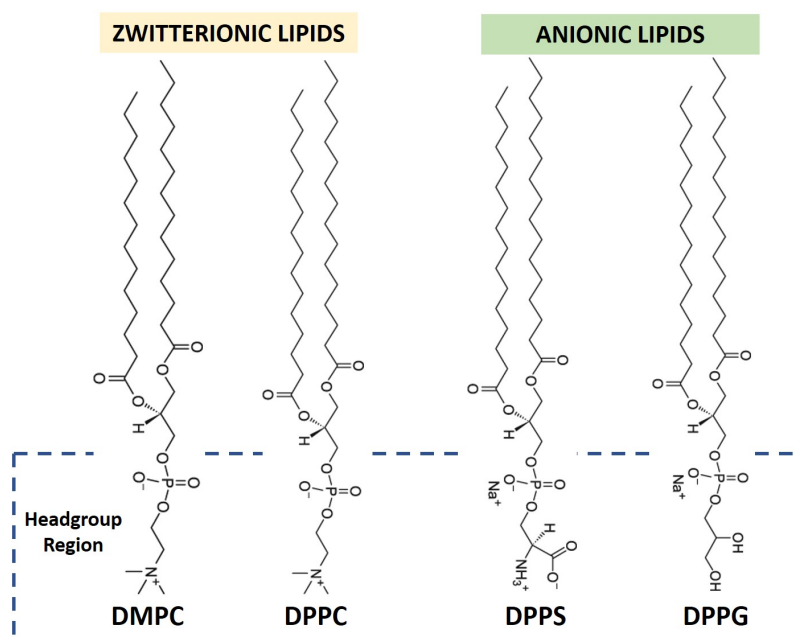


Figure 4.5: Structure of membrane phospholipids studied throughout this thesis.

4.2.2 Physicochemical characterization of liposomes

Undoubtedly, it is mandatory to characterize liposomes in terms of their size distribution, physical conformational integrity, drug-liposome interactions, encapsulation efficiency and drug delivery rates, particularly, if these systems are proposed as therapeutic agents, because these properties regulate the pharmacokinetic behavior of liposomes. Furthermore, these characterization techniques allow to analyze the batch to batch reproducibility and thus the quality of liposomes.

4.2.2.1 EGCG–liposome interactions analysis: spectroscopy

4.2.2.1.1 UV-visible Spectroscopy (UV-vis) Ultraviolet and visible (UV–vis) spectroscopy is a technique that determines the concentration of a particular sample by considering the energy absorbed by this sample at a certain wavelength. During the procedure, the electromagnetic radiation in the UV-Visible region passes through a sample and, when absorbed, it changes the distribution of electrons in the sample and promotes the electron migration from the ground state to higher energy levels (electronic transitions). This energy absorbed (ΔE) can be calculated using the Planck–Einstein equation:

$$\Delta E = h_p \nu = \frac{h_p c_L}{\lambda} \quad (4.12)$$

where h_p is the Planck's constant ($6.62607004 \times 10^{-34} \text{ m}^2 \text{ kg/s}$), ν is the frequency, c_L the speed of light in vacuum ($2.998 \times 10^8 \text{ m/s}$) and λ the wavelength, which depends of the structure of the molecule on its neighborhood. Most of the polyatomic organic molecules absorb in the near UV and visible region of the electromagnetic spectrum so, the electronic transitions from a stationary state orbital to a higher energy orbital involve π (double bonds) and n (lone pair) electrons and, usually, they appear in the absorption spectrum. According to the Beer-Lambert Law the absorbance of a given sample, at a certain wavelength, is proportional to concentration. This relationship is defined by the equation 4.13:

$$A = \varepsilon_a l c = \log\left(\frac{I_0}{I}\right) \quad (4.13)$$

where A is the absorbance, ε_a is the molar absorption coefficient (probability that the photon of that particular wavelength will be absorbed by the material), l is the optical path length, c is the molar concentration, I_0 and I is the intensity of the light beam before and after passing the cuvette with the sample. Absorption spectrum is sensitive to minor changes in chemical structure of a molecule and, sometimes, these are noticeable after occurring shifts in the absorption spectra of a particular molecule towards lower (hypsochromic shift) or higher (bathochromic shift) wavelengths.

In thesis work, the UV-Vis spectroscopy was used to verify the possible interactions EGCG-liposomes, or at least, their co-existence in solution after liposomes preparation. This technique was also used to measure the quantity of EGCG entrapped inside liposomes following dialysis and to determine the *in vitro* release of catechin from liposomes (see further details in results section). Finally,

UV-Vis spectroscopy was used as a primary technique to verify the effect of UV irradiation on the antioxidant activity of EGCG on lipid molecules.

4.2.2.1.2 Fourier Transform Infrared Spectroscopy In Fourier transform infrared spectroscopy (FTIR) measurements, some of the infrared polychromatic radiation impinged on the sample is absorbed at a particular energy, indicating that the incident radiation interacted and displaced the dipole moment of the molecule leading to a vibrational transition. So, each peak displayed on the collected absorption infrared spectrum corresponds to the frequency of a characteristic transition in vibrational state of a certain functional group that compose the molecules. In thesis work, the molecular interaction between liposomes and EGCG were characterized by using FTIR. The liposomes preparations consist of encapsulated and unencapsulated EGCG were adsorbed on calcium fluoride (CaF_2) substrates and the FTIR absorption spectrum was collected in the frequency range from 400 to 4000 cm^{-1} , with a resolution of 4 cm^{-1} , at Tensor 27 FTIR spectrometer (Bruker, Germany). The FTIR spectra provide information concerning the location of EGCG at the liposome structure and its effect on the membrane polar and nonpolar region. Additionally, the antioxidant action of EGCG on liposomes against radiation-induced damage was also investigated by the analysis of FTIR spectrum for all liposomes preparations before and after UV irradiation for different times. More specifically, the changes in the frequency and bandwidth of the characteristics bands of lipid such as, the stretching vibrations of phosphate, carbonyl and hydrocarbon chains, are monitored revealing if the presence of EGCG in the vicinity of these lipid groups decreases sensitivity to radiation. These results were complemented with data obtained by UV-vis technique.

4.2.2.1.3 Fluorescence Spectroscopy The intrinsic fluorescence of EGCG was used in the fluorescence anisotropy measurements in an attempt to determine the distribution of EGCG in the liposomal bilayer and monitor the implications of incorporation of the different EGCG concentrations (10-30 mol%) on bilayer fluidity. Polarization measurements were performed on a Horiba Jobin Yvon Spex Fluorolog 3-22 spectrofluorometer (Kyoto, Japan) with excitation at 275 nm (slit width 5 nm) and emission at 353 nm (slit width 5 nm). Also, ratiometric fluorescence measurements of di-8-ANEPPS were used to monitor the effect of increasing amounts of EGCG in the bilayer dipole potential. Shortly, after staining liposomes with di-8-ANEPPS overnight, the changes in membrane dipole potential are monitored considering the ratio of the fluorescence intensity at 630 nm of

di-8-ANEPPS excited at 420 nm to that excited at 520 nm (for further detail see chapter 8).

4.2.2.2 Drug–liposome interactions analysis: molecular simulations

Molecular simulations were used to study the dynamic interactions between atoms and molecules at specific time periods and the forces acting on each atom. These forces were determined by solving Newton’s motion equations obtaining new position coordinates and the velocities for each atom. Furthermore, the interactions between the molecules are modelled by a potential energy function (known as force field) that considers the sum of individual potentials associated to bond lengths, bond angles and torsions (covalent contributions) and also those from the non-bonding van der Waals and Coulomb interactions between atoms (simplified equation 4.14).

$$V(\vec{r}) = V_{bonds} + V_{angle} + V_{dihe} + V_{imp} + V_{vdW} + V_{Coulomb} \quad (4.14)$$

All atom molecular dynamics simulations were carried out using the Gromacs package (version 2016) and the Gromos 54A7 as the atom force field and so, a general force field can be written as follows (equation 4.15):

$$\begin{aligned} V(\vec{r}^N) = & \sum_{bonds}^N \frac{1}{4} k_b [b_n^2 - b_0^2]^2 + \sum_{angle}^N \frac{1}{2} k_\theta [\cos(\theta) - \cos(\theta_0)]^2 \\ & + \sum_{dihe}^N \frac{1}{2} k_\varphi [1 + \cos(\delta_n) \cos(m_n \varphi_n)] + \sum_{imp}^N \frac{1}{2} k_\xi [\xi_n - \xi_0]^2 \\ & + \sum_{vdw} 4\varepsilon_{ij} \left[\left(\frac{\sigma_{ij}}{r_{ij}} \right)^{12} - \left(\frac{\sigma_{ij}}{r_{ij}} \right)^6 \right] + \sum_{Coulomb}^N \frac{q_i q_j}{4\pi \varepsilon_0 \varepsilon_r r_{ij}} \end{aligned} \quad (4.15)$$

where V is the potential energy function, \vec{r} is the position vector for N atoms, b and r_{ij} the inter-particle distance, θ is the bond angle, φ is the dihedral angle, m_n is the dihedral multiplicity and δ_n the phase angle. Also, the ξ_n is the improper dihedral angle, the q is the partial charge, ε_r is the relative permittivity, the σ is a finite distance where the net electric potential is zero. Finally, the k_{bonds} , k_θ , k_φ and k_ξ represent the respective forces constants.

The specific details for the molecular dynamics simulations are discussed in respective chapter 8. In the thesis scope, a coarse-grained liposome model was developed by colleagues from Machuqueiro’ Simulation Group (FCUL institution), to model the distribution and interactions of EGCG inside of the lipid bilayer at

molecular level, thus providing the basis for improve the efficiency of experimentally designed liposomes.

4.2.2.3 Liposomes size analysis

In thesis work, the liposome size distribution was determined in the Zetasizer Nano ZS90 apparatus (Malvern Instruments Inc. He–Ne laser of 633 nm, detection angle of 90 °) using the Photon correlation spectroscopy also known as dynamic light scattering (DLS). During the procedure, a monochromatic laser beam hits the liposomal suspension and the time-dependent fluctuations of the light scattered from particles are measured in a photon detector. The light scattering results from random motion (Brownian motion) of the particles, since they are continually colliding and interacting with solvent molecules. According to Stokes-Einstein equation (equation 4.16) the movement (diffusion, D_T) of these particles is inversely proportional to their size, meaning that larger particles diffuse more slowly than small ones.

$$D_T = \frac{k_B T}{6\pi\eta R_H} \quad (4.16)$$

In the equation, k_B is the Boltzmann constant, D_T is the diffusion velocity of the particle, which depends of the temperature (T) and the viscosity of the solution (η), and R_H is the hydrodynamic radius of the particle.

4.2.3 UVC irradiation setup

For the UV irradiation experiments, the liposomal suspensions consist of encapsulated and unencapsulated EGCG were placed in closed quartz cells or adsorbed on CaF_2 substrates and then, irradiated with a 254 nm UVC germicid lamp (Philips TUV PL-S 55W/2P 1CT) at a radiance of 1.9 W/m^2 . Afterwards, the damage caused by UV radiation was recorded by measuring the UV–vis and infrared absorption spectra of the liposomal suspensions and cast films, respectively, over the irradiation time.

4.2.4 Immobilization of EGCG-loaded liposomes on nanofibers: electrospinning

Electrospinning was used to incorporate EGCG-loaded liposomes into nanofibers. During the procedure, a highly viscous synthetic or natural polymeric solution of choice is placed in a syringe, pumped at a constant flow rate and is injected

through a needle, due to the high voltage electric field applied to the tip of the needle (usually between 10 and 30 kV) and the collector. The polymeric solution is only successfully electrospun into nanofibers when the electric field distort the polymeric droplet at the tip of the needle into a conical shape (Taylor cone) thus ejecting a charged jet of fluid towards the collector (for further details see Chapter 9). The surface morphology and size of the nanofibers were evaluated using a Zeiss Auriga scanning electron microscope (SEM).

4.2.5 Cellular studies

4.2.5.1 Cell lines

Vero cells (monkey kidney epithelial cells) were used for the in vitro cytotoxicity assays of EGCG and of nanofibers extracts. Human fetal foreskin fibroblasts (HFFF2, European Collection of Authenticated Cell Cultures, UK), were used in cell survival assays after cell exposure to H_2O_2 or UV radiation (for further details about cell culture conditions used in cytotoxicity and cell viability assays see Chapter 9).

4.2.6 Statistical Analysis

The Principal Component Analysis (PCA) and 2D–correlation spectroscopy were two mathematical techniques applied to the UV–vis or the IR spectra of each irradiated liposomal suspension, to analyse small changes in measured signals and then, extract information about the protective role of EGCG against UV damage (more details are shown in Chapter 7).

For cell-based experiments, one-way or two-way ANOVA with Tukey’s post-tests were performed to determine significant differences. All the experiments were performed in triplicate. P values lower than 0.05 (*), 0.01 (**), and 0.001 (***) indicates that differences are statistically significant. Mean \pm SEM was plotted on all graphs.

References

- [1] C. Constantino, A Dhanabalan, and O. Oliveira Jr. “Experimental artifacts in the surface pressure measurement for lignin monolayers in Langmuir troughs.” In: *Review of scientific instruments* 70.9 (1999), pp. 3674–3680.
- [2] K. Lee and Y. C. “Collapse mechanisms of Langmuir monolayers.” In: *Annu. Rev. Phys. Chem.* 59 (2008), pp. 771–791.

-
- [3] H Mohwald, R Lipowsky, and E Sackmann. In: *Handbook of biological physics*. Elsevier Science, 1995.
- [4] R Seoane, P Dynarowicz-Tstka, J Minones Jr, and I Rey-Gomez-Serranillos. “Mixed Langmuir monolayers of cholesterol and essential fatty acids.” In: *Colloid and Polymer Science* 279.6 (2001), pp. 562–570.
- [5] R. J. Demchak and T. Fort Jr. “Surface dipole moments of close-packed un-ionized monolayers at the air-water interface.” In: *Journal of Colloid and Interface Science* 46.2 (1974), pp. 191–202.
- [6] O. N. Oliveira and C. Bonardi. “The surface potential of Langmuir monolayers revisited.” In: *Langmuir* 13.22 (1997), pp. 5920–5924.
- [7] R. Mendelsohn, G. Mao, and C. R. Flach. “Infrared reflection–absorption spectroscopy: principles and applications to lipid–protein interaction in Langmuir films.” In: *Biochimica et Biophysica Acta (BBA)-Biomembranes* 1798.4 (2010), pp. 788–800.
- [8] D. Hoenig and D. Moebius. “Direct visualization of monolayers at the air-water interface by Brewster angle microscopy.” In: *The Journal of Physical Chemistry* 95.12 (1991), pp. 4590–4592.
- [9] S Hénon and J Meunier. “Microscope at the Brewster angle: Direct observation of first-order phase transitions in monolayers.” In: *Review of Scientific Instruments* 62.4 (1991), pp. 936–939.

MONOLAYER RESULTS

Effect of blue light irradiation on the stability of phospholipid molecules in the presence of epigallocatechin-3-gallate¹

Abstract

In this paper, we report on the effects from epigallocatechin-3-gallate (EGCG), a phytochemical flavonoid present in green tea, on Langmuir monolayers of 1,2-dipalmitoyl-*sn*-glycero-3-[phospho-*rac*-(1-glycerol)] (sodium salt) (DPPG), including experiments with blue light irradiation. EGCG was found to interact with both the DPPG headgroups and hydrophobic tails, thus affecting the lipid packing according to surface pressure and surface potential isotherms and polarization-modulated infrared reflection absorption spectroscopy (PM-IRRAS) data. Blue light irradiation caused considerable changes in the surface pressure isotherms and PM-IRRAS spectra of DPPG monolayers, but the effects were considerably less when EGCG was present. For the surface pressure isotherms, for instance, no irradiation effect could be measured for mixed EGCG-DPPG monolayers. It is concluded that EGCG protected the DPPG molecules from degrading upon blue light irradiation, which means that EGCG may be a preventive and therapeutic agent to decrease photosensitivity of phospholipids to blue light oxidative damage, a pathogenic mechanism in skin disorders.

¹This chapter is based on the following publication:

Pires, F., Geraldo, V. P., Antunes, A., Marletta, A., Oliveira Jr, O. N., and Raposo, M.. Effect of blue light irradiation on the stability of phospholipid molecules in the presence of epigallocatechin-3-gallate. *Colloids and Surfaces B: Biointerfaces* 2019, 177: 50-57, DOI:10.1016/j.colsurfb.2019.01.042

5.1 Introduction

Natural sunlight is photocarcinogenic to human skin owing to its ionizing radiation (UV radiation) as extreme exposure to UVB (290-320 nm) and UVA (320-400 nm) light triggers mutagenic effects on DNA to form cyclobutane pyrimidine dimers.[1, 2, 3] In recent years, there has been evidence that blue light (400-495 nm) is also phototoxic, causing skin ageing and pigmentation.[4, 5, 6] Kushibiki et al. reported cytotoxic effects from blue laser irradiation with power density of 100 mW/cm^2 on fibroblasts, lung cancer cells, and human cervix adenocarcinoma cells, owing to a marked increase in the synthesis of intracellular reactive oxygen species (ROS). This increment in ROS generation in the cytoplasm was not observed for cells exposed to red or near-infrared lasers, although some mitochondrial ROS could have been produced but not detected with the fluorescent CM-H2DCFDA probe used.[7] Blue light photons are also absorbed by enzymes (flavins), flavoproteins, photoreceptors (cryptochrome 2) and cell mitochondrial respiratory components (cytochrome c oxidase), and therefore prolonged exposure could impair intracellular events and contribute to tumorigenesis.[8, 9, 10]

Furthermore, ROS resulting from blue light-induced mitochondrial oxidative stress may cause DNA lesions, induce membrane lipid oxidation, increase the rate of ATP depletion and the membrane permeability, which for retinal pigment epithelial cells leads to cell dysfunction and retina aging.[11, 12, 13, 14, 15, 16]

Such photoinduced effects can be at least partially mitigated with incorporation of some herbal drugs into daily diet. For example, the polyphenol flavonoid catechins, which are present in green tea, protect biomolecules from radiation-induced damage by acting as antioxidant and free radical scavengers. This activity is believed to occur due to the affinity of catechins to lipid bilayers that make the framework of cell membranes.[17, 18, 19, 20] This activity is believed to occur due to the affinity of catechins to lipid bilayers that make the framework of cell membranes.[21] The interaction between catechins and cell membranes has been investigated with techniques such as Flicker spectroscopy, nuclear magnetic resonance (NMR), differential scanning calorimetry (DSC), and fluorescence spectroscopy. [22, 23, 24, 25, 26] However, to our knowledge the number of studies on molecular-level interactions with the lipids at the membrane is rather scarce. Since the cell membrane is complex, with a varied composition of phospholipids and proteins, this type of investigation is performed with simplified models such as Langmuir monolayers[27] as it was done by Collado et al.[28] for catechins. Another possible model involves liposomes made with different types of lipids, as in recent works from our groups where the lipid electrical charge was found to

be relevant for incorporation of phytomolecules that affect the level of protection against oxidizing agents.[29, 30]

In this paper, we report on the interaction between epigallocatechin-3-gallate (EGCG), the major catechin in green tea leaves, and monolayers of 1,2-dipalmitoyl-*sn*-glycero-3-[phospho-*rac*-(1-glycerol) (sodium salt) (DPPG), with special emphasis on effects of blue light irradiation. DPPG is a negatively-charged unsaturated phospholipid found in the pulmonary surfactant that confers protection to the surfactant protein B against oxidation, thus decreasing the risk of respiratory diseases.[31, 32] It was chosen for this study to infer possible synergistic effects with EGCG in protecting cells against irradiation, and because it has fusogenic properties that seem to increase the liposome uptake into target cells.[33, 34, 35] In order to probe the intermolecular interactions and the effect from blue light irradiation, the monolayer properties were evaluated using surface pressure isotherms and polarization-modulated infrared reflection absorption spectroscopy (PM-IRRAS).

5.2 Experimental Details

5.2.1 Chemicals

EGCG (M.W. 458.4 g/mol) and DPPG (M.W. 744.96 g/mol) were purchased from Sigma-Aldrich and Avanti Polar Lipids, respectively.

5.2.2 Langmuir monolayers

The co-spreading methodology was used to prepare Langmuir monolayers to study the interaction between EGCG and DPPG. DPPG and EGCG were dissolved in a chloroform and methanol (4:1) mixture in concentrations of 0.5 mg/mL and 0.3 mg/mL, respectively. These values have been chosen to maintain the same number of moles in each solution. Aliquots of 50 μ L of pure DPPG or DPPG-EGCG mixtures, namely, DPPG(95%)-EGCG(5%), DPPG(93%)-EGCG(7%) and DPPG(87%)-EGCG(13%), were spread on an aqueous subphase to obtain Langmuir monolayers. Milli-Q water at $24 \pm 1^\circ$ C was used as the subphase. After spreading the solvent was allowed to evaporate for 10 min. The surface activity of EGCG was assessed without spreading the phospholipids by compressing the barrier and measuring the surface pressure, π , using the Wilhelmy plate method. All experiments were repeated at least three times to ensure reproducibility of the isotherms. The mean molecular area (A_m) is calculated using:

$$A_m = \frac{A_{LT} \times M}{c \times N_A \times V} \quad (5.1)$$

where the A_{LT} is the Langmuir trough area, M is the molecular mass, c is the concentration, N_A is the Avogadro number and V is the solution's volume spread. In the case of DPPG+EGCG mixtures, the average molar mass (MMA) obtained with the molar fractions of EGCG and DPPG was used as M value. The experimental molecular areas were compared with the theoretical molecular areas predicted by the additivity rule (see later). Surface potential and surface pressure measurements were made with a Langmuir mini trough from KSV Instruments, in a class 10,000 clean room. Film compression was carried out using two symmetrically movable barriers at a constant barrier speed of 10 mm/min. The stability of the mixed DPPG-EGCG monolayers at the air-water interface was verified through hysteresis measurements, which consisted of successive compression/decompression cycles (11 cycles). Surface potential was measured using the vibrating plate method (frequency 300 Hz) with a KSV Kelvin probe. Both reference and vibrating plate electrodes are made of platinum and the probe was located roughly 1-2 mm above the water surface. The irradiation experiments were performed with the barriers open to promote enhanced ROS via water radiolysis as the number of solvating water molecules is higher for large areas per lipid. A blue LED (ca. 460 nm, with nominal light intensity of 77.1 mW/cm^2) was positioned perpendicularly to the Langmuir trough 25 cm above the surface illuminating the entire trough area during 1 h. After irradiation, film compression was carried out at a constant barrier speed of 10 mm/min. Control experiments were performed with the same setup but without the blue LED source. Polarization-modulated infrared reflection absorption spectra (PM-IRRAS) measurements were performed using a KSV PMI 550 instrument (KSV Instruments, Finland) at an incidence angle of 80° . The DPPG-EGCG mixtures were spread on an aqueous subphase, and then compressed up to 30 mN/m. The spectra were measured for *s*- and *p*- polarizations at a high frequency. All the spectra shown were obtained by subtracting the baseline which corresponded to the spectrum of a pure water subphase.

5.3 Results and Discussion

5.3.1 Surface Pressure Isotherms

The surface pressure isotherms for monolayers containing guest molecules can be represented either in terms of area per molecule - with the guest molecules being

assumed to occupy an area at the interface and being therefore considered in the number of total molecules - or area per lipid molecule. In the latter case, the total number of molecules used in the calculations is the number of lipid molecules (hence area per lipid molecule is used in the x-axis of the isotherms), disregarding the number of guest molecules. The isotherms so obtained for monolayers of DPPG-EGCG mixtures are given in Figure A.1 in the Appendix A . The surface pressure isotherms with area per molecule are shown in Figure 5.1A. The isotherm for pure DPPG does not display any coexistence region of liquid expanded and liquid condensed (LE-LC) phases, in contrast to what was observed by Dicko et al.[36] and Vollhardt et al.[37]. The LE-LC transition is very sensitive to parameters such as temperature and ionic strength. Vollhardt et al. mentioned that the LE-LC transition plateau is only observed in the temperature range between 26° and 37°C for a pure water subphase. Dicko et al. used 150mM NaCl subphase. Therefore, the reason why we did not observe the LE-LC transition may be the use of a pure water subphase at a lower temperature (24°C) than in other studies. The incorporation of EGCG causes no appreciable change in the collapse pressure, typically around 55-57 mN/m. DPPG+EGCG isotherms are shifted to smaller areas per molecule with increasing EGCG concentration from 5 to 13% in mol, suggesting that EGCG condenses the monolayer. Effects from the EGCG concentration changes are better seen in the area versus concentration plot in the inset of Figure 5.1A, which deviates from the straight line predicted by the additivity rule according to which the area per molecule should be: $A_{theoretical} = X_{lipid} A_{lipid} + X_{EGCG} A_{EGCG}$, where X_{lipid} and X_{EGCG} are the mole fractions of each component, and A_{lipid} and A_{EGCG} are the areas occupied by each component in neat Langmuir monolayers. Because the measured areas are smaller than predicted from the additivity rule, one infers there are attractive interactions between EGCG and DPPG. It is worth mentioning that EGCG did not form a Langmuir film on its own as it was necessary to spread a large number of molecules to obtain the surface pressure isotherm. The area per molecule thus calculated as if a true monolayer had been formed is much smaller than expected for the size of the molecule. The results of the additivity rule are therefore only useful for the characterization of the mixed films.

The surface compressional modulus (C_s^{-1}), calculated from the surface pressure isotherms using $C_s^{-1} = -A \left(\frac{\partial \pi}{\partial A} \right)_T$, is used to explain qualitatively changes in the mechanical properties of the monolayer. Differences in lipid phase transitions (e.g. LE-LC) as well as in monolayer elasticity can be probed. A decrease in C_s^{-1} means that the monolayer is more compressible/flexible, thus the lipids are not closely packed. Values of C_s^{-1} below 100 mN/m indicate that the monolayer is

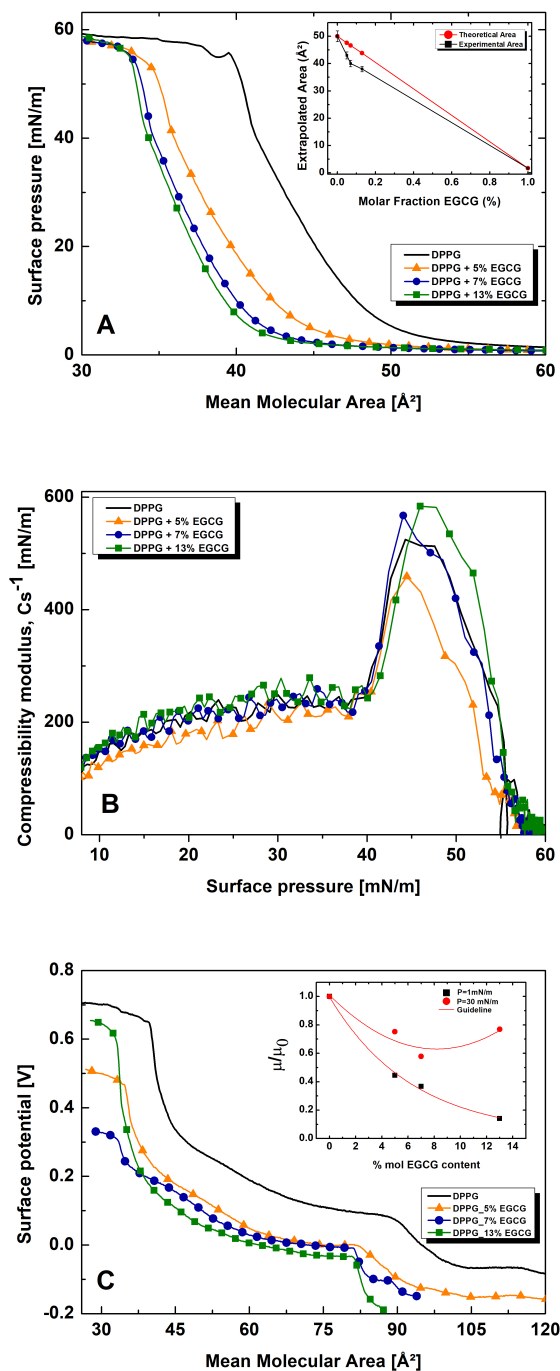


Figure 5.1: Surface Pressure for DPPG monolayers with different contents of EGCG at the water interface. In the inset is shown the additivity rule data obtained from DPPG+EGCG pressure area isotherms, with evidence for the attractive interactions between EGCG and DPPG with slight deviation from the theoretical area. B. Compressional modulus vs surface pressure for DPPG and DPPG + EGCG monolayers at the air/water interface. C. Surface Potential isotherms of DPPG + EGCG monolayers at various concentrations. The top-right inset in C shows the ratio between the apparent dipole moment of DPPG + EGCG (μ) and pure DPPG (μ_0) vs. EGCG concentration at 1 mN/m and 30 mN/m. The solid lines in the graph are only to guide the eyes

in a LE phase. For Cs^{-1} between 100-250 mN/m the monolayer is considered as being in a LC phase, while values higher than 250 mN/m denote that the monolayer is in a solid state.[38] Figure 5.1B shows that DPPG reaches a Cs^{-1} value of 500 mN/m, i.e. in the solid state. The introduction of 5 mol% EGCG practically does not affect Cs^{-1} at surface pressures below 40 mN/m. Above 40 mN/m, Cs^{-1} decreases from 524 mN/m for DPPG to 451 mN/m for 5% EGCG cospread. For the higher concentrations of EGCG (7-13 mol %), Cs^{-1} at surface pressures above 40 mN/m is higher than for DPPG, indicating that the incorporation of EGCG turns the monolayer more rigid (less compressible).

The surface potential depends on the charge and orientation of the molecules on the surface, being more sensitive than pressure for area-dependent effects. The curve for neat DPPG in Figure 5.1C starts off at a negative surface potential (- 0.1 V) for large areas per molecule due to the electrical double layer, arising from the negatively-charged DPPG headgroups and the counter-ions in the subphase solution.[39] It increases abruptly upon packing of the molecules. The introduction of 5-13 mol% of EGCG into the DPPG monolayer caused an overall decrease in surface potential. Such a decrease could be caused by additional charge brought by EGCG[40], as EGCG molecules should be partially charged at the interface (the pKa for the charged groups of EGCG are 7.6 and 10.7). However, the surface potential for the monolayer with 13% mol of EGCG is higher than for the smaller concentrations, and therefore the additional charge cannot be the sole factor to explain the changes in potential. Additional factors should be taken into account, and indeed there is a competition of effects to explain the non-monotonic dependence on concentration of the apparent dipole moment in the inset of Figure 5.1C. These factors may include the intrinsic dipole moment of catechins [41, 42], and the changes induced by EGCG on the packing of DPPG molecules, as inferred from the surface pressure isotherms. Furthermore, as we shall see when the PM-IRRAS spectra are discussed, the incorporation of EGCG affects the hydration and conformation of DPPG headgroups, which causes the monolayer surface potential to change.

5.3.2 PM-IRRAS

The PM-IRRAS spectra for neat DPPG and EGCG monolayers and mixed DPPG + EGCG monolayers at 30 mN/m are shown in Figure 5.2A for distinct wavenumber regions. These spectra were subtracted from the spectrum of the water interface obtained without film. In the region between 3000 to 2800 cm^{-1} (Figure 5.2A), information is inferred about CH_2 groups. Two strong bands appear at 2919

cm^{-1} and 2851 cm^{-1} for DPPG, with the band at 2919 cm^{-1} being decomposed into two Gaussian bands at 2947 cm^{-1} and 2919 cm^{-1} while the band at 2851 cm^{-1} can be decomposed into two Gaussian bands at 2880 cm^{-1} and 2851 cm^{-1} . The inset in Figure 5.2A shows this decomposition. The positions of these bands are close to those obtained by Dicko et al.[36] The bands at 2919 cm^{-1} and 2851 cm^{-1} are assigned to CH_2 antisymmetric and symmetric stretching vibrations, respectively, while the weak bands at 2947 cm^{-1} and 2880 cm^{-1} are assigned to the antisymmetric and symmetric stretching vibrations, respectively, of terminal CH_3 groups. The changes in wavenumber and width of the methylene infrared bands provide information about chain conformation.[43] The parameter of order, calculated from the ratio between the intensity of these bands $\left(\frac{I_{2916}}{I_{2851}}\right)$ [44], is 1.9, 2.0, 1.7, 1.8 as EGCG concentration increased from 0 to 13%. Therefore, the order parameter is little influenced by EGCG. However, with increasing percentage of EGCG the band position for the antisymmetric stretching of methylene groups was shifted to lower wavenumbers. In addition, the affinity between EGCG and DPPG phospholipids is also suggested by the changes in intensity and band width at 2920 cm^{-1} after incorporation of EGCG, consistent with the change in surface potential of the DPPG monolayer in Figure 5.1C.

The region of C=O vibrations in Figure 5.2C can be decomposed into two Gaussian bands at 1740 cm^{-1} and 1760 cm^{-1} , assigned to hydrogen and non-hydrogen bonded carbonyl groups, respectively.[45, 46] According to the literature [47, 48], phosphate and carbonyl groups are hydration centers surrounded by a layer of water molecules at the interface that modulates the thermodynamics and surface membrane properties such as dipole potential. The carbonyl stretching mode is strongly affected by EGCG since it is a polyhydroxylated molecule that decreases the number of water molecules bound to carbonyl groups. As a consequence, the C=O orientation may change to affect the dipole moment (and surface potential). In addition, the changes in degree of freedom of carbonyl induced by EGCG modify the exposure of hydrocarbon chains of phospholipids, which tend to minimize the area exposed to water since they are hydrophobic.

The spectra region between 1200 and 1300 cm^{-1} in Figure 5.2C is associated with the lipid head groups, hydrogen bonds and hydration. The band at 1257 cm^{-1} in DPPG is decomposed into two Gaussian bands at 1230 cm^{-1} and 1257 cm^{-1} corresponding to P=O antisymmetric stretching of PO_4^- group and P=O antisymmetric stretching of hydrated PO_4^- group, respectively. In DPPG cast films these bands appear at 1222 cm^{-1} and 1241 cm^{-1} , respectively. For DPPG+EGCG, the Gaussian decomposition yields two bands at 1235 cm^{-1} and 1262 cm^{-1} , suggesting that the presence of EGCG shifted the spectra to higher wavenumbers. In

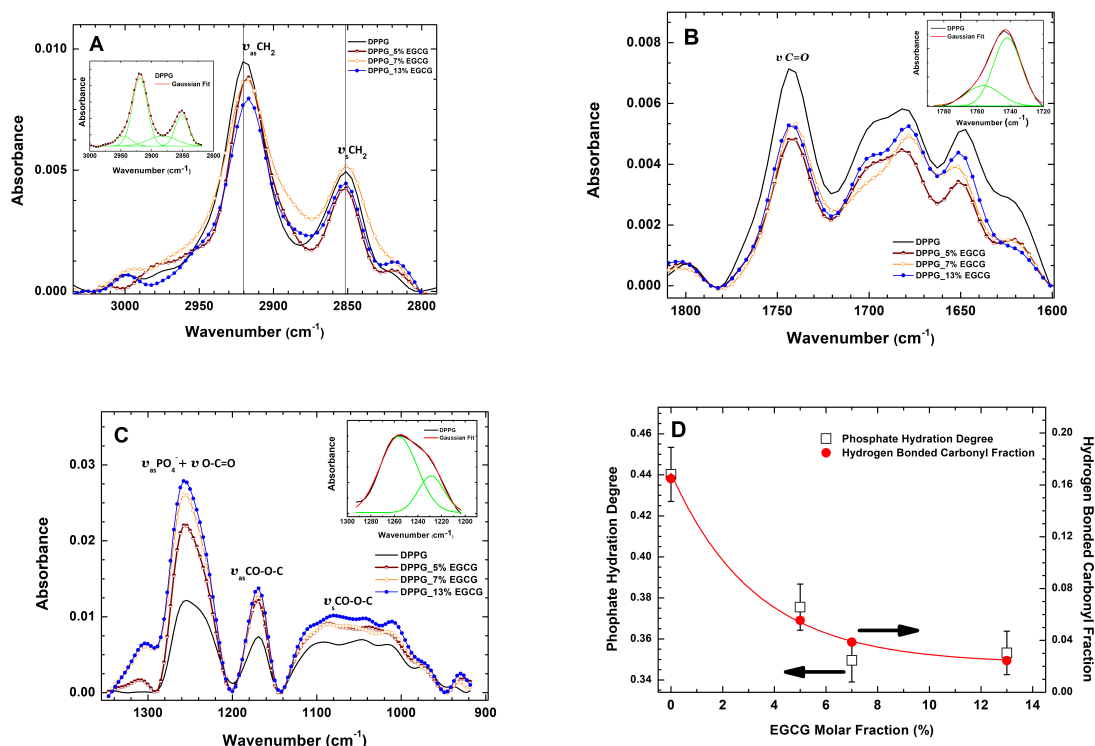


Figure 5.2: PM-IRRAS spectra of DPPG monolayers with different EGCG percentages in aqueous solutions at a surface pressure of 30 mN/m in the wavelength region of: A. 3000 to 2600 cm^{-1} ; B. 1800 to 1600 cm^{-1} and C. 1350 to 900 cm^{-1} . The plot shows the degree of hydration of phosphate groups and hydrogen bonded carbonyl groups fraction ions calculated by fitting the IRRAS spectra (D). The solid line is a fitting with an exponential function.

DPPG, the presence of the glycerol esterified to phosphate inserts a charge at the surface which is sufficient to change water organization. Analyzing the bands at 1257 cm^{-1} (PO_4^- hydrated groups) in Figure 5.2C and 1743 cm^{-1} (C=O) in Figure 5.2B, one notes that EGCG affects hydrogen bonding of PO_4^- groups with water molecules. Note that the band at 1257 cm^{-1} is shifted from 1236 cm^{-1} assigned to the stretching mode of O-C=O group of EGCG. In fact, EGCG has affinity to phosphate groups creating a hydration stress, since these molecules compete with water molecules excluded from the surface or replace them nearby the phosphate groups, affecting the thermodynamic balance of the membrane. The increase in intensity of the phosphate band of DPPG with increasing EGCG concentration in Figure 5.2C is due to the absorption of carboxylate groups of EGCG. For DPPG, this region can be represented by two Gaussian bands, with correlation coefficient of 0.99976, at $1232.2 \pm 0.8 cm^{-1}$ and at $1260.4 \pm 0.7 cm^{-1}$, with width at half maximum of $29 \pm 1 cm^{-1}$ and $28.1 \pm 0.6 cm^{-1}$. The bands are assigned to the most

and least hydrated phosphates, respectively. [49] For EGCG, this region is represented by a Gaussian band, with correlation coefficient of 0.99659, at $1255.8 \pm 0.3 \text{ cm}^{-1}$ and with width at half maximum of $55 \pm 2 \text{ cm}^{-1}$. The relation between the most and least hydrated phosphates was obtained by fitting the spectra of the mixtures of DPPG with EGCG with the three Gaussian bands mentioned above. From the areas of these bands the ratio $\left(\frac{A_{1232}}{A_{1232}+A_{1260}}\right)$, where A_{1232} and A_{1260} are the areas under the bands at 1232 cm^{-1} and 1260 cm^{-1} , respectively. Within the same rationale, the fraction of hydrogen-bonded carbonyl groups was obtained by dividing the area under the band at 1740 cm^{-1} by the total area of the bands ($A_{1740} + A_{1760}$). The ratios representing the degrees of hydration were plotted as a function of EGCG concentration in Figure 5.2D, where a decrease in phosphate as well as carbonyl hydration is observed with increasing EGCG concentration.

In summary, the PM-IRRAS results provided significant evidence of structural rearrangements in the DPPG monolayer induced by EGCG. Differences appeared in the vibrational modes of carbonyl and phosphate groups, caused by competition among EGCG and water molecules. This competition alters hydrogen bonding between phosphate groups-water molecules and induces structural rearrangements, e.g. in carbonyl groups (C=O) of DPPG, which may be the reason for the changes in surface potential shown in Figure 5.1C.

5.3.3 Irradiation of phospholipid monolayers

DPPG monolayers were exposed to a blue LED in the presence and absence of EGCG. Figure 5.3A shows that this exposure shifted the isotherm of pure DPPG monolayer to larger molecular areas, e.g. with the minimum phospholipid area changing from $44 \pm 7 \text{ \AA}^2$ to $50 \pm 3 \text{ \AA}^2$ after 1h of exposure. In contrast, for the mixed EGCG-containing monolayers in Figure 5.3B, blue light irradiation does not affect the surface pressure isotherms, for any of the EGCG concentrations tested. For example, the minimum area for the DPPG+13% EGCG monolayer was $47 \pm 2 \text{ \AA}^2$ and $47 \pm 5 \text{ \AA}^2$ with and without exposure to blue light, respectively. Significantly, the irradiated mixed monolayers were stable, as confirmed with hysteresis measurements in compression-decompression cycles and area versus times measurements in Figure A.2 in the Appendix A.

Because the changes in the surface pressure isotherms owing to blue light exposure were small for pure DPPG and negligible for the EGCG-containing mixed monolayers, we investigated the possible role of EGCG with PM-IRRAS spectroscopy. We selected the composition with the highest EGCG concentration

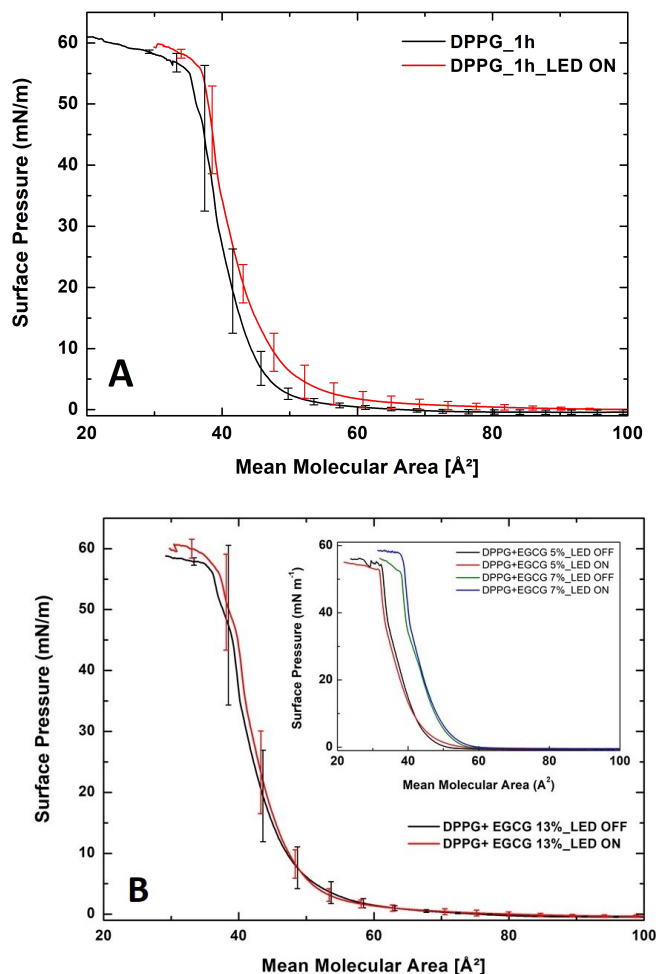


Figure 5.3: Irradiation with blue light of pure DPPG (A) and DPPG+13 mol% EGCG (B) monolayers isotherms. The top-right inset in B shows the blue light-irradiated DPPG monolayers in the presence of 5 and 7% EGCG. The error bars represent the standard deviation (SD) of 3 independent experiments.

(13%) as stronger effects are expected. The PM-IRRAS spectra are shown in Figure 5.4 for monolayers of DPPG and DPPG+EGCG 13%, before and after 1 h of blue light irradiation. The first thing to be noted in the three regions of the spectra analysed is that irradiation does affect the monolayers, with effects being stronger for pure DPPG. In the spectral region corresponding to the hydrocarbon chains in Figure 5.4A, irradiation induced a decrease in the intensity and a slight shift in the frequency of the symmetric and antisymmetric stretching of lipid acyl chains from $2851 \pm 3 \text{ cm}^{-1}$ and $2919 \pm 1 \text{ cm}^{-1}$ to $2844 \pm 1 \text{ cm}^{-1}$ and $2911 \pm 2 \text{ cm}^{-1}$, respectively. In the absence of EGCG, radiation leads to a disordering effect on phospholipid fatty acids chains, observed by the decrease in the ratio

of 2920/2850 band intensity, which reflects the balance between trans-gauche conformations. Thus, the decrease of this ratio means that the number of gauche conformers is increasing with radiation exposure. Figure 5.4B shows that even in the presence of 13 mol% of EGCG, the DPPG acyl chains are affected by irradiation as seen with the appearance of a small shoulder at 2971 cm^{-1} (CH_3 antisymmetric stretching).

The effect of irradiation on the phosphate moiety of DPPG was investigated by analysing the P=O stretching band in Figure 5.4C, which is decomposed into three Gaussian bands at $1222 \pm 4\text{ cm}^{-1}$, $1238 \pm 2\text{ cm}^{-1}$ and $1260 \pm 2\text{ cm}^{-1}$, with width at half maximum of $21 \pm 3\text{ cm}^{-1}$, $25 \pm 6\text{ cm}^{-1}$ and $28 \pm 1\text{ cm}^{-1}$. These bands are assigned to dihydrated, monohydrated and dehydrated PO_2^- groups, respectively. Upon irradiation, the band assigned to partially hydrated phosphates (1260 cm^{-1}) shifted to lower wavenumbers (1247 cm^{-1}), meaning that the resulting free radicals strongly disturb phosphate-water interactions. The drastic shift in the band frequency of the PO_2^- antisymmetric stretching to lower wavenumbers indicates formation of hydrogen bonding between DPPG phosphate groups and water molecules (increase in the ratio of hydrated phosphate vs dehydrated phosphate). Also, the exposure to blue light narrowed the bandwidth (bandwidth = 42.44, breakdown factor = 1.18) suggesting that the released ROS interferes in the lipid phosphate mobility. The decomposed spectrum of P=O band for the DPPG+13% EGCG monolayer in Figure 5.4D has two Gaussian bands at $1237.5 \pm 1.6\text{ cm}^{-1}$ and $1261.8 \pm 0.9\text{ cm}^{-1}$, with width at half maximum of $34 \pm 2\text{ cm}^{-1}$ and $27 \pm 1\text{ cm}^{-1}$. Upon irradiation, this phosphate band changes in shape exhibiting two well-defined bands at 1262 cm^{-1} and 1227 cm^{-1} assigned to dehydrated and hydrated phosphate groups, respectively. Although the split into two bands suggests a heterogenous population, the population of hydrated phosphates is lower in the presence of EGCG, even after irradiation, in contrast to what was observed for the pure DPPG monolayer.

As already mentioned, the presence of EGCG weakens membrane-water interactions by competing with water to bind to the phosphate moiety of the lipids, dehydrating the lipids. Our results also show that the blue light irradiation is sufficient to alter the proportion of hydrated and dehydrated phosphate groups, possibly because some EGCG molecules are damaged and water molecules are more easily bound to the phosphate. Deconvolution of the carbonyl band of DPPG monolayer in Figure 5.4E revealed two bands at 1743 cm^{-1} and 1765 cm^{-1} corresponding to the hydrogen and non-hydrogen bonded carbonyl groups, respectively. Upon irradiation, the bandwidth for the C=O region increases, both in the absence or presence of EGCG, reflecting a heterogenous carbonyl population

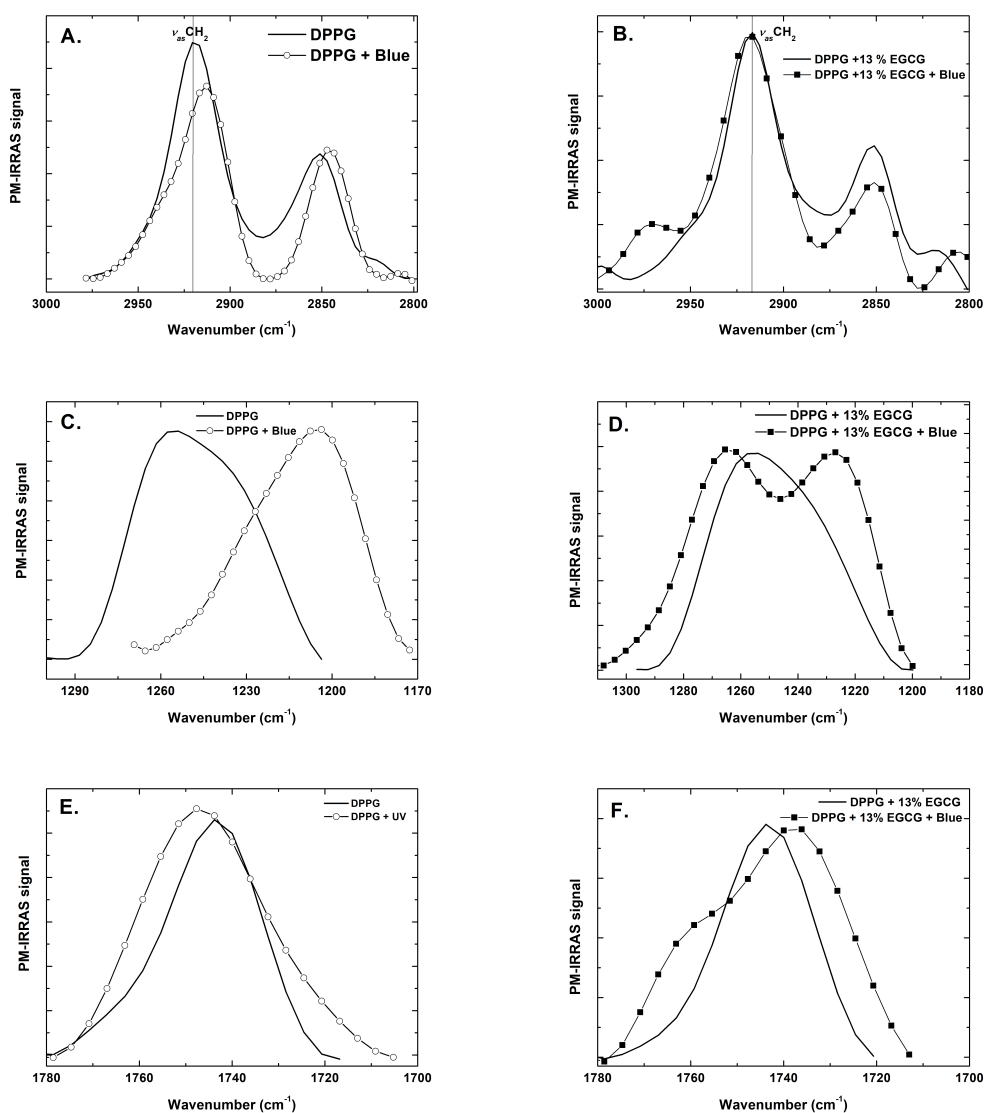


Figure 5.4: PM-IRRAS spectra of DPPG (A, C, E) and DPPG+13%EGCG (B, D, F) monolayers, before and after blue light irradiation.

with distinct hydrogen bonding capacity. The appearance of the two well-defined bands after irradiation for the DPPG+13%EGCG spectrum in Figure 4F corroborates this observation. The spectra in Figures 5.4E and 5.4F obtained after irradiation are better explained if each spectrum is fitted with 3 Gaussians, two of which already used (at 1740 and 1760 cm^{-1}) and another one at ca. 1720 cm^{-1} associated with hydrogen bonded carbonyl groups. For pure DPPG, the percentage of hydrogen-bonded carbonyl groups increases upon irradiation, possibly due to the attack of light-induced radicals to the water molecules strongly bound to the carbonyls (one should recall that in the absence of EGCG, DPPG has the highest degree of hydration (Figure 5.2D)). When EGCG is present, the ratio between hydrated and total C=O bands is not affected by irradiation if we exclude the new

carbonyl groups associated with the 1720 cm^{-1} band appearing with the irradiation. This lack of effect can be attributed to three factors: (1) competition between EGCG and water molecules to bind to the carbonyl group; (2) condensing effect of EGCG on the DPPG monolayer hampers diffusion of ROS across the monolayer, and (3) scavenging activity of EGCG eliminates ROS in the vicinity of carbonyl groups of DPPG lipids.

In conclusion, irradiation affected DPPG in pure monolayers and even in the presence of EGCG. But the effects were stronger in the absence of EGCG, especially for the head groups of DPPG. These findings are in line with our previous work, where we irradiated DPPG liposomes containing EGCG with ultraviolet radiation (254 nm) at fixed times and concluded that EGCG is a good shield against UV light that slows down the cascade of oxidizing events, efficiently protecting the hydration sites of DPPG lipids (carbonyl and phosphate groups) from degradation. A prolonged exposure to UV light disrupted the integrity of EGCG by opening the pyrogallol ring, a starting point to initiate lipid damage.[50] The results presented here are also consistent with previous studies according to which ROS induced by blue light increases significantly the lipid membrane permeability and the level of lipid peroxidation, eventually leading to cell death.[51, 52, 53]

5.4 Conclusions

The effects from catechin EGCG on DPPG Langmuir monolayers have been analysed from the point of view of interactions and from damage induced by blue light irradiation. The incorporation of EGCG in DPPG monolayers caused significant changes in the structuring of the lipid molecules, and this could be confirmed with PM-IRRAS and surface potential isotherms. The combination of distinct methods to characterize the monolayers was important to probe the intermolecular interactions. For instance, the decrease in surface potential caused by EGCG is most likely related to the changes in the dipole moment of C=O groups from DPPG whose band in the PM-IRRAS spectra was considerably altered. The effects did not change monotonically with the relative concentration of EGCG, which means that EGCG cannot be incorporated indefinitely into the DPPG monolayer. Also relevant for the molecular-level interactions was the competition among EGCG and water molecules for H-bonding, thus inducing structural rearrangements of DPPG molecules. As observed with liposomes, EGCG was found to protect the DPPG monolayer against blue light irradiation.

Regarding the biological implications, the results presented here point to a physiological action of EGCG protecting lipids from the free radicals induced by wavelengths beyond the UV spectrum. In the future, EGCG+DPPG monolayers should be exposed to a combination of different wavelengths within and beyond UV, mimicking natural sunlight. This is relevant to improve sunscreen products in the market. In dermatology, the uncontrolled generation of lipid peroxidation end products and the depleted level of antioxidants are pathogenic mechanisms for inflammatory skin diseases such as atopic/photocontact dermatitis and acne. Therefore, based on the findings of this study, one may envisage EGCG as promising to control inflammatory diseases related to oxidative stress, by decreasing the photosensitivity and susceptibility of phospholipids to blue light oxidative damage. Also, blue light may be beneficial by inactivating and killing bacterial pathogens, in spite of the damage it may cause to eyes (macular degeneration) and skin. Since the damage/protection balance depends on the wavelength and dose used, experiments with EGCG and various blue light wavelengths could indicate whether the anti-inflammatory and antibacterial action of catechins may be enhanced by blue light irradiation to treat skin conditions.

5.5 Acknowledgements

The authors acknowledge the financial support from FEDER, through Programa Operacional Factores de Competitividade – COMPETE and Fundação para a Ciência e a Tecnologia – FCT, by the project PTDC/FIS-NAN/0909/2014 and for the Portuguese research Grant No. PEst-OE/FIS/UI0068/2011 and UID/FIS/00068/2013 through FCTMEC(Portugal) and by FAPESP (2013/14262-7) and CNPq (Brazil). Filipa Pires acknowledges the fellowship PD/BD/106036/2015 from RABBIT Doctoral Programme (Portugal).

References

- [1] M.-C. D. Desgarnier and P. J. Rochette. “Enhancement of UVB-induced DNA damage repair after a chronic low-dose UVB pre-stimulation.” In: *DNA repair* 63 (2018), pp. 56–62.
- [2] H. Ikehata, T. Mori, T. Douki, J. Cadet, and M. Yamamoto. “Quantitative analysis of UV photolesions suggests that cyclobutane pyrimidine dimers produced in mouse skin by UVB are more mutagenic than those produced

- by UVC.” In: *Photochemical & Photobiological Sciences* 17.4 (2018), pp. 404–413.
- [3] S. Kimeswenger, R. Dingelmaier-Hovorka, D. Foedinger, and C. Jantschitsch. “UVA1 impairs the repair of UVB – induced DNA damage in normal human melanocytes.” In: *Experimental dermatology* 27.3 (2018), pp. 276–279.
- [4] S. Grether-Beck, A. Marini, T. Jaenicke, and J. Krutmann. “Photoprotection of human skin beyond ultraviolet radiation.” In: *Photodermatology, photoimmunology & photomedicine* 30.2-3 (2014), pp. 167–174.
- [5] L. Duteil, N. Cardot-Leccia, C. Queille-Roussel, Y. Maubert, Y. Harmelin, F. Boukari, D. Ambrosetti, J.-P. Lacour, and T. Passeron. “Differences in visible light-induced pigmentation according to wavelengths: a clinical and histological study in comparison with UVB exposure.” In: *Pigment cell & melanoma research* 27.5 (2014), pp. 822–826.
- [6] B. H. Mahmoud, E. Ruvolo, C. L. Hexsel, Y. Liu, M. R. Owen, N. Kollias, H. W. Lim, and I. H. Hamzavi. “Impact of long-wavelength UVA and visible light on melanocompetent skin.” In: *Journal of investigative dermatology* 130.8 (2010), pp. 2092–2097.
- [7] T. Kushibiki, T. Hirasawa, S. Okawa, and M. Ishihara. “Blue laser irradiation generates intracellular reactive oxygen species in various types of cells.” In: *Photomedicine and laser surgery* 31.3 (2013), pp. 95–104.
- [8] A. C.-H. Chen, Y.-Y. Huang, P. R. Arany, and M. R. Hamblin. “Role of reactive oxygen species in low level light therapy.” In: *Proceedings Mechanisms for Low-Light Therapy IV*. Vol. 7165. 716502–716506. 2009.
- [9] C. Ash, G. Town, R. Whittall, L. Tooze, and J. Phillips. “Lasers and intense pulsed light (IPL) association with cancerous lesions.” In: *Lasers in medical science* 32.8 (2017), pp. 1927–1933.
- [10] A. N. Osipov, T. V. Machneva, E. A. Buravlev, and Y. A. Vladimirov. “Effects of laser radiation on mitochondria and mitochondrial proteins subjected to nitric oxide.” In: *Frontiers in medicine* 5.112 (2018), pp. 1–6.
- [11] F.-Q. Liang and B. F. Godley. “Oxidative stress-induced mitochondrial DNA damage in human retinal pigment epithelial cells: a possible mechanism for RPE aging and age-related macular degeneration.” In: *Experimental eye research* 76.4 (2003), pp. 397–403.

- [12] S. Stoelzle, T. Kagawa, M. Wada, R. Hedrich, and P. Dietrich. “Blue light activates calcium-permeable channels in *Arabidopsis mesophyll* cells via the phototropin signaling pathway.” In: *Proceedings of the National Academy of Sciences* 100.3 (2003), pp. 1456–1461.
- [13] B. F. Godley, F. A. Shamsi, F.-Q. Liang, S. G. Jarrett, S. Davies, and M. Boulton. “Blue light induces mitochondrial DNA damage and free radical production in epithelial cells.” In: *Journal of Biological Chemistry* 280.22 (2005), pp. 21061–21066.
- [14] L. Knels, M. Valtink, C. Roehlecke, A. Lupp, J. de la Vega, M. Mehner, and R. H. Funk. “Blue light stress in retinal neuronal (R28) cells is dependent on wavelength range and irradiance.” In: *European Journal of Neuroscience* 34.4 (2011), pp. 548–558.
- [15] P. Ramakrishnan, M. Maclean, S. J. MacGregor, J. G. Anderson, and M. H. Grant. “Cytotoxic responses to 405 nm light exposure in mammalian and bacterial cells: involvement of reactive oxygen species.” In: *Toxicology in Vitro* 33 (2016), pp. 54–62.
- [16] C. Núñez-Álvarez, C. Suárez-Barrio, S. del Olmo Aguado, and N. N. Osborne. “Blue light negatively affects the survival of ARPE 19 cells through an action on their mitochondria and blunted by red light.” In: *Acta Ophthalmologica* 97.1 (2019), pp. 103–115.
- [17] T. Devasagayam, J. Tilak, K. Bloor, K. S. Sane, S. S. Ghaskadbi, and R. Lele. “Free radicals and antioxidants in human health: current status and future prospects.” In: *Journal of Association of Physicians of India* 52.4 (2004), pp. 794–804.
- [18] J. P. Silva and O. P. Coutinho. “Free radicals in the regulation of damage and cell death—basic mechanisms and prevention.” In: *Drug Discoveries & Therapeutics* 4.3 (2010), pp. 144–167.
- [19] L. Chen, X. Yang, H. Jiao, and B. Zhao. “Tea catechins protect against lead-induced ROS formation, mitochondrial dysfunction, and calcium dysregulation in PC12 cells.” In: *Chemical Research in Toxicology* 16.9 (2003), pp. 1155–1161.
- [20] M. D. Farrar, A. Nicolaou, K. A. Clarke, S. Mason, K. A. Massey, T. P. Dew, R. E. Watson, G. Williamson, and L. E. Rhodes. “A randomized controlled trial of green tea catechins in protection against ultraviolet radiation-induced cutaneous inflammation, 2.” In: *The American Journal of Clinical Nutrition* 102.3 (2015), pp. 608–615.

- [21] J.-Y. Fang, C.-F. Hung, T.-L. Hwang, and Y.-L. Huang. “Physicochemical characteristics and in vivo deposition of liposome-encapsulated tea catechins by topical and intratumor administrations.” In: *Journal of Drug Targeting* 13.1 (2005), pp. 19–27.
- [22] T. Nakayama, K. Kajiya, and S. Kumazawa. “Interaction of plant polyphenols with liposomes.” In: *Advances in Planar Lipid Bilayers and Liposomes* 4 (2006), pp. 107–133.
- [23] Y. Tamba, S. Ohba, M. Kubota, H. Yoshioka, H. Yoshioka, and M. Yamazaki. “Single GUV method reveals interaction of tea catechin (-)-epigallocatechin gallate with lipid membranes.” In: *Biophysical Journal* 92.9 (2007), pp. 3178–3194.
- [24] Y. Sun, W.-C. Hung, F.-Y. Chen, C.-C. Lee, and H. W. Huang. “Interaction of Tea Catechin (-)-Epigallocatechin Gallate with Lipid Bilayers.” In: *Biophysical Journal* 96.3 (2009), 1026—1035.
- [25] Y. Uekusa, M. Kamihira-Ishijima, O. Sugimoto, T. Ishii, S. Kumazawa, K. Nakamura, K.-i. Tanji, A. Naito, and T. Nakayama. “Interaction of epicatechin gallate with phospholipid membranes as revealed by solid-state NMR spectroscopy.” In: *Biochimica et Biophysica Acta (BBA)-Biomembranes* 1808.6 (2011), pp. 1654–1660.
- [26] T. Matsuzaki, H. Ito, V. Chevyreva, A. Makky, S. Kaufmann, K. Okano, N. Kobayashi, M. Suganuma, S. Nakabayashi, H. Y. Yoshikawa, and M. Tanaka. “Adsorption of galloyl catechin aggregates significantly modulates membrane mechanics in the absence of biochemical cues.” In: *Physical Chemistry Chemical Physics* 19.30 (2017), pp. 19937–19947.
- [27] T. M. Nobre, F. J. Pavinatto, L. Caseli, A. Barros-Timmons, P. Dynarowicz-Łątka, and O. N. Oliveira Jr. “Interactions of bioactive molecules & nanomaterials with Langmuir monolayers as cell membrane models.” In: *Thin Solid Films* 593 (2015), pp. 158–188.
- [28] A. d.A. M. Collado, F. G. Dupuy, R. D. Morero, and C. Minahk. “Cholesterol induces surface localization of polyphenols in model membranes thus enhancing vesicle stability against lysozyme, but reduces protection of distant double bonds from reactive-oxygen species.” In: *Biochimica et Biophysica Acta (BBA)-Biomembranes* 1858.7 (2016), pp. 1479–1487.
- [29] F Pires and M Raposo. “Artificial nanosystems to decode natural antioxidants – cellular membrane interactions.” In: *Conf. Proc. 13th Int. Meet. Comput. Intell. Methods Bioinforma. Biostat. CIBB*. 2016, pp. 190–195.

- [30] F. Pires, G. Magalhães-Mota, P. A. Ribeiro, and M. Raposo. "Effect of UV Radiation on DPPG and DMPC Liposomes in Presence of Catechin Molecules." In: *International Meeting on Computational Intelligence Methods for Bioinformatics and Biostatistics*. Springer. 2016, pp. 172–183.
- [31] R. Veldhuizen, K. Nag, S. Orgeig, and F. Possmayer. "The role of lipids in pulmonary surfactant." In: *Biochimica et Biophysica Acta (BBA)-Molecular Basis of Disease* 1408.2-3 (1998), pp. 90–108.
- [32] M. Al-Saiedy, R. Pratt, P. Lai, E. Kerek, H. Joyce, E. Prenner, F. Green, C.-C. Ling, R. Veldhuizen, S. Ghandorah, and M. Amrein. "Dysfunction of pulmonary surfactant mediated by phospholipid oxidation is cholesterol-dependent." In: *Biochimica et Biophysica Acta (BBA)-General Subjects* 1862.4 (2018), pp. 1040–1049.
- [33] S. Zellmer and G. Cevc. "Tumor targeting in vivo by means of thermolabile fusogenic liposomes." In: *Journal of drug targeting* 4.1 (1996), pp. 19–29.
- [34] T. Boulikas. "Clinical overview on Lipoplatin™: a successful liposomal formulation of cisplatin." In: *Expert opinion on investigational drugs* 18.8 (2009), pp. 1197–1218.
- [35] E. Marzban, S. H. Alavizadeh, M. Ghiadi, M. Khoshangosht, Z. Khashayarmanesh, A. Abbasi, and M. R. Jaafari. "Optimizing the therapeutic efficacy of cisplatin PEGylated liposomes via incorporation of different DPPG ratios: In vitro and in vivo studies." In: *Colloids and Surfaces B: Biointerfaces* 136 (2015), pp. 885–891.
- [36] A. Dicko, H. Bourque, and M. Pézolet. "Study by infrared spectroscopy of the conformation of dipalmitoylphosphatidylglycerol monolayers at the air–water interface and transferred on solid substrates." In: *Chemistry and physics of lipids* 96.1-2 (1998), pp. 125–139.
- [37] D. Vollhardt, V. Fainerman, and S. Siegel. "Thermodynamic and textural characterization of DPPG phospholipid monolayers." In: *The Journal of Physical Chemistry B* 104.17 (2000), pp. 4115–4121.
- [38] V. P. Geraldo, F. J. Pavinatto, T. M. Nobre, L. Caseli, and O. N. Oliveira Jr. "Langmuir films containing ibuprofen and phospholipids." In: *Chemical Physics Letters* 559 (2013), pp. 99–106.
- [39] O. N. Oliveira and C. Bonardi. "The surface potential of Langmuir monolayers revisited." In: *Langmuir* 13.22 (1997), pp. 5920–5924.

- [40] M. Kumamoto, T. Sonda, K. Nagayama, and M. Tabata. "Effects of pH and metal ions on antioxidative activities of catechins." In: *Bioscience, biotechnology, and biochemistry* 65.1 (2001), pp. 126–132.
- [41] E. N. Bentz, A. B. Pomilio, and R. M. Lobayan. "Structure and electronic properties of (+)-catechin: aqueous solvent effects." In: *Journal of Molecular Modeling* 20.2 (2014), pp. 20–2105.
- [42] E. N. Bentz, A. B. Pomilio, and R. M. Lobayan. "Exploratory conformational study of (+)-catechin. Modeling of the polarizability and electric dipole moment." In: *Journal of Molecular Modeling* 20.2522 (2014), pp. 1–10.
- [43] H. L. Casal and H. H. Mantsch. "Polymorphic phase behaviour of phospholipid membranes studied by infrared spectroscopy." In: *Biochimica et Biophysica Acta (BBA)-Reviews on Biomembranes* 779.4 (1984), pp. 381–401.
- [44] I. Levin, T. Thompson, Y Barenholz, and C.-h. Huang. "Two types of hydrocarbon chain interdigitation in sphingomyelin bilayers." In: *Biochemistry* 24.22 (1985), pp. 6282–6286.
- [45] R. Lewis, R. N. McElhaney, W. Pohle, and H. H. Mantsch. "Components of the carbonyl stretching band in the infrared spectra of hydrated 1, 2-diacylglycerolipid bilayers: a reevaluation." In: *Biophysical journal* 67.6 (1994), pp. 2367–2375.
- [46] M. d.l. A. Frías and E. A. Dissalvo. "Configuration of carbonyl groups at the lipid interphases of different topological arrangements of lipid dispersions." In: *Langmuir* 25.14 (2009), pp. 8187–8191.
- [47] E. Disalvo, F Lairion, F Martini, E Tymczyszyn, M Frías, H Almaleck, and G. Gordillo. "Structural and functional properties of hydration and confined water in membrane interfaces." In: *Biochimica et Biophysica Acta (BBA)-Biomembranes* 1778.12 (2008), pp. 2655–2670.
- [48] X. Chen, W. Hua, Z. Huang, and H. C. Allen. "Interfacial water structure associated with phospholipid membranes studied by phase-sensitive vibrational sum frequency generation spectroscopy." In: *Journal of the American Chemical Society* 132.32 (2010), pp. 11336–11342.
- [49] N. E. Levinger, R. Costard, E. T. Nibbering, and T. Elsaesser. "Ultrafast energy migration pathways in self-assembled phospholipids interacting with confined water." In: *The Journal of Physical Chemistry A* 115.43 (2011), pp. 11952–11959.

-
- [50] F. Pires, V. P. Geraldo, A. Antunes, A. Marletta, O. N. Oliveira Jr, and M. Raposo. "On the role of epigallocatechin-3-gallate in protecting phospholipid molecules against UV irradiation." In: *Colloids and Surfaces B: Biointerfaces* 173 (2019), pp. 312–319.
- [51] X. Chen, H. Hall, J. P. Simpson, W. D. Leon-Salas, D. F. Ready, and V. M. Weake. "Cytochrome b5 protects photoreceptors from light stress-induced lipid peroxidation and retinal degeneration." In: *NPJ Aging and Mechanisms of Disease* 3.1 (2017), pp. 1–9.
- [52] C. Grangeteau, F. Lepinois, P. Winckler, J.-M. Perrier-Cornet, S. Dupont, and L. Beney. "Cell death mechanisms induced by photo-oxidation studied at the cell scale in the yeast *Saccharomyces cerevisiae*." In: *Frontiers in Microbiology* 9.2640 (2018), pp. 1–9.
- [53] J. Wu, Z. Chu, Z. Ruan, X. Wang, T. Dai, and X. Hu. "Changes of Intracellular Porphyrin, Reactive Oxygen Species, and Fatty Acids Profiles During Inactivation of Methicillin-Resistant *Staphylococcus aureus* by Antimicrobial Blue Light." In: *Frontiers in physiology* 9.1658 (2018), pp. 1–10.

RESULTS

The impact of blue light in monolayers representing tumorigenic and nontumorigenic cell membranes containing EGCG¹

Abstract

Natural products such as epigallocatechin-3-gallate (EGCG) have been suggested for complementary treatments of cancer, since they lower toxic side effects of anticancer drugs, and possess anti-inflammatory and antioxidant properties that inhibit carcinogenesis. Their effects on cancer cells depend on interactions with the membrane, which is the motivation to investigate Langmuir monolayers as simplified membrane models. In this study, EGCG was incorporated in zwitterionic dipalmitoyl phosphatidyl choline (DPPC) and anionic dipalmitoyl phosphatidyl serine (DPPS) Langmuir monolayers to simulate healthy and cancer cells membranes, respectively. EGCG induces condensation in surface pressure isotherms for both DPPC and DPPS monolayers, interacting mainly via electrostatic forces and hydrogen bonding with the choline and phosphate groups of the phospholipids, according to data from polarization-modulated infrared reflection absorption spectroscopy (PM-IRRAS). Both monolayers become more compressible upon interaction with EGCG, which may be correlated to the synergy between EGCG and anticancer drugs reported in the literature. The interaction with EGCG is stronger for DPPC, leading to stronger morphological changes in

¹This chapter is based on the submitted publication:

Pires, F., Magalhães-Mota, G., Geraldo, V. P., Oliveira Jr, O. N., and Raposo, M. The impact of blue light in monolayers representing tumorigenic and nontumorigenic cell membranes containing EGCG. COLSUB, 2019.

Brewster Angle Microscopy (BAM) images and higher degree of condensation in the surface pressure isotherms. The changes induced by blue irradiation on DPPC and DPPS monolayers were largely precluded when EGCG was incorporated, thus confirming its antioxidant capacity for both types of membrane.

6.1 Introduction

Ionizing radiation may ionize biomolecules such as proteins, phospholipids, and nucleic acids, also impairing the genome stability in cells to yield unrepaired DNA lesions.[1] A prolonged exposure to ultraviolet radiation (100–400 nm) affects the homeostasis of cell membranes by altering the ratio of saturated/unsaturated phospholipids and disturbing packing and the stiffness of lipid membranes.[2, 3] These cell abnormalities increase with the radiation dose and may be correlated with cancer progression. Upon long-term exposure, even the blue light (400 - 480 nm) from electronic devices (computers, smartphones) may produce reactive oxygen species (ROS) that affect the cells metabolic activity, dehydrate the epidermis and accelerate skin ageing, by promoting fragmentation of collagen fibers and appearance of wrinkles.[4, 5, 6, 7, 8] Since preventing complete exposure is not possible, strategies have to be sought for reducing or eliminating radiation damage. This has been attempted with natural products, including antioxidants, antibacterial and antimutagenic compounds, which may help prevent cellular injuries from radiation.[9, 10, 11]

One antioxidant that has been suggested to foster protection against irradiation is epigallocatechin –3–gallate (EGCG), found in herb teas. EGCG has hydroxyphenol rings (ring B and gallate group) that are chelators to reduce ROS species, as in the case of hydroxyl radicals to suppress *in vitro* 'Fenton-like' reactions.[12] Since the antioxidant properties of EGCG could be related to their affinity toward cell membranes, studies have been performed to investigate interaction between EGCG and Langmuir monolayers, which represent simplified membrane models.[13, 14] In fact, Langmuir monolayers have long been used to elucidate the partitioning of several molecules into the cell membrane.[15, 16] For EGCG, in particular, we have found that it is incorporated in dipalmitoyl phosphatidyl glycerol (DPPG) monolayers spread on an aqueous subphase (pH 6) and is able to reduce damage caused by blue irradiation in DPPG molecules.[17]

We have decided to extend the study to other phospholipids that could mimic

healthy and cancerous cell membranes, in addition to verifying if the antioxidant effectiveness of EGCG can be compromised upon oxidation of the phenolic rings, which depends on irradiation, temperature and pH.[18, 19, 20] The phospholipids chosen were dipalmitoylphosphatidylcholine (DPPC)[21, 22] and dipalmitoyl phosphatidyl serine (DPPS)[23, 24, 25], representing the healthy and cancer cell membranes, respectively. We concentrated on probing whether the partitioning of EGCG in the membrane is conditioned by lipid membrane composition (lipid net charge, polar termination, head orientation). Furthermore, we investigated the effects from blue light irradiation at a neutral subphase (pH 7.4) to analyse possible changes in EGCG structure that could lead to a conversion of an antioxidant into a prooxidant behavior, i.e. EGCG could then damage rather than protect the lipid monolayers.

6.2 Experimental

1,2-dipalmitoyl-sn-glycero-3-phosphocholine (DPPC) and 1,2-dipalmitoyl-sn-glycero-3-phospho-L-serine (sodium salt) (DPPS) were obtained from Avanti Polar Lipids. DPPC were dissolved in chloroform to result in a concentration of 0.5 mg/mL. In the case of DPPS, this phospholipid were dissolved in a mixture of chloroform:methanol:water (65:30:5 v/v) to obtain a concentration of 0.5 mg/mL. The EGCG (M.W. 458.4 g/mol) was purchased from Sigma- Aldrich and dissolved in chloroform to render a 0.3 mg/mL solution.

Langmuir monolayers were obtained after spreading aliquots of the lipid solutions on the phosphate buffer saline subphase of the Langmuir minitrough from KSV Instruments. After 10 min the solvent evaporated and two symmetric barriers start to move at a constant speed of 10 mm.min⁻¹, initiating the surface pressure measurements. All the experiments were carried out in a class 10,000 clean room and they were repeated at least three times to ensure reproducibility of the isotherms. The membrane compressibility modulus (C_s^{-1}) was obtained from isotherms using the following equation: $C_s^{-1} = -A \left(\frac{\partial \pi}{\partial A} \right)_T$, where A is the average area per lipid and π is the monolayer surface pressure. The polarization-modulated infrared reflection absorption spectroscopy (PM-IRRAS) measurements were carried out in a KSV PMI 550 instrument (KSV Instruments, Finland), operating at a high frequency and at an incidence angle of 80°, after compress the monolayer up to 30 mN m⁻¹. All the lipid spectra shown were obtained by subtracting the spectrum of a phosphate buffer solution subphase at

the same temperature as that of samples. The morphology of the Langmuir monolayers at air/water interface was studied by Brewster angle microscopy (BAM). Imaging apparatus consists in an ultra-objective BAM 2 Plus microscope (Nano Film EP4 Technology, Germany) connected to a high quality GigE CCD camera and to a light source (480 nm laser). The evident contrast in BAM images displays the clean water surface (no reflection, dark regions) and the monolayer domains (reflection, bright regions).

In irradiation experiments, the lipid monolayers were exposed to blue led light (ca. 460 nm, with nominal light intensity of 77.1 mW/cm^2) for 1h. The light source was placed perpendicularly to the Langmuir trough (25 cm above the surface) to irradiate the entire monolayer surface. Control experiments were performed with the same setup but without the blue LED source. Also, the changes in lipid chemical composition and morphology due to irradiation were analysed by PM-IRRAS spectroscopy and BAM microscopy, respectively.

6.3 Results

6.3.1 Effect of EGCG on DPPC and DPPS monolayers: analysis of surface–pressure isotherms

The surface pressure-area isotherm for pure DPPC on a PBS subphase in Figure 6.1A displays a first-order transition from the liquid expanded to liquid-condensed (LE/LC) phases, with a plateau at 5-10 mN/m. The DPPC monolayer collapsed at $62.1 \pm 1.5 \text{ mN/m}$, a collapse pressure similar to those reported in the literature [26, 27]. Regardless of the composition of the mixed DPPC/EGCG monolayers, the presence of EGCG shifts the surface pressure-area isotherms to smaller areas. Moreover, the LE/LC transition is less pronounced (although still present) when large amounts of EGCG were incorporated, consistent with the condensing effect of EGCG on DPPC monolayers. The compressional modulus (C_s^{-1}) is a measure of the monolayer elasticity, where values below 100 mN/m denote the LE state and values ranging from 100 to 250 mN/m are typical of the LC state [22]. Here, at the surface pressure mimicking the cell membrane (30 mN/m), $C_s^{-1} = 159 \pm 16 \text{ mN/m}$ for a pure DPPC monolayer (i.e. in the LC phase), while for DPPC+50%EGCG mixture $C_s^{-1} = 97 \pm 11 \text{ mN/m}$, which means that EGCG incorporation turns the DPPC monolayer more compressible. Furthermore, the differences in the compressional modulus indicate that EGCG affects

the lipid chain packing and modifies the orientation of DPPC headgroups with respect to the membrane plane. Figure 6.1B shows a typical isotherm for DPPS with a collapse surface pressure of 63.4 ± 1.4 mN/m, consistent with the literature [28, 29, 30]. As observed for DPPC, the presence of EGCG shifted the DPPS isotherms to smaller molecular areas. The decrease in lipid area with EGCG concentration in the monolayer at 30 mN/m is plotted in Figure 6.1C, where the condensing effect of EGCG on the DPPC monolayer is more pronounced than on DPPS monolayer. Moreover, the compressibility of DPPC monolayer (inset in Figure 6.1A) decreased with all the EGCG concentrations studied, whereas the compressibility of the DPPS monolayer was only significantly affected by the highest EGCG concentration (50 mol%). Both DPPC and DPPS phospholipids have the same tail length but their headgroups are distinct, particularly in the surface charge density. While electrostatic repulsion is expected among the anionic DPPS headgroups, intermolecular hydrogen bonding may occur between the phosphate and NH_3^+ groups of two adjacent DPPS molecules.[31] It seems that the result of these opposing trends is a decrease in area per molecule induced by EGCG that is larger for DPPC than for DPPS. The reason why these intermolecular interactions in DPPC are stronger than in DPPS could be the difference in lipid packing density as the phase transition temperatures are 41° and 54° for DPPC[32] and DPPS[33].

Thus, from the analysis of these physical parameters, i.e. area per lipid and compressional modulus, one infers that EGCG interacts with both neutral and anionic phospholipids, promoting monolayer condensation. The differences in the headgroups seem to regulate the strength of the intermolecular interactions that take place at the monolayer/water interface, which might determine the degree of monolayer condensation triggered by EGCG (see PM-IRRAS results for further discussion).

6.3.2 Molecular reorganization of neat and mixed monolayers upon blue irradiation: PM-IRRAS study

Phospholipids exhibit characteristic vibrational bands at $2920\text{--}2850\text{ cm}^{-1}$, $1710\text{--}1740\text{ cm}^{-1}$ and $1220\text{--}1090\text{ cm}^{-1}$ assigned to the acyl CH_2 chains, carbonyl groups and phosphate groups, respectively. These are very sensitive to the environmental factors, such as dipolar interactions, protonation state, hydration force changes, and can thus reflect subtle lipid conformational changes due to blue irradiation exposure. Table 6.1 shows the assignments of the main vibrational modes of DPPC monolayer along with the shifts caused by EGCG and upon blue light irradiation. In the PM-IRRAS spectrum of neat DPPC monolayer, Figure 6.2A, the

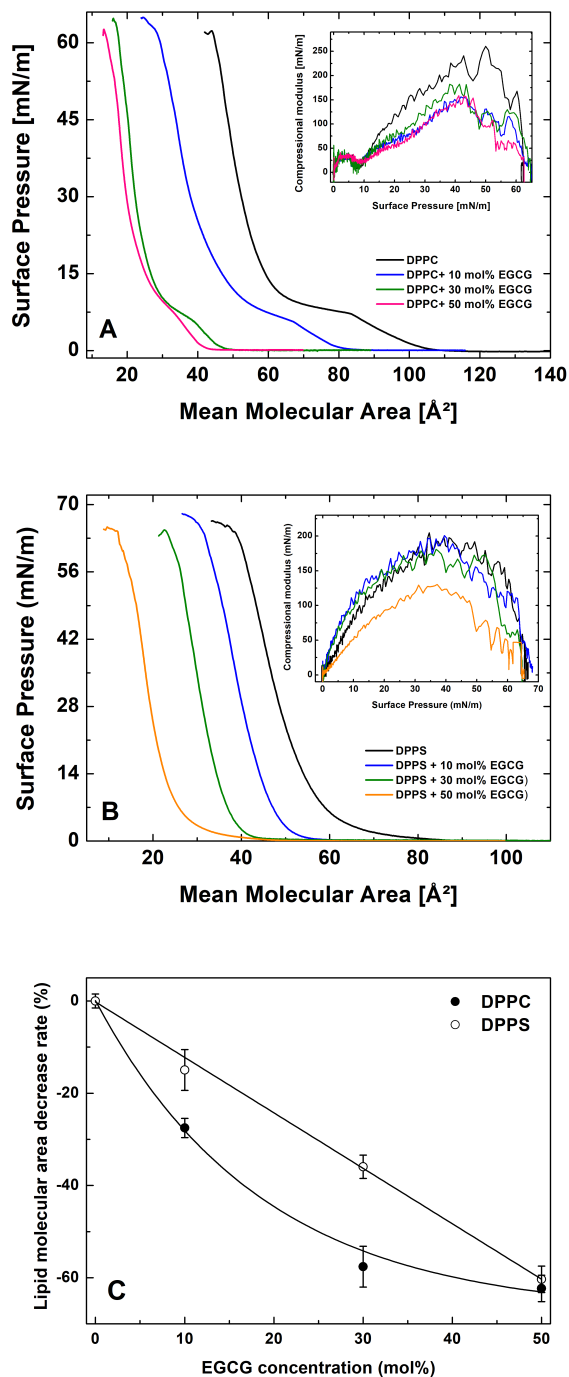


Figure 6.1: Surface pressure isotherms registered for DPPC (A) and DPPS (B) monolayers containing different EGCG molar fractions. The compressional modulus corresponding to each monolayer is shown in inset. At the surface pressure of 30 mN/m, the lipid molecular area decreases as the amount of EGCG increases in the monolayer (C).

bands at 2909 cm^{-1} and 2852 cm^{-1} are ascribed to the asymmetric and symmetric CH_2 stretching, respectively. The shift of these bands to higher frequencies (2919 and 2857 cm^{-1}) upon blue irradiation is clear evidence of the increase in the number of gauche conformers, and hence of a conformational disordering of the lipid alkyl chains. In the mixed EGCG/DPPC monolayer, these bands are located at 2930 and 2828 cm^{-1} . The data suggest that the geometric accommodation of EGCG and the interactions established at the headgroup region seem to imply conformational changes in the lipid tails, as illustrated schematically in Figure 6.4B. This is consistent with the compressional modulus measurements, where the EGCG/DPPC monolayer was more fluid than a neat DPPC monolayer. Furthermore, these bands shifted to lower frequencies when the monolayer was submitted to radiation, suggesting a new organization of the hydrocarbon tails, possibly because radiation affects the EGCG molecules and promotes their migration towards the water interface. The shift in the asymmetric and symmetric CH_2 stretching bands towards higher frequencies also occurred in DPPS/EGCG monolayers (Figure 6.2 D), thus indicating that EGCG disturbs the packing of DPPS alkyl chains similarly to that observed for DPPC. After irradiation, a new band at 2820 cm^{-1} appeared in Figure 6.2C for the DPPS monolayer. This band is assigned to the symmetric CH_3 stretching, being indicative of disordering of the alkyl chains arising from the vulnerability of DPPS lipids to radiation. Table 6.2 shows the assignments of the main vibrational modes of DPPS monolayer along with the shifts caused by EGCG and upon blue light irradiation. For the mixed EGCG/DPPS monolayer in Figure 6.2D, a new band appeared at 2959 cm^{-1} (asymmetric CH_3 stretching) and the asymmetric CH_2 stretching band was red-shifted to a wavenumber close to that of pure DPPS monolayer. The relative intensity of this band increases, possibly because some EGCG molecules are expelled from the monolayer, which elicits conformational changes in lipid tails. The interaction between EGCG and DPPC seems to be stronger than with DPPS, or at least the EGCG seems to be inserted more deeply into the DPPC membrane, as the CH_2 stretching bands in the mixed EGCG/DPPC monolayer did not change markedly upon irradiation. Finally, our results suggest that the membrane fluidity is strongly dependent on EGCG concentration, and therefore EGCG can be used to enhance the intracellular trafficking of chemotherapeutic drugs across cell membranes to destroy abnormal DNA.

We also analyzed the vibrational mode assigned to the ester carbonyl $\text{C}=\text{O}$ stretching (1736 cm^{-1}), the asymmetrical stretching mode of phosphate group (1265 cm^{-1}) and of the choline group ($^+\text{N}(\text{CH}_3)_3$, 970 cm^{-1}). The carbonyl ($\text{C}=\text{O}$) band in neat DPPC monolayer is split into two bands at 1747 cm^{-1} and 1735 cm^{-1}

CHAPTER 6. THE IMPACT OF BLUE LIGHT IN TUMORIGENIC AND NONTUMORIGENIC MONOLAYERS CONTAINING EGCG

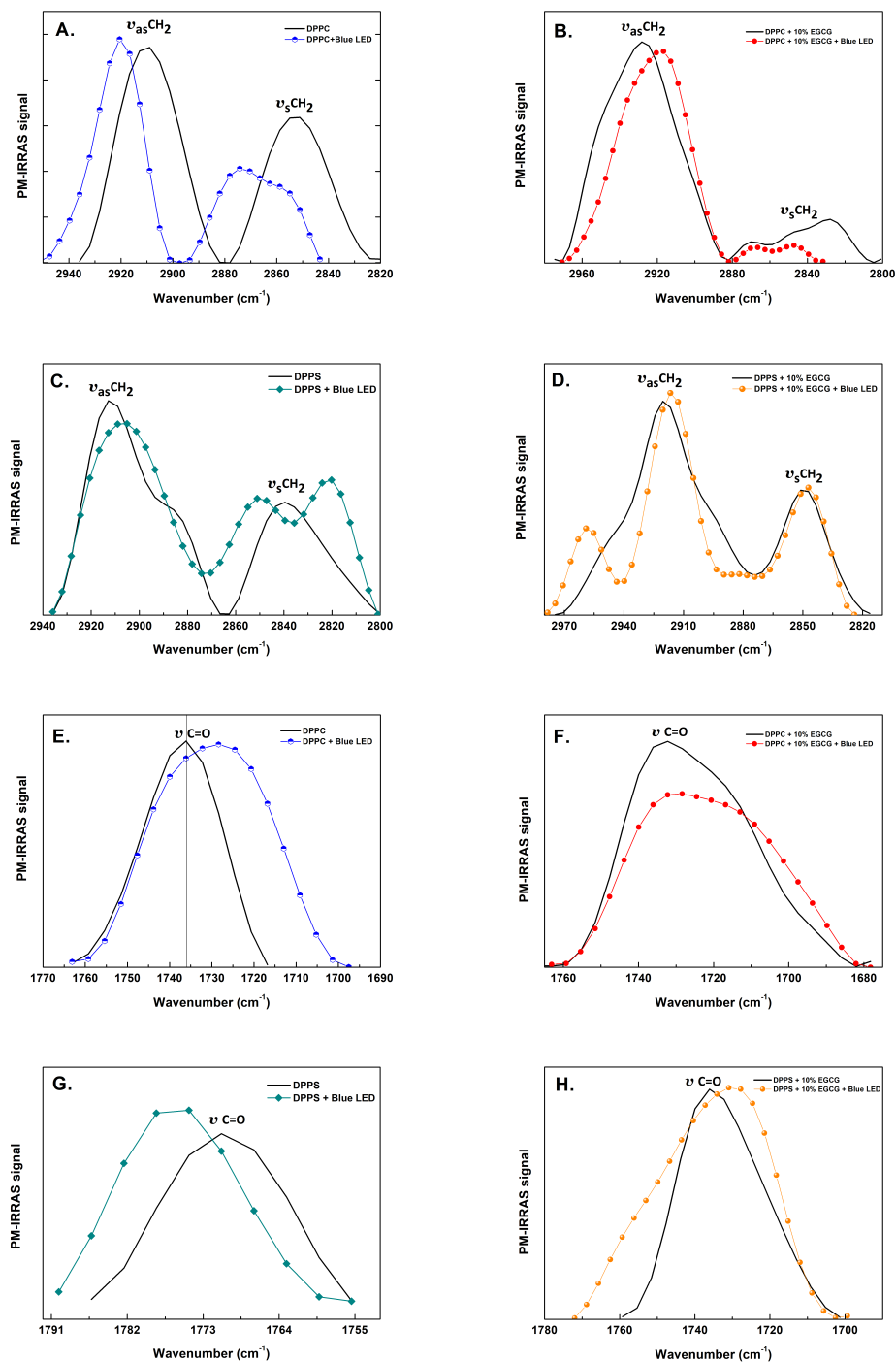


Figure 6.2: PM-IRRAS spectra for neat DPPC, mixed EGCG/DPPC, neat DPPS and mixed EGCG/DPPS monolayer in the lipid alkyl chains (A-D) and carbonyl (E-H) region, before and after blue light irradiation.

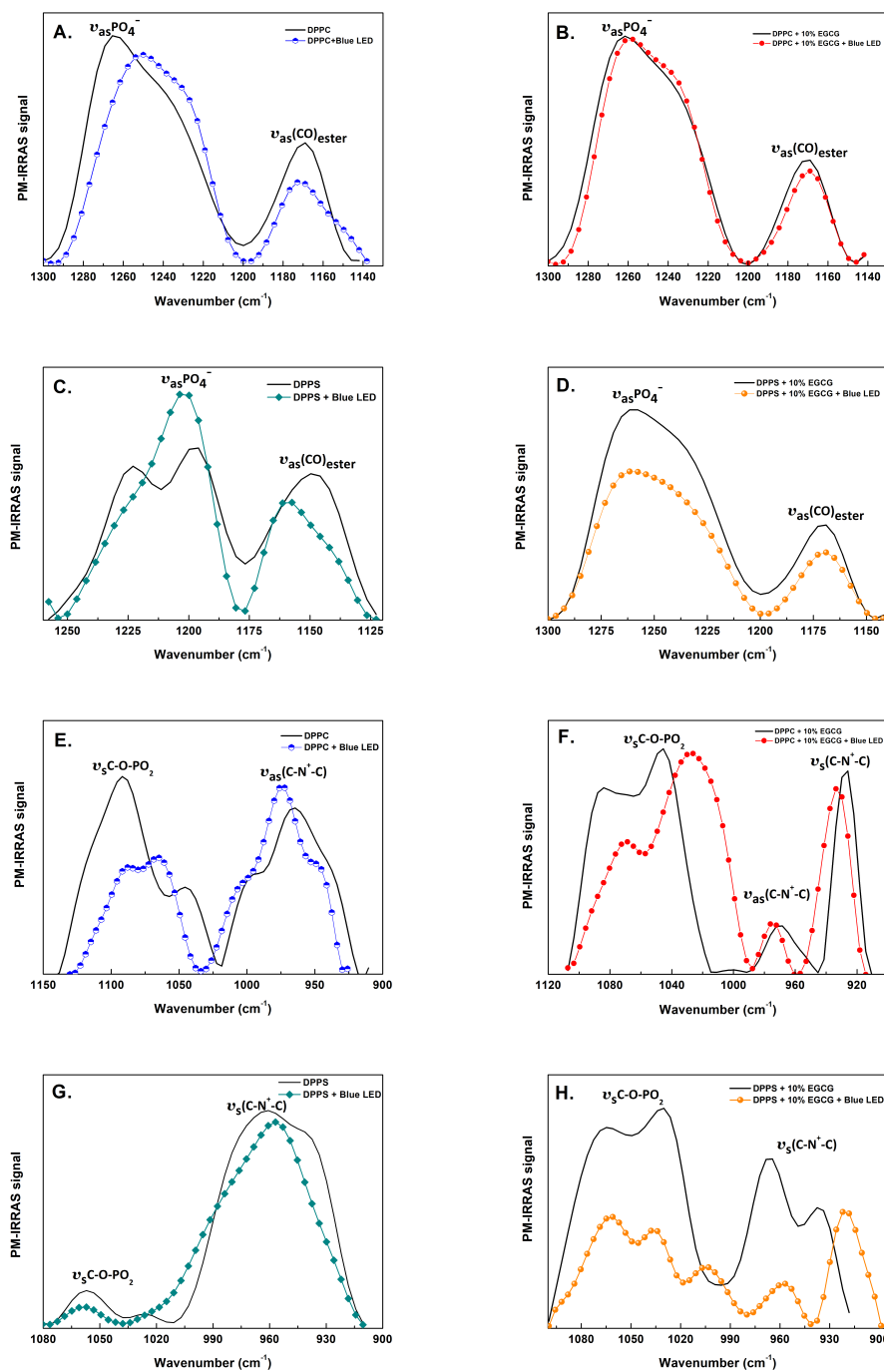


Figure 6.3: PM-IRRAS spectra for neat DPPC, mixed EGCG/DPPC, neat DPPS and mixed EGCG/DPPS monolayer in the phosphate (A-D) and choline (E-H) region, before and after blue light irradiation.

assigned to non-hydrated and hydrated carbonyl groups close to the headgroup, respectively. Upon blue irradiation the carbonyl band in Figure 6.2E becomes broader and the bands shift to lower frequencies (1740 and 1722 cm^{-1}). The fraction of hydrated carbonyl groups decreases from 79.4% to 55.3% (1.4 fold decrease) upon irradiation, indicating disruption in hydrogen bonding between DPPC lipids. In the presence of EGCG, the bands associated with non-hydrated and hydrated carbonyl groups are shifted to lower frequencies (1738 and 1720 cm^{-1}), probably due to interactions with the phenolic rings of EGCG. It seems that such interactions are responsible for protecting carbonyl groups from radiation damage, as indicated by the small change in the fraction of hydrated carbonyl groups after irradiation (from 68.9% to 61.3%). Furthermore, the well defined peak at 1435 cm^{-1} assigned to δCH_2 methylene deformation (Appendix B) indicates that EGCG also binds electrostatically to positively charged quaternary ammonium headgroups of DPPC lipids, in addition to hydrogen bonding with the carbonyl groups.

The strong intermolecular interactions between the amine hydrogen and serine carbonyl oxygen groups in DPPS lead to a pronounced aggregation associated with disordering in the acyl chains, which affects the water movement from the interface to the lipid tail chains and restricts the headgroup motion.[31] Accordingly, the carbonyl bands of DPPS in Figure 6.2G are located at higher frequencies (1774 and 1765 cm^{-1}) compared to that in DPPC phospholipids (1747 and 1735 cm^{-1}). Also, the DPPS monolayer has a lower fraction of hydrated carbonyl groups (35.4 %) than DPPC (79.4%). Regardless of the orientational distribution of the interfacial water molecules in the lipids, dehydration resulted from irradiation on the carbonyl groups of each lipid. Figure 6.2H shows that EGCG induces a large red shift of 36 cm^{-1} in the carbonyl band owing to hydrogen bonding between the phenol ring of EGCG and carbonyl groups of DPPS, similarly to that observed in DPPC monolayer. Again, the anchorage of EGCG on carbonyl groups of DPPS slows down the rate of oxidation of these groups due to radiation exposure.

The effect of EGCG on the hydration of the phosphate group of both DPPC and DPPS phospholipids was also addressed. The spectra of neat DPPC monolayer in Figure 6.3A show an intense band at 1265 cm^{-1} assigned to the antisymmetric P=O stretching, consisting in two overlapping bands at 1242 cm^{-1} and 1269 cm^{-1} corresponding to hydrated and partially hydrated PO_2^- groups, respectively. Blue light irradiation during 1 h on the Langmuir trough led to a slight decrease (4%) in the area per molecule for DPPC (Figure B.2 of Appendix B). This was accompanied by a shift to lower frequencies (1227 and 1255 cm^{-1}) in the antisymmetric P=O band and broadening of the (CO) ester stretching band (at 1169

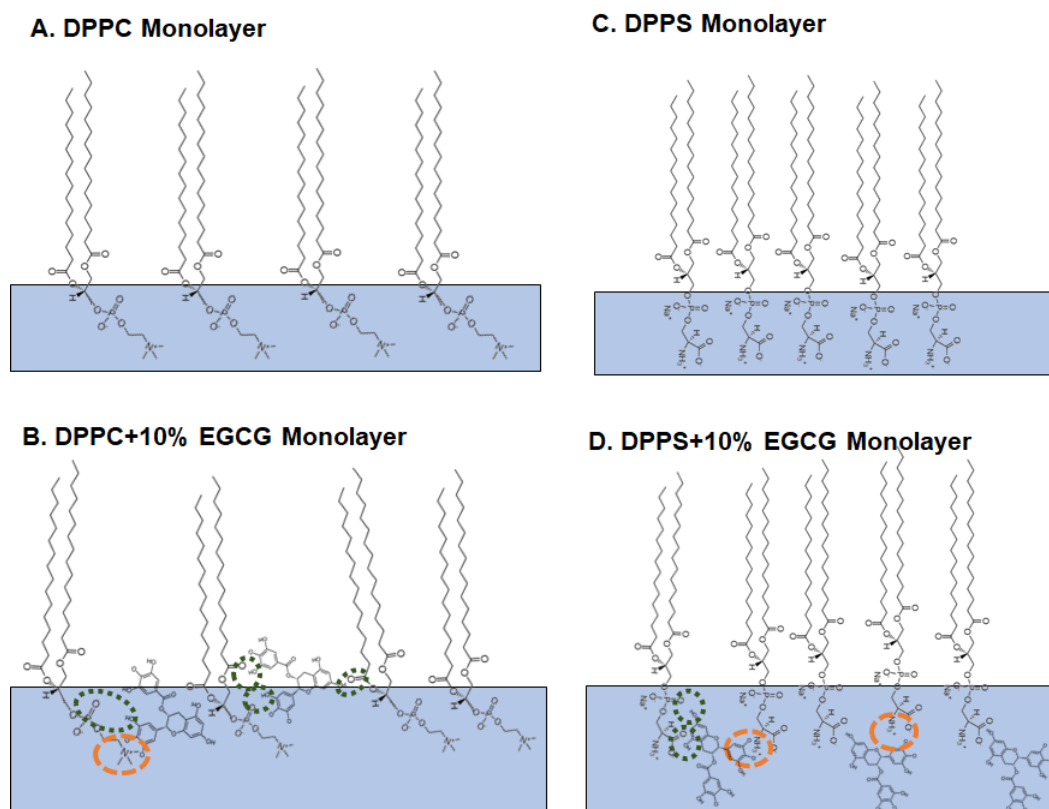


Figure 6.4: Illustrative model for DPPC monolayer (A) and EGCG interaction with a DPPC monolayer (B). EGCG intercalates among DPPC molecules at the air/water interface establishing H-bonding between the OH groups of EGCG and P=O and C=O groups of DPPC (green circle), in addition to ion pairing interactions between the charged oxygen groups of EGCG and the quaternary N⁺ of DPPC (orange circle). From the differences in the ordering of acyl chains, it seems that EGCG can insert into the hydrophobic region of the lipids. C. Illustrative model for DPPS monolayer. D. Illustrative model for EGCG interaction with a closely packed DPPS monolayer. The tighter packing of the DPPS monolayer prevents EGCG penetration to the hydrophobic lipid chains. EGCG binds onto the DPPS surface at the interface through H-bonding between the OH groups of EGCG and P=O and C=O groups of DPPS (green circle), in addition to the electrostatic interactions between the charged oxygen groups of EGCG and the protonated amine NH₃⁺ of DPPS (orange circle).

cm^{-1}), suggesting some nucleophilic attack to DPPC polar moiety by oxidant species produced by radiation. The red-shift of the antisymmetric P=O band points to weakening of the P=O bonds and loss of electron density.[34]

The location of EGCG in the DPPC monolayer may be inferred from a combined analysis of PM-IRRAS data and surface pressure isotherms. One of the most important physicochemical property of a drug that affects its location and orientation in a phospholipid monolayer is its ionization state. In an alkaline pH

CHAPTER 6. THE IMPACT OF BLUE LIGHT IN TUMORIGENIC AND NONTUMORIGENIC MONOLAYERS CONTAINING EGCG

Table 6.1: Vibrational assignments and changes in band position of DPPC monolayer after blue light irradiation and interaction with EGCG.

Assignment	PC	PC+Blue	PC+EG	PC+EG+Blue
Asymmetric CH ₂ tails	2909	2919	2930	2915
Symmetric CH ₂ tails	2852	2857	2828	2848
Carbonyl	1747/1735	1740/1722	1738/1720	1736/1713
% Hydrated Carbonyl	79.4%	55.3%	68.8%	61.3%
Phosphate	1269/1242	1255/1227	1265/1236	1263/1236
% Hydrated Phosphate	64.6%	34.4%	44.4%	48.4%
Symmetric Phosphate	1093	1088	1083	1073
Asymmetric Choline	965	974	976	977
Symmetric Choline	935	945	928/963	933/970

environment, some of the phenol hydroxyl groups of EGCG are electron-donors since they are deprotonated (pKa 7.8-8.7) [35, 36, 37], whereas DPPC molecules are neutral. Hence, electrostatic interactions may occur: (i) between the hydrogen of EGCG hydroxyl groups and the negative oxygen of DPPC phosphate groups, and (ii) between EGCG oxygen groups and the nitrogen of DPPC choline group. In a previous study[14], the incorporation of EGCG molecules was found to trigger a reorganization of hydration water in the polar sites of dimyristoyl phosphatidyl choline (DMPC) due to their ability to form hydrogen bonding with phosphate groups. Here, such hydrogen bonding is revealed by the slight shift in the antisymmetric P=O stretching to lower frequencies (1236 and 1265 cm⁻¹) and the decrease in the fraction of hydrated phosphate groups (44.4%) compared to neat DPPC monolayer (64.6%). Dehydration of phosphate groups is consistent with the decrease in area per molecule by incorporating EGCG in Figure 6.1A. Upon blue irradiation. The antisymmetric P=O and (CO)ester stretching bands were not affected significantly in position and shape in the mixed EGCG/DPPC monolayer, in contrast to what was observed in a neat DPPC monolayer. The percentage of hydrated phosphate groups slightly increases (44.4% to 48.4%) in the mixed EGCG/DPPC monolayer with irradiation because some EGCG are degraded. Upon being degraded, EGCG molecules no longer interact with the DPPC headgroup, thus giving some space to water molecules to bind.

When examining the hydration status of DPPS phospholipids, the bands assigned to the hydrated and non-hydrated phosphate groups of DPPS in Figure 6.3C are seen at lower frequencies, 1196 and 1223 cm⁻¹, respectively, than for DPPC. Indeed, the orientation of the headgroup in relation to the surface plane is distinct between zwitterionic and anionic phospholipids, with DPPS headgroup

oriented perpendicularly whereas the DPPC headgroup is parallel to the monolayer plane [38, 39, 40, 41]. Hence, the results in Figure 6.3C suggest that the phosphate groups of DPPS are oriented more vertically in relation to the interface, maximizing intermolecular hydrogen bonding with the adjacent water molecules. After irradiation, the (CO) ester band shifted from 1150 to 1157 cm^{-1} and the pattern of the antisymmetric phosphate band changed. In particular, there was a significant increase in the hydrated phosphate component, thus indicating that part of the intermolecular H bonds formed between lipids has been disrupted to generate sufficient space for water molecules to reorganize and bind to the phosphate groups. Also, irradiation may affect phosphate – sodium counterions interactions, which are responsible for the decrease in the repulsive headgroup interactions. This may result in the faster release of counterions and uptake of water molecules by the phosphate groups of DPPS. Upon EGCG addition, the phosphate bands shifted to higher wavenumbers (1228 and 1260 cm^{-1}), suggesting that the binding of EGCG to phosphate groups involves replacement of water molecules (Figure 6.3D). These results are consistent with those observed for EGCG/DPPG and EGCG/DMPC monolayers in an aqueous subphase.[14, 17] It is worth noting that EGCG molecules hamper the changes induced by blue irradiation on the band position in the PM-IRRAS spectra and fraction of hydrated phosphate groups in mixed EGCG/DPPS monolayers. The protecting effect is similar to that for EGCG/DPPC monolayers.

The damage induced by irradiation on the charged headgroups of DPPC and DPPS was analyzed in the presence and absence of EGCG. Blue irradiation induced shifts to higher frequencies on the bands assigned to the choline moiety of DPPC. The bands at 935 and 965 cm^{-1} , corresponding to the symmetric and asymmetric $(NCH_3)_3^+$ stretching, shifted to 945 and 974 cm^{-1} . In the mixed EGCG/DPPC monolayer, the asymmetric $(NCH_3)_3^+$ band (at 968 cm^{-1}) was deconvoluted into two bands at 963 and 975 cm^{-1} assigned to $(NCH_3)_3^+$ of DPPC lipids and CH groups in the aromatic groups of EGCG, respectively. With EGCG, the symmetric and asymmetric $(NCH_3)_3^+$ bands shifted to 927 and 963 cm^{-1} owing to electrostatic interactions, with the choline group being oriented in a more vertical position than in pure DPPC monolayer, thus reflecting the condensing effect caused by EGCG. Upon irradiation, the shift in the choline band towards higher frequencies was slightly smaller in the EGCG/DPPC monolayer (to 933 and 970 cm^{-1} , i.e. a spectral difference $\sim 6 cm^{-1}$) than in the neat DPPC monolayer (spectral difference $\sim 10 cm^{-1}$). Moreover, blue irradiation did not yield a significant change in area per molecule for DPPC in the presence of EGCG molecules, given

the similarity between the surface-pressure isotherms for EGCG/DPPC monolayer with and without irradiation (Figure B.2 of Appendix B).

The effect from blue light irradiation is stronger in the surface pressure isotherms of DPPS than in the DPPC monolayer, according to Figure B.3A of Appendix B. This can be attributed to the carboxylate and protonated amine NH_3^+ groups in DPPS, which are more susceptible to radiation-damage than the $(\text{N}(\text{CH}_3)_3)$ choline group of DPPC. Indeed, the significant shift of 30 cm^{-1} in the choline band of the monolayer under irradiation in Figure 6.3G indicates that this functional group in the DPPS headgroup was attacked by irradiation. Nonetheless, the incorporation of EGCG seems to shield these functional groups from radiation since no considerable changes in surface pressure isotherms were caused upon blue light irradiation in Figure B.3B of Appendix B. Accordingly, the wavenumber position of choline bands in the spectra of the DPPS monolayers containing EGCG were shifted from 958 to 966 cm^{-1} , indicating hydrogen bonding between the oxygen groups of EGCG and the protons of amine NH_3^+ of the DPPS headgroup (Figure 6.3H). In this case, the spectral shift in the antisymmetric choline band induced by irradiation was not so drastic for DPPS monolayers containing EGCG than for the pure DPPS ones.

In summary, EGCG molecules are incorporated into the headgroup region of the DPPC monolayer, forming a very condensed monolayer that is more resistant against oxidative stress-induced by blue irradiation than pure DPPC monolayers. EGCG also binds onto a DPPS membrane as illustrated in Figure 6.4D and is capable of scavenging the oxidant species arising from blue irradiation. In this case, however, the EGCG insertion into the hydrophobic region of DPPS phospholipids is hampered since the DPPS monolayer itself is dense and tightly packed due to the strong intramolecular interactions between the quaternary ammonium groups of DPPS and the phosphate or serine carbonyl groups of adjacent lipids.

6.3.3 Morphology and organization of neat and mixed monolayers: BAM analysis

The BAM images indicate that EGCG affects lateral film organization and viscoelastic properties of a DPPC monolayer, consistent with the surface pressure measurements. At the LE–LC plateau region in the surface pressure-area isotherms (7 mN/m), the BAM images in Figure 6.5 show large chiral multilobed domains of pure DPPC that fuse together, forming a homogeneous monolayer at $\pi = 20 \text{ mN/m}$. Also, blue irradiation causes significant decrease in the number and size of DPPC domains, which delays the monolayer condensation ($\pi = 10\text{--}15 \text{ mN/m}$).

Table 6.2: Vibrational assignments and changes in band position of DPPS monolayer after blue light irradiation and interaction with EGCG.

Assignment	PS	PS+Blue	PS+EG	PS+EG+Blue
Asymmetric CH ₂ tails	2912	2912	2921	2916
Symmetric CH ₂ tails	2842	2850	2849	2847
Carbonyl	1774/1765	1778/1769	1738/1724	1744/1719
% Hydrated Carbonyl	35.4%	20.3%	43.3%	38.4%
Phosphate	1223/1196	1221/1200	1260/1228	1262/1233
% Hydrated Phosphate	42.5%	50.4%	31.1%	26.3%
Symmetric Phosphate	1056	1058	1069	1062
Asymmetric Choline	958	988	966	960
Symmetric Choline	934	954	935	919

For instance, upon irradiation the DPPC domains at 10 mN/m are not so condensed and have a more rounded contour upon irradiation. The incorporation of 10 mol% EGCG interferes with the domain formation and shape in the DPPC monolayer, turning the domains smaller and rounded-shaped. At $\pi = 10$ mN/m, a different morphology with branched domains was observed for DPPC+10% EGCG monolayer since EGCG disturbs intermolecular interactions. Upon further compression, these irregular domains merge and the monolayer becomes completely homogeneous. After blue irradiation, the BAM images of EGCG/DPPC monolayer taken at a surface pressure of 10 mN/m suggest that EGCG potentially increases the stability of the monolayer against radiation, since there are no such great differences in morphological appearance of the domains as in the neat DPPC monolayer.

The BAM images of pure DPPS and DPPS+10% EGCG are shown in Figure 6.6, which illustrate the impact of EGCG on the morphology and fluidity of phospholipids domains at LE (7-10 mN/m) and LC (15-30 mN/m) phases. At 7 mN/m, DPPS displayed irregular domains (size range: $7-20 \pm 3 \mu\text{m}$) dispersed within the LE matrix, resulting from the intermolecular attractions between amine and carboxylic groups of DPPS molecules [42, 43]. These domains coalesced and formed a homogeneous monolayer upon further compression. Morphological changes were seen in the BAM images upon irradiation, with DPPS domains becoming more rounded and smaller. After further monolayer compression, it is possible to distinguish these domains in the irradiated DPPS monolayer. The BAM micrographs of DPPS+10% EGCG monolayer showed condensed domains relatively large (size range: $78 \pm 7 \mu\text{m}$) with a distinct circular shape. Blue light does not seem to affect the domain shape so drastically, although still two domain populations can be distinguished at $\pi = 7$ mN/m. It is worth mentioning that the

CHAPTER 6. THE IMPACT OF BLUE LIGHT IN TUMORIGENIC AND NONTUMORIGENIC MONOLAYERS CONTAINING EGCG

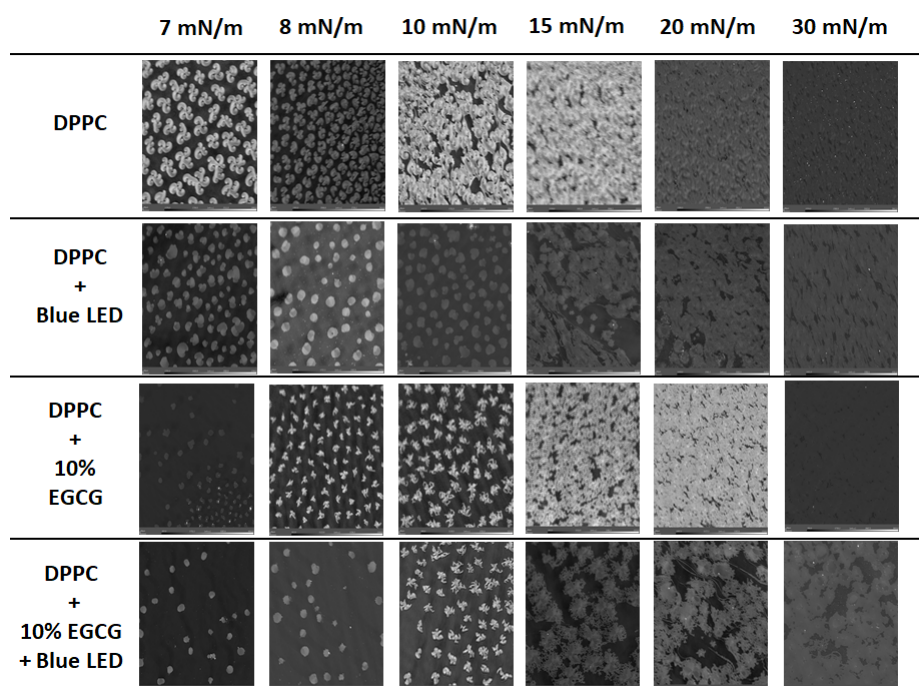


Figure 6.5: BAM micrographs of DPPC and DPPC+10% EGCG monolayers at several surface pressures before and after blue light irradiation.

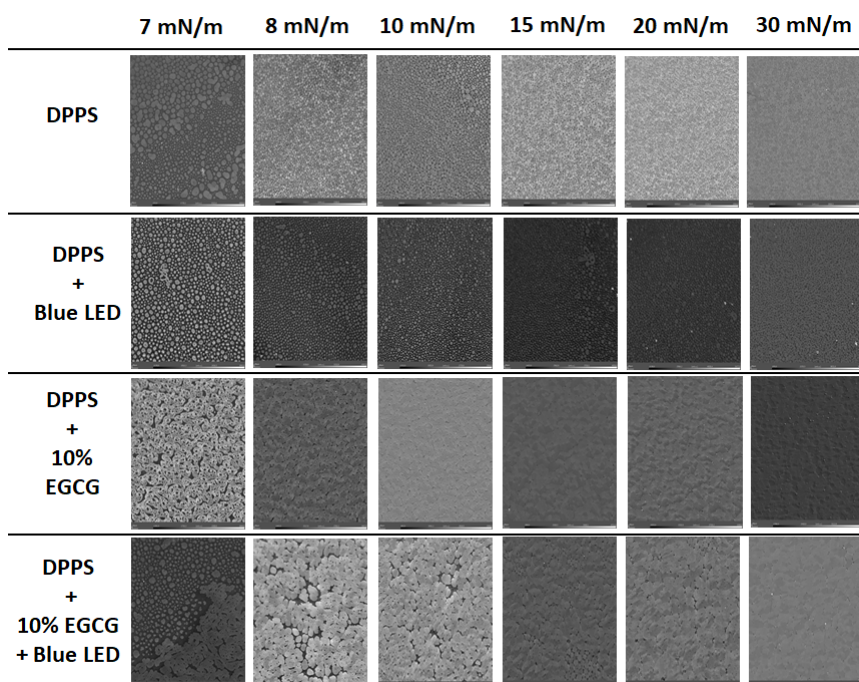


Figure 6.6: BAM micrographs of DPPS and DPPS+10% EGCG monolayers obtained at several surface pressures before and after blue light irradiation.

domains are much more condensed than for DPPS monolayer, suggesting that EGCG effectively confers antioxidant protection under stress conditions.

6.4 Conclusion

The findings from this study indicate that the incorporation of EGCG affects the physicochemical properties of the zwitterionic (DPPC) and anionic (DPPS) Langmuir monolayer, causing condensation of the monolayers. According to the PM-IRRAS spectra, EGCG interacts with the lipid headgroup region, establishing H-bonding with the phosphate and carbonyl groups of the lipids. The charged oxygen groups of EGCG interact electrostatically with the protonated amine NH_3^+ groups of DPPS lipids. EGCG was found to affect the ordering of the DPPC hydrocarbon tails considerably, much more than it does with DPPS, which suggest that EGCG inserts more deeply in the DPPC monolayer, possibly because the quaternization of the amine group ($\text{N}(\text{CH}_3)_3$) of DPPC reduces the interactions at the interface. Despite these differences, the blue light irradiation experiments showed that EGCG has an antioxidant action independently of the phospholipid headgroup properties, hence protecting the phosphate and carbonyl groups from radiation in both monolayers. Nonetheless, the EGCG location in the lipid membrane depends on the headgroup hydration and orientation in relation to the membrane plane. The degree of intermolecular and intramolecular interactions regulate the EGCG penetration into the hydrophobic region. Taken together, the results presented here may have important implications for cancer therapy. It has been shown that the effectiveness of chemotherapeutic agents is higher in cancer cells when combined with EGCG [44, 45, 46, 47]. From our results we may speculate that EGCG can enhance the intracellular trafficking of chemotherapeutic agents across cell membranes to destroy abnormal DNA because it increases membrane fluidity in a concentration-dependent manner. Additionally, some of these chemotherapeutic agents are inducers of apoptosis, a phenomenon presumably more intense in the presence of EGCG due to an induced membrane fluidization and destabilization, thus resulting in much lower survival of cancer cells.

6.5 Acknowledgements

The authors acknowledge the financial support from FEDER, through Programa Operacional Factores de Competitividade – COMPETE and Fundação para a Ciência e a Tecnologia – FCT, by the project PTDC/FIS-NAN/0909/2014 and for the Portuguese research Grant No. PEst-OE/FIS/UI0068/2011 and UID/FIS/00068/2013 through FCTMEC (Portugal) and by FAPESP (2013/14262-7) and CNPq (Brazil). Filipa Pires acknowledges the fellowship PD/BD/106036/2015 from RABBIT Doctoral Programme (Portugal).

References

- [1] J. Cadet, K. J. Davies, M. H. Medeiros, P. Di Mascio, and J. R. Wagner. “Formation and repair of oxidatively generated damage in cellular DNA.” In: *Free Radic Biol Med* 107 (2017), pp. 13–34.
- [2] M. Choe, C. Jackson, and B. P. Yu. “Lipid peroxidation contributes to age-related membrane rigidity.” In: *Free Radical Biology and Medicine* 18.6 (1995), pp. 977–984.
- [3] S Pillai, C Oresajo, and J Hayward. “Ultraviolet radiation and skin aging: roles of reactive oxygen species, inflammation and protease activation, and strategies for prevention of inflammation-induced matrix degradation—a review.” In: *Int. J. Cosmet. Sci.* 27.1 (2005), pp. 17–34.
- [4] K. P. Lawrence, T. Douki, R. P. Sarkany, S. Acker, B. Herzog, and A. R. Young. “The UV/Visible Radiation Boundary Region (385–405 nm) Damages Skin Cells and Induces ‘dark’ Cyclobutane Pyrimidine Dimers in Human Skin in vivo.” In: *Sci. Rep.* 8 (2018), pp. 12710–12722.
- [5] C. Roehlecke, A. Schaller, L. Knels, and R. H. Funk. “The influence of sublethal blue light exposure on human RPE cells.” In: *Molecular Vision* 15 (2009), pp. 1929–1938.
- [6] N. N. Osborne, C. Nunez-Alvarez, and S. del Olmo-Aguado. “The effect of visual blue light on mitochondrial function associated with retinal ganglions cells.” In: *Exp. Eye Res.* 128 (2014), pp. 8–14.
- [7] S. Hopkins, B Siewert, S. Askes, P Veldhuizen, R Zwier, M. Heger, and S. Bonnet. “An in vitro cell irradiation protocol for testing photopharmaceuticals and the effect of blue, green, and red light on human cancer cell lines.” In: *Photochem Photobiol Sci* 15.5 (2016), pp. 644–653.
- [8] C. Opländer, A. Deck, C. M. Volkmar, M. Kirsch, J. Liebmann, M. Born, F. Van Abeelen, E. E. Van Faassen, K.-D. Kröncke, and J. Windolf. “Mechanism and biological relevance of blue-light (420–453 nm)-induced nonenzymatic nitric oxide generation from photolabile nitric oxide derivatives in human skin in vitro and in vivo.” In: *Free Radic Biol Med* 65 (2013), pp. 1363–1377.
- [9] N. Mulinacci, A. Valletta, V. Pasqualetti, M. Innocenti, C. Giuliani, M. Bellumori, G. De Angelis, A. Carnevale, V. Locato, and C. Di Venanzio.

- “Effects of ionizing radiation on bio-active plant extracts useful for preventing oxidative damages.” In: *NAT PROD RES.* 33.8 (2019), pp. 1106–1114.
- [10] R. Pathak, S. K. Shah, and M. Hauer-Jensen. “Therapeutic potential of natural plant products and their metabolites in preventing radiation enteropathy resulting from abdominal or pelvic irradiation.” In: *Int J Radiat Biol* 95.4 (2019), pp. 493–505.
- [11] N. Fischer, E.-J. Seo, and T. Efferth. “Prevention from radiation damage by natural products.” In: *Phytomedicine* 47 (2018), pp. 192–200.
- [12] N. Zhu, M. Wang, G.-J. Wei, J.-K. Lin, C. S. Yang, and C.-T. Ho. “Identification of reaction products of (-)-epigallocatechin,(-)-epigallocatechin gallate and pyrogallol with 2, 2-diphenyl-1-picrylhydrazyl radical.” In: *Food Chem* 73.3 (2001), pp. 345–349.
- [13] G. Brezesinski and H. Möhwald. “Langmuir monolayers to study interactions at model membrane surfaces.” In: *ADV COLLOID INTERFAC* 100 (2003), pp. 563–584.
- [14] F. Pires, V. P. Geraldo, B. Rodrigues, A. d. Granada-Flor, R. F. de Almeida, O. N. Oliveira, B. L. Victor, M. Machuqueiro, and M. Raposo. “Evaluation of EGCG loading capacity in DMPC membranes.” In: *Langmuir* 20 (2019), pp. 6771–6781.
- [15] T. M. Nobre, F. J. Pavinatto, L. Caseli, A. Barros-Timmons, P. Dynarowicz-Łątka, and O. N. Oliveira Jr. “Interactions of bioactive molecules & nanomaterials with Langmuir monolayers as cell membrane models.” In: *Thin Solid Films* 593 (2015), pp. 158–188.
- [16] E. Rascol, J.-M. Devoisselle, and J. Chopineau. “The relevance of membrane models to understand nanoparticles–cell membrane interactions.” In: *Nanoscale* 8.9 (2016), pp. 4780–4798.
- [17] F. Pires, V. P. Geraldo, A. Antunes, A. Marletta, O. N. Oliveira Jr, and M. Raposo. “Effect of blue light irradiation on the stability of phospholipid molecules in the presence of epigallocatechin-3-gallate.” In: *Colloids Surf B* 177 (2019), pp. 50–57.
- [18] F. Pires, V. P. Geraldo, A. Antunes, A. Marletta, O. N. Oliveira Jr, and M. Raposo. “On the role of epigallocatechin-3-gallate in protecting phospholipid molecules against UV irradiation.” In: *Colloids and Surfaces B: Biointerfaces* 173 (2019), pp. 312–319.

- [19] M.-J. Yang, Y.-A. Hung, T.-W. Wong, N.-Y. Lee, J.-M. Yuann, S.-T. Huang, C.-Y. Wu, I.-Z. Chen, and J.-Y. Liang. “Effects of blue-light-induced free radical formation from catechin hydrate on the inactivation of *Acinetobacter baumannii*, including a carbapenem-resistant strain.” In: *Molecules* 23.7 (2018), pp. 1631–1648.
- [20] J.-Y. Liang, J.-Y. Wu, M.-Y. Yang, A. Hu, and L.-Y. Chen. “Photo-catalytic polymerization of catechin molecules in alkaline aqueous.” In: *J Photochem Photobiol B* 165 (2016), pp. 115–120.
- [21] R. Veldhuizen, K. Nag, S. Orgeig, and F. Possmayer. “The role of lipids in pulmonary surfactant.” In: *Biochimica et Biophysica Acta (BBA)-Molecular Basis of Disease* 1408.2-3 (1998), pp. 90–108.
- [22] G. Ma and H. C. Allen. “DPPC Langmuir monolayer at the air- water interface: probing the tail and head groups by vibrational sum frequency generation spectroscopy.” In: *Langmuir* 22.12 (2006), pp. 5341–5349.
- [23] S. Ran and P. E. Thorpe. “Phosphatidylserine is a marker of tumor vasculature and a potential target for cancer imaging and therapy.” In: *Int. J. Radiat. Oncol. Biol. Phys.* 54.5 (2002), pp. 1479–1484.
- [24] T. Utsugi, A. J. Schroit, J. Connor, C. D. Bucana, and I. J. Fidler. “Elevated expression of phosphatidylserine in the outer membrane leaflet of human tumor cells and recognition by activated human blood monocytes.” In: *Cancer Res.* 51.11 (1991), pp. 3062–3066.
- [25] J. Lin, H. Zhang, Z. Chen, and Y. Zheng. “Penetration of lipid membranes by gold nanoparticles: insights into cellular uptake, cytotoxicity, and their relationship.” In: *ACS Nano* 4.9 (2010), pp. 5421–5429.
- [26] K. Gong, S.-S. Feng, M. L. Go, and P. H. Soew. “Effects of pH on the stability and compressibility of DPPC/cholesterol monolayers at the air-water interface.” In: *COLLOID SURF A PHYSICOCHEM ENG ASP* 207.1-3 (2002), pp. 113–125.
- [27] E. V. Lage, J. Magalhães, M. Pinheiro, and S. Reis. “Effect of the alkyl group in the piperazine N-substitution on the therapeutic action of rifamycins: A drug-membrane interaction study.” In: *Chem Biol Interact* 289 (2018), pp. 75–80.
- [28] L. Van Deenen, U. Houtsmuller, G. De Haas, and E Mulder. “Monomolecular layers of synthetic phosphatides.” In: *J Pharm Pharmacol* 14.1 (1962), pp. 429–444.

- [29] A. V. Agasøsler, L. M. Tungodden, D. Āejka, E. Bakstad, L. K. Sydnes, and H. Holmsen. "Chorpromazine-induced increase in dipalmitoylphosphatidylserine surface area in monolayers at room temperature." In: *Biochem. Pharmacol* 61.7 (2001), pp. 817–825.
- [30] P. Wydro. "The interactions between cholesterol and phospholipids located in the inner leaflet of human erythrocytes membrane (DPPE and DPPS) in binary and ternary films – The effect of sodium and calcium ions." In: *Colloids Surf B* 82.1 (2011), pp. 209–216.
- [31] J. Lopez Cascales, J. Garca de la Torre, S. J. Marrink, and H. J. Berendsen. "Molecular dynamics simulation of a charged biological membrane." In: *The Journal of chemical physics* 104.7 (1996), pp. 2713–2720.
- [32] S. Leekumjorn and A. K. Sum. "Molecular studies of the gel to liquid-crystalline phase transition for fully hydrated DPPC and DPPE bilayers." In: *BBA–BIOMEMBRANES* 1768.2 (2007), pp. 354–365.
- [33] J. L. Browning and J. Seelig. "Bilayers of phosphatidylserine: a deuterium and phosphorus nuclear magnetic resonance study." In: *Biochemistry* 19.6 (1980), pp. 1262–1270.
- [34] I. Zawisza, G. Wittstock, R. Boukherroub, and S. Szunerits. "Polarization modulation infrared reflection absorption spectroscopy investigations of thin silica films deposited on gold. 2. Structural analysis of a 1, 2-dimyristoyl-sn-glycero-3-phosphocholine bilayer." In: *Langmuir* 24.8 (2008), pp. 3922–3929.
- [35] S. Wu, K. Sun, X. Wang, D. Wang, X. Wan, and J. Zhang. "Protonation of epigallocatechin-3-gallate (EGCG) results in massive aggregation and reduced oral bioavailability of EGCG-dispersed selenium nanoparticles." In: *J Agric Food Chem* 61.30 (2013), pp. 7268–7275.
- [36] S. H.A.R.I. M. Muzolf Małgorzata and B. Tyrakowska. "pH-dependent radical scavenging capacity of green tea catechins." In: *J Agric Food Chem* 56.3 (2008), pp. 816–823.
- [37] D.-W. Tang, S.-H. Yu, Y.-C. Ho, B.-Q. Huang, G.-J. Tsai, H.-Y. Hsieh, H.-W. Sung, and F.-L. Mi. "Characterization of tea catechins-loaded nanoparticles prepared from chitosan and an edible polypeptide." In: *Food Hydrocoll.* 30.1 (2013), pp. 33–41.
- [38] S. L. Duncan and R. G. Larson. "Comparing experimental and simulated pressure-area isotherms for DPPC." In: *Biophys. J.* 94.8 (2008), pp. 2965–2986.

- [39] S. A. Pandit, D. Bostick, and M. L. Berkowitz. “Molecular dynamics simulation of a dipalmitoylphosphatidylcholine bilayer with NaCl.” In: *Biophys. J.* 84.6 (2003), pp. 3743–3750.
- [40] Y. Chen, H. I. Okur, C. Lutgebaucks, and S. Roke. “Zwitterionic and charged lipids form remarkably different structures on nanoscale oil droplets in aqueous solution.” In: *Langmuir* 34.3 (2017), pp. 1042–1050.
- [41] H. I. Okur, O. B. Tarun, and S. Roke. “The Chemistry of Lipid Membranes—from Models to Living Systems: A Perspective of Hydration, Surface Potential, Curvature, Confinement and Heterogeneity.” In: *J. Am. Chem. Soc.* 141.31 (2019), pp. 12168–12181.
- [42] X. Chen, Z. Huang, W. Hua, H. Castada, and H. C. Allen. “Reorganization and caging of DPPC, DPPE, DPPG, and DPPS monolayers caused by dimethylsulfoxide observed using Brewster angle microscopy.” In: *Langmuir* 26.24 (2010), pp. 18902–18908.
- [43] J Miñones Jr, J. R. Patino, O Conde, C Carrera, and R Seoane. “The effect of polar groups on structural characteristics of phospholipid monolayers spread at the air–water interface.” In: *COLLOID SURF A PHYSICOCHEM ENG ASP* 203.1-3 (2002), pp. 273–286.
- [44] N. M. Yunos, P. Beale, J. Q. Yu, and F. Huq. “Synergism from sequenced combinations of curcumin and epigallocatechin-3-gallate with cisplatin in the killing of human ovarian cancer cells.” In: *Anticancer Res.* 31.4 (2011), pp. 1131–1140.
- [45] L. Chen, H.-L. Ye, G. Zhang, W.-M. Yao, X.-Z. Chen, F.-C. Zhang, and G. Liang. “Autophagy inhibition contributes to the synergistic interaction between EGCG and doxorubicin to kill the hepatoma Hep3B cells.” In: *PLoS One* 9.1 (2014), e85771.
- [46] G.-J. Du, C.-Z. Wang, L.-W. Qi, Z.-Y. Zhang, T. Calway, T.-C. He, W. Du, and C.-S. Yuan. “The synergistic apoptotic interaction of panaxadiol and epigallocatechin gallate in human colorectal cancer cells.” In: *Phytother Res* 27.2 (2013), pp. 272–277.
- [47] D. Pal, S. Sur, R. Roy, S. Mandal, and C. Kumar Panda. “Epigallocatechin gallate in combination with eugenol or amarogentin shows synergistic chemotherapeutic potential in cervical cancer cell line.” In: *J Cell Physiol* 234.1 (2019), pp. 825–836.

RESULTS

On the role of epigallocatechin-3-gallate in protecting phospholipid molecules against UV irradiation¹**Abstract**

Catechin molecules such as epigallocatechin-3-gallate (EGCG) are capable of attenuating the biomolecular damage induced by UV radiation, possibly through molecular mechanisms involving the cell membranes. In this study, we confirmed the protective role of EGCG against UV of 1,2-dipalmitoyl-*sn*-glycero-3-[phospho-*rac*-(1-glycerol)] (sodium salt) (DPPG) in liposomes and cast films. The incorporation of EGCG increased the stability of DPPG liposomes as indicated by UV-vis absorption spectra. Using 2D correlation spectroscopy to analyse the spectra, we found that DPPG and EGCG are co-helpers and complement each other against degradation induced by UV. At the molecular level, UV irradiation affects the phosphate and carbonyl groups of DPPG, in addition to triggering the oxidation and opening of the pyrogallol ring of EGCG. Since EGCG can be incorporated into liposomes and is a strong shield against UV radiation, one may envisage its use in anti-ageing and sunscreen creams, and in dermal drug delivery.

¹This chapter is based on the following publication:

Pires, F., Geraldo, V. P., Antunes, A., Marletta, A., Oliveira Jr, O. N., and Raposo, M.. On the role of epigallocatechin-3-gallate in protecting phospholipid molecules against UV irradiation. *Colloids and Surfaces B: Biointerfaces* 2019, 173: 312-319, DOI:10.1016/j.colsurfb.2018.09.065

7.1 Introduction

Excessive exposure to ultraviolet (UV) radiation, either natural (sunlight) or artificial (tanning beds), is the main driving force for the dramatic increase in skin cancer cases around the world. The exposure to a high dose of UV radiation produces reactive oxygen species (ROS) through water radiolysis, which weakens the immune system, affects the integrity and homeostasis of cell membranes, and ultimately causes DNA damage and premature photoaging.[1, 2] Candidate – molecules for photoprotection of DNA and lipids may be involved both in displacing surrounding water, thus reducing production of hydroxyl groups from collision between secondary radiation/particles (radiation track) and water, and in local quenching/neutralization of ROS to reduce breaks in DNA strands caused by radiation exposure. Catechin molecules, such as epigallocatechin–3–gallate (EGCG), are possible candidates since they are strong antioxidants present in large quantities in green tea, which attenuate and repair the damage of biomolecules induced by radiation.[3, 4, 5, 6] After 1h of drinking a cup of green tea, the concentration of catechins in the bloodstream is sufficient to hinder formation of intracellular ROS, thus reducing the oxidation-induced lesions in DNA. [7]

The efficiency of catechins, however, depends on the diffusion rate towards the extracellular medium/cell membrane interface, which is hindered by their vulnerability to chemical degradation (dimerization, glycosylation and oxidation) and by the rapid clearance from the systemic circulation. Therefore, nano–systems such as liposomes[8], transfersomes [9], nanoethosomes [10, 11] and nanoparticles [12, 13] have been designed to increase the therapeutic efficiency of catechins on the layer skin (stratum corneum and epidermis) [14, 15, 16] and on the deepest epidermal layers (stratum basale)[17, 18]. This allows for a localized, controlled release of catechins to protect skin from UV-induced damage. In addition to oral administration of EGCG, topical application of EGCG solution minimizes complications such as pain, itching and burning feeling in patients with radiation-induced dermatitis, a side effect of breast cancer radiotherapy.[19] In Fang et al.[20], liposomes of egg phosphatidylcholine alone or mixed with anionic species were prepared to topically deliver EGCG on the skin and locally in the tumour to treat basal cell carcinoma in female nude mice. They showed that the presence of the gallate moiety in EGCG, and not in other catechins, increases the lipophilicity of EGCG and leads to a higher encapsulation efficiency, yielding a higher, faster uptake in the skin and tumour than for other catechins.

In this paper, we assess the protective role of EGCG against UV of 1,2 – di-palmitoyl – *sn* – glycerol – 3 – [phospho – rac – (1 – glycerol)] (sodium salt) (DPPG) in liposomes in solution, in addition to comparing with cast films. DPPG was chosen because we wish to test the hypothesis of whether EGCG can be encapsulated into DPPG liposomes for pulmonary and skin administration, which can decrease inflammation and the side – effects of oxidative stress. DPPG liposomes have fusogenic properties that allow for a direct fusion of liposomes with cell membranes and act like skin-penetration enhancers for dermal applications.[21, 22] Furthermore, DPPG liposomes may incorporate magnetic nanoparticles that would be less toxic than if encapsulated in cationic liposomes.[23, 24, 25]

7.2 Experimental details

7.2.1 Materials

EGCG (M.W. 458.4 g/mol) and DPPG (M.W. 744.96 g/mol), whose chemical structures are shown in the insets of Figure 7.1, were purchased from Sigma-Aldrich and Avanti Polar Lipids, respectively.

7.2.2 Liposomes Preparation

DPPG liposomes were prepared using the dry film method [23, 26], with a mixture of chloroform and methanol 4:1 (v:v) to dissolve 5mM DPPG. A gentle stream of nitrogen was used to evaporate the solvent and form a thin lipid film on the walls of a falcon tube. To remove the residual traces of solvent, the falcon tube was placed in a primary vacuum system overnight. Then, the lipid films were hydrated for 2h with ultrapure water or with a 450 μ M EGCG aqueous solution to obtain DPPG or DPPG + EGCG liposomes, respectively, in suspensions with a lipid concentration of 5mM. All the liposomes were prepared with Milli-Q ultrapure water (Millipore GmbH, Billerica, MA). A tip sonicator (UP50H, Hielscher Ultrasonics, GmbH, Germany) was used to sonicate the vesicle suspensions, in an ice bath, to obtain small unilamellar vesicles (SUVs). The procedure was repeated 15 times with 1 min interval between sonication cycles of 30 s. For DPPG+EGCG liposomes, dialysis membranes of regenerated cellulose (Spectra/Pro, Biotech USA) were used to discard non-bound or non-entrapped EGCG molecules in the liposomes. DPPG + EGCG suspensions (10 mL) were placed into the dialysis membrane with the cutoff size of 8–10 kDa and dialyzed against 1000 mL H_2O Milli-Q in a water bath at 37 °C for 48h. The percentage of encapsulated

EGCG molecules was determined from the absorbance spectra measured with a Shimadzu UV-vis spectrometer, model UV 2101, before and after the dialysis procedure. The encapsulation efficiency of ca. 67% was estimated by calculating the ratio between the absorbance at 274 nm of the vesicle suspensions DPPG + EGCG after and before dialysis. The equilibrium dialysis technique was also used to determine the liposome/water partition coefficient (Kp) for EGCG using the equation below:

$$Kp = \frac{n_L \times V_{water}}{n_W \times V_{Lipid}} \quad (7.1)$$

where n_L and n_W are the numbers of moles of EGCG in the lipid bilayer and in the water at the equilibrium, respectively, and V_L and V_W are the volumes of liposomes inside the dialysis bag and in water, respectively. The partition coefficient of EGCG into DPPG liposomes was 1.9, i.e. EGCG is a lipophilic compound that easily incorporates into the vesicles.

7.2.3 Irradiation of samples

The irradiation studies were performed using aqueous solutions of 15 μ M EGCG and vesicle suspension of 0.5mM DPPG and DPPG + EGCG after dialysis. Cast films were prepared using the drop casting method, i.e, depositing some drops of aqueous solutions and vesicle suspensions onto calcium fluoride (CaF_2) substrates that had been cleaned with a 2% mucasol solution, ethanol, ultrapure water and then dried with a nitrogen flux. The vesicle suspensions placed in closed quartz cells as well the cast films deposited on CaF_2 substrates were irradiated with a 254 nm UVC germicide lamp (Philips TUV PL-S 55W/2P 1CT) at a radiance of 1.9 W/m^2 . The damage caused by UV radiation was recorded by measuring the UV-vis and infrared absorption spectra of the solution/vesicle suspension and cast films, respectively, over the irradiation time. The infrared measurements were performed with a Fourier transform infrared (FTIR) spectroscope Thermo Scientific Nicolet-model 530 (Waltham, MA, USA) in the transmittance mode at a resolution of 4 cm^{-1} and 128 scans.

7.2.4 Principal component analysis

Principal component analysis (PCA) is a statistical method that converts a set of data of correlated variables into a set of values of linearly uncorrelated variables (principal components).[27, 28] PCA was performed using a correlation matrix, where the original variables are all standardized and the total variance is equal

to one. The data matrix was built using the UV–vis or the IR spectra for different UV irradiation times. The UV–vis region analysed was between 190–400 nm. For IR, the regions chosen were between 1145–1319 cm^{-1} , 1315–1541 cm^{-1} and 1700–1760 cm^{-1} , corresponding to absorption bands assigned to phosphate stretching, CH_2 scissoring and carbonyl stretching, respectively. The PCA analysis was applied to samples of DPPG and DPPG + EGCG to extract information about the protective role of EGCG against UV damage.

7.2.5 2D–correlation spectroscopy

Since the changes in the UV–vis spectra induced by irradiation are not straightforward to analyse, 2D-correlation spectroscopy was also applied. This mathematical technique is used to analyse small changes in measured signals when a sample is subjected to an external perturbation. In the present case, the perturbation comes from irradiation and the measured signals are the UV–vis spectra. This technique consists in obtaining the 2D correlation spectrum, $X(\lambda_1, \lambda_2)$, which allows for a quantitative comparison of variation patterns in spectral intensities at two different spectral variables, the wavelength λ_1 and λ_2 , along the external variable of perturbation. Here, this variable is the time, t , represented by the expression:[29]

$$X(\lambda_1, \lambda_2) = \langle \tilde{y}(\lambda_1, t) \cdot \tilde{y}(\lambda_2, t) \rangle = \Phi(\lambda_1, \lambda_2) + i\Psi(\lambda_1, \lambda_2) \quad (7.2)$$

where the symbol $\langle \rangle$ is a cross-correlation function to compare the dependence patterns of the chosen quantities $\tilde{y}(\lambda_1, t)$ and $\tilde{y}(\lambda_2, t)$. These are also designated as dynamic spectra, which can be obtained when a perturbation-induced variation is observed during a fixed interval of irradiation time t . Considering a perturbation-induced variation of a spectral intensity, $y(\lambda_2, t)$ measured over a limited range with minimum time (t_{min}) and maximum time (t_{max}), one can calculate the dynamic spectra, by:

$$\tilde{y},(\lambda, t) = y(\lambda, t) - \frac{1}{(t_{max} - t_{min})} \int_{t_{min}}^{t_{max}} (\lambda, t) dt \quad (7.3)$$

The 2D correlation spectrum can be also treated as a complex number function where the real component, $\Phi(\lambda_1, \lambda_2)$ corresponds to the synchronous 2D correlation intensity map and the imaginary part yields the asynchronous 2D correlation intensity map, $\Psi(\lambda_1, \lambda_2)$. The first represents the similarity or coincidental absorbance changes at a given wavelength when a sample is submitted to a perturbation-time changing from t_{min} to t_{max} . The second part is the asynchronous 2D correlation spectrum, representing absorbance variations out-of

phase or dissimilarities (the events occur at different irradiation times).[29, 30] It should be noted that the horizontal and vertical axes of these maps correspond to the wavelengths (λ) of the UV–vis spectra measured. As for the interpretation, the synchronous maps are symmetric in respect to a diagonal line corresponding to wavelength coordinates $\lambda_1 = \lambda_2$. If the UV–vis spectra change with irradiation time, peaks will appear in the diagonal (auto-peaks) and off-diagonal positions.[31] 2D Shige software for two-dimensional correlation spectroscopy, a free software by Shigeaki Morita (Osaka Electro-Communication University, Japan)[29, 31], was employed to verify radiation induced-damage on cast films of DPPG, EGCG and DPPG + EGCG by using UV–vis spectra.

7.3 Results and discussion

7.3.1 UV radiation influence on EGCG incorporated in liposomes

7.3.1.1 Analysis of UV damage via UV–vis spectroscopy

UV–vis spectroscopy was used to analyse the damage caused on EGCG solutions and DPPG and DPPG + EGCG vesicle suspensions exposed to 254 nm UV light. We recall that EGCG + DPPG vesicle suspension was subjected to dialysis prior to irradiation to eliminate EGCG molecules that were not interacting with the liposomes. The encapsulation efficiency for EGCG into the liposomes was 67%. The absorption spectrum of EGCG in pure water in Figure 7.1a exhibits two bands at 206 nm and 274 nm, assigned to electronic transitions on aromatic rings and $n-\pi^*$ transition involving oxygen electrons from the gallic acid group[32, 33], respectively. Even in the dark at room temperature, EGCG aqueous solutions (not exposed to UV) are already changed over time, as indicated by the slight decrease in intensity of the peaks at 206 nm and 274 nm in Figure 7.1a. Such changes could be attributed to the tendency of EGCG to suffer dimerization in aqueous solutions owing to its amphipathic nature and the number of hydroxyl groups in its aromatic rings.[34, 35] As expected, the band intensity decreased sharply upon exposure to UV radiation, with the EGCG solution being almost entirely bleached after 2340 min (39 h) of irradiation in Figure 7.1b.

The spectra of DPPG liposomes in Figure 7.1c display an absorption band near 198 nm, consistent with the typical band at 194.4 ± 0.7 nm[36] for DPPG molecules assigned either to the transition from the lone-pair on the carbonyl oxygen to the

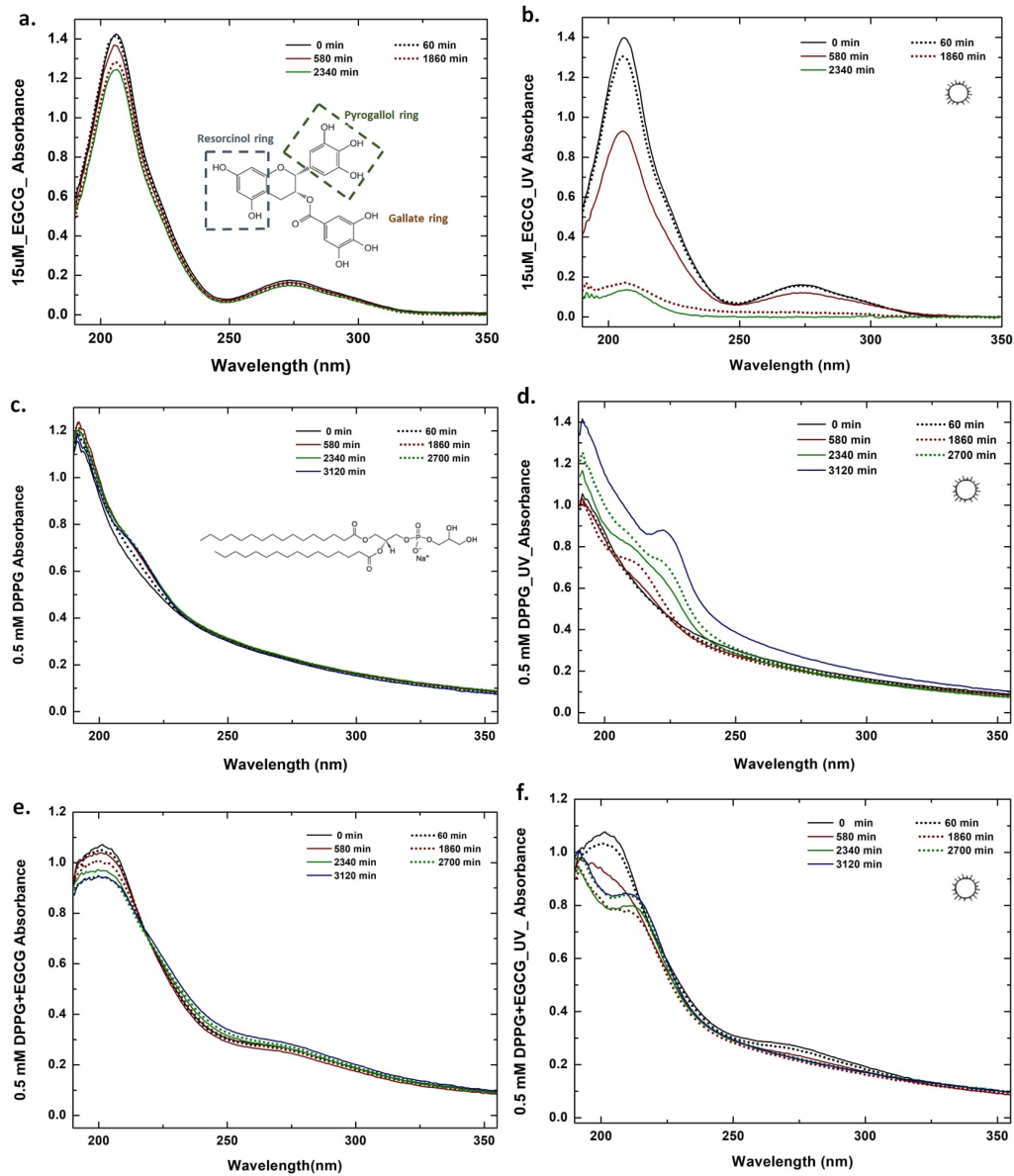


Figure 7.1: Absorption spectra of EGCG (a,b), DPPG liposomes (c,d) and DPPG + EGCG liposomes (e,f). Samples of control group (a,c,e) were maintained in the dark and the absorbance spectra were recorded over time in order to analyse the stability of each sample during storage. The remaining samples (b,d,f) were exposed to 254 nm UV light over time.

antibonding π_{CO} valence orbital[37, 38], $n_0 \rightarrow \pi_{CO}^*$, or to the valence shell electronic excitations of hydroxyl groups.[39, 40, 41, 42] The appearance of a new band at 215 nm shows that during storage the DPPG molecules undergo a possible oxidation process. This oxidation is enhanced upon exposure to UV radiation, with the band at 215 nm increasing with irradiation time and shifting to 222 nm after prolonged irradiation in Figure 7.1d. Hydrolysis and oxidation are the main degradation pathways of lipids. Ionizing radiation triggers water radiolysis to form radicals such as hydroxyl (OH), hydrogen peroxide (H_2O_2) and hydroperoxyl. In polyunsaturated lipids, these radicals attack the hydrogen of methylene groups, with rearrangement of carbon double bonds to form conjugated dienes. Oxidation of these lipids can be monitored by measuring the absorption band of conjugated dienes between 215 and 250 nm.[43] In saturated phospholipids, the ester bonds and hydroxyl groups attached to the polar moiety are attacked by radicals arising from the radiation exposure. For DPPG, irradiation leads to degradation products such as dipalmitoylphosphatidic acid, 1,2-dipalmitoyl-*sn*-glycerol-3-phospho-(1,3-dihydroxyacetone), dipalmitoyl-*sn*-glycerol-3-phosphoryl, (1,2-dihydroxypropaldehyde), 1-palmitoyl-*sn*-propanediol-3-phosphorylglycerol and 1,2-dipalmitoyl-*sn*-glycerol-3-phosphorylethanol.[44]

The spectra of DPPG + EGCG samples not exposed to radiation in Figure 7.1e suggest that the addition of EGCG enhanced liposomes stability since there was no evidence of the peak at 215 nm. In the spectra of irradiated DPPG + EGCG liposomes in Figure 7.1f, the peak at 215 nm only appeared after the characteristic peaks of EGCG, now centred at 202 nm and 276 nm, disappeared, indicating that the EGCG molecules were subjected to damage. From these data, we suggest that part of EGCG molecule, viz. the gallate group responsible for the peak at 276 nm, penetrates the phospholipid bilayer leaving the other groups of the molecule (202 nm) outward facing. These groups act as a protection shield for the liposomes, being directly exposed to UV radiation instead of DPPG molecules. After 2340 min, the EGCG protecting shield was disrupted and UV radiation began to attack the phospholipids (thus causing the 215 nm band to appear). From the absorbance data we conclude that EGCG has affinity to the lipid bilayer and this interaction is sufficient to protect DPPG from oxidation during ca. 1860 min (31 h). The absorbance spectra for DPPG and DPPG + EGCG taken before and after irradiation are displayed in Figure 7.2a for comparison.

The effects from UV irradiation time are more clearly seen by plotting the absorbance at 206 nm in Figure 7.2a, with the following worth observing features: I) for EGCG solution, absorbance decreases exponentially with the irradiation time, with a characteristic time of 650 ± 20 min ($10.8 \pm 0.4h$) and correlation of

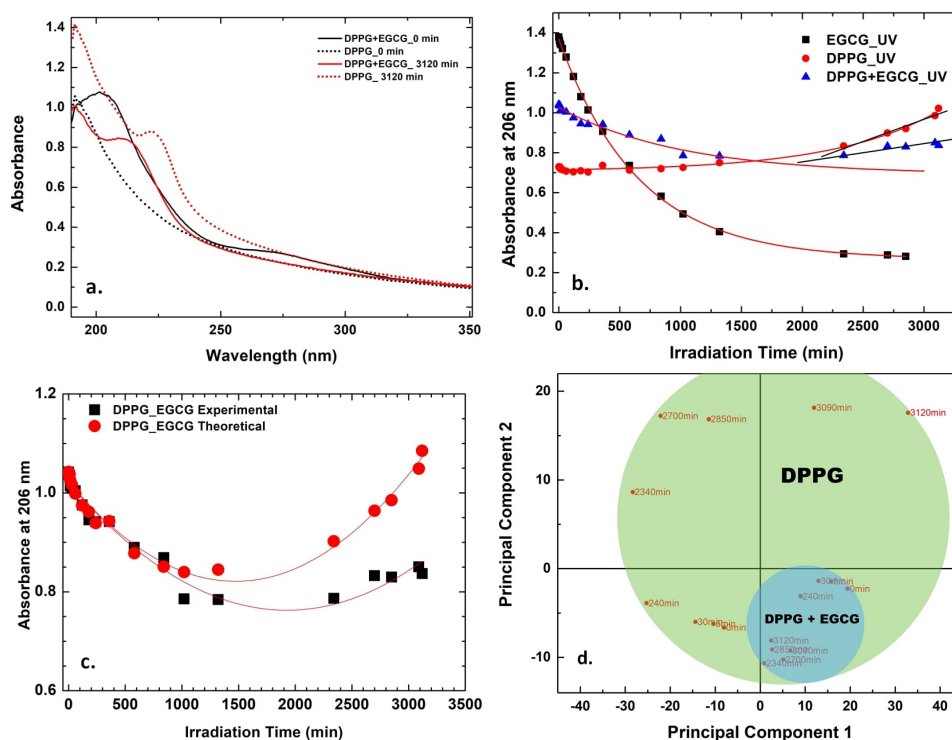


Figure 7.2: a. Absorption spectra of DPPG liposomes and DPPG + EGCG liposomes before and after irradiation. b. Absorbance at 206 nm of DPPG (black square), EGCG (black circle) and of EGCG encapsulated or on DPPG liposomes (empty triangle) as a function of UV irradiation time. The solid lines represent the fittings. c. Experimental and calculated absorbance at 206 nm of EGCG encapsulated in DPPG liposomes (red circle) versus irradiation time. The lines are only to guide the eyes. d. PCA for the UV-vis spectra of DPPG and DPPG + EGCG liposomes, in the region between 190–400 nm, over irradiation time

0.996; II) for DPPG vesicle suspension, absorbance is practically unaffected until 1860 min (31 h) of irradiation, then increased linearly with time at a slope of $(2.3 \pm 0.2) \times 10^{-4} \text{ min}^{-1}$ and correlation coefficient of 0.986; III) for DPPG + EGCG vesicle suspension after dialysis the absorbance decreased exponentially until an irradiation time of 840 min with a characteristic time of 960 ± 60 min (16 ± 1 h) and correlation coefficient of 0.981, followed by a slight increase. The analysis of the UV effects is complicated by the fact that for EGCG the absorbance always decreases while for DPPG there is an increase in absorption after long exposure. If we assume that the damages caused by UV on the two types of molecule were independent, the absorbance at 206 nm should follow the curve in Figure 7.2b labelled as DPPG + EGCG calculated data. This latter curve was obtained from the measured absorbance at 206 nm in Figure 7.2a versus the irradiation time of the

EGCG and DPPG samples, and then normalized taking into account the respective concentrations of EGCG and DPPG. The absorbance values for each EGCG and DPPG samples were then added to yield the calculated curve in Figure 7.2c. The actual dependence (DPPG + EGCG experimental data), also shown in this figure, indicates that EGCG molecules protect DPPG from being oxidized, as the increase in absorbance is much less than the predicted based on independent processes.

Figure 7.2d shows the PCA plot for the UV-vis spectra of DPPG and DPPG + EGCG samples, where each dot represents a sample of DPPG or DPPG + EGCG liposomes irradiated with UV light over a specific time. The general idea is that if liposomes are more resistant against UV damage the PCA data should cluster. In the PCA analysis, clustering results from the transformation of the dataset to a coordinate two dimensions system: first principal component and second principal component. So, the dots are spread out along a diagonal line (the two endpoints of this line represent the maximum variation in the dataset), PC1, but also, they are spread out above and below this line (representing the second most variation), PC2. Thus new X and Y axes are created which describe the variation in the dataset. The negative and positive signs suggest the direction a given variable in that principal component axis is going for along that single dimension vector. The magnitude gives the strongest/weakest correlation of a variable with each component axis. Figure 7.2d shows the PCA biplot for the UV-vis spectra of DPPG and DPPG + EGCG samples, where the cumulative variance is 91.15% for the two first components (PC1 and PC2). There is clear separation of the points corresponding to DPPG liposomes, indicating dissimilarities in the samples resulting from the lipid-structural changes induced by UV radiation exposure. In contrast, the points corresponding to the DPPG + EGCG liposomes are closer to each other, thus suggesting that EGCG molecules slowdown the cascade of oxidant events responsible for damaging the lipid, at least to a certain extent.

7.3.2 2D-Correlation Spectroscopy applied to UV-vis spectra

Two-dimensional (2D) analysis on 200–400 nm region over radiation time range 0–3120 min was performed and the results are shown in Figure 7.3. In the synchronous map of EGCG (Figure 7.3 Ia), one autopeak at 206 nm was obtained, indicating a change in the absorbance. The peak at 206 nm, associated to the aromatic ring of EGCG, decreased exponentially with the irradiation time. In the asynchronous map in Figure 7.3 Ib, two positive cross-peaks ((206, 225 nm), (206, 276 nm) and one negative correlation peak (198, 206 nm) appear. According to

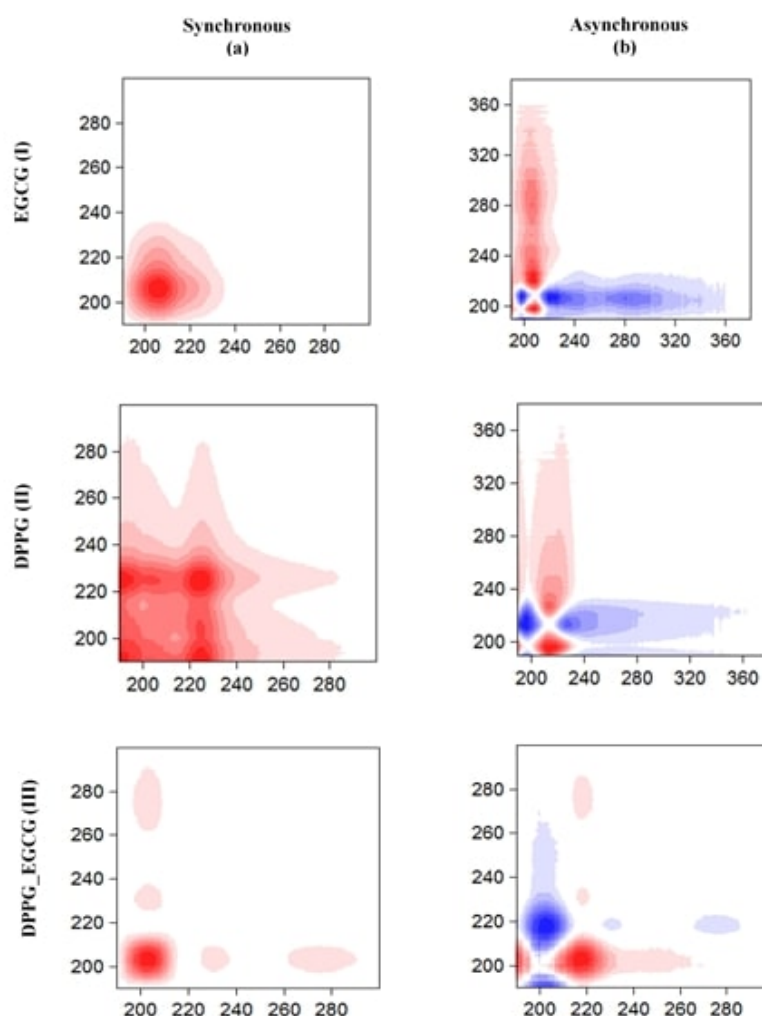


Figure 7.3: a) Synchronous and b) asynchronous 2D correlation maps in the wavelength region between 190 and 300 nm of aqueous solutions of EGCG, vesicle suspension of DPPG and DPPG + EGCG. All these solutions and vesicle suspension were irradiated with 254 nm UV during different periods of time. Red and blue colours mean positive and negative correlation, respectively.

Noda's rule, the cross-peaks become positive if the absorbance change at 206 nm (abscissa scale (λ_1)) occurs prior to the change in absorbance at 225 and 276 nm (ordinates scale (λ_2)). On the other hand, the negative crosspeak appears when the change at $\lambda_1 = 198$ nm occurs predominantly after $\lambda_2 = 206$ nm. Based on these results, it is inferred that the UV light damages the band at 206 nm in the first place, and then the bands at 225 and 276 nm associated with the gallic acid ring of EGCG.

The synchronous map for DPPG in Figure 7.3 IIa presents two auto-peaks at 193 and 225 nm and a positive crosspeak (193, 226 nm). This indicates that these

bands, assigned to the carbonyl oxygen and hydroxyl groups of DPPG, are affected by UV light simultaneously. The asynchronous maps reveal the sequential changes of the spectral intensities in response to radiation time showing, in the case of DPPG, one positive crosspeak at (215, 226 nm) and another negative crosspeak at (198, 215 nm). According to Noda's rule, as the crosspeaks (193, 226 nm) and (198, 215 nm) in the synchronous and asynchronous maps, respectively, have opposite signs, the change in intensity of the 198 nm absorbance peak occurs after the change in the 215 nm absorbance peak. The absorbance spectra in Figure 7.1 corroborate this interpretation.

For DPPG + EGCG, the synchronous map in Figure 7.3 IIIa) displays one autopeak at 203 nm and two positive cross-peaks at (203, 232 nm) and (203, 275 nm), indicating that the spectral intensity variation of the 203 nm peak is related to the changes in the 232 nm and 275 nm peaks. In other words, the change in the 203 nm peak is correlated to the UV-induced damage on the phospholipid structure (peak at 232 nm) and gallate ring of EGCG (275 nm). It should also be mentioned that the notorious absence of the autopeak at 225 nm in the DPPG + EGCG synchronous maps, previously observed in the DPPG synchronous maps, indicates that EGCG molecules protect the lipid's integrity against oxidative stress to a certain extent. The two positive crosspeaks at (219, 232 nm), (219, 275 nm) and the negative crosspeak at (203, 219 nm) in the asynchronous maps of DPPG + EGCG, in Figure 7.3 IIIb), indicate that the 219 nm peak changes prior to the change in the 232 nm and 275 nm peaks, while the change in the 203 nm peak occurs predominantly after the change in the 219 nm peak. These results show that DPPG protects EGCG molecules from radiation since the absorbance peaks of DPPG (219 and 232 nm) were affected before those of EGCG (203 and 275 nm). In summary, EGCG and DPPG are co-helpers against oxidative stress-induced by UV radiation.

7.3.3 Analysis of UV damage via infrared spectroscopy

The effects from UV irradiation are seen in the FTIR-spectra of EGCG, DPPG and DPPG + EGCG cast films in Figure 7.4a. The FTIR spectra of EGCG shown in this Figure are altered considerably by UV irradiation, especially at the 1340 and 3360 cm^{-1} band assigned to O-C=O of gallic acid and OH-attached to aromatic rings of EGCG, respectively. Furthermore, in the case of EGCG samples, some molecules may have come off the solid support during the successive irradiation procedure. The entire assignment for the bands in Figure 7.4a is given in Table 7.1, Table 7.2. The DPPG liposomes deposited onto a solid support are much less affected

by UV irradiation, though some degradation occurs in hydrophobic hydrocarbon tails and in phosphate headgroups, as seen by the decrease in intensity of the peaks at 1093 cm^{-1} and 1221 cm^{-1} , respectively. Significantly, for the liposomes containing EGCG, i.e. DPPG + EGCG, there is practically no degradation induced by UV irradiation, as demonstrated in Figure 7.4a.

Since in both DPPG and DPPG + EGCG liposomes the lipid hydrocarbon chains practically remain unaltered after radiation, the intensity of the symmetric stretching of CH_2 at 2850 cm^{-1} was assigned a value of 1 and the intensities of the phosphate and carbonyl groups of phospholipids were normalized to this value. The objective was to infer if the rate of oxidizing events on these hydration centers changes in the presence of EGCG. As expected, radiation exposure leads to an accentuated decrease in absorbance of the peaks corresponding to phosphate and carbonyl groups of DPPG liposomes. This confirms that these hydration centers are very sensitive and easily damaged. Such damage seems to be slowed down when EGCG molecules are present in the lipid bilayer (Fig. C.1).

Table 7.1: Characteristic infrared absorptions of EGCG cast films prepared onto CaF_2 solid supports. The assignments were performed having into account.[45, 46]

EGCG band frequency (cm^{-1})	Assignment
975	Stretching of C-H group in the aromatic ring
1016	Stretching C-H group in the aromatic ring
1035	C-O-C group that links the chroman ring and trihydroxy benzoate ring
1095	Bending of C-OH alcohols
1144	Bending of C-OH alcohols
1238	Carboxylate stretching
1340	Stretching of O-C=O
1458	Stretching of C-H group in chroman ring
1519	C=C aromatic ring
1610	C=CH ₃ that links the trihydroxybenzoate group and chroman group
1695	Stretching of C=O of gallic acid that links the trihydroxybenzoate group and chroman group
3360	Stretching of O-H group attached to aromatic ring

The IR regions between $1145\text{--}1319\text{ cm}^{-1}$, $1315\text{--}1541\text{ cm}^{-1}$ and $1700\text{--}1760\text{ cm}^{-1}$ due to absorption bands of phosphate stretching, CH_2 scissoring and carbonyl stretching, respectively, were selected to perform the PCA analysis. The plot in Figure 7.4b has a cumulative variance of 84.51% and shows two well-defined

CHAPTER 7. ON THE ROLE OF EGCG IN PROTECTING PHOSPHOLIPID MOLECULES AGAINST UV IRRADIATION

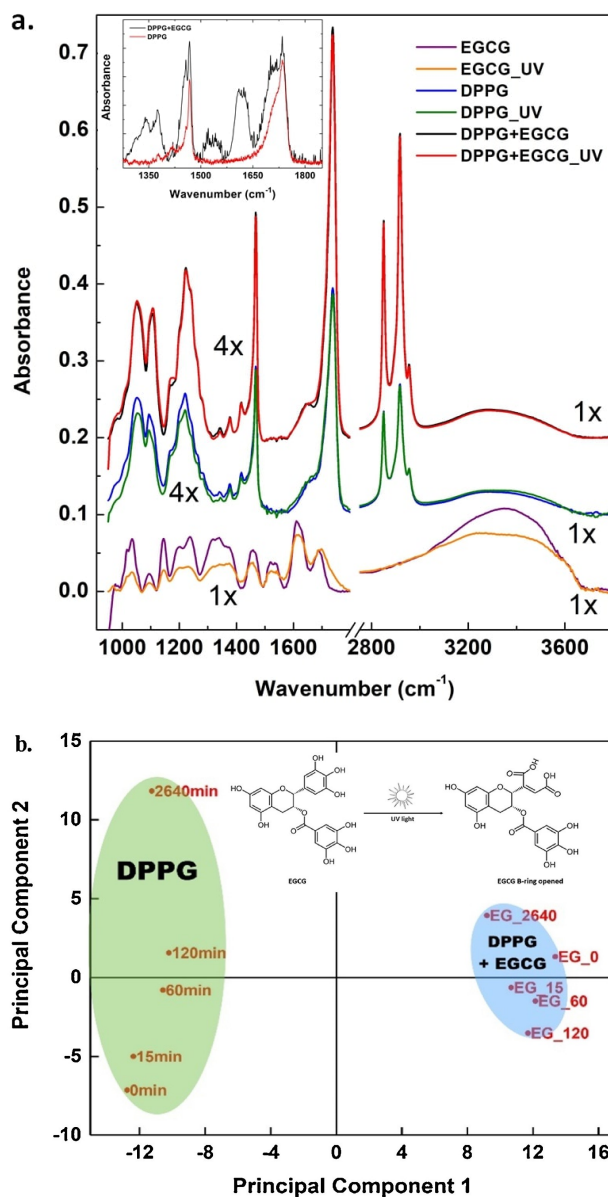


Figure 7.4: a. FTIR spectra for cast films of EGCG, DPPG and DPPG + EGCG before and after UV irradiation. The inset shows the FTIR spectra of DPPG and DPPG + EGCG mixture with similar concentrations, measured using a FTIR spectrometer purging high-purity nitrogen, revealing typical bands of EGCG at 1350, 1519 and 1695 cm^{-1} . b. PCA for IR spectra of DPPG (green circle) and DPPG + EGCG (blue circle) liposomes over irradiation time. The biplot of the first two principal components showed 84.51% of the cumulative variance. In the inset is shown the scheme of a possible reaction pathway that leads to oxidation of the B-ring of EGCG (pyrogallol ring) and to the opening of the ring.

clusters corresponding to DPPG (left-side) and DPPG + EGCG (right-side) liposomes data. This clear separation indicates that UV radiation induces different effects on these types of liposomes. Similarly to what was observed in the PCA analysis of absorbance data, the DPPG + EGCG points are grouped closer than the DPPG points. Therefore, in the absence of EGCG molecules, UV irradiation causes more drastic changes in DPPG, mainly in the IR regions assigned to phosphate and carbonyl groups. EGCG molecules can act like a shield against UV light because they can be accommodated below the phosphate groups of DPPG in the lipids ester region, where the hydroxyl groups (hydrogen bond donors) of EGCG can interact with the negative oxygen groups of DPPG (hydrogen bond acceptors). This is possible owing to the liposomal membrane-water partition coefficient for EGCG ($K_p = 1.9$) and the hydrophobicity of the molecule.

Table 7.2: Characteristic infrared absorptions of DPPG cast films prepared onto CaF_2 solid supports. The assignments were done having in to account and references therein.[46]

DPPG band frequency (cm^{-1})	Assignment
1053	Symmetric stretching of C-O-C
1094	Symmetric stretching of CO-O-C
1169	Asymmetric stretching of CO-O-C
1220	P=O antisymmetric stretching of PO_4^- group
1240	Anti-symmetric stretching of hydrated PO_4^- group
1418	in plane bending of C-O-H group
1468	CH_2 Scissoring
1738	Stretching of carbonyl group (C=O)
2851	Symmetric C-H stretching of the phospholipid hydrocarbon: CH_2
2918	Antisymmetric C-H stretching of the phospholipid hydrocarbon: CH_2
3325	OH group of glycerol and H_2O retained in liposomes

From the UV-vis absorbance data, one notes that 2340 min is sufficient to degrade EGCG molecules. Hence, oxidation of the lipids heads is expected (Figure 7.4a) followed by a decrease in CO due to the loss of EGCG molecules that shield the liposomes, as suggested by the analysis of the UV-vis spectra. But Figure 7.4a shows that the absorbance of CO does not change even after 2340 min. This may be due to water that would contribute with additional oxygen atoms to trigger oxidation pathways of the B-ring of EGCG (pyrogallol ring), thus opening this ring (scheme in Figure 7.4b) and creating new CO bonds. Such a hypothesis is consistent with the scavenging activity of ROS by the gallate group and the B-ring

of EGCG, which is crucial to prevent lipid peroxidation. [47, 48, 49] According to Salah et al, the conversion of trihydroxylphenyl B-ring to o-dihydroxylphenyl B-ring is efficient to decrease the scavenger activity of EGCG.[48] In fact, if UV light leads to this conversion of EGCG, the intensity of the 1738 cm^{-1} band comes from contributions of CO of DPPG and of the opened B-ring of EGCG. One should note that in the DPPG + EGCG liposomes the decrease in intensity of the phosphate band at 1221 cm^{-1} and the increase in CO-O-C band at 1169 cm^{-1} only occurred after 2340 min of irradiation, possibly linked to the decrease in the scavenging activity of EGCG.

The spectra between 2400 and 3800 cm^{-1} for DPPG and DPPG + EGCG indicate that the CH stretching in CH_2 and CH_3 of DPPG at 2850 and 2915 cm^{-1} , respectively, was not affected by UV irradiation. Hence, the presence of EGCG had no appreciable effect on these hydrocarbon groups. However, the changes in the DPPG spectrum for the region between 3200 and 3600 cm^{-1} , in contrast to the lack of changes in DPPG + EGCG liposomes, point to DPPG being more vulnerable to UV light.

We conclude that lipid oxidation is prevented by addition of EGCG, since the binding of EGCG to lipid molecules through hydrogen bonding decreases the number of water molecules near the phosphate ($\text{P}=\text{O}$) and carbonyl ($\text{C}=\text{O}$) groups of the lipids, thus decreasing the ROS production rate during UV exposure. In addition, EGCG exerts antioxidant activity, quenching the generated ROS that induces lipid oxidation.

7.4 Conclusion

The effects from the catechin EGCG on two types of DPPG assemblies have been investigated, namely in liposomes and cast films from the liposome solutions. In all systems, EGCG was found to protect DPPG molecules from damage induced by UV irradiation. The changes observed with UV-vis and FTIR spectroscopies may be interpreted in terms of molecular-level interactions involving the aromatic rings (gallic acid moiety) of EGCG and carbonyl and phosphate groups of DPPG. The presence of a micromolar amount of EGCG is sufficient to decrease the UV-induced damage in COC, phosphate and carbonyl ($\text{C}=\text{O}$) group of DPPG, for example. After a certain irradiation time (or radiation dose), UV light attacks and opens the B-ring of EGCG (pyrogallol ring) dismantling this biological shield against lipid oxidation.

Within a colloid and interface science context, results from this study contribute to the understanding of how EGCG regulates the physicochemical properties of the water-lipid interface in the liposome to protect it against radiation damage. Important issues to address in future studies include a detailed analysis of oxidation index and formation of photoproducts with the radiation dose. Furthermore, experimental and theoretical work should be performed to investigate the interaction between EGCG at distinct concentrations and monolayers at the air/water interfaces, preferably with lipid mixtures to better represent the complexity of a cell membrane (mixture of saturated/polyunsaturated lipids and cholesterol). This would provide a framework to understand the antioxidant paradox and determine the behavior of EGCG at the water-oil environment in complex systems. Such basic knowledge is required to correlate molecular-level properties of EGCG and its possible ability to be used in treating human diseases. Indeed, liposomal formulations able to encapsulate EGCG may be relevant for cosmetics (anti-ageing and sunscreen creams) and in dermal drug delivery.

7.5 Acknowledgments

The authors acknowledge the financial support from FEDER, through Programa Operacional Factores de Competitividade – COMPETE and Fundação para a Ciência e a Tecnologia–FCT, by the project PTDC/FIS-NAN/0909/2014 and for the Portuguese research Grant No. PEst-OE/FIS/UI0068/2011 and UID/FIS/00068/2013 through FCT-MEC (Portugal) and by FAPESP (2013/14262-7) and CNPq (Brazil). Filipa Pires acknowledges the fellowship PD/BD/106036/2015 from RABBIT Doctoral Programme (Portugal).

References

- [1] S. Beissert and K. Loser. “Molecular and cellular mechanisms of photocarcinogenesis.” In: *Photochemistry and photobiology* 84.1 (2008), pp. 29–34.
- [2] A. Svobodova, D. Walterova, J. Vostalova, et al. “Ultraviolet light induced alteration to the skin.” In: *Biomedical Papers-Palacky University in Olomouc* 150.1 (2006), pp. 25–38.

- [3] T. Devasagayam, J. Tilak, K. Bloor, K. S. Sane, S. S. Ghaskadbi, and R. Lele. "Free radicals and antioxidants in human health: current status and future prospects." In: *Journal of Association of Physicians of India* 52.4 (2004), pp. 794–804.
- [4] J. P. Silva and O. P. Coutinho. "Free radicals in the regulation of damage and cell death—basic mechanisms and prevention." In: *Drug Discoveries & Therapeutics* 4.3 (2010), pp. 144–167.
- [5] L. Chen, X. Yang, H. Jiao, and B. Zhao. "Tea catechins protect against lead-induced ROS formation, mitochondrial dysfunction, and calcium dysregulation in PC12 cells." In: *Chemical research in toxicology* 16.9 (2003), pp. 1155–1161.
- [6] M. D. Farrar, A. Nicolaou, K. A. Clarke, S. Mason, K. A. Massey, T. P. Dew, R. E. Watson, G. Williamson, and L. E. Rhodes. "A randomized controlled trial of green tea catechins in protection against ultraviolet radiation-induced cutaneous inflammation, 2." In: *The American journal of clinical nutrition* 102.3 (2015), pp. 608–615.
- [7] C. K. Ho, S.-w. Choi, P. M. Siu, and I. F. Benzie. "Effects of single dose and regular intake of green tea (*Camellia sinensis*) on DNA damage, DNA repair, and heme oxygenase-1 expression in a randomized controlled human supplementation study." In: *Molecular Nutrition & Food Research* 58.6 (2014), pp. 1379–1383.
- [8] F. Pires and M. Raposo. "Artificial nanosystems to decode natural antioxidants – cellular membrane interactions." In: *Conference. Proceedings. 13th International Meeting Computational Intelligence Methods for Bioinformatics and Biostatistics (CIBB)*. 2016, pp. 190–195.
- [9] K. S. Avadhani, J. Manikkath, M. Tiwari, M. Chandrasekhar, A. Godavarthi, S. M. Vidya, R. C. Hariharapura, G. Kalthur, N. Udupa, and S. Mutalik. "Skin delivery of epigallocatechin-3-gallate (EGCG) and hyaluronic acid loaded nano-transfersomes for antioxidant and anti-aging effects in UV radiation induced skin damage." In: *Drug delivery* 24.1 (2017), pp. 61–74.
- [10] B. Liao, H. Ying, C. Yu, Z. Fan, W. Zhang, J. Shi, H. Ying, N. Ravichandran, Y. Xu, J. Yin, et al. "(-)-Epigallocatechin gallate (EGCG)-nanoethosomes as a transdermal delivery system for docetaxel to treat implanted human melanoma cell tumors in mice." In: *International journal of pharmaceuticals* 512.1 (2016), pp. 22–31.

- [11] W. Zhang, Y. Yang, T. Lv, Z. Fan, Y. Xu, J. Yin, B. Liao, H. Ying, N. Ravichandran, and Q. Du. "Sucrose esters improve the colloidal stability of nanoethosomal suspensions of (-)-epigallocatechin gallate for enhancing the effectiveness against UVB-induced skin damage." In: *Journal of Biomedical Materials Research Part B: Applied Biomaterials* 105.8 (2017), pp. 2416–2425.
- [12] J.-G. Leu, S.-A. Chen, H.-M. Chen, W.-M. Wu, C.-F. Hung, Y.-D. Yao, C.-S. Tu, and Y.-J. Liang. "The effects of gold nanoparticles in wound healing with antioxidant epigallocatechin gallate and α -lipoic acid." In: *Nanomedicine: Nanotechnology, Biology and Medicine* 8.5 (2012), pp. 767–775.
- [13] R. Radhakrishnan, H. Kulhari, D. Pooja, S. Gudem, S. Bhargava, R. Shukla, and R. Sistla. "Encapsulation of biophenolic phytochemical EGCG within lipid nanoparticles enhances its stability and cytotoxicity against cancer." In: *Chemistry and physics of lipids* 198 (2016), pp. 51–60.
- [14] J. Kim, J.-S. Hwang, Y.-K. Cho, Y. Han, Y.-J. Jeon, and K.-H. Yang. "Protective effects of (-)-epigallocatechin-3-gallate on UVA- and UVB-induced skin damage." In: *Skin Pharmacology and Physiology* 14.1 (2001), pp. 11–19.
- [15] S. Chaudhury, S. Bag, M. Bose, A. K. Das, A. K. Ghosh, and S. Dasgupta. "Protection of human γ B-crystallin from UV-induced damage by epigallocatechin gallate: spectroscopic and docking studies." In: *Molecular BioSystems* 12.9 (2016), pp. 2901–2909.
- [16] C. Liu, X.-Q. Zheng, L.-P. Xiang, J.-L. Lu, C. A. Polito, and Y.-R. Liang. "Protective effect of (-)-epigallocatechin gallate on ultraviolet b-induced skin damage in hairless mice." In: *Tropical Journal of Pharmaceutical Research* 15.6 (2016), pp. 1183–1189.
- [17] Y.-R. Liang, S. Kang, L. Deng, L.-P. Xiang, and X.-Q. Zheng. "Inhibitory effects of (-)-epigallocatechin-3-gallate on melanogenesis in ultraviolet A-induced B16 murine melanoma cell." In: *Tropical Journal of Pharmaceutical Research* 13.11 (2014), pp. 1825–1831.
- [18] W Ning, S Wang, D Liu, L Fu, R Jin, and A Xu. "Potent effects of peracetylated (-)-epigallocatechin-3-gallate against hydrogen peroxide-induced damage in human epidermal melanocytes via attenuation of oxidative stress and apoptosis." In: *Clinical and experimental dermatology* 41.6 (2016), pp. 616–624.

- [19] W. Zhu, L. Jia, G. Chen, H. Zhao, X. Sun, X. Meng, X. Zhao, L. Xing, J. Yu, and M. Zheng. “Epigallocatechin-3-gallate ameliorates radiation-induced acute skin damage in breast cancer patients undergoing adjuvant radiotherapy.” In: *Oncotarget* 7.30 (2016), pp. 48607–48613.
- [20] J.-Y. Fang, C.-F. Hung, T.-L. Hwang, and Y.-L. Huang. “Physicochemical characteristics and in vivo deposition of liposome-encapsulated tea catechins by topical and intratumor administrations.” In: *Journal of drug targeting* 13.1 (2005), pp. 19–27.
- [21] P. P. Campos, L. F. Fraceto, and M. Ferreira. “Layer-by-layer films containing emodin or emodin encapsulated in liposomes for transdermal applications.” In: *Colloids and Surfaces B: Biointerfaces* 162 (2018), pp. 69–75.
- [22] P. Sakdiset, A. Okada, H. Todo, and K. Sugibayashi. “Selection of phospholipids to design liposome preparations with high skin penetration-enhancing effects.” In: *Journal of Drug Delivery Science and Technology* 44 (2018), pp. 58–64.
- [23] A. A. Duarte, A. M. Botelho do Rego, M. Salerno, P. A. Ribeiro, N. El Bari, B. Bouchikhi, and M. Raposo. “DPPG liposomes adsorbed on polymer cushions: effect of roughness on amount, surface composition and topography.” In: *The Journal of Physical Chemistry B* 119.27 (2015), pp. 8544–8552.
- [24] A. A. Duarte, S. L. Filipe, L. M. Abegão, P. J. Gomes, P. A. Ribeiro, and M. Raposo. “Adsorption kinetics of DPPG liposome layers: a quantitative analysis of surface roughness.” In: *Microscopy and Microanalysis* 19.4 (2013), pp. 867–875.
- [25] Y. Kono, T. Nakai, H. Taguchi, and T. Fujita. “Development of magnetic anionic liposome/atelocollagen complexes for efficient magnetic drug targeting.” In: *Drug delivery* 24.1 (2017), pp. 1740–1749.
- [26] M. L. Moraes, P. J. Gomes, P. A. Ribeiro, P. Vieira, A. A. Freitas, R. Köhler, O. N. Oliveira Jr, and M. Raposo. “Polymeric scaffolds for enhanced stability of melanin incorporated in liposomes.” In: *Journal of colloid and interface science* 350.1 (2010), pp. 268–274.
- [27] J. E. Jackson. *A user’s guide to principal components*. Vol. 587. John Wiley & Sons, 2005.
- [28] R. A. Johnson and D. Wichern. “Multivariate analysis.” In: *Wiley StatsRef: Statistics Reference Online* (2014), pp. 1–20.

- [29] I. Noda and Y. Ozaki. *Two-dimensional correlation spectroscopy: applications in vibrational and optical spectroscopy*. John Wiley & Sons, 2005.
- [30] I. Noda. “Advances in two-dimensional correlation spectroscopy.” In: *Vibrational Spectroscopy* 36.2 (2004), pp. 143–165.
- [31] M. Raposo, M. Coelho, P. J. Gomes, P. Vieira, P. A. Ribeiro, N. J. Mason, C. A. Hunniford, and R. W. McCullough. “DNA damage induced by carbon ions (C3+) beam accessed by independent component analysis of infrared spectra.” In: *International journal of radiation biology* 90.5 (2014), pp. 344–350.
- [32] K. Polewski, S. Kniat, and D. Slawinska. “Gallic acid, a natural antioxidant, in aqueous and micellar environment: spectroscopic studies.” In: *Current Topics in Biophysics* 26.2 (2002), pp. 217–227.
- [33] X.-Q. Lin, F. Li, Y.-Q. Pang, and H. Cui. “Flow injection analysis of gallic acid with inhibited electrochemiluminescence detection.” In: *Analytical and Bioanalytical Chemistry* 378.8 (2004), pp. 2028–2033.
- [34] R. Wang, W. Zhou, and X. Jiang. “Reaction kinetics of degradation and epimerization of epigallocatechin gallate (EGCG) in aqueous system over a wide temperature range.” In: *Journal of Agricultural and Food Chemistry* 56.8 (2008), pp. 2694–2701.
- [35] S. Sang, M.-J. Lee, Z. Hou, C.-T. Ho, and C. S. Yang. “Stability of tea polyphenol (-)-epigallocatechin-3-gallate and formation of dimers and epimers under common experimental conditions.” In: *Journal of Agricultural and Food Chemistry* 53.24 (2005), pp. 9478–9484.
- [36] A. A. Duarte, P. J. Gomes, J. H. Ribeiro, P. A. Ribeiro, S. V. Hoffmann, N. J. Mason, O. N. Oliveira, and M. Raposo. “Characterization of PAH/DPPG layer-by-layer films by VUV spectroscopy.” In: *The European Physical Journal E* 36.9 (2013), pp. 36–98.
- [37] E. E. Barnes and W. T. Simpson. “Correlations among electronic transitions for carbonyl and for carboxyl in the vacuum ultraviolet.” In: *The Journal of Chemical Physics* 39.3 (1963), pp. 670–675.
- [38] T. Ari and M. H. Güven. “Valence-shell electron energy-loss spectra of formic acid and acetic acid.” In: *Journal of Electron Spectroscopy and Related Phenomena* 106.1 (2000), pp. 29–35.

- [39] K. Xu, G. Amaral, and J. Zhang. “Photodissociation dynamics of ethanol at 193.3 nm: The H-atom channel and ethoxy vibrational distribution.” In: *The Journal of chemical physics* 111.14 (1999), pp. 6271–6282.
- [40] S. Satyapal, J. Park, R. Bersohn, and B. Katz. “Dissociation of methanol and ethanol activated by a chemical reaction or by light.” In: *The Journal of Chemical Physics* 91.11 (1989), pp. 6873–6879.
- [41] Y Wen, J Segall, M Dulligan, and C Wittig. “Photodissociation of methanol at 193.3 nm: Translational energy release spectra.” In: *The Journal of chemical physics* 101.7 (1994), pp. 5665–5671.
- [42] S Harich, J. Lin, Y. Lee, and X Yang. “Competing atomic and molecular hydrogen pathways in the photodissociation of methanol at 157 nm.” In: *The Journal of chemical physics* 111.1 (1999), pp. 5–9.
- [43] E. A. Glende Jr and R. O. Recknagel. “Spectrophotometric Detection of Lipid-Conjugated Dienes.” In: *In Vitro Toxicity Indicators*. Academic Press San Diego, 1994, pp. 400–406.
- [44] N. J. Zuidam, C. Versluis, E. A. Vernooy, and D. J. Crommelin. “Gamma-irradiation of liposomes composed of saturated phospholipids. Effect of bilayer composition, size, concentration and absorbed dose on chemical degradation and physical destabilization of liposomes.” In: *Biochimica et Biophysica Acta (BBA)-Biomembranes* 1280.1 (1996), pp. 135–148.
- [45] J. Garcia, M.-F. Hsieh, B. Doma, D. Peruelo, I.-H. Chen, and H.-M. Lee. “Synthesis of gelatin- γ -polyglutamic acid-based hydrogel for the in vitro controlled release of epigallocatechin gallate (EGCG) from *Camellia sinensis*.” In: *Polymers* 6.1 (2014), pp. 39–58.
- [46] L. Zeng, J. Yan, L. Luo, M. Ma, and H. Zhu. “Preparation and characterization of (-)-Epigallocatechin-3-gallate (EGCG)-loaded nanoparticles and their inhibitory effects on Human breast cancer MCF-7 cells.” In: *Scientific reports* 7.45521 (2017), pp. 1–15.
- [47] J. Terao, M. Piskula, and Q. Yao. “Protective effect of epicatechin, epicatechin gallate, and quercetin on lipid peroxidation in phospholipid bilayers.” In: *Archives of Biochemistry and Biophysics* 308.1 (1994), pp. 278–284.
- [48] N. Salah, N. J. Miller, G. Paganga, L. Tijburg, G. P. Bolwell, and C. Ricevans. “Polyphenolic flavanols as scavengers of aqueous phase radicals and as chain-breaking antioxidants.” In: *Archives of biochemistry and biophysics* 322.2 (1995), pp. 339–346.

- [49] S. V. Jovanovic, S. Steenken, Y. Hara, and M. G. Simic. "Reduction potentials of flavonoid and model phenoxyl radicals. Which ring in flavonoids is responsible for antioxidant activity?" In: *Journal of the Chemical Society, Perkin Transactions 2* 11 (1996), pp. 2497–2504.

RESULTS

Evaluation of EGCG loading capacity in DMPC membranes¹**Abstract**

Catechins are molecules with potential use in different pathologies such as diabetes and cancer, but their pharmaceutical applications are often hindered by their instability in the bloodstream. This issue can be circumvented by using liposomes as their nanocarriers for *in vivo* delivery. In this work, we studied the molecular details of (-)-epigallocatechin-3-gallate (EGCG) interacting with 1,2-dimyristoyl-*sn*-glycero-3-phosphocholine (DMPC) monolayer/bilayer systems to understand the catechin loading ability and liposome stability, using experimental and computational techniques. The molecular dynamics simulations show the EGCG molecules deep inside the lipid bilayer, positioned below the lipid ester groups, generating a concentration-dependent lipid condensation. This effect was also inferred from the surface pressure isotherms of DMPC monolayers. In the PM-IRRAS assays, the predominant effect at higher concentrations of EGCG (e.g. 20 mol%) was an increase in lipid tail disorder. The steady-state fluorescence data confirmed this disordered state, indicating that the catechin-induced liposome aggregation out-weights the condensation effects. Therefore, by adding more than 10 mol% EGCG to the liposomes, a destabilization of the vesicles occurs with the ensuing release of entrapped catechins. The loading capacity for

¹This chapter is based on the following publication:

Pires, F., Geraldo, V. P.N., Rodrigues, B., Granada-Flor, A., Almeida, R.F.M., Oliveira Jr, O. N., Victor, B.L., Machuqueiro, M. and Raposo, M.. Evaluation of EGCG loading capacity in DMPC membranes. *Langmuir* 2019, 35, 20, 6771:6781, DOI:10.1021/acs.langmuir.9b00372

DMPC seems to be limited by its disordered lipid arrangements, typical of a fluid phase. To further increase the liposomes clinical usefulness, lipid bilayers with more stable and organized assemblies should be employed to avoid aggregation at large concentrations of catechin.

8.1 Introduction

Epigallocatechin-3-gallate (EGCG; Figure 8.1) is the most abundant catechin in the *Camellia sinensis* green tea, whose potential for cancer therapy has been studied owing to its ability to modulate membrane organization and coordinate intracellular signalling pathways in the various steps of tumorigenesis.[1, 2] EGCG is known to partition favourably to lipid bilayers,[3, 4, 5] and can even induce membrane disruption at high concentrations.[3] Also, EGCG can lead to aggregation of phosphatidylcholine (PC) liposomes, rapidly potentiating the cargo release from the liposome in a concentration-dependent manner [6]. Using phase-contrast fluorescence microscopy, it has been shown that EGCG can induce calcein leakage from egg PC giant unilamellar vesicles, where their prolate shape changed to two spheres connected by a narrow neck. [3, 7] EGCG modulates biological pathways [8, 9, 10, 11] by altering membrane properties and acting as pan-assay interference compounds (PAINS) [12, 13]. Adsorption kinetics studies of different catechins on DMPC phospholipid surface showed that the catechins bearing gallate moiety bind more strongly to lipid membranes than non-gallolylated catechins, due to the additional phenolic OH groups. [14] Additionally, the stereochemical structure also seems to affect the kinetic behaviour of catechins. [15] The *cis* configurations have more favourable conformations for hydrogen bonding since the trihydroxyl groups are better oriented and closer to the bilayer surface.

From the clinical point of view, the major limitation in the oral administration of EGCG is its poor bioavailability in the bloodstream. The susceptibility of its phenolic groups to deprotonation, oxidation and metabolic reactions within the living system [16] makes this catechin very unstable. Fortunately, drug carriers including liposomes [17, 18, 19], nanoparticles [20, 21] and microparticles [22, 23], can be used to overcome this problem, and therefore loading EGCG into nanocarriers is a promising natural chemopreventive and chemotherapeutic agent for brain, [24, 25] breast, [26, 27] prostate, [28, 29] lung, [30, 31] and skin[32, 33] cancers. Many reports have focused on the design of nanocarrier formulations and the use of new production techniques to improve encapsulation efficiency and enhance the cellular uptake of liposomes [34, 35, 36, 37]. These developments

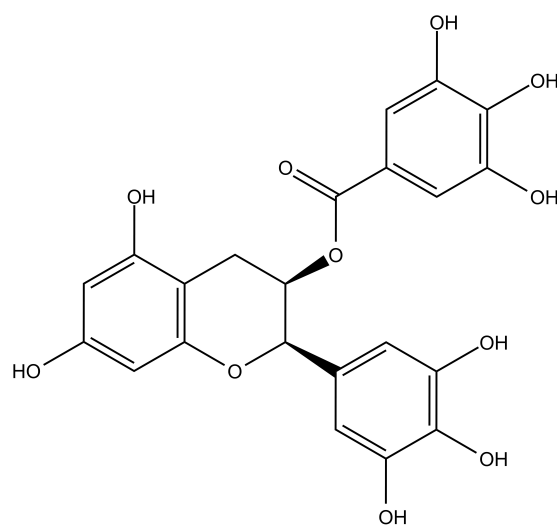


Figure 8.1: Schematic chemical structure of Epigallocatechin-3-gallate (EGCG).

should be guided by molecular-level information regarding the interaction of EGCG in lipidic model systems. For instance, details on the catechin preferred location, membrane stability and other monolayer/bilayer structural properties are useful to evaluate and improve encapsulation efficiency.

This type of information can be obtained by Molecular Dynamics (MD) simulations, which have been used to investigate interactions between membranes and small drugs, [38, 39] larger compounds, [40, 41] peptides [42, 43, 44], and catechins. [4, 15, 45, 46, 47, 48, 49] This *in silico* technique can provide a detailed picture of the molecular interactions and allow the prediction of several properties that are usually very difficult to tackle using experimental techniques. [50] MD studies on EGCG insertion into lipid bilayers showed that these molecules adopted a more ordered configuration in membranes composed of phosphatidyl ethanolamine: phosphatidyl choline (PE:PC) lipids (1:1 ratio), [15, 45, 46] which is significantly different from pure PC. The molecular interactions of four green tea catechin compounds, including EGCG, with a POPC pure bilayer have also been studied, where EGCG was found to establish hydrogen bonds with the lipids ester region, inducing only a small local condensing effect on the bilayer, probably due to the presence of only one catechin molecule per leaflet.[4] Recently, EGCG was observed to insert into two different membrane models, resembling either a plasma membrane or a late endosome membrane, without a clear tendency to aggregate.[49] Furthermore, the ability of EGCG to insert into neutral and anionic membrane models was modulated by the presence of salt, especially divalent Ca^{++} and Mg^{++} . [47, 48] Despite growing evidence of the health benefits

of catechins, EGCG has not been thoroughly studied using Langmuir monolayers models. These experimental membrane models mimic half a liposome/cell membrane, providing valuable information on drug-lipid interactions, particularly its impact on the physicochemical properties of the system under study (degree of molecular packing, molecular organization, and surface potential). [51, 52, 53]

In this work, we carried out a detailed study of the molecular interactions between EGCG and DMPC model membranes. The carrier loading capacity and the effects of the catechin on the membrane were studied using a multidisciplinary approach combining Langmuir monolayers, infrared and fluorescence spectroscopies, and MD simulations. The results obtained provide an accurate evaluation of liposomes as nanocarriers and catechins encapsulation agents, which is relevant for future use in food packaging, cosmetics, and cancer therapeutics.

8.2 Experimental

8.2.1 Materials

EGCG (M.W. 458.4 g/mol) and dimyristoylphosphatidylcholine (DMPC) phospholipid (M.W. 677.93 g/mol) were purchased from Sigma–Aldrich and Avanti Polar Lipids, respectively. 4-(2-[6-(dioctylamino)-2-naphthalenyl]ethyl)-1-(3-sulfopropyl)-pyridinium (di-8-ANEPPS) was purchased from Biotium.

8.2.2 Langmuir Monolayers Studies

The Langmuir monolayers were prepared using the co-spreading methodology. Firstly, DMPC and EGCG were dissolved in chloroform at concentrations of 0.5 mg/ml and 0.3 mg/ml, respectively, leading to the same molar concentration in each solution. Langmuir monolayers were obtained after spreading the pure DMPC or EGCG/DMPC mixtures, (1.6, 5, 10, and 20 mol%), on an aqueous subphase (Milli-Q water at 297 ± 1 K). Surface pressure measurements started after the solvent was allowed to evaporate for 10 min. The experiments were carried out in a Langmuir minitrough from KSV Instruments (model 2000, KSV Nima, Helsinki, Finland), in a class 10,000 clean room and were repeated at least three times to ensure reproducibility of the isotherms. During film compression, two symmetric barriers moved at a constant speed of $10 \text{ mm}\cdot\text{min}^{-1}$.

In the isotherms analyses, the EGCG molecules were considered to also occupy an area on the Langmuir monolayer, in addition to the DMPC molecules. Therefore, the area per lipid (i.e. per DMPC molecule) (A_l) was calculated by dividing

the trough area by the number of DMPC molecules after subtracting the estimated area occupied by the EGCG molecules. This procedure was necessary because the area occupied by each EGCG molecule varied with its concentration, since not all EGCG molecules are expected to be at the interface. We also used the results from MD simulations to estimate the EGCG area at the interface. Finally, the area of DMPC was calculated from the total area of the Langmuir minitrough occupied by the DMPC phospholipid (area of the Langmuir minitrough minus the total area occupied by EGCG molecules) and the number of DMPC molecules spread in each condition. The compressional modulus (C_s^{-1}) and the minimum area per lipid (A_l) were estimated from the π - A_l compression isotherms. C_s^{-1} was calculated using: $C_s^{-1} = -A_l \left(\frac{\partial \pi}{\partial A_l} \right)_T$, where π is the monolayer surface pressure. The minimum area per lipid was derived by extrapolating the tangent to the inflection point on the condensed region of the isotherm, indicating the area occupied by one lipid molecule at the air/water interface. The surface potential and surface pressure-area isotherms were recorded simultaneously in a Langmuir minitrough equipped with a surface potential sensor (KSV Kelvin probe, Biolin Scientific Oy, Helsinki, Finland), during the compression of the spread mixed EGCG/DMPC monolayers with selected ratios. The surface potential sensor measures the potential difference between the vibrating plate (placed roughly 1–2 mm above the monolayer) and the reference electrode immersed into the water subphase, thus reflecting the changes in surface potential.[54]

8.2.3 PM-IRRAS Studies

Polarization-modulated infrared reflection absorption spectra (PM-IRRAS) measurements were performed using a KSV PMI 550 instrument (KSV Instruments Ltd, Helsinki, Finland) at an incidence angle of 80° . The EGCG/DMPC mixtures were spread on an aqueous subphase at 297 ± 1 K, and then compressed up to 30 mN m^{-1} . The spectra were measured for s- and p-polarizations at a high frequency. All the spectra were obtained by subtracting the spectrum of a pure water subphase at the same temperature as that of samples. Spectra of lipid samples were cut to a frequency range between 3000 and 900 cm^{-1} and were baseline corrected with a straight line. Spectra deconvolution using Gaussian lineshape was used to reveal the components of the phosphate and carbonyl bands as well as the band position and bandwidth of these components. The phosphate region of DMPC consists of two bands from the phosphate hydrogen-bonding to water (1237 cm^{-1}) and "free" non-bound phosphates (1261 cm^{-1}). The phosphate hydration degree of DMPC was assessed from the ratio between the area under

the band at 1237 cm^{-1} and the total area under the curve. The carbonyl band was deconvoluted into two Gaussian bands at 1737 cm^{-1} and 1746 cm^{-1} , which can be attributed to the hydrogen-bonded ester carbonyl groups and free ester carbonyl groups, respectively. Within the same rationale, the hydration degree of the carbonyl groups was calculated from the ratio between the area of the band at 1737 cm^{-1} and the total area under the curve. The orientational order parameter of the CH_2 lipid hydrocarbon chains was obtained from the band area ratios $A(2920\text{ cm}^{-1})/A(2855\text{ cm}^{-1})$. [55]

8.2.4 Fluorescence Studies

Steady-state fluorescence anisotropy measurements were performed for EGCG in DMPC unilamellar vesicles (LUVs) suspensions. Briefly, the required amount of lipid to obtain a final lipid concentration in the LUVs suspension of 0.25 mM [56] was dissolved in chloroform and the solvent was evaporated using a gentle stream of nitrogen, followed by vacuum desiccation for 4h to remove the last traces of solvent. The dried phospholipid films were dispersed in buffer (10 mM HEPES, 0.1 mM EDTA, 100 mM NaCl, pH 7.4) at 308 K (above the gel to liquid-crystalline transition temperature of DMPC, which is ca. 297 K [57]) and vortex-mixed. The resulting multilamellar vesicle suspensions were subjected to five freeze/thaw cycles and extruded 21 times through polycarbonate membranes with a pore diameter of 100 nm to form the LUVs and left to equilibrate overnight. Then, EGCG (at 5, 10, 20 or 30 mol%) was added to the sample at 303 K and incubated for 2h before the measurements.

Fluorescence spectroscopy measurements were performed in a Horiba Jobin Yvon Spex Fluorolog 3-22 spectrofluorometer (Kyoto, Japan) with excitation at 275 nm (slit width 5 nm) and emission at 353 nm (slit width 5 nm), i.e. at the maximum of the excitation and emission spectra under our conditions. The fluorescence anisotropy, $\langle r \rangle$, was calculated using equation 8.1:

$$\langle r \rangle = \frac{I_{VV} - GI_{VH}}{I_{VV} + 2GI_{VH}} \quad (8.1)$$

where the fluorescence emission I had subscripts V and H for the vertical and horizontal orientations of the polarizers. The G -factor is a correction factor for detector sensitivity and is calculated as $G = \frac{I_{HV}}{I_{HH}}$. A total of seven readings for each intensity component were taken per sample using an integration time of 0.1 s . For each intensity reading, the background obtained for a DMPC suspension (without EGCG) was subtracted. All measurements were performed for 3

independent samples at 303 K, which was confirmed directly inside the cuvette using a temperature probe in a thermostated cuvette holder.

To detect the changes in the bilayer dipole potential, the lipid suspensions were labelled with di-8-ANEPPS (1:500 probe/lipid mole ratio [41]) overnight. The ratio of the fluorescence intensity at 630 nm of di-8-ANEPPS excited at 420 nm to that excited at 520 nm was used to evaluate the membrane dipole potential. [58, 59]

8.2.5 Computational Details

8.2.6 Molecular Dynamics

MD simulations were performed with GROMACS 2016.4 [60] and the GROMOS 54A7 force field [61, 62]. Initial parameters for the EGCG molecule were obtained with the Automated Topology Builder (ATB) and Repository [63, 64] and manually curated. The pairs section were modified to exclude 1-4 interactions in the aromatic rings. The charge set was obtained from a RESP[65] fitting protocol, using the electrostatic potential calculated with Gaussian 09[66], the B3LYP functional [67, 68, 69] and 6-31G*[70] basis set. We have not explicitly accounted for the anionic form of EGCG ($pK_a \sim 7.7$)[71] since the neutral form is the most abundant. Additionally, when interacting with lipid bilayers, anionic groups have their neutral forms stabilized.[43]. Two types of MD simulations were performed: the insertion and the concentration sets. In the insertion simulations, two EGCG molecules were introduced to a pre-equilibrated 128 lipid DMPC membrane patch, either outside (in the water phase), or inside the membrane (Figure 8.2A). These two molecules were not allowed to interact (they are always at distances larger than 1.0 nm, which is the PME cutoff) and were analyzed as independent replicates. For the concentration simulations set, we created systems with 0, 2, 6, 12 and 24 EGCG molecules, corresponding to 0, 1.6, 4.7, 9.4, and 18.8 mol% of EGCG. Note that these molar fractions will slightly differ from the molar fractions in the experiments. Furthermore, the choice for DMPC was based on its small size, which leads to faster simulations, while keeping the correct lipid fluid phase.

The simulations were performed using the v-rescale heat bath [72] at 298 K with separate couplings for water and solute (DMPC and EGCG), with a relaxation time of 0.1 ps. A Parrinello-Rahman [73] semi-isotropic pressure couple was used to keep the pressure at 1 bar with isothermal compressibility of $4.5 \times 10^{-5} \text{ bar}^{-1}$, and a relaxation time of 2.0 ps. All bonds were constrained with the parallel

version of the LINCS algorithm [74], and the SETTLE algorithm [75] was used for water (SPC [76]). A time step of 2 fs were used in the integration of the equations of motion, with the neighbor lists being updated every 10 steps. The Particle-Mesh Ewald (PME) [77] electrostatics was applied using 0.12 nm for the maximum grid spacing of the Fast Fourier Transform and a cutoff distance of 1.0 nm for Lennard-Jones and Coulomb interactions. The interpolation order for PME was 4 (cubic).

Energy minimization of all systems was performed using two steps with the steepest-descent algorithm, with LINCS constraints turned on in the second step. The initialization was achieved in a 250 ps MD simulation with harmonic restraints in both DMPC and EGCG, followed with 500 ps with restraints only on DMPC phosphorous atoms, always with a restraint force of 1000 kJ/(mol nm²). We ran 5 replicate simulations (3 in the insertion set) of 200 ns and all equilibrium properties were obtained from the last 100 ns. In the insertion set, we doubled our replicates by following the two EGCG molecules independently.

8.2.7 Analyses and error calculations

The computational analyses were performed using in-house scripts and GRO-MACS analysis utilities. All simulations and experiments were done with replicates. The error bars represent the standard error of the mean and were determined with a leave-one-out resampling method.

8.3 Results and discussion

8.3.1 EGCG insertion into DMPC bilayers

We used MD simulations to study the interaction of EGCG with a lipid bilayer at the molecular level. We setup different systems where EGCG (catechin) was introduced either in the water phase or at the bilayer hydrophobic region (Figure 8.2A). Regardless of the starting positions, all EGCG molecules accumulate in the membrane at ~ 10 Å below the average phosphorous atoms positions (Figure 8.2B-C). There is only a small energy barrier around the phosphate region, which is easily overcome by the molecules within 100 ns. The preferred position is in good agreement with the minimum region of the reported potential of mean force [13], even though completely different force fields were used. In another separate set of MD simulations, Sirk *et al* did not observe the complete insertion

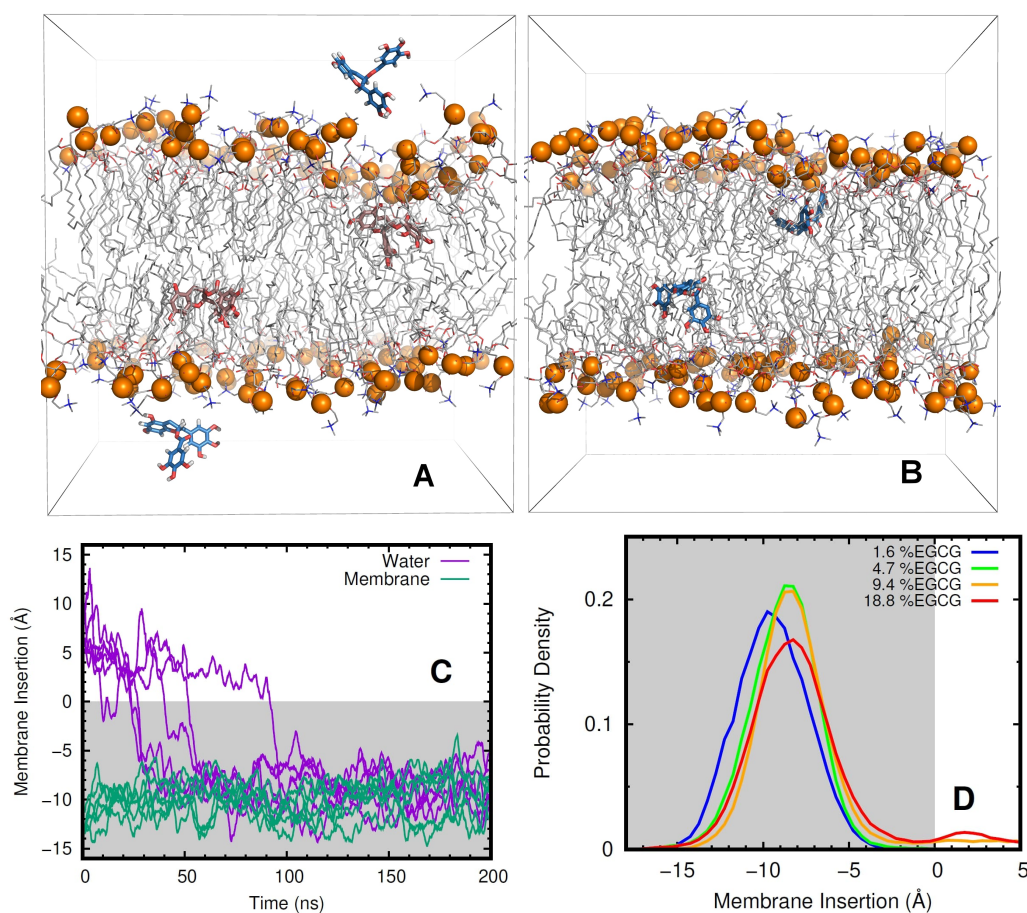


Figure 8.2: Initial (A) and final (B) conformations of the EGCG membrane insertion process. The catechin molecules were added near either the water/membrane interface (blue sticks) or the membrane center (pink sticks). Even though the catechin molecules started from the water phase, we observe full insertion in all simulations (B). The membrane is shown as thin grey sticks with the phosphorous atoms in spheres to highlight the polar interface. Membrane insertion of all EGCG molecules over time (C) and the corresponding histograms for the different molar ratios of the EGCG/DMPC systems (D). The catechin molecules tend to accumulate within the membrane (in each monolayer), regardless of its original position. Negative insertion values correspond to positions below the average phosphorous atoms positions, which were used as reference.

of EGCG into POPC membranes, probably due to the lack of sampling on their simulations where the catechins were placed at the water region. [4]

The large number of hydrogen bond donor groups in EGCG molecule makes it ideal to interact with the lipids ester region, where there are plenty of hydrogen bond acceptors. This feature and the significant hydrophobicity of EGCG explain its membrane location and the most commonly observed conformations where its OH groups preferentially interact with the lipid esters (Figure 8.2D).

8.3.2 Effects of increasing EGCG concentration on DMPC lipid organization

In the MD simulations, we also built EGCG/DMPC mixtures at different molar ratios: 0, 1.6, 4.7, 9.4, and 18.8, corresponding to 0, 2, 6, 12, and 24 ~EGCG molecules in 128 ~DMPC lipids, respectively. The EGCG molecules always remained mainly at the membrane preferred position (~ 10 Å below the average position of the phosphorous atoms). Only for 9.4 and 18.8 molar ratios did we observe some catechin exchange between solvent and membrane (Figure 8.2D). The A_1 values calculated specifically for DMPC indicate significant condensation with increasing concentrations of EGCG (Figure 8.3A), even though the system is expanded due to the presence of the catechin (Figure D.1 of Appendix D). The catechin specific area per molecule was calculated from the MD simulations to be 82.6, 88.2, 96.8, and 89.6 Å², for the 1.6, 5, 10, and 20 mol% EGCG mixtures, respectively. The surface pressure of DMPC Langmuir monolayers displays a gaseous (100–80 Å²) and a liquid-expanded (LE) phase (molecular areas lower than 80 Å²), without a well-defined LE/LC transition (Figure 8.3B). The surface pressure increased monotonically up to ~ 49 mN/m, reaching values of compressional modulus of ~ 96 mN/m (Figure 8.3C). On further compression, the monolayer collapses to a three-dimensional state at $\pi_c \sim 49$ mN/m.

The A_1 values from Figure 8.3B are in good agreement with those obtained from MD simulations (Figure 8.3A). The addition of EGCG to the phospholipid monolayers caused a shift in the isotherms towards lower A_1 , a trend similar to the condensing effect due to the presence of cholesterol in PC membranes at the air-water interface [81, 82, 83, 84]. As an example, in DMPC monolayers at 30 mN/m, cholesterol concentrations of 4%, 8% and 21% promote molecular area contractions to 53 Å², 50 Å² and 48 Å², respectively. [85] Therefore, it seems that EGCG has an even larger condensing effect on DMPC than cholesterol. Interestingly, although EGCG causes condensation of DMPC monolayers, this monotonic dependence on concentration was not observed in the compressional modulus. The surface pressure isotherms in Figure 8.3C indicate that small amounts of EGCG (1.6 and 5 mol%) turn the DMPC membrane more rigid as reflected by the increased compressional modulus. This agrees with the MD simulations, in particular with the observed increase in the lipid tail order parameter (Figure 8.4A). These results are also consistent with the literature where a slight, approximately linear, decrease of fluidity at the acyl chain level was observed in DMPC LUVs in the fluid phase with increasing EGCG.[86] In addition, the rigidifying effects of EGCG are believed to be responsible for the anti-migratory and anti-metastatic

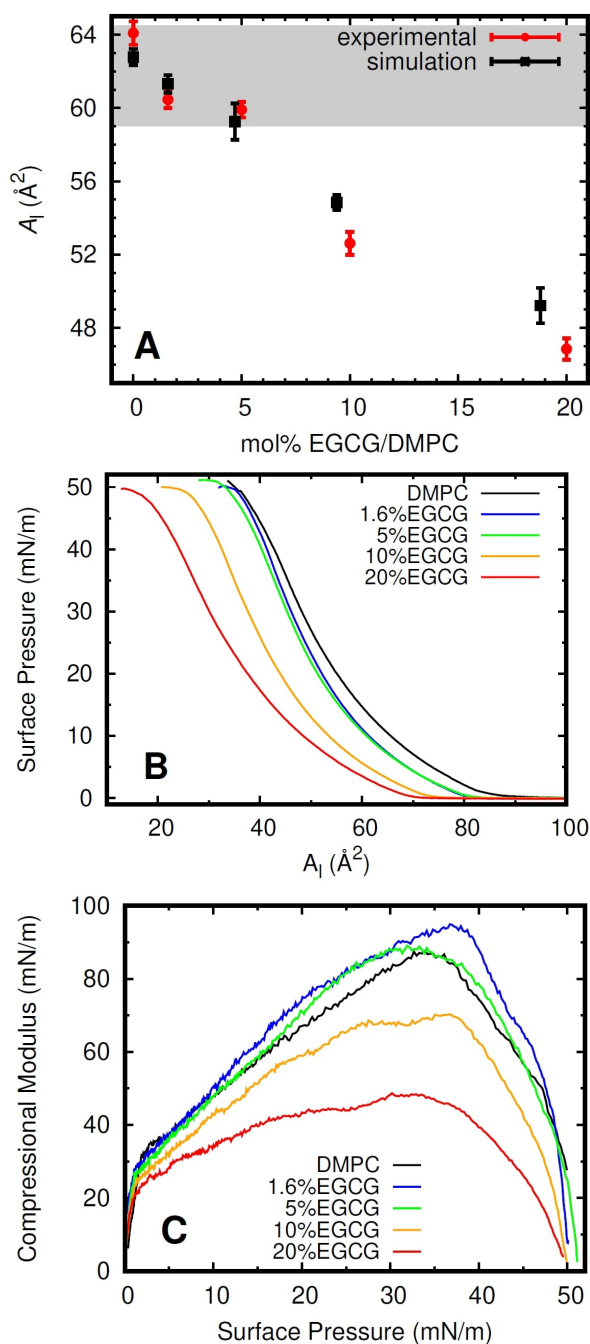


Figure 8.3: Area per lipid (A_1) values of DMPC calculated in the presence of different amounts of EGCG (A). The simulation A_1 values were calculated using GridMAT-MD[78], while the experimental details are given in the Experimental section. The gray shaded region corresponds to the values measured experimentally for pure DMPC in the fluid phase.[79, 80] Surface pressure isotherms for monolayers of neat DMPC (black), 1.6% (blue), 5% (green), 10% (orange) and 20% w/w EGCG in DMPC (red) are shown (B). The respective compressional modulus as a function of surface pressure at the air/water interface are also shown (C).

effects on lung cancer cells [87, 88, 89, 90, 91]. Rigidification slows down disintegration of drug-loaded liposomes, thus improving stability although compromising drug entrapment efficiency [92]. However, for higher concentrations of EGCG, the compressional modulus decreases, i.e. the DMPC monolayer becomes more compressible (membrane fluidization). The latter change was not captured in the MD simulation, probably because the short time scales used are inadequate to probe lipid lateral diffusion (several hundreds of nanoseconds are needed[93] to observe EGCG aggregation). Additionally, the small membrane patch used (128 lipids) may not capture EGCG-induced phase separation and/or membrane curvature phenomena. When a large number of EGCG molecules are inserted into the DMPC monolayer, an anisotropic molecular packing is likely to occur upon the formation of EGCG aggregates.

The preferred location of the EGCG molecules in the lipid bilayer, as inferred from the MD simulations (Figure 8.2D), indicates that catechin can have different concentration-dependent effects on the lipid head and tail groups. The membrane thickness and the order parameter of lipid aliphatic tails can provide decoupled information on which region is most affected by the presence of the catechin. In pure bilayers, these properties are usually highly coupled to the A_1 values. In mixtures, however, specific parts of the lipids can be altered while little or no impact is observed in the overall A_1 values. The DMPC membrane thickness can be measured by following the distance between average position of the phosphorous atoms in each monolayer. In our simulations, there are no significant differences in the membrane thickness values, even in the presence of higher amounts of EGCG (Figure D.2 of Appendix D). A membrane condensation effect, as suggested by the A_1 values (Figure 8.3A), is often associated with an increase in the membrane thickness values, which is not observed. Therefore, these simulations suggest that EGCG could be accommodated in the DMPC bilayer, without perturbing too much the lipid head groups.

The changes in the DMPC membrane ordering, caused by increasing molar ratios of EGCG, can be analyzed by calculating the deuterium order parameter on the lipid tails and by PM-IRRAS spectroscopy of DMPC+EGCG monolayers. The deuterium order parameter values ($-S_{CD}$) increase significantly with the molar fraction of EGCG (Figure D.3 of Appendix D). The $-S_{CD}$ plateau, usually observed at the 6th methylene group of aliphatic chains, highlights the EGCG induced gain of order in this membrane region (Figure 8.4A). These results indicate that the condensing effect observed in the MD simulations can be attributed to a better packing of the lipid hydrocarbon chains in the presence of EGCG.

In the experiments using Langmuir monolayers, the arrangement of the acyl

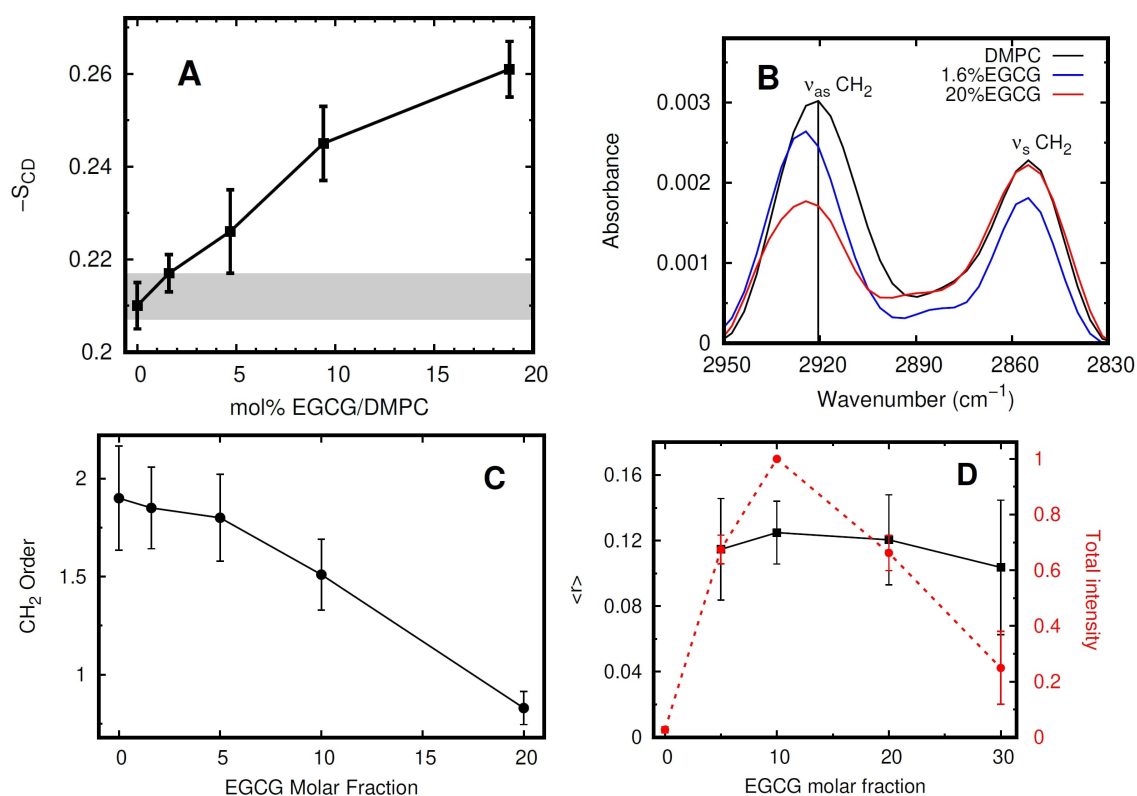


Figure 8.4: Lipid tails order in the presence of different molar ratios of EGCG. Deuterium order parameter ($-S_{CD}$) values for the 6th methylene group in DMPC (A). The 6th positions correspond to a plateau in the $-S_{CD}$ profiles (Figure D.3 of Appendix D). The gray shaded region corresponds to the experimental value (0.212 ± 0.005) for pure DMPC in fluid phase[79]. PM-IRRAS measurements for different EGCG molar fractions in the region of DMPC methylene (CH_2) groups (B), from which the asymmetric/symmetric bands ratios were obtained (C). EGCG fluorescence anisotropy $\langle r \rangle$ in the presence of DMPC vesicles (D). Total fluorescence intensity corresponds to the sum of $I_{VV} + 2GI_{VH}$ retrieved from anisotropy measurements, corrected for inner filter effects[94] and normalized for the max value in each sample. All values correspond to the average of, at least, 3 independent samples. Error bars = \pm standard deviation.

chains was assessed by analyzing the shifts and shape changes of the peaks assigned to the CH_2 stretching modes. As shown in Figure 8.4B, the positions of the bands at 2855 cm^{-1} and 2921 cm^{-1} assigned to the symmetric and anti-symmetric stretching of CH_2 in the DMPC monolayer, respectively, were not significantly affected by the incorporation of EGCG. However, the experimental hydrocarbon ordering parameter (Figure 8.4C), calculated using the ratio between the CH_2 anti-symmetric and symmetric stretching bands, revealed that EGCG may have a disordering effect on the trans-gauche conformational equilibrium of DMPC. Indeed, even though at lower concentrations we see no significant effect on the CH_2 order parameter (the values fall within their error bars), at a larger EGCG concentration (20 mol%) a clear loss of lipid tail ordering is observed in the monolayer. This disordering effect is not consistent with the $-S_{CD}$ data from the MD simulations, probably due to EGCG aggregation effects, which were not accounted for in the *in silico* studies even at higher concentrations.

The EGCG molecules intrinsic fluorescence is environment sensitive, [56] which allows one to monitor its interaction with the membrane. The fluorescence anisotropy of the catechin in the presence of DMPC vesicles remains unaltered at different mol% values (Figure 8.4D). However, the catechin fluorescence intensity increases significantly up to 10 mol%, which indicates that most catechin molecules are incorporated in the liposomes, since EGCG quantum yield is larger in the lipid bilayer than in the water phase. [56] This increase is reverted at higher EGCG concentrations (20 and 30 mol%), probably due to instabilities and the increase of scattering from the suspension associated with catechin and liposome aggregation (observable with the naked eye after sample preparation) and/or a change of the catechin microenvironment. These results at high EGCG concentrations are consistent with the disordering effect observed in the phospholipid monolayers, pointing to the role of aggregation in limiting the catechin loading capacity of DMPC. In fact, from the MD simulations, which exclude the aggregation effects, one could expect a higher loading capacity according to the increased $-S_{CD}$ values (Figure 8.4A) and the low catechin exchange from the membrane to the water phase, which is only present at 18.8 mol% (Figure 8.2D).

8.3.3 Effects of increasing EGCG concentration on DMPC dipolar properties

Membrane dynamical properties are usually strongly coupled to the electric field generated by the anisotropic organization of the charged, polar head groups. This will include the glycerol ester moiety, the first water solvation shells, and even

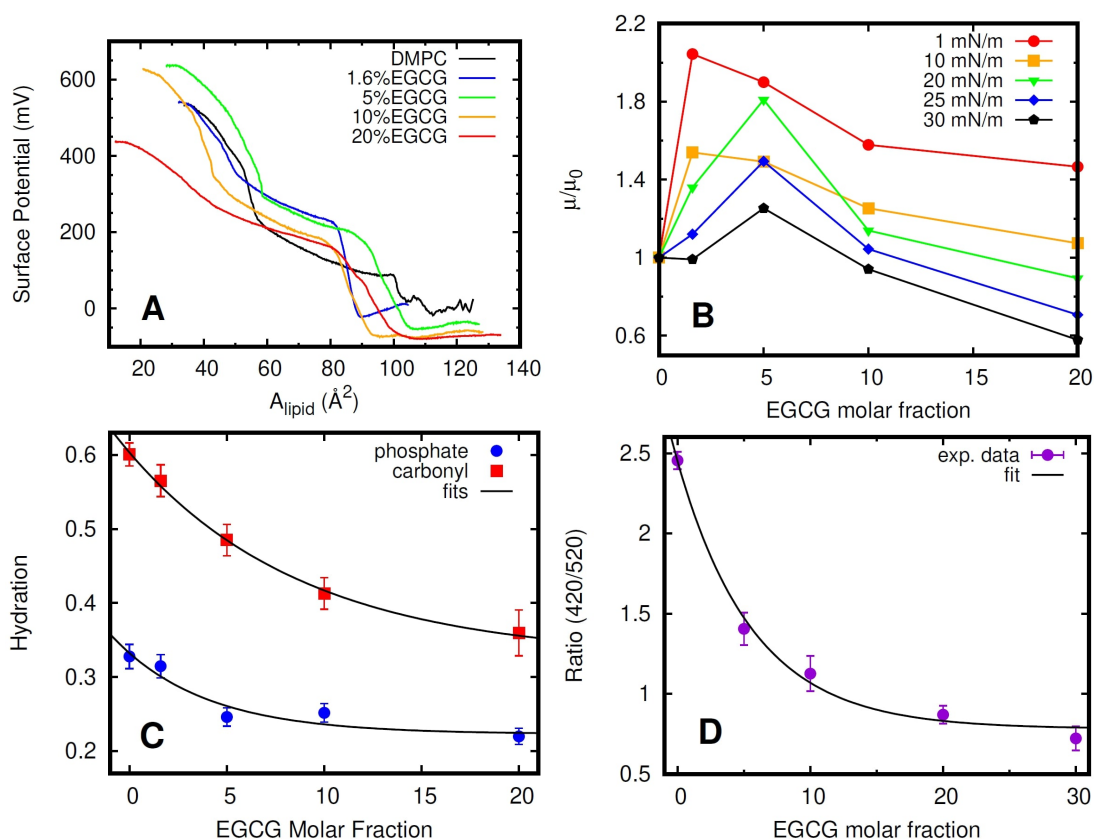


Figure 8.5: Surface potential at different A_1 values for the different EGCG molar fractions in DMPC monolayers (A). The ratio between the apparent dipole moment of EGCG and DMPC (μ) and neat DMPC (μ_0) when varying the EGCG molar fractions for different surface pressures (B). DMPC carbonyl and phosphate hydration degrees (C) obtained from their carbonyl and asymmetric phosphate bands (see Figure D.4 A-B from Appendix D), respectively. Effect of EGCG concentration on the fluorescence ratio reflecting the membrane dipole potential of DMPC vesicles labeled with di-8-ANEPPS (D). The exponential functions, which are also shown (black), were fitted to the data points. Error bars = \pm standard deviation of 4 independent samples.

the solution electrolytes, acting as counterions. The transmembrane potential, the surface potential and the dipole potential are the three types of membrane electrical potential, which are known to play important roles in the structure and permeability of biological membranes [59, 95, 96, 97]. A surface potential (ΔV) is generated due to the charge difference that exists between the aqueous interface (ions in bulk water) and the membrane monolayer surface (charged head groups of lipids). [95, 98].

We assessed the effect of EGCG on DMPC membrane potential using the lipid monolayer/bilayer as a model. Figure 8.5 shows the surface potential isotherms. In pure DMPC, contributions to the surface potential arise from the intrinsic

dipoles of choline, phosphate and ester (carbonyl) groups, and the interfacial water molecules in the lipid headgroup region [98, 99]. Surface potential becomes non zero at large A_1 values ($\sim 104 \text{ \AA}^2$) due to the initial assembling of the lipid molecules in the liquid expanded state, which leads to an increase in the normal component of the dipole moment (black curve in Figure 8.5A). At A_1 of $\sim 58 \text{ \AA}^2$ the surface potential increases further, probably related to a LE/LC transition (not completely clear from the isotherm), where dipoles are even more aligned to the membrane normal. At too small A_1 values, the monolayer collapses with the highest surface potential observed of $\sim 530 \text{ mV}$. The A_1 vs. ΔV curves for the EGCG/DMPC mixtures have similar profiles to pure DMPC. However, some differences can be noted, namely, the negative ΔV values at high A_1 , or the significantly higher ΔV values observed for 5 and 10% EGCG/DMPC systems ($\sim 610 \text{ mV}$), at monolayer pre-collapsing A_1 values (Figure 8.5A). It seems that EGCG contributes with up to 80 mV to the total membrane surface potential. The potential functions do not exhibit a monotonic behavior due to the distinct effect of low and large amounts of EGCG in the packing of DMPC phospholipids molecules, as should be expected from the PM-IRRAS and steady-state fluorescence measurements. For the 20% EGCG/DMPC mixture, the membrane surface potential decreases drastically at small A_1 , being only $\sim 410 \text{ mV}$ near the monolayer collapse. This is probably due to the significant increase in the physical distance between DMPC head groups, promoted by the presence of EGCG, which surpasses any condensing effect that may have occurred at lower mol% values. This extra space between the choline/phosphate groups is generated by the presence of the catechin molecules (Figure D.1 of Appendix D), which are usually inserted at higher depth (Figure 8.2D), and allows for significant bending of the head group, leading to a decrease in its total membrane surface potential (Figure D.5 of Appendix D). This effect is also captured in the apparent dipole ratios between EGCG/DMPC and neat DMPC at different EGCG molar fractions, for different surface pressures (Figure 8.5B). Indeed, the predominant effect at small amounts of EGCG seems to be the lipid monolayer condensation, which is indicated by the compressional modulus (Figure 8.3C) and, to some extent, by the PM-IRRAS measurements (Figure 8.4C). This seems to be related to an increase in the apparent dipole moment. However, at larger EGCG mol% fractions, the dipole moment decreases probably due to the DMPC head group bending, as suggested above. Shifts in the choline group ($N(\text{CH}_3)_3^+$) asymmetric stretching band from 978 to 963 cm^{-1} with 1.6 mol% EGCG in the PM-IRRAS measurements (Figure D.4C of Appendix D) also suggest a condensation effect, since a shift of this band to a lower wavenumber indicates a decrease in the choline group bending[100].

The asymmetric stretching band observed for the 20 mol% fraction (969 cm^{-1}) suggests a larger choline bending when compared with the 1.6 mol% system, but still not fully consistent with the pure DMPC measurements. Furthermore, the head group bending can also explain why the membrane thickness profile does not change significantly in the MD simulations, even though the A_1 of DMPC decreases with increased EGCG concentration. The limitations of our MD simulations to describe the membrane stability are the main reason why these data were not used further to help interpret the surface potential and PM-IRRAS results.

Considering the relationship between lipid hydration and membrane dipole potential, the region between $1100\text{--}1800\text{ cm}^{-1}$ in the PM-IRRAS spectra was analyzed in more detail. This analysis provides information about the spatial arrangement of the water molecules in the vicinity of the ester (carbonyl) and phosphate groups of lipids, and about its hydrogen bond network (Figures D.4A-B of Appendix D). The absorption band assigned to the carbonyl group (C=O) was deconvoluted with two components at 1737 cm^{-1} and 1746 cm^{-1} corresponding to the water-bound ester carbonyl groups and free carbonyl groups, respectively.[101] At lower concentrations (1.6–5 mol% EGCG) there is a shift to higher wavenumbers, reflecting a reduction in hydrogen bonding to carbonyl groups. The hydration of DMPC carbonyl groups decreases in Figure 8.5C, probably due to replacement of water molecules by EGCG, which can act as hydrogen bond donors to the oxygen atoms in the DMPC carbonyl groups. Similar results were obtained for the phosphate region in Figure 8.5C, where the absorption band assigned to the phosphate group (P=O) antisymmetric stretching was deconvoluted with two components at 1232 cm^{-1} and 1261 cm^{-1} corresponding to water hydrogen bonding and “free” phosphate groups, respectively.[102] The hydration level of DMPC phosphate groups also decreased upon addition of EGCG, following a similar exponential decay trend.

The dipole potential changes in the presence of EGCG measured in DMPC monolayers were compared with similar data in DMPC bilayers using fluorescence spectroscopy. The DMPC vesicles were labeled with di-8-ANEPPS, a probe that is very sensitive to the dipole potential changes in the membrane.[58] The addition of EGCG leads to a decrease of the dipole potential of DMPC vesicles (Figure 8.5D), following an exponential decrease that is more analogous to the monolayer dehydration profiles (Figure 8.5C) than to their dipole moment values (Figure 8.5B). In fact, this decrease in dipole moment is paralleled with the reduced polarity/hydration at the hydrophilic-hydrophobic interface in DMPC vesicles assessed through the generalized polarization of Laurdan. [86] This suggests that the displacement of the water molecules by catechin in lipid bilayers is

a key factor in the dipole moment decrease. Moreover, the addition of EGCG induces DMPC headgroup bending due to increased P–P distances or lipid disorder, which could be related with liposomes aggregation at higher EGCG concentrations.

8.4 Conclusion

The effects of embedding EGCG into DMPC membranes were studied using Langmuir monolayer techniques, lipid vesicles and MD simulations of lipid bilayers. This interdisciplinary study showed that EGCG accumulates at the lipids ester region, displacing the water molecules and establishing hydrogen bond interactions with all available hydrogen bond acceptors (phosphate and ester groups) of DMPC lipids. The presence of EGCG induces changes in several physical properties of DMPC monolayers/bilayers. The computational data suggests that the main effect is a condensation, reminiscent of what has been described for cholesterol. [81, 82, 83, 84] The PM-IRRAS data on lipid monolayers showed that such an effect appears only at low catechin concentrations, since at higher values the predominant effect was of increased disorder, which could be confirmed by the lowering of the dipole moments. The steady-state fluorescence data at higher EGCG concentrations (> 10 mol%) corroborated that a catechin-induced liposome aggregation process overtakes any condensation effect. Furthermore, the membrane dipole potential of DMPC vesicles, followed using a di-8-ANEPPS label, shows that EGCG induces lipid bending in the bilayer and confirms that catechin loading capacity in DMPC liposomes is ~ 10 mol%. This loading capacity indicates that liposomes are promising as nanocarriers and catechins encapsulation agents. Nonetheless, it may be desirable to develop formulations that stably retain larger molar fractions of EGCG. From our results we infer that more stable and organized liposomes (e.g. DPPC), [103] may circumvent the aggregation process at larger concentrations of catechin. Finally, this work contributes to better understanding the extent of molecular interactions between EGCG and PC lipids and reveal how these interactions influence the loading efficiency and stability of liposomes. EGCG encapsulation in PC-based liposomes can promote its antioxidant and antimicrobial activities by triggering its sustained and controlled release over time. Looking ahead, these liposomal systems can be included in: (1) food packaging – as an active coating that extends the food shelf life by preventing oxidation; (2) cosmetic formulations – with increased EGCG absorption into human skin; and (3) cancer therapies – as vehicles that provide higher EGCG

accumulation within tumour cells.

8.5 Acknowledgements

The authors acknowledge the financial support from FEDER, through Programa Operacional Factores de Competitividade COMPETE and Fundação para a Ciência e a Tecnologia through research project grants PEst-OE/FIS/UI0068/2011, UID/FIS/00068/2013, UID/FIS/00068/2019, UID/MULTI/00612/2019, UID / MULTI/ 04046/2019, PTDC/FIS-NAN/0909/2014, PTDC/QEQ-COM/5904/2014 and PTDC/BBB-BQB/6071/2014. The Conselho Nacional de Desenvolvimento Científico e Tecnológico and Fundação de Amparo à Pesquisa do Estado de São Paulo are also acknowledged. MM acknowledges fellowship SFRH / BPD / 110491 / 2015 and contract CEECIND/02300/2017 grants, and FP acknowledges the fellowship grant PD/BD/106036/2015 from RABBIT Doctoral Programme (Portugal).

References

- [1] J. Crous-Masó, S. Palomeras, J. Relat, C. Camó, Ú. Martínez-Garza, M. Planas, L. Feliu, and T. Puig. “(-)-Epigallocatechin 3-Gallate Synthetic Analogues Inhibit Fatty Acid Synthase and Show Anticancer Activity in Triple Negative Breast Cancer.” In: *Molecules* 23.5 (2018), pp. 1160–1172.
- [2] K.-W. Luo, W.-Y. Lung, X.-L. L. Chun-Xie, and W.-R. Huang. “EGCG inhibited bladder cancer T24 and 5637 cell proliferation and migration via PI3K/AKT pathway.” In: *Oncotarget* 9.15 (2018), 12261—12272.
- [3] Y. Tamba, S. Ohba, M. Kubota, H. Yoshioka, H. Yoshioka, and M. Yamazaki. “Single GUV method reveals interaction of tea catechin (-)-epigallocatechin gallate with lipid membranes.” In: *Biophysical Journal* 92.9 (2007), pp. 3178–3194.
- [4] T. W. Sirk, E. F. Brown, M. Friedman, and A. K. Sum. “Molecular binding of catechins to biomembranes: relationship to biological activity.” In: *Journal of Agricultural and Food Chemistry* 57.15 (2009), pp. 6720–6728.
- [5] Y. Sun, W.-C. Hung, F.-Y. Chen, C.-C. Lee, and H. W. Huang. “Interaction of tea catechin (—)-epigallocatechin gallate with lipid bilayers.” In: *Biophysical Journal* 96.3 (2009), pp. 1026–1035.

- [6] H. Ikigai, T. Nakae, Y. Hara, and T. Shimamura. "Bactericidal catechins damage the lipid bilayer." In: *Biochimica et Biophysica Acta (BBA) – Biomembranes* 1147.1 (1993), pp. 132–136.
- [7] M. Yamazaki. "The single GUV method to reveal elementary processes of leakage of internal contents from liposomes induced by antimicrobial substances." In: *Advances in Planar Lipid Bilayers Liposomes* 7 (2008), pp. 121–142.
- [8] M. Shimizu and I. B. Weinstein. "Modulation of signal transduction by tea catechins and related phytochemicals." In: *Mutation Research/Fundamental and Molecular Mechanisms of Mutagenesis* 591.1 (2005), pp. 147–160.
- [9] N. Khan, F. Afaq, M. Saleem, N. Ahmad, and H. Mukhtar. "Targeting multiple signaling pathways by green tea polyphenol (-)-epigallocatechin-3-gallate." In: *Cancer Research* 66.5 (2006), pp. 2500–2505.
- [10] D. G. Nagle, D. Ferreira, and Y.-D. Zhou. "Epigallocatechin-3-gallate (EGCG): chemical and biomedical perspectives." In: *Phytochemistry* 67.17 (2006), pp. 1849–1855.
- [11] S. Prasad, K. Phromnoi, V. R. Yadav, M. M. Chaturvedi, and B. B. Aggarwal. "Targeting inflammatory pathways by flavonoids for prevention and treatment of cancer." In: *Planta Medica* 76.11 (2010), pp. 1044–1063.
- [12] J. Baell and M. A. Walters. "Chemical con artists foil drug discovery." In: *Nature* 513.7519 (2014), pp. 481–483.
- [13] H. I. Ingólfsson, P. Thakur, K. F. Herold, E. A. Hobart, N. B. Ramsey, X. Periole, D. H. De Jong, M. Zwama, D. Yilmaz, K. Hall, T. Maretzky, H. C. Hemmings Jr., C. Blobel, S. J. Marrink, A. Kocer, J. T. Sack, and A. O. S. "Phytochemicals perturb membranes and promiscuously alter protein function." In: *Chemical Biology* 9.8 (2014), pp. 1788–1798.
- [14] M. Kamihira, H. Nakazawa, A. Kira, Y. Mizutani, M. Nakamura, and T. Nakayama. "Interaction of tea catechins with lipid bilayers investigated by a quartz-crystal microbalance analysis." In: *Bioscience, Biotechnology, and Biochemistry* 72.5 (2008), pp. 1372–1375.
- [15] T. W. Sirk, E. F. Brown, A. K. Sum, and M. Friedman. "Molecular dynamics study on the biophysical interactions of seven green tea catechins with lipid bilayers of cell membranes." In: *Journal of Agricultural and Food Chemistry* 56.17 (2008), pp. 7750–7758.

- [16] L. H. Long, M. V. Clement, and B. Halliwell. "Artifacts in cell culture: rapid generation of hydrogen peroxide on addition of (-)-epigallocatechin, (-)-epigallocatechin gallate, (+)-catechin, and quercetin to commonly used cell culture media." In: *Biochemical and Biophysical Research Communications* 273.1 (2000), pp. 50–53.
- [17] M. K. Riaz, M. A. Riaz, X. Zhang, C. Lin, K. H. Wong, X. Chen, G. Zhang, A. Lu, and Z. Yang. "Surface Functionalization and Targeting Strategies of Liposomes in Solid Tumor Therapy: A Review." In: *International Journal of Molecular Sciences* 19 (2018), pp. 195–222.
- [18] T. O. Olusanya, R. R. Haj Ahmad, D. M. Ibegbu, J. R. Smith, and A. A. Elkordy. "Liposomal drug delivery systems and anticancer drugs." In: *Molecules* 23.4 (2018), pp. 907–924.
- [19] V. P. Torchilin. "Immobilization of specific proteins on liposome surface: systems for drug targeting." In: *Liposome Technology* 3 (2018), pp. 75–94.
- [20] B. Hu, Y. Ting, X. Yang, W. Tang, X. Zeng, and Q. Huang. "Nanochemoprevention by encapsulation of (-)-epigallocatechin-3-gallate with bioactive peptides/chitosan nanoparticles for enhancement of its bioavailability." In: *Chemical Communications* 48.18 (2012), pp. 2421–2423.
- [21] J. Liang, H. Yan, P. Puligundla, X. Gao, Y. Zhou, and X. Wan. "Applications of chitosan nanoparticles to enhance absorption and bioavailability of tea polyphenols: A review." In: *Food Hydrocolloids* 69 (2017), pp. 286–292.
- [22] K. Istenič, R. Cerc Korošec, and N. Poklar Ulrih. "Encapsulation of (-)-epigallocatechin gallate into liposomes and into alginate or chitosan microparticles reinforced with liposomes." In: *Journal of the Science of Food and Agriculture* 96.13 (2016), pp. 4623–4632.
- [23] L. G. Gómez-Mascaraque, G. Sanchez, and A. López-Rubio. "Impact of molecular weight on the formation of electrosprayed chitosan microcapsules as delivery vehicles for bioactive compounds." In: *Carbohydrate Polymers* 150 (2016), pp. 121–130.
- [24] W. Hong, Y. Zhao, Y. Guo, C. Huang, P. Qiu, J. Zhu, C. Chu, H. Shi, and M. Liu. "PEGylated Self-Assembled Nano-Bacitracin A: Probing the Antibacterial Mechanism and Real-Time Tracing of Target Delivery in Vivo." In: *Applied Materials & Interfaces* 10.13 (2018), pp. 10688–10705.

- [25] Y. Zhang, S.-X. Wang, J.-W. Ma, H.-Y. Li, J.-C. Ye, S.-M. Xie, B. Du, and X.-Y. Zhong. “EGCG inhibits properties of glioma stem-like cells and synergizes with temozolomide through downregulation of P-glycoprotein inhibition.” In: *Journal of Neuro-Oncology* 121.1 (2015), pp. 41–52.
- [26] H. Hajipour, H. Hamishehkar, S. Nazari Soltan Ahmad, S. Barghi, N. F. Maroufi, and R. A. Taheri. “Improved anticancer effects of epigallocatechin gallate using RGD-containing nanostructured lipid carriers.” In: *Artificial cells, Nanomedicine, and Biotechnology* (2018), pp. 1–10.
- [27] S. K. Ramadass, N. V. Anantharaman, S. Subramanian, S. Sivasubramanian, and B. Madhan. “Paclitaxel/epigallocatechin gallate coloaded liposome: a synergistic delivery to control the invasiveness of MDA-MB-231 breast cancer cells.” In: *Colloids and Surfaces Biointerfaces* 125 (2015), pp. 65–72.
- [28] V. Sanna, C. K. Singh, R. Jashari, V. M. Adhami, J. C. Chamcheu, I. Rady, M. Sechi, H. Mukhtar, and I. A. Siddiqui. “Targeted nanoparticles encapsulating (-)-epigallocatechin-3-gallate for prostate cancer prevention and therapy.” In: *Scientific Reports* 7.41573 (2017), pp. 1–15.
- [29] L.-C. Tsai, H.-Y. Hsieh, K.-Y. Lu, S.-Y. Wang, and F.-L. Mi. “EGCG/gelatin-doxorubicin gold nanoparticles enhance therapeutic efficacy of doxorubicin for prostate cancer treatment.” In: *Nanomedicine* 11.1 (2016), pp. 9–30.
- [30] S. K. Dhatwalia, M. Kumar, and D. K. Dhawan. “Role of EGCG in Containing the Progression of Lung Tumorigenesis—A Multistage Targeting Approach.” In: *Nutrition and Cancer* 70.3 (2018), pp. 334–349.
- [31] Y. Ma, J. Yang, S. Li, and W. Yu. “Synergic Inhibition of Lung Carcinoma 95-D Cell Proliferation and Invasion by Combination with (-) – Epigallocatechin – 3 – Gallate and Ascorbic Acid.” In: *Wuhan University Journal of Natural Sciences* 23.3 (2018), pp. 270–276.
- [32] D. Ramadan, A. W. Goldie, and E. Anwar. “Novel Transdermal Ethosomal Gel Containing Green Tea (*Camellia sinensis* L. Kuntze) Leaves Extract: Formulation and In vitro Penetration Study.” In: *Journal of Young Pharmacists* 9.3 (2017), pp. 336–340.
- [33] J. Zhang, Z. Lei, Z. Huang, X. Zhang, Y. Zhou, Z. Luo, W. Zeng, J. Su, C. Peng, and X. Chen. “Epigallocatechin-3-gallate (EGCG) suppresses melanoma cell growth and metastasis by targeting TRAF6 activity.” In: *Oncotarget* 7.48 (2016), 79557–79571.

- [34] S. Akhavan, E. Assadpour, I. Katouzian, and S. M. Jafari. "Lipid nano scale cargos for the protection and delivery of food bioactive ingredients and nutraceuticals." In: *Trends in Food Science & Technology* 7 (2018), pp. 132–146.
- [35] A. Zoghi, K. Khosravi-Darani, and A. Omri. "Process Variables and Design of Experiments in Liposome and Nanoliposome Research." In: *Mini reviews in Medicinal Chemistry* 18.4 (2018), pp. 324–344.
- [36] A. F. Esfanjani, E. Assadpour, and S. M. Jafari. "Improving the bioavailability of phenolic compounds by loading them within lipid-based nanocarriers." In: *Trends in Food Science & Technology* 76 (2018), pp. 56–66.
- [37] R. F. Gonçalves, J. T. Martins, C. M. Duarte, A. A. Vicente, and A. C. Pinheiro. "Advances in nutraceutical delivery systems: From formulation design for bioavailability enhancement to efficacy and safety evaluation." In: *Trends in Food Science & Technology* 78 (2018), pp. 270–291.
- [38] W. Kopeć, J. Telenius, and H. Khandelia. "Molecular dynamics simulations of the interactions of medicinal plant extracts and drugs with lipid bilayer membranes." In: *FEBS Journal* 280.12 (2013), pp. 2785–2805.
- [39] D. Vila-Viçosa, B. L. Victor, J. Ramos, D. Machado, M. Viveiros, J. Switala, P. C. Loewen, R. Leitaó, F. Martins, and M. Machuqueiro. "Insights on the mechanism of action of INH-C₁₀ as an antitubercular prodrug." In: *Molecular Pharmaceutics* 14.12 (2017), pp. 4597–4605.
- [40] J. Wong-Ekkabut, S. Baoukina, W. Triampo, I.-M. Tang, D. P. Tieleman, and L. Monticelli. "Computer simulation study of fullerene translocation through lipid membranes." In: *Nature Nanotechnology* 3.6 (2008), pp. 363–368.
- [41] H. A. Filipe, C. Sousa, J. T. Marques, D. Vila-Viçosa, A. de Granada-Flor, A. S. Viana, M. S. C. Santos, M. Machuqueiro, and R. F. de Almeida. "Differential targeting of membrane lipid domains by caffeic acid and its ester derivatives." In: *Free Radical Biology and Medicine* 115 (2018), pp. 232–245.
- [42] A. E. Cardenas, R. Shrestha, L. J. Webb, and R. Elber. "Membrane Permeation of a Peptide: It is Better to be Positive." In: *The Journal of Physical Chemistry B* 119.21 (2015), pp. 6412–6420.
- [43] V. H. Teixeira, D. Vila-Viçosa, P. B.P. S. Reis, and M. Machuqueiro. "pK_a Values of Titrable Amino Acids at the Water/Membrane Interface." In: *Journal of Chemical Theory and Computation* 12.3 (2016), pp. 930–934.

- [44] D. Vila-Viçosa, T. F. Silva, G. Slaybaugh, Y. K. Reshetnyak, O. A. Andreev, and M. Machuqueiro. “Membrane-Induced pK_a shifts in *wt*-pHLIP and its L16H Variant.” In: *Journal of Chemical Theory and Computation* 14.6 (2018), pp. 3289–3297.
- [45] W. Zhu, L. Jia, G. Chen, H. Zhao, X. Sun, X. Meng, X. Zhao, L. Xing, J. Yu, and M. Zheng. “Epigallocatechin-3-gallate ameliorates radiation-induced acute skin damage in breast cancer patients undergoing adjuvant radiotherapy.” In: *Oncotarget* 7.30 (2016), pp. 48607–48613.
- [46] W. Zhu, I. Khalifa, J. Peng, and C. Li. “Position and orientation of gallated proanthocyanidins in lipid bilayer membranes: influence of polymerization degree and linkage type.” In: *Journal of Biomolecular Structure and Dynamics* (2017), pp. 1–14.
- [47] E. Laudadio, G. Mobbili, C. Minnelli, L. Massaccesi, and R. Galeazzi. “Salts influence catechins and flavonoids encapsulation in liposomes: A molecular dynamics investigation.” In: *Molecular Informatics* 36.11 (2017), pp. 1700059–1700072.
- [48] E. Laudadio, C. Minnelli, A. Amici, L. Massaccesi, G. Mobbili, and R. Galeazzi. “Liposomal formulations for an efficient encapsulation of epigallocatechin – 3 – gallate: An in-silico/experimental approach.” In: *Molecules* 23.2 (2018), pp. 441–459.
- [49] J. Villalaín. “Epigallocatechin-3-gallate location and interaction with late endosomal and plasma membrane model membranes by molecular dynamics.” In: *Journal of Biomolecular Structure and Dynamics* 37.12 (2018), pp. 1–13.
- [50] A. Hospital, J. R. Goñi, M. Orozco, and J. L. Gelpí. “Molecular dynamics simulations: advances and applications.” In: *Advances and Applications in Bioinformatics and Chemistry* 8 (2015), pp. 37–47.
- [51] M. Elderdfi and A. F. Sikorski. “Langmuir-Monolayer Methodologies for Characterizing Protein-Lipid Interactions.” In: *Chemistry and Physics of Lipids* 212 (2018), pp. 61–72.
- [52] T. M. Nobre, F. J. Pavinatto, L. Caseli, A. Barros-Timmons, P. Dynarowicz-Łątka, and O. N. Oliveira Jr. “Interactions of bioactive molecules & nano-materials with Langmuir monolayers as cell membrane models.” In: *Thin Solid Films* 593 (2015), pp. 158–188.

- [53] J. J. Giner-Casares, G. Brezesinski, and H. Möhwald. “Langmuir monolayers as unique physical models.” In: *Current opinion in Colloid & Interface Science* 19.3 (2014), pp. 176–182.
- [54] O. N. Oliveira, D. M. Taylor, T. J. Lewis, S. Salvagno, and C. J. Stirling. “Estimation of group dipole moments from surface potential measurements on Langmuir monolayers.” In: *Journal of the Chemical Society Faraday Transactions* 85.4 (1989), pp. 1009–1018.
- [55] I. Levin, T. Thompson, Y Barenholz, and C.-h. Huang. “Two types of hydrocarbon chain interdigitation in sphingomyelin bilayers.” In: *Biochemistry* 24.22 (1985), pp. 6282–6286.
- [56] N. Caturla, E. Vera-Samper, J. Villalaín, C. R. Mateo, and V. Micol. “The relationship between the antioxidant and the antibacterial properties of galloylated catechins and the structure of phospholipid model membranes.” In: *Free Radical Biology and Medicine* 34.6 (2003), pp. 648–662.
- [57] S. Mabrey and J. M. Sturtevant. “Investigation of phase transitions of lipids and lipid mixtures by sensitivity differential scanning calorimetry.” In: *Proceedings of the National Academy of Sciences* 73.11 (1976), pp. 3862–3866.
- [58] R. J. Clarke. “The dipole potential of phospholipid membranes and methods for its detection.” In: *Advances in Colloid and Interface Science* 89 (2001), pp. 263–281.
- [59] A. Khmelinskaia, M. Ibarguren, R. F. de Almeida, D. J. López, V. A. Paixão, H. Ahyayauch, F. M. Goñi, and P. V. Escribá. “Changes in membrane organization upon spontaneous insertion of 2-hydroxylated unsaturated fatty acids in the lipid bilayer.” In: *Langmuir* 30.8 (2014), pp. 2117–2128.
- [60] M. J. Abraham, T. Murtola, R. Schulz, S. Páll, J. C. Smith, B. Hess, and E. Lindahl. “GROMACS: High performance molecular simulations through multi-level parallelism from laptops to supercomputers.” In: *SoftwareX* 1-2 (2015), pp. 19–25.
- [61] N. Schmid, A. P. Eichenberger, A. Choutko, S. Riniker, M. Winger, A. E. Mark, and W. F. Van Gunsteren. “Definition and testing of the GROMOS force-field versions 54A7 and 54B7.” In: *European Biophysics Journal* 40 (2011), pp. 843–856.
- [62] W. Huang, Z. Lin, and W. F. van Gunsteren. “Validation of the GROMOS 54A7 Force Field with Respect to β -Peptide Folding.” In: *Journal of Chemical Theory and Computation* 7.5 (2011), pp. 1237–1243.

- [63] A. K. Malde, L. Zuo, M. Breeze, M. Stroet, D. Poger, P. C. Nair, C. Oostenbrink, and A. E. Mark. “An automated force field topology builder (ATB) and repository: version 1.0.” In: *Journal of Chemical Theory and Computation* 7.12 (2011), pp. 4026–4037.
- [64] K. B. Koziara, M. Stroet, A. K. Malde, and A. E. Mark. “Testing and validation of the Automated Topology Builder (ATB) version 2.0: prediction of hydration free enthalpies.” In: *Journal of Computer-Aided Molecular Design* 28.3 (2014), pp. 221–233.
- [65] C. I. Bayly, P. Cieplak, W. D. Cornell, and P. A. Kollman. “A Well Behaved Electrostatic Based Method Using Charge Restraints For Deriving Atomic Charges: The RESP Model.” In: *The Journal of Physical Chemistry* 97 (1993), pp. 10269–10280.
- [66] M. Frisch, G. Trucks, H. Schlegel, G. Scuseria, M. Robb, J. Cheeseman, G. Scalmani, V. Barone, G. Petersson, H. Nakatsuji, X. Li, M. Caricato, A. Marenich, J. Bloino, B. Janesko, R. Gomperts, B. Mennucci, H. Hratchian, J. Ortiz, A. Izmaylov, J. Sonnenberg, D. Williams-Young, F. Ding, F. Lipparini, F. Egidi, J. Goings, B. Peng, A. Petrone, T. Henderson, D. Ranasinghe, V. Zakrzewski, J. Gao, N. Rega, G. Zheng, W. Liang, M. Hada, M. Ehara, K. Toyota, R. Fukuda, J. Hasegawa, M. Ishida, T. Nakajima, Y. Honda, O. Kitao, H. Nakai, T. Vreven, K. Throssell, J. Montgomery, J. A., J. Peralta, F. Ogliaro, M. Bearpark, J. Heyd, E. Brothers, K. Kudin, V. Staroverov, T. Keith, R. Kobayashi, J. Normand, K. Raghavachari, A. Rendell, J. Burant, S. Iyengar, J. Tomasi, M. Cossi, J. Millam, M. Klene, C. Adamo, R. Cammi, J. Ochterski, R. Martin, K. Morokuma, O. Farkas, J. Foresman, and D. Fox. *Gaussian 09, Revision A.02*. Gaussian, Inc., Wallingford, CT, 2016.
- [67] S. H. Vosko, L. Wilk, and M. Nusair. “Accurate spin-dependent electron liquid correlation energies for local spin density calculations: a critical analysis.” In: *Canadian Journal of Physics* 58.8 (1980), pp. 1200–1211.
- [68] C. Lee, W. Yang, and R. G. Parr. “Development of the Colle-Salvetti correlation-energy formula into a functional of the electron density.” In: *Physical Review B* 37.2 (1988), pp. 785–789.
- [69] A. D. Becke. “Density-functional thermochemistry. III. The role of exact exchange.” In: *The Journal of Chemical Physics* 98.7 (1993), pp. 5648–5652.

- [70] P. C. Hariharan and J. A. Pople. "The influence of polarization functions on molecular orbital hydrogenation energies." In: *Theoretica Chimica Acta* 28.3 (1973), pp. 213–222.
- [71] M. Muzolf, H. Szymusiak, A. Gliszczyńska-Świgło, I. M. Rietjens, and B. Tyrakowska. "pH-dependent radical scavenging capacity of green tea catechins." In: *Journal of Agricultural and Food Chemistry* 56.3 (2008), pp. 816–823.
- [72] G. Bussi, D. Donadio, and M. Parrinello. "Canonical sampling through velocity rescaling." In: *The Journal of Chemical Physics* 126.014101 (2007), pp. 1–8.
- [73] M. Parrinello and A. Rahman. "Polymorphic transitions in single crystals: A new molecular dynamics method." In: *Journal of Applied Physics* 52.12 (1981). ISSN: 0021-8979.
- [74] B. Hess. "P-LINCS: A Parallel Linear Constraint Solver for Molecular Simulation." In: *Journal of Chemical Theory and Computation* 4 (2008), pp. 116–122.
- [75] S. Miyamoto and P. A. Kollman. "SETTLE: An analytical version of the SHAKE and RATTLE algorithm for rigid water models." In: *Journal of Computational Chemistry* 13 (1992), pp. 952–962.
- [76] J. Hermans, H. J. C. Berendsen, W. F. van Gunsteren, and J. P. M. Postma. "A Consistent Empirical Potential for Water-Protein Interactions." In: *Biopolymers : Original Research on Biomolecules* 23 (1984), pp. 1513–1518.
- [77] T. Darden, D. York, and L. Pedersen. "Particle mesh Ewald: An Nlog(N) method for Ewald sums in large systems." In: *The Journal of Chemical Physics* 98 (1993), pp. 10089–10092.
- [78] W. J. Allen, J. A. Lemkul, and D. R. Bevan. "GridMAT-MD: A grid-based membrane analysis tool for use with molecular dynamics." In: *Journal of Computational Chemistry* 30.12 (2009), pp. 1952–1958.
- [79] H. I. Petrache, S. W. Dodd, and M. F. Brown. "Area per lipid and acyl length distributions in fluid phosphatidylcholines determined by ^2H -NMR spectroscopy." In: *Biophysical Journal* 79 (2000), pp. 3172–3192.
- [80] J. F. Nagle and S. Tristram-Nagle. "Structure of lipid bilayers." In: *Biochimica et Biophysica Acta (BBA)– Reviews on Biomembranes* 1469.3 (2000), pp. 159–195.

- [81] P. Wydro and K. Hac-Wydro. "Thermodynamic description of the interactions between lipids in ternary Langmuir monolayers: the study of cholesterol distribution in membranes." In: *The Journal of Physical Chemistry B* 111.10 (2007), pp. 2495–2502.
- [82] Y. Su, Q. Li, L. Chen, and Z. Yu. "Condensation effect of cholesterol, stigmasterol, and sitosterol on dipalmitoylphosphatidylcholine in molecular monolayers." In: *Colloids and Surfaces A: Physicochemical and Engineering Aspects* 293.1-3 (2007), pp. 123–129.
- [83] K. Gong, S.-S. Feng, M. L. Go, and P. H. Soew. "Effects of pH on the stability and compressibility of DPPC/cholesterol monolayers at the air–water interface." In: *Colloids and Surfaces A: Physicochemical and Engineering Aspects* 207.1-3 (2002), pp. 113–125.
- [84] K. Sabatini, J.-P. Mattila, and P. K. Kinnunen. "Interfacial behavior of cholesterol, ergosterol, and lanosterol in mixtures with DPPC and DMPC." In: *Biophysical Journal* 95.5 (2008), pp. 2340–2355.
- [85] T. Miyoshi and S. Kato. "Detailed analysis of the surface area and elasticity in the saturated 1, 2-diacylphosphatidylcholine/cholesterol binary monolayer system." In: *Langmuir* 31.33 (2015), pp. 9086–9096.
- [86] J. R. Colina, M. Suwalsky, M. Manrique-Moreno, K. Petit, L. F. Aguilar, M. Jemiola-Rzeminska, and K. Strzalka. "Protective effect of epigallocatechin gallate on human erythrocytes." In: *Colloids and Surfaces B: Biointerfaces* 173 (2019), pp. 742–750.
- [87] A. Takahashi, T. Watanabe, A. Mondal, K. Suzuki, M. Kurusu-Kanno, Z. Li, T. Yamazaki, H. Fujiki, and M. Suganuma. "Mechanism-based inhibition of cancer metastasis with (-)-epigallocatechin gallate." In: *Biochemical and Biophysical Research Communications* 443.1 (2014), pp. 1–6.
- [88] Q. Luo, D. Kuang, B. Zhang, and G. Song. "Cell stiffness determined by atomic force microscopy and its correlation with cell motility." In: *Biochimica et Biophysica Acta (BBA)-General Subjects* 1860.9 (2016), pp. 1953–1960.
- [89] M. Suganuma, A. Takahashi, T. Watanabe, K. Iida, T. Matsuzaki, H. Y. Yoshikawa, and H. Fujiki. "Biophysical approach to mechanisms of cancer prevention and treatment with green tea catechins." In: *Molecules* 21.11 (2016), pp. 1566–1583.
- [90] H. Tsuchiya, M. Nagayama, T. Tanaka, M. Furusawa, M. Kashimata, and H. Takeuchi. "Membrane-rigidifying effects of anti-cancer dietary factors." In: *Biofactors* 16.3,4 (2002), pp. 45–56.

- [91] H. Tsuchiya. "Effects of green tea catechins on membrane fluidity." In: *Pharmacology* 59.1 (1999), pp. 34–44.
- [92] S. Holzschuh, K. Kaeß, G. V. Bossa, C. Decker, A. Fahr, and S. May. "Investigations of the influence of liposome composition on vesicle stability and drug transfer in human plasma: a transfer study." In: *J. Liposome Res.* 28.1 (2018), pp. 22–34.
- [93] W. L. C. Vaz, R. M. Clegg, and D. Hallmann. "Translational diffusion of lipids in liquid crystalline phase phosphatidylcholine multibilayers. A comparison of experiment with theory." In: *Biochemistry* 24.3 (1985), pp. 781–786.
- [94] M. Kubista, R. Sjöback, S. Eriksson, and B. Albinsson. "Experimental correction for the inner-filter effect in fluorescence spectra." In: *Analyst* 119.3 (1994), pp. 417–419.
- [95] L. Wang. "Measurements and implications of the membrane dipole potential." In: *Annual Review of Biochemistry* 81 (2012), pp. 615–635.
- [96] F. Lakhdar-Ghazal, J.-L. Tichadou, and J.-F. Tocanne. "Effect of pH and monovalent cations on the ionization state of phosphatidylglycerol in monolayers." In: *European Journal of Biochemistry* 134 (1983), pp. 531–537.
- [97] O. Oliveira Jr, A Riul Jr, and G. L. Ferreira. "Surface potentials of mixed Langmuir films: a model consistent with a domain-structured monolayer." In: *Thin Solid Films* 242.1-2 (1994), pp. 239–242.
- [98] H. Brockman. "Dipole potential of lipid membranes." In: *Chemistry and Physics of Lipids* 73.1-2 (1994), pp. 57–79.
- [99] U. Peterson, D. A. Mannock, R. N. Lewis, P. Pohl, R. N. McElhaney, and E. E. Pohl. "Origin of membrane dipole potential: Contribution of the phospholipid fatty acid chains." In: *Chemistry and Physics of Lipids* 117.1 (2002), pp. 19–27.
- [100] W. Terakosolphan, J. L. Trick, P. G. Royall, S. E. Rogers, O. Lamberti, C. D. Lorenz, B. Forbes, and R. D. Harvey. "Glycerol solvates DPPC headgroups and localises in the interfacial regions of model pulmonary interfaces altering bilayer structure." In: *Langmuir* 34.23 (2018), pp. 6941–6954.

- [101] A. Dicko, H. Bourque, and M. Pérolet. “Study by infrared spectroscopy of the conformation of dipalmitoylphosphatidylglycerol monolayers at the air–water interface and transferred on solid substrates.” In: *Chemistry and Physics of Lipids* 96.1 (1998), pp. 125–139.
- [102] N. E. Levinger, R. Costard, E. T. Nibbering, and T. Elsaesser. “Ultrafast energy migration pathways in self-assembled phospholipids interacting with confined water.” In: *The Journal of Physical Chemistry A* 115.43 (2011), pp. 11952–11959.
- [103] J. Adler-Moore and R. T. Proffitt. “AmBisome: Liposomal formulation, structure, mechanism of action and pre-clinical experience.” In: *Journal of Antimicrobial Chemotherapy* 49.1 (2002), pp. 21–30.

CELL-BASED RESULTS

Polycaprolactone/gelatin nanofiber membranes containing epigallocatechin-3-gallate loaded liposomes and their potential use for skin regeneration¹

Abstract

Polymeric scaffolds incorporating plant-derived compounds, produced by electrospinning, have attracted attention in the field of skin tissue engineering. This study evaluates the sustained antioxidant activity of polycaprolactone (PCL) / gelatin nanofibers prepared by electrospinning and incorporating loaded liposomes of epigallocatechin-3-gallate (EGCG), a strong antibacterial and antioxidant molecule found in green tea, that significantly accelerates the wound healing process. The morphology and the structural properties of the membranes were characterized by scanning electron microscopy (SEM) and FTIR spectroscopy. Results revealed that the EGCG released from PCL+Gelatin nanofibers scavenges the toxic ROS species generated by exposure either to H₂O₂ or UV radiation and slows down the oxidation events associated with damage. This study provides basis for developing new and promising nanofiber formulations containing EGCG that might enhance repair/regeneration of skin tissue.

¹This chapter is based on the following publication in press:

Pires, F., Santos, JF., Bitoque, D., Silva, GA., Marletta, A., Nunes, VA., Ribeiro, PA., Silva, JC. and Raposo, M..Polycaprolactone/gelatin nanofiber membranes containing epigallocatechin-3-gallate loaded liposomes and their potential use for skin regeneration. Applied Bio Materials, 2019,DOI:10.1021/acsabm.9b00524

9.1 Introduction

Skin is a crucial organ of the human body that confers immunologic protection against pathogenic invasion and provides shielding against harmful physical and chemical agents such as exposure to ultraviolet radiation (UV), toxic metals, cigarette smoke, among others.[1, 2, 3] These agents contribute to an excessive generation and accumulation of highly toxic reactive oxygen species (ROS), which have been associated to skin aging,[4, 5] cancer progression enhancement[6, 7, 8] and delay in the wound healing process.[9] Wound healing is a complex and highly dynamic process that requires a balance between ROS species production and detoxification, and involves multiple steps including inflammation, proliferation, and tissue remodeling. Remarkably, low levels of ROS are required to activate cell signaling pathways and angiogenesis that participate in the elimination of invading pathogens, whereas high ROS levels trigger oxidative stress that seriously compromises tissue repair, resulting in chronic non-healing wounds that can be painful and require expensive and long-term treatments.[10, 11] Fortunately, the advances in the skin tissue engineering field allowed successful design of new biomaterials and scaffolds, that after surface functionalization with specific biomolecules (growth factors,[12, 13] vitamins,[14, 15] antibiotics [16, 17]), can prevent infection and promote quick revascularization and re-epithelialization, thus significantly improving wound healing. The biomaterials used should be biocompatible and biodegradable and the scaffolds should be permeable to moisture and oxygen and able to absorb wound exudate, avoid infections and mechanical irritations and provide an architecture that sustains cell adhesion, infiltration and proliferation.

One of the approaches used to produce scaffolds for skin tissue engineering is the electrospinning technique. This technique has been widely used for nanofiber scaffold production and is gaining more and more interest since the membranes obtained architecturally resemble the fibrillary structure of the extracellular matrix, thus enhancing cell attachment.[18, 19] Biocompatible scaffolds, with good mechanical properties for tissue engineering [20, 21, 22, 23, 24, 25], can be produced by mixing, for instance, the synthetic polyester poly(ϵ -caprolactone) (PCL) with natural polymers such as gelatin. Over the past few decades, the electrospinning technology was also used for loading 3D scaffolds with plant-derived bioactive compounds, molecules that display antimicrobial, antiviral, antioxidant, anti-inflammatory and antitumor activity, thereby offering a great potential for skin tissue engineering applications ([26] and references therein). Moreover, the main advantages of this technology over other conventional encapsulating

methods are its relatively low cost and high production rate without compromising the structural stability/activity of the bioactive molecule. For instance, the stability of epigallocatechin-3-gallate (EGCG), a natural antioxidant present in green tea leaves, was greatly increased after encapsulation into PCL/multi-walled carbon nanotubes (MWCNTs) composite nanofibers produced by electrospinning.[27] According to this study, the nanofibers produced were non-toxic for normal osteoblast cells but markedly inhibited hepatocellular tumor cell proliferation, being the rate of EGCG release strongly influenced by the MWCNTs content in the nanofibers. In another study, EGCG-loaded PCL nanofibers also displayed anticancer activity towards gastric cancer cells, through activation of apoptotic pathways by EGCG.[28] More recently, given the potent angiogenic and antioxidant activity of EGCG, different sets of nanocomposite membranes carrying EGCG were prepared for wound healing applications.[29, 30, 31] Moreover, previous studies showed that the encapsulation of EGCG within liposomes, specifically within the lipid bilayer, ensures an optimum antioxidant activity against UV-induced damage.[32]

In this study, PCL/gelatin nanofibers containing EGCG-loaded liposomes were produced by electrospinning and their drug release and antioxidant behavior against oxidative stress induced either by H_2O_2 or UV radiation was investigated. The main purpose of this study is to develop a scaffold that sustains cell growth while at the same time efficiently scavenging ROS species as a novel strategy for the enhancement of the wound healing process.

9.2 Methodology

9.2.1 Materials

The phospholipid 1,2-dipalmitoyl-*sn*-glycero-3-phosphocholine (DPPC) was purchased from Avanti Polar Lipids. Polycaprolactone (PCL, Mw = 70–90 kDa), epigallocatechin-3-gallate (EGCG), hydrogen peroxide solution (H_2O_2 , 30 wt% in H_2O), gelatin from cold water fish skin (Mw = 60 kDa), glutaraldehyde (50 wt% in H_2O) and Dulbecco's Modified Eagle Medium (DMEM) were obtained from Sigma-Aldrich. Fetal bovine serum (FBS), streptomycin, penicillin, dichlorofluorescein diacetate (DCFDA) and Hoechst 33342 fluorescent stain were purchased from ThermoFisher Scientific. All chemicals were used without further purification.

9.2.2 Preparation and characterization of EGCG-loaded liposomes

The liposomal formulations used in this work are summarized in Table 9.1 . The liposomal formulation 1 (LF1) consists only of pure 1,2-dipalmitoyl-*sn*-glycero-3-phosphocholine (DPPC) phospholipids. In order to increase the stability of liposomes,[31, 33] the surfactant Tween 80 was added to DPPC, liposomal formulation 2 (LF2), in a corresponding molar ratio of 10:1 (DPPC:Tween80). As a third liposomal formulation (LF3), PEG6000 was added to the pre-formed DPPC:Tween 80 liposome vesicles to reach a DPPC:EGCG:Tween80:PEG6000 molar ratio of 10:1:1:0.1, respectively. After incubation at 54°C for 2 h, PEG chains are anchored on the surface of liposomes, which is a useful strategy to increase the *in vivo* half-life of liposomes. The PEG chains adsorbed onto liposome's surface work as a steric barrier that confers protection against the clearance by serum components and, sometimes, can further extend the drug release duration.[34, 35] All the liposomal formulations were prepared by the thin-film hydration method[36]. Briefly, EGCG was co-dissolved with DPPC, at a molar ratio of 1:10, in a chloroform: methanol (4:1) solution. Then, the organic solvents were evaporated under a stream of nitrogen, being the residual traces removed in a vacuum desiccator for 4 h in the dark. To maximize the encapsulation efficiency, the mixture was hydrated by magnesium chloride dissolved in distilled water (in a 5:1 molar ratio of magnesium/EGCG)[37], stirred at 54°C until it was dispersed and then cooled down to 25°C, resulting in a multilamellar vesicle suspension. This was followed by sonication (UP50H, Hielscher Ultrasonics, GmbH, Germany) in an ice bath, where each cycle consisted of 30 s sonication followed by a 1 minute rest. These cycles were repeated 15 times. The untrapped EGCG was then removed from DPPC liposomes by dialysis (regenerated cellulose membranes, 8–10 kDa cutoff size, Spectra/Pro, Biotech USA) at 4 °C for 48 h. The concentration of EGCG entrapped in DPPC liposomes was determined by spectrophotometry (Shimadzu UV-vis spectrometer, model UV 2101) at 274 nm. The encapsulation efficiency (EE%) and the drug loading capacity (LC%) of liposomes were calculated by the following equations 9.1 and 9.2:

$$EE\% = \frac{C_{encap}}{C_{total}} \times 100 \quad (9.1)$$

$$LC\% = \frac{C_{encap}}{C_{lipid}} \times 100 \quad (9.2)$$

where: C_{encap} is the amount of EGCG encapsulated in liposomes after dialysis, C_{total} is the amount of EGCG in liposomes before dialysis and the C_{lipid} is the total lipid concentration. The size and polydispersity index of the liposome vesicles were determined by dynamic light scattering (DLS) measurements (Zetasizer Nano ZS Malvern Instrument Ltd, UK).

9.2.3 Immobilization of liposomes onto electrospun fibers

Nanofibers were prepared using a horizontal electrospinning setup as described in ref.[38] Briefly, PCL was dissolved in glacial acetic acid at a concentration of 20 wt%. A 40 wt% aqueous gelatin solution was prepared after dissolving in distilled water (control nanofibers) or in EGCG-liposomal suspension for 12 h, at room temperature, under agitation and in dark conditions. The solutions were independently loaded in 2 mL syringes connected to 23 G blunt-tip needles, being pumped at a flow rate of 0.15 mL/h using two syringe pumps. High voltage DC power supplies were connected to the needle tips and set at 10.0 kV and 12.5 kV for PCL and gelatin solutions, respectively. The resulting nanofibers were collected on a 6 cm diameter cylindrical rotating collector covered with aluminum foil placed at a distance of 15 cm from the needle tips. Nanofibers for cell culture were produced by attaching glass coverslips (12 mm diameter) to the collector. Nanofibers were vacuum dried at room temperature and were crosslinked with 5 wt% GTA vapor in an oven at 40 °C for 5 h. The residual traces of unreacted GTA were removed by incubation in an oven at 37 °C overnight.

9.2.4 *In vitro* release of EGCG from scaffolds

Samples of PCL/gelatin membranes loaded with EGCG liposomes and weighing about 25 mg were immersed in 5 mL phosphate buffer saline (pH 7.4) under magnetic stirring at 37 °C. Aliquots of 1 mL were taken at predetermined time intervals from the release medium. Moreover, 1 mL of fresh medium was added at each sampling time to keep the release medium volume constant. The amount of EGCG was quantified at 274 nm using a Shimadzu UV-vis spectrometer. Each measurement was performed in triplicates ($n = 3$) and the results obtained are expressed as mean \pm standard deviation (S.D.). The cumulative release of each nanofiber sampling was calculated by the following equation 9.3:

$$Q\% = \frac{C_n V_0 + \sum_{i=1}^n C_{n-1} V}{M_t} \times 100 \quad (9.3)$$

where: Q is the quantity of released EGCG, C_n is the EGCG concentration measured for the n^{th} time, V_0 is the total volume of the release medium, V is the sampling volume and M_t is the total EGCG content incorporated in each membrane.

9.2.5 Scaffolds characterization

The surface morphology and size of the nanofibers were evaluated using a Zeiss Auriga scanning electron microscope (SEM). Samples were sputter-coated with iridium (Q300T D Quorum sputter coater) before analysis. ATR-FTIR spectroscopy analysis was also carried out to study the chemical modifications upon GTA crosslinking and to detect the presence of EGCG-loaded liposomes at the fibers surface. The ATR-FTIR measurements were obtained with an ATR-FTIR spectrometer Nicolet Nexus Continuum in the spectral region from 500 to 4500 cm^{-1} at a 4 cm^{-1} resolution.

9.2.6 Cell-based studies

9.2.6.1 Cell culture

Vero cells (monkey kidney epithelial cells) were used for the *in vitro* cytotoxicity assays of EGCG and of nanofibers extracts. Human fetal foreskin fibroblasts (HFFF2, European Collection of Authenticated Cell Cultures, UK), were used in cell survival assays after cell exposure to H_2O_2 or UV radiation. Cells were cultured in Dulbecco's Modified Eagle Medium (DMEM) with 10% fetal bovine serum (FBS) and streptomycin (100 $\mu\text{g}/\text{mL}$) and penicillin (100 U/ mL), in a humidified 5% CO_2 atmosphere at 37 °C (Sanyo MCO-19AIC-UV).

9.2.6.2 Cytotoxicity assay for antioxidant EGCG screening

The cytotoxicity of EGCG was evaluated following the ISO10993-5 standard test method.[39] Vero cells were seeded at a concentration of 2×10^4 cells/ cm^2 in a 96 well plate, in standard DMEM culture medium, and allowed to attach for 24 h in the incubator at 37 °C in a 5% CO_2 humidified atmosphere. Then, the medium was aspirated and replaced with fresh medium supplemented with EGCG (10 mM stock solution of EGCG was diluted with PBS) to obtain the desired EGCG concentration range of 0.1-1000 μM and cells were left exposed to this medium for 24 h and 48 h. Cells treated with DMEM containing 10% DMSO were used as positive control. Resazurin dye test was used to assess the viability of cells following treatment with EGCG solutions. Resazurin is a non-toxic and stable dye that

is converted into resorufin due to cellular energy metabolism, leading to a color change from blue to pink.[40] Cells were incubated with DMEM containing 10% v/v of the stock solution of resazurin (0.2 mg/mL in PBS) for 3 h. Subsequently, the absorbance was read at 570 nm and 600 nm on ELX800UV microplate reader (Biotek Instruments, E.U.A.). The absorbance values of the samples were normalized to control absorbance (Vero cells grown in DMEM medium).

9.2.6.3 Cytotoxicity assay for scaffolds

The cytotoxicity of the electrospun nanofibers was also evaluated following the ISO10993-5 standard.[39] The extraction media were prepared by immersing each scaffold (total weight ~ 25 mg per mL) in serum-free DMEM at 37 °C for 24 h. The Vero cells were seeded at a concentration of $2 \times 10^4/\text{cm}^2$ in a 96 well plate, in standard DMEM, and allowed to attach for 24 h prior to the addition of extraction media. Afterwards, cells were incubated with extraction media for 24 and 72 h, being their viability determined with the resazurin dye test. Vero cells cultured with DMEM were used as control.

9.2.6.4 Cell attachment on scaffolds

Scaffolds for cell seeding were firstly immersed in 0.1 M glycine aqueous solution to block unreacted aldehyde groups introduced by GTA crosslinking and further washed twice with PBS solution. Afterwards, the scaffolds (electrospun nanofibers covered glass coverslips) were transferred to home-made Teflon[®] supports[22], which have a surface area of 0.5 cm^2 for cell adhesion. A density of 2×10^4 HFFF2 cells/ cm^2 were seeded onto scaffolds and maintained in the incubator at 37 °C in a 5% CO₂ humidified atmosphere for 7 days. At days 3 and 5, cells were fixed with 3.7% paraformaldehyde in PBS overnight, washed twice with ultrapure water for visualization of cell morphology by SEM microscopy.

9.2.6.5 Antioxidant property of extracts from nanofibers against intracellular ROS production

The antioxidant activity of the scaffolds against intracellular ROS production was indirectly determined by DCFDA fluorescence-based assay[41, 42]. HFFF2 fibroblasts were seeded in a 96 well culture plate (density of $2 \times 10^4/\text{cm}^2$) and, after 1 day of culture, they were treated with the nanofibers' extracts diluted in DMEM (1:1, 1:2 and 1:4 v/v) for 24 h. Then, the oxidative stress was induced by exposure of HFFF2 cells to 50 μM H₂O₂ in PBS for 30 min. Next, for indirect intracellular ROS quantification, cells were incubated with the DCFDA dye (10 μM in PBS)

for 30 min, at 37 °C in dark, and the fluorescence was measured at $\lambda_{\text{excitation}} = 480$ nm and $\lambda_{\text{emission}} = 530$ nm on a Synergy H1 microplate reader (Biotek Instruments, E.U.A.). For fluorescence microscopy studies, the HFFF2 cells were seeded on glass coverslips (density of $2 \times 10^4/\text{cm}^2$) and incubated with the nanofibers' extracts for 24 h. Then, cells were exposed to 50 μM H_2O_2 in PBS for 30 min. Afterwards, cells were washed with PBS and incubated with DCFDA dye (1.5 μM in PBS) at 37 °C for 10 min. Cells were washed twice with PBS, nuclei stained with Hoechst 33342 dye (2 μM in PBS) and fixed with 3.4% paraformaldehyde for 15 min. The fluorescence imaging was done on epi-fluorescence microscope Nikon Ti-S and the images were analyzed using the software ImageJ.

9.2.6.6 Antioxidant property of nanofibers against ROS induced by H_2O_2 and UV radiation

The antioxidant and cytoprotective properties of the scaffolds were also evaluated after generating *in vitro* oxidative stress, by incubating HFFF2 cells with an H_2O_2 solution or by exposing cells to UV radiation. In both experiments, a density of 2×10^4 HFFF2 cells/ cm^2 were seeded onto scaffolds and the cells were allowed to attach for 48 h. After this period, the cells were exposed to 50 μM H_2O_2 for 1 h to induce ROS production. In UV irradiation experiments, DMEM was replaced by PBS and the cells were exposed to 220–280 nm radiation from a UVC lamp at a radiance dose of 2 and 8 J/cm^2 . After treatment with H_2O_2 or UV exposure, cells were cultured with fresh DMEM and incubated with resazurin to assess cell viability after 4, 24 and 72 h. HFFF2 cells not exposed to H_2O_2 nor UVC radiation were used as control.

9.2.6.7 Statistical Analysis

All the experiments were performed in triplicates and all the results are expressed as mean \pm standard deviation of the mean. Microscopy images were analyzed using the software ImageJ.[43] The statistical differences were analyzed by one or two-way ANOVA followed by Turkey's post-hoc analyses using GraphPad Prism (version 5.0).[44] *P* values lower than 0.05 (*), 0.01 (**), and 0.001 (***) indicates that differences are statistically significant.

9.2.7 Results

9.2.7.1 Cytotoxic activity of EGCG

To screen the in vitro concentration responsible for the antioxidant and prooxidant behavior of EGCG, Vero cells were exposed to a wide range of EGCG concentrations (0.1-1000 μM) for 24 and 48h. The dose-response curve shows that 200 μM was the highest EGCG non-toxic concentration for Vero cell metabolism (Figure 9.1). The LD50 values represent the concentration that causes 50% of cell death and, in this study, the LD50 values were approximately 800-1000 μM for 24 h treatment. Furthermore, a marked enhancement of EGCG cytotoxicity occurred after a prolonged in vitro exposure of Vero cells to high EGCG concentrations (400-1000 μM), probably related to inherent instability of EGCG in culture medium, which generates many secondary metabolites that decrease cell proliferation and, ultimately, may cause cell death.[45, 46]

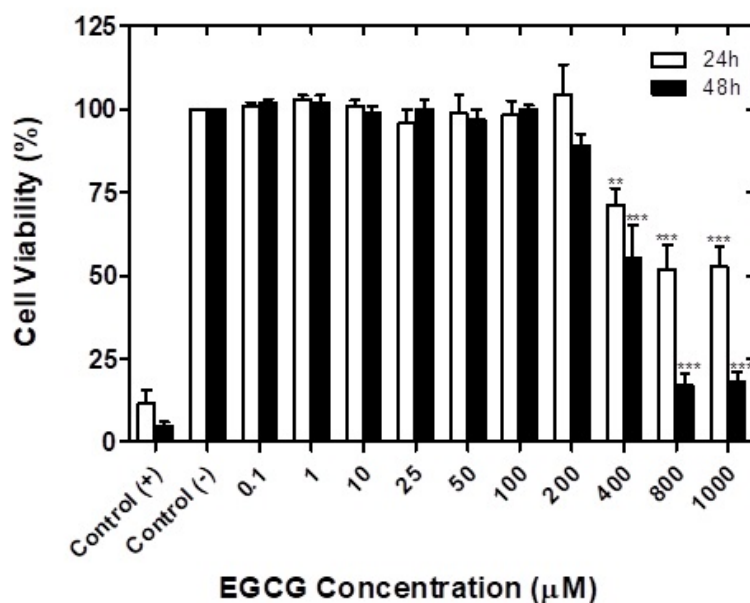


Figure 9.1: Dose-dependent cytotoxic effects of EGCG in Vero cells. The cytotoxicity of EGCG was evaluated following the ISO10993-5 standard test method using cells cultured with DMEM and DMEM+10% DMSO (toxic) as negative and positive control, respectively. Values are presented as the mean \pm SD of three independent experiments. Statistical analysis was performed by repeated measures two-way ANOVA followed by Tukey's Multiple Comparison Test and ** $p < 0.01$ and *** $p < 0.001$ indicates significance in relation to negative control.

9.2.7.2 Characterization of liposomes

In this study, three different liposome drug delivery systems were developed to avoid EGCG degradation and, at the same time, to control its release to the cell culture medium. Theoretically, in this way, EGCG secondary metabolite formation rate is slowed down and the antioxidant activity of EGCG is increased. Table 9.1 shows that all the different liposomal formulations have high encapsulation efficiencies. The liposome formulations F1, F2 and F3 had encapsulation efficiencies of 90.6 ± 2.8 , 80.1 ± 2.1 and 82.4 ± 1.9 and loading capacities of 24.8 ± 1.6 , 9.3 ± 0.4 and 10.9 ± 0.2 , respectively. Regarding the liposome size, the experimental results showed that the mean particle diameter of F1, F2 and F3 liposomes were 221 ± 21 nm, 97 ± 13 nm and 114 ± 22 nm, respectively, with polydispersity indices below 0.4 for all the formulations. These findings show that the insertion of Tween 80 in the liposomal formulation decreased around 10% the EGCG encapsulation efficiency and drastically decreased the size of liposomes by two-fold. Tween 80 monomers have affinity to the DPPC hydrocarbon tail but also to the liposome surface. The presence of a large amount of the Tween 80 molecules at the outer surface of liposome is sufficient to increase the degree of liposome curvature, that consequently imply a decrease in particle size (turbidity of liposomal solution decreased substantially).[47] The decrease in encapsulation efficiency of EGCG was possibly caused by the accommodation of Tween 80 molecules into the liposomes, which can lead to some liposomal bilayer's destruction. Moreover, the unsaturated alkyl chain of the Tween 80 molecules can loosen the packing of the hydrocarbon tails of DPPC and thus increase the permeability of liposomes.[48, 49] Additionally, the increase in F3 liposome size confirmed the presence of PEG coating on the liposomes.

Table 9.1: Composition of liposomal formulations adsorbed on PCL / gelatin nanofibers.

Liposomal Formulation	Lipid Composition	Molar Ratio	Size (nm)	Encapsulation Efficiency (%)	Loading Capacity (%)
F1	DPPC:EGCG	10:1	221±21	90.6±2.8	24.8±1.6
F2	DPPC:EGCG: T80	10:1:1	97±13	80.1±2.1	9.3±0.4
F3	DPPC:EGCG: T80:PEG	10:1:1:0.1	114±22	82.4±1.9	10.9±0.2

9.2.7.3 Fiber morphology of EGCG-containing PCL nanofibers

The morphology of the electrospun nanofibers, before and after the GTA crosslinking process, is shown in Figure 9.2. The SEM images show that randomly oriented and bead-free nanofibers assembled in highly porous mats were obtained for all tested conditions. The addition of EGCG-loaded liposomes seems to slightly increase the average diameter of the nanofibers, which were 398 ± 80 nm for PCL/gelatin, 415 ± 70 nm for PCL/EGCG, 491 ± 196 nm PCL/EGCG/T80 and 427 ± 50 nm for PCL/EGCG/PEG, respectively (Table 9.2). After GTA crosslinking, the average diameter of the nanofibers was 459 ± 60 nm for PCL/gelatin, 477 ± 220 nm for PCL/EGCG, 672 ± 240 nm PCL/EGCG/T80 and 539 ± 110 nm for PCL/EGCG/PEG, respectively. EGCG contains several hydroxyl groups attached to its phenol rings that display a tendency for hydrogen bond formation with gelatin, which might increase the gelatin solution viscosity, thereby raising the nanofiber diameter.[50, 51] The changes in nanofiber mean diameter suggest that EGCG-loaded liposomes are present and attached to nanofiber surface. Regarding the effect of GTA vapor crosslinking process on nanofiber morphology, it can be seen that this treatment did not appreciably change the morphology of PCL/gelatin membranes. In this work, GTA crosslinking process was used not only to stabilize gelatin and avoid its dissolution but also as a means to immobilize EGCG-loaded liposomes on the scaffolds, since the amino groups of DPPC liposomes react with the aldehyde groups of GTA molecules. Hence, this interaction between GTA and DPPC molecules caused some morphological change in PCL/EGCG and PCL/EGCG/T80 membranes (Figure 2). However, this change was not so evident in membranes containing PEG, because the shielding layer of PEG hindered the attack of GTA molecules to amino groups of DPPC.

Table 9.2: Average nanofiber diameter before and after GTA vapor crosslinking.

Nanofiber Formulation	Before Crosslinking	After Crosslinking
PCL/gelatin	398 ± 80	459 ± 60
PCL/EGCG	415 ± 70	477 ± 220
PCL/EGCG/T80	491 ± 196	672 ± 240
PCL/EGCG/PEG	427 ± 50	539 ± 110

Additionally, the SEM images of PCL/gelatin nanofibers containing liposomes did not show any liposomes possibly because (1) the weight ratio liposome/gelatin is low and the liposomes may not be in the focus field-of-view and (2) the blend electrospinning methodology used to prepare the nanofibers may have disrupted the integrity of the liposomes giving rise to phospholipid bilayers instead

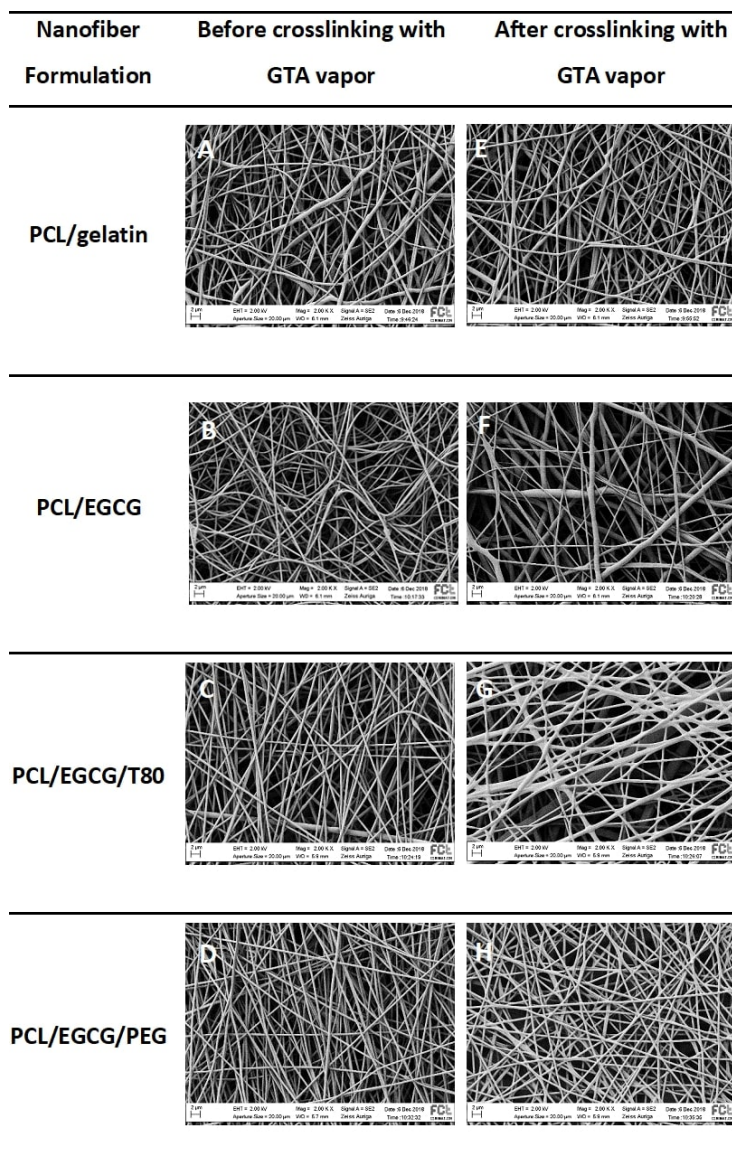


Figure 9.2: SEM images showing the morphology of PCL+GEL nanofibers containing liposomal formulations with EGCG, EGCG+T80 and EGCG+T80+PEG before (A, B, C, D) and after (E, F, G, H) GTA crosslinking. This process did not significantly change the nanofibers morphology, which remained randomly oriented, bead-free and arranged in a highly porous structure. X2000 magnification, scale bar 2 μm .

of spherical liposome-structures. The rupture and transformation of liposomes into phospholipid bilayers influences the rate of EGCG release from nanofibers, but still a good antioxidant activity of these nanofibers is expected.

9.2.7.4 EGCG immobilization on PCL nanofibers: ATR-FTIR analysis

ATR-FTIR spectroscopy was used to confirm the reaction of GTA with the amino groups of gelatin and DPPC. The ATR-FTIR spectrum for PCL/gelatin nanofibers is shown in Figure 9.3. The typical characteristic bands of PCL are observed at 2942 cm^{-1} , 2863 cm^{-1} , 1722 cm^{-1} , 1294 cm^{-1} and 1240 cm^{-1} due to asymmetric CH_2 stretching, symmetric CH_2 stretching, $\text{C}=\text{O}$ stretching, $\text{C}-\text{C}$ stretching and asymmetric $\text{C}-\text{O}-\text{C}$ stretching, respectively. Additionally, characteristic bands of gelatin are centered at 3300 cm^{-1} , 1651 cm^{-1} , 1538 cm^{-1} and 1240 cm^{-1} , which are attributed to NH stretching, amide I ($\text{C}=\text{O}$ stretching) and amides II and III (both originating from CN stretching and NH bending vibrations), respectively. Regarding the crosslinking process, the intensity ratio ($1651\text{ cm}^{-1}/1538\text{ cm}^{-1}$) increased from 1.1 to 1.5 due to the formation of Schiff bases (aldimine linkages) showing the efficiency of GTA vapor process in hardening the gelatin fibers. The increase of the relative peak intensity at 1722 cm^{-1} is correlated with the presence of unreacted aldehyde groups, thus increasing the carbonyl content in the samples.

The GTA vapor process may also crosslink the DPPC liposomes amino groups, improving their adsorption onto the PCL/gelatin nanofibers as well as the EGCG release profile from the fibers. The DPPC liposomes[52] exhibited characteristic peaks at 2920 cm^{-1} , 1730 cm^{-1} , 1220 cm^{-1} and 1080 cm^{-1} assigned to asymmetric CH_2 hydrocarbon stretching, $\text{C}=\text{O}$ stretching, asymmetric and symmetric $\text{P}=\text{O}$ stretching, respectively, having the major bands in the fingerprinting region of PCL. Moreover, typical EGCG peaks[32] were located around 3360 cm^{-1} (phenyl OH stretching), 1695 cm^{-1} ($\text{C}=\text{O}$ gallic acid stretching), 1519 cm^{-1} ($\text{C}=\text{C}$ stretching) and 1016 cm^{-1} (CH stretching of aromatic rings). The ATR-FTIR spectra of PCL/gelatin fibers containing EGCG-loaded liposomes were very similar and indistinguishable from control sample (PCL/gelatin fibers), firstly because only a small number of liposomes were incorporated onto these fibers (much smaller intensity), and secondly, given the overlap of the DPPC absorption bands with the main bands of PCL/gelatin.

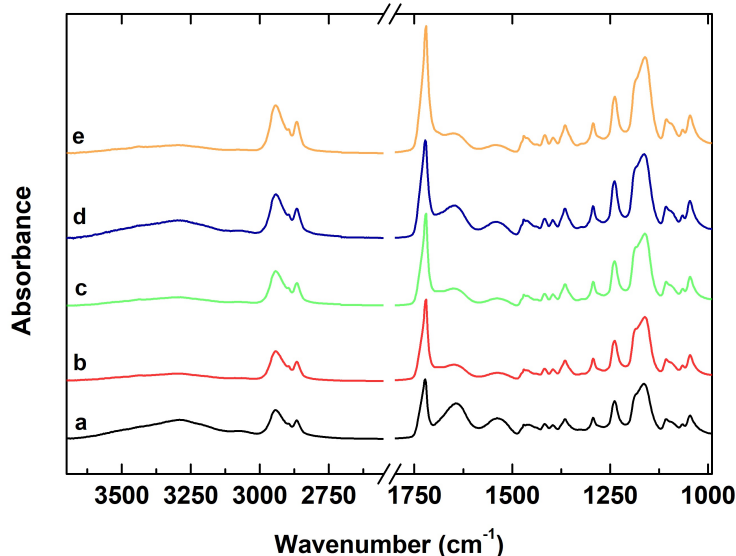


Figure 9.3: ATR-FTIR spectra of the PCL/gelatin nanofibers before (a) and after (b) GTA crosslinking process. ATR-FTIR spectra of the PCL/gelatin nanofibers containing the F1 (c), F2 (d) and F3 (e) liposomal formulation after GTA crosslinking process.

9.2.7.5 EGCG release from liposomes immobilized on PCL nanofibers

The *in vitro* release profiles of EGCG, obtained from the different liposomal formulations immobilized on PCL/gelatin nanofibers, is shown in Figure 9.4. Despite the improvements carried out in optimization of liposome design, namely the addition of PEG and Tween 80, these did not prevent the initial burst release of EGCG. Release profiles show that all the liposomal formulations are characterized by an initial burst during the first hour, releasing on average 30% of their EGCG cargo, followed by a more sustained release of the encapsulated EGCG. In addition, it can be observed that the coating of liposomes with PEG results in a faster release rate and higher total amounts of EGCG released than for conventional DPPC+EGCG liposomes. Indeed, this phenomenon has also been reported by other authors, showing that PEGylation increases the liposome stability and plasma circulation time, but also affects the bilayer fluidity in the water interfacial region, which in turn, may influence the drug release kinetics.[53, 54, 55] According to previous studies, EGCG binds to phosphate and choline groups of lipid at the interface.[56] At the same time, it is also known that the PEG polymer chains are tethered to lipids at the air-water interface[57, 58] which, in turn, is likely to weaken part of the hydrogen bonds between EGCG and DPPC in this region. So, the addition of PEG can interfere with hydrogen bond network at

the interface, which compromises the trapping efficiency of liposomes and, thus increases the burst release as well as EGCG release in the later hours.

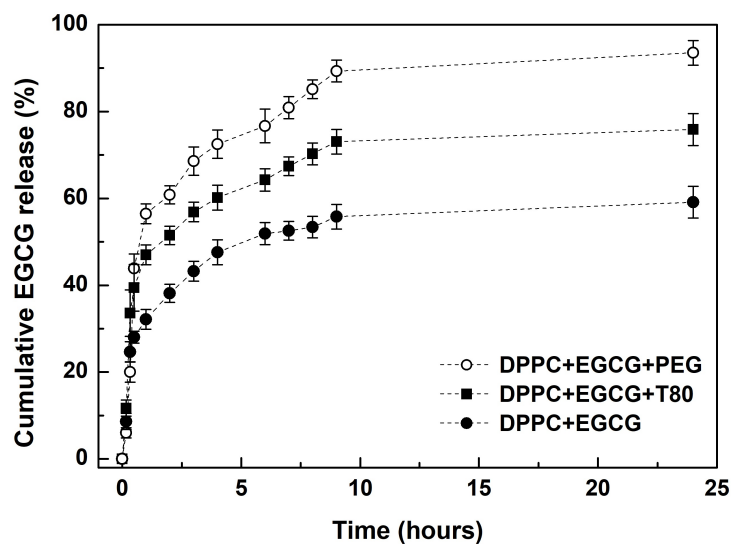


Figure 9.4: Release profiles of EGCG from each type of PCL/gelatin membranes that were immersed in PBS solution (pH = 7.4) at 37 °C. All values represent the mean \pm SD (n = 3).

9.2.7.6 Cytotoxicity test of the nanofiber's extracts

Cytotoxicity assays were performed to determine the biocompatibility of the different types of the PCL/gelatin membranes. As seen in Figure 9.5, all four types of the membranes displayed cell viabilities above 90% compared to the negative control (Table 9.3) after both 1 and 3 days of cell exposure to the extracts. Thus, none of the membranes have cytotoxic effects since the amount of EGCG released did not disturb Vero cells normal metabolism and are, therefore, suitable as substrates for cell adhesion.

9.2.7.7 Cell morphology

The changes in cell morphology in response to underlying nanofibers topography was studied by SEM microscopy. As shown in Figure 9.6, HFFF2 cells adhered to and spread along the nanofibers from day 1 to day 7. At day 3, the images suggest that HFFF2 cells on PEG-liposomes-containing membranes adhered well, grew and almost reached confluence by day 7. This finding is consistent with some

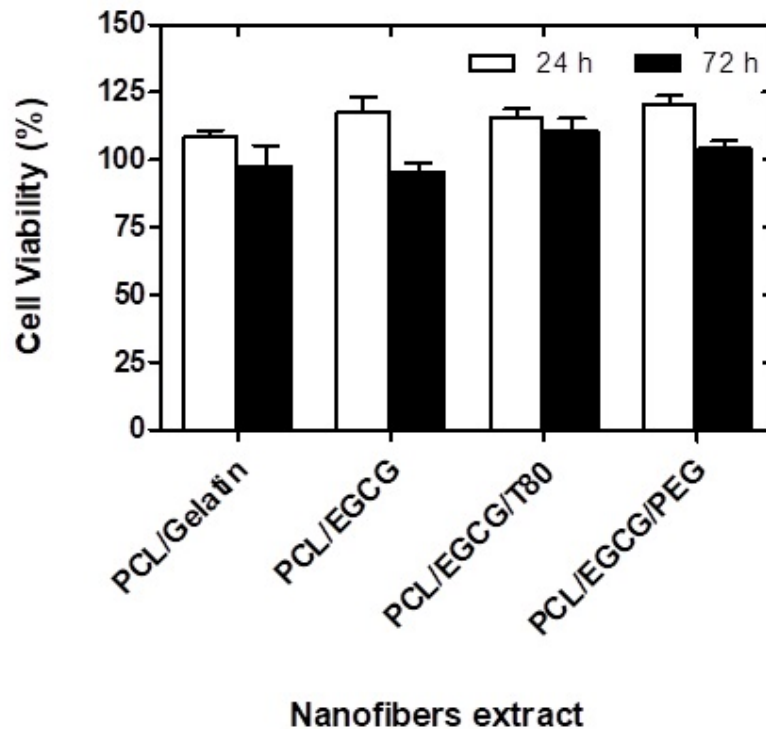


Figure 9.5: Results of the cytotoxicity test using extracts of the PCL/gelatin nanofibers containing different liposomal formulations. The Vero cells were exposed to the extracts for 24 and 72h. Cell viability was measured with the resazurin method and the results showed that all the extracts are not cytotoxic. Values are presented as the mean \pm SD of three independent experiments.

Table 9.3: VERO cells viability relative to the negative control after 1 and 3 days of culture with nanofibers-extracted media. Values are presented as the mean \pm SD of three or more independent experiments.

Nanofiber Formulation	Day 1	Day3
PCL/gelatin	108.7 \pm 2.1	97.6 \pm 7.9
PCL/EGCG	117.7 \pm 5.1	95.5 \pm 3.3
PCL/EGCG/T80	115.6 \pm 3.2	110.9 \pm 4.3
PCL/EGCG/PEG	120.5 \pm 3.3	104.1 \pm 3.1

previous studies, which found that the presence of PEG in PCL/gelatin membranes increased porosity and hydrophilicity, resulting in a significant increase in cell attachment and proliferation[59, 60, 61]. Overall, the results evidence the good biocompatibility of all membranes that provide a high surface area for cell adhesion.

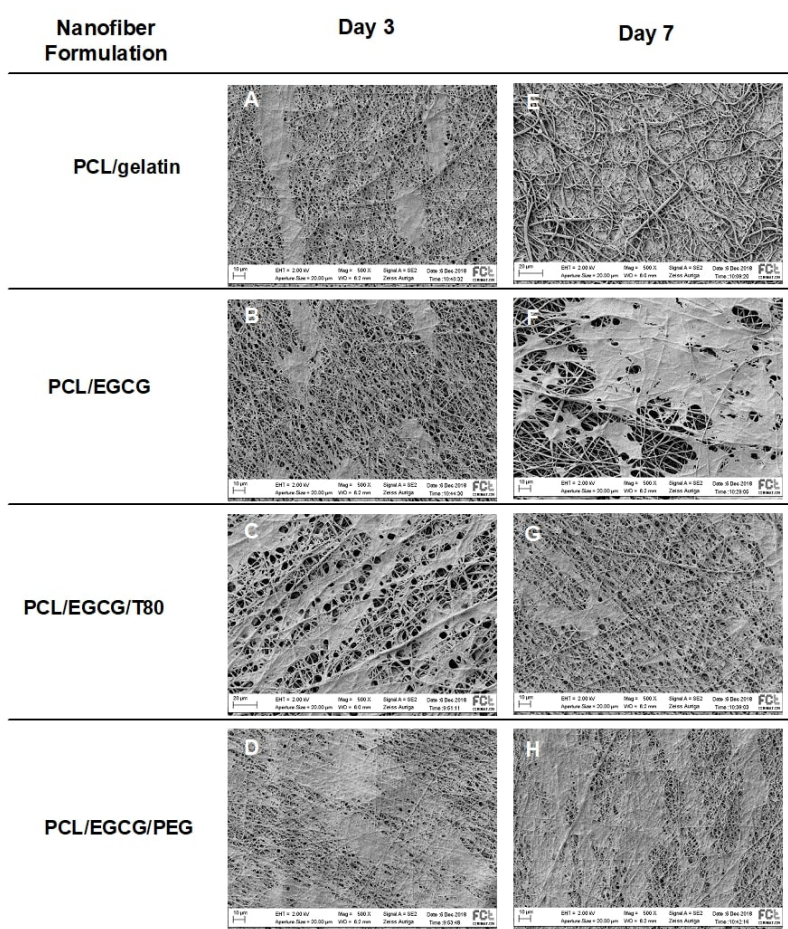


Figure 9.6: SEM micrographs of HFFF2 cells seeded over PCL/gelatin membranes containing liposomal formulations with EGCG, EGCG+T80 and EGCG+T80+PEG after 3 (A, B, C, D) and 7 (E, F, G, H) days of culture, respectively. x 500 magnification, scale bar 10 μm .

9.2.7.8 *In vitro* antioxidant effect of the nanofibers against H_2O_2

9.2.7.8.1 Cell viability after damage The antioxidant activity of each type of membrane was tested following 50 μM H_2O_2 exposure for 1 h; the results for cell survival are shown in Figure 9.7. After 4 h of H_2O_2 exposure, a significant reduction in cell viability on conventional PCL/gelatin membranes ($\sim 37\%$ of viable cells) was observed, whereas the changes in cell viability were not so drastic on EGCG-loaded PCL/gelatin membranes ($\sim 60\%$ of viable cells). Indeed, all the antioxidant functionalized nanofibers showed an improvement in cell viability, where their antioxidant efficiency was seen to be increased in the order PCL/EGCG < PCL/EGCG/T80 < PCL/EGCG/PEG. After 24 h of H_2O_2 treatment, a time sufficient for cells to metabolize H_2O_2 , the percentage of viable cells was again calculated to further elucidate if the damage caused by H_2O_2 is

too severe to be repaired or if damage was completely repaired. The viable cell population in PCL/gelatin membranes drops to $\sim 20\%$ as compared to $\sim 45\%$ in PCL/gelatin membranes containing PEG-liposomes. Indeed, a significantly higher number of viable cells ($p < 0.05$) was always observed in PCL/EGCG/T80 and PCL/EGCG/PEG membranes for each day of culture. Nonetheless, the results also showed that from day 1 to day 3 after H_2O_2 exposure, the cells continued dying regardless of EGCG presence in cell culture medium. The dose-response for H_2O_2 toxicity in eukaryotic cells is discontinuous, specifically, several studies reported that a micromolar concentration of H_2O_2 is much more severe than a millimolar concentration, because of the difference in the association of Fe^{2+} with DNA [62, 63]. So, in this study, we may suggest that the cell damage caused by $50 \mu M H_2O_2$ exposure was enough to disrupt cell membrane integrity and affect the cellular respiratory pathways, hampering the DNA repair and cell renewal. Hence, the results showed that the liposome-coated PCL/gelatin membranes continuously deliver EGCG reducing H_2O_2 -induced damage in HFFF2 cells but did not completely block the oxidant action of this compound.

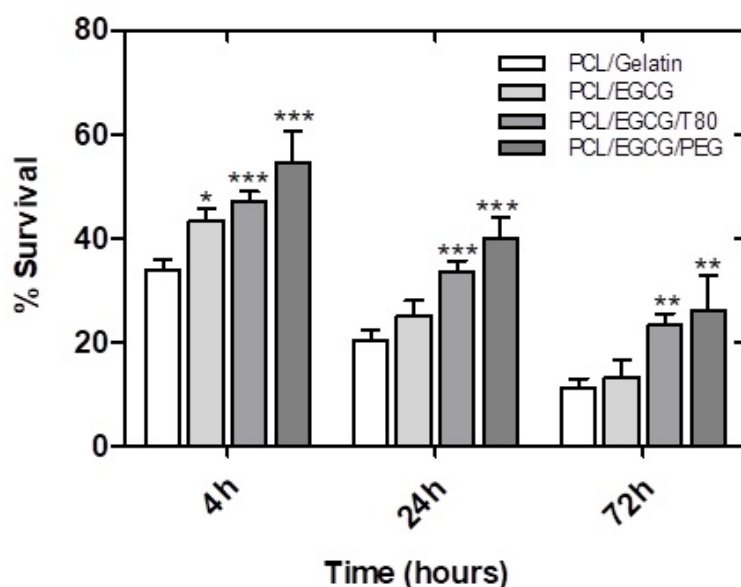


Figure 9.7: Cell viability of HFFF2 cells cultured on PCL/gelatin nanofibers containing different liposomal formulations after 4, 24 and 72 h of oxidative stress induced by $50 \mu M H_2O_2$ treatment. Values are presented as the mean \pm SD of the three independent experiments. * $p < 0.05$, ** $p < 0.01$ and *** $p < 0.001$ indicates significance in relation to conventional PCL+GEL nanofibers treated with $50 \mu M H_2O_2$.

9.2.7.8.2 Detection of intracellular ROS production According to previous results, a higher percentage of viable cells is achieved in PCL/gelatin membranes containing EGCG-loaded liposomes under stress conditions, which may be correlated with a decrease in ROS species production. We studied this correlation by using the DCFDA fluorescence assay that detects the generation of intracellular ROS in cells. H₂DCFDA is a non-fluorescent molecule that is readily cleaved to 2',7'-dichlorofluorescein (DCF, a fluorescent molecule) by intracellular esterases or following oxidation, being used for evaluation of changes in the intracellular redox state. HFFF2 cells were exposed to 50 μ M H₂O₂ for 30 min and treated with the extracts from the unloaded and from each liposome containing PCL/gelatin nanofibers. Results are shown in Figure 9.8. After 50 μ M H₂O₂ exposure, treatment with the extracts from all the nanofibers containing EGCG caused a significantly decrease in fluorescence intensity compared to the control PCL/gelatin group, which is indicative of the potent antioxidant activity of these nanofibers against H₂O₂-induced damage (Figure 9.8).

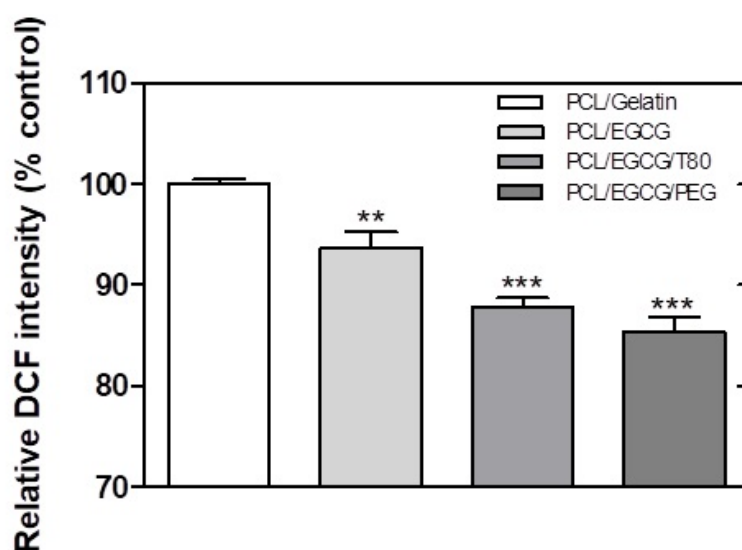


Figure 9.8: Assessment of ROS formation in HFFF2 cells following incubation with 50 μ M H₂O₂ (30min) based on the fluorescence intensity of DCFDA dye. Values are presented as the mean \pm SD of three independent experiments. ** ($p < 0.01$) and *** ($p < 0.001$) indicates significance in comparison to PCL/gelatin (control).

Fluorescence microscopy images show a strong and bright green signal in HFFF2 cells cultured with the extracts from PCL/gelatin scaffolds, associated with the enhancement of the endogenous ROS species, as can be seen in Figure 9.9. Cells treated with the extracts from EGCG-containing nanofibers displayed low

green fluorescence intensities, more specifically, the number of green fluorescent cells decreases in the order $\text{PCL/EGCG/PEG} \leq \text{PCL/EGCG/T80} < \text{PCL/EGCG}$. Also, the reduction in the observed fluorescence intensity can be directly related to radical-scavenging activity of EGCG that reduced the presence of ROS species and delayed the oxidation. These results corroborate the findings of cell viability assay (Figure 9.7, indicating that the inclusion of EGCG into PCL/gelatin nanofibers was effective in decreasing the H_2O_2 -induced overproduction of ROS in HFFF2 cells.

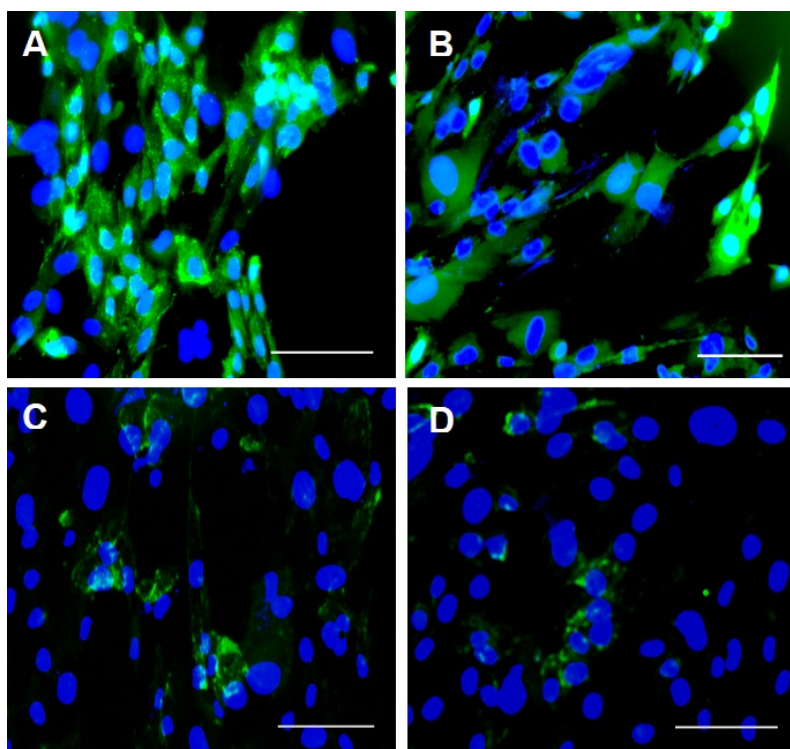


Figure 9.9: Fluorescence images of HFFF2 cells seeded on unloaded PCL/gelatin (A), PCL/EGCG (B), PCL/EGCG/T80 (C) and PCL/EGCG/PEG (D) membranes. The HFFF2 cells were stained with DCFDA (ROS sensitive dye, green color) and Hoechst (cell nuclei dye, blue color) to check formation of intracellular ROS after oxidative stress. Scale bar = 100 μM .

9.2.7.9 *In vitro* antioxidant effect against UV radiation

In UV irradiation experiments, the HFFF2 cells were exposed to two UV doses (2 and 8 J/cm^2), triggering a distinct rate of ROS generation, that allows to infer about the relationship between ROS concentration and antioxidant potential of EGCG containing nanofibers. Figure 9.10 shows that upon exposure to a low UV-dose (2 J/cm^2), the cell survival percentage was approximately 76.9%, 84.7%

and 96.1% in EGCG, EGCG+T80, EGCG+PEG formulations, respectively, contrasting with the 52.9% in the PCL/gelatin control nanofibers. According to these results, the cell survival percentages were higher in the nanofibers containing the antioxidant EGCG, being significantly different from that in PCL/gelatin control nanofibers, demonstrating that EGCG confers cell resistance and can effectively reduce the UVC induced-oxidative stress.

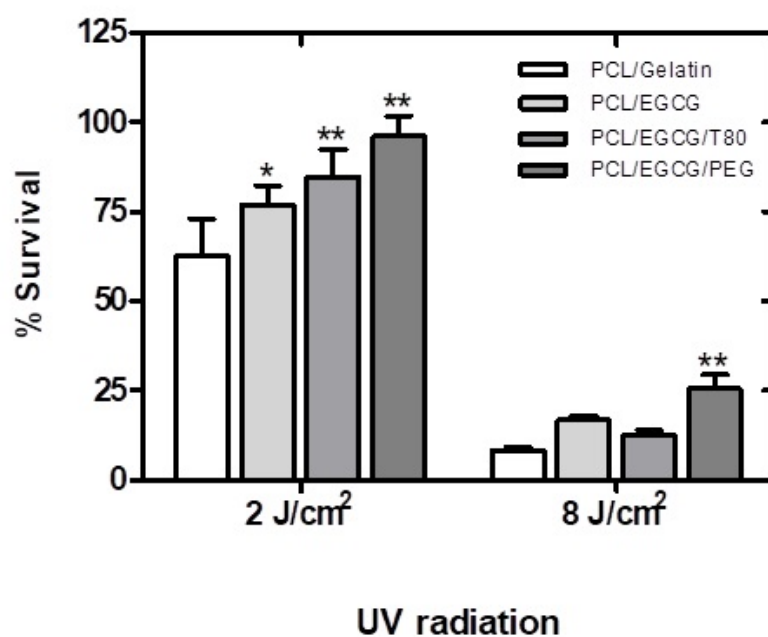


Figure 9.10: Cell viability of HFFF2 cells cultured on PCL/gelatin nanofibers containing different liposomal formulations after oxidative stress induced by UVC light exposure at a dose of 2 or 8 J/cm². Values are presented as the mean \pm SD of three independent experiments. * $p < 0.05$ and ** $p < 0.01$ indicates significance in relation to conventional PCL+GEL nanofibers exposed to UVC light.

At high-UV-dose (8 J/cm²), cell viability percentages reduced to 16.7%, 12.5%, 25.4%, contrasting with the 8.3% of the control. A higher radiation dose may impair the DNA integrity and also decline the activity of the DNA repair machinery and the cellular antioxidant defense system, leading to much lower survival percentages.[64] For instance, after the 8 J/cm² dose, the cell survival percentage in PCL/EGCG/PEG nanofibers was still significantly higher than in the control group, but is much lower (almost 4 fold) when compared to the one obtained at 2 J/cm². Therefore, these results suggest that high UV doses could photodegrade EGCG [65, 66] and the others fiber components resulting in oxidant and

toxic sub-products that may lead to additional cell damage. After UV irradiation, an increased number of ROS, matrix metalloproteinases (MMPs) and pro-inflammatory cytokines are produced contributing to the development of chronic inflammation that is the main reason for failure/delay of wound healing.[67, 68, 69] Numerous studies have incorporated natural antioxidant molecules in PCL-based scaffolds to suppress chronic inflammation and to facilitate skin re-epithelization/tissue regeneration.[70, 71, 72, 73] Curiously, in spite of the well-known anti-inflammatory and anti-bacterial properties of EGCG only a few studies immobilized this molecule into scaffolds. In a recent study, collagen scaffolds incorporating EGCG were synthesized that have ability to decrease the production of pro-inflammatory cytokines (such as IL-8, IL-1 and TNF- α) and proteolytic enzymes. Further, these scaffolds also controlled the macrophage recruitment into wounds that accelerates the tissue remodeling.[74] Regarding the photoprotective role of EGCG against UV damage, some studies showed that EGCG inhibits the UVA/UVB radiation induced-apoptosis in vitro in human HaCaT keratinocytes by preventing the activation of caspase pathway, which significantly reduces the degree of DNA fragmentation.[75, 76, 77, 78] Huang et al. also found that EGCG (1-100 μ M) treatment prior to UVA irradiation renders high cell survival rates due to a reduction in intracellular H₂O₂ production and through blockage of the ERK signalling pathway, which prevents cell matrix degradation.[79] So, there is a remarkable agreement between our results and these published studies, showing that EGCG treatment improves the ability of human fibroblasts to survive UV damage and also support the appreciation that our scaffolds can be used for skin wound healing.

9.3 Conclusion

In this study, DPPC liposomes carrying EGCG were designed to be immobilized in PCL/gelatin nanofibers mats through a blend electrospinning technique. The SEM images of PCL/gelatin nanofibers containing DPPC+EGCG liposomes did not show any intact liposomes suggesting that the blend electrospinning methodology used to prepare the nanofibers disrupts the integrity of the liposomes and leads to a premature EGCG leakage. Nevertheless, this technique successfully gave rise to PCL/gelatin nanofiber supported DPPC+EGCG phospholipid bilayers, that are highly biocompatible and have a cellular antioxidant capacity superior to that of raw PCL/gelatin nanofibers. The EGCG released from the DPPC

phospholipid bilayers immobilized at the surface of PCL+GEL nanofibers guarantees higher cell survival rates after oxidative stress induced either by H₂O₂ (induced ± 2.3 fold increase in cell survival over control within 72 h) or UV radiation (up to ± 3 fold increased in cell survival over control after high-UV-dose). Therefore, the results showed that the EGCG-containing nanofibers slows down oxidative-stress related cell damage and could be used for wound healing and skin tissue engineering. Looking ahead, the coaxial electrospinning technique may be used in future studies since it conserves the integrity of liposomes rendering a better performance of the nanofibers against oxidative damage.

9.4 Acknowledgments

The authors acknowledge the financial support from FEDER, through Programa Operacional Factores de Competitividade COMPETE and Fundação para a Ciência e a Tecnologia through research project grants, UID/FIS/00068/2013, PTDC/FIS-NAN/0909/2014, UID/CTM/50025/2013 and UID/FIS/00068/2019 and to Portugal Brazil Bilateral Project. The Conselho Nacional de Desenvolvimento Científico e Tecnológico and Fundação de Amparo à Pesquisa do Estado de São Paulo (2013/14262-7) are also acknowledged. FP acknowledges the fellowship grant PD/BD/106036/2015 from RABBIT Doctoral Programme (Portugal).

References

- [1] M. Norouzi, S. M. Boroujeni, N. Omidvarkordshouli, and M. Soleimani. “Advances in skin regeneration: application of electrospun scaffolds.” In: *Advanced Healthcare Materials* 4.8 (2015), pp. 1114–1133.
- [2] S. Q. Wang, R. Setlow, M. Berwick, D. Polsky, A. A. Marghoob, A. W. Kopf, and R. S. Bart. “Ultraviolet A and melanoma: a review.” In: *Journal of the American Academy of Dermatology* 44.5 (2001), pp. 837–846.
- [3] D. Mohania, S. Chandel, P. Kumar, V. Verma, K. Digvijay, D. Tripathi, K. Choudhury, S. K. Mitten, and D. Shah. “Ultraviolet radiations: skin defense-damage mechanism.” In: *Ultraviolet Light in Human Health, Diseases and Environment*. Springer, 2017, pp. 71–87.
- [4] L. Rittié and G. J. Fisher. “UV-light-induced signal cascades and skin aging.” In: *Ageing Research Reviews* 1.4 (2002), pp. 705–720.

- [5] G. J. Fisher, S. Kang, J. Varani, Z. Bata-Csorgo, Y. Wan, S. Datta, and J. J. Voorhees. “Mechanisms of photoaging and chronological skin aging.” In: *Archives of Dermatology* 138.11 (2002), pp. 1462–1470.
- [6] F. R. de Grujil, H. J. van Kranen, and L. H. Mullenders. “UV-induced DNA damage, repair, mutations and oncogenic pathways in skin cancer.” In: *Journal of Photochemistry and Photobiology B: Biology* 63.1-3 (2001), pp. 19–27.
- [7] G. P. Pfeifer and A. Besaratinia. “UV wavelength-dependent DNA damage and human non-melanoma and melanoma skin cancer.” In: *Photochemical & Photobiological Sciences* 11.1 (2012), pp. 90–97.
- [8] P. C. Ikwegbue, P. Masamba, L. S. Mbatha, B. E. Oyinloye, and A. P. Kappo. “Interplay between heat shock proteins, inflammation and cancer: a potential cancer therapeutic target.” In: *American Journal of Cancer Research* 9.2 (2019), pp. 242–249.
- [9] M. Schäfer and S. Werner. “Oxidative stress in normal and impaired wound repair.” In: *Pharmacological Research* 58.2 (2008), pp. 165–171.
- [10] P. G. Rodriguez, F. N. Felix, D. T. Woodley, and E. K. Shim. “The role of oxygen in wound healing: a review of the literature.” In: *Dermatologic Surgery* 34.9 (2008), pp. 1159–1169.
- [11] C. Dunnill, T. Patton, J. Brennan, J. Barrett, M. Dryden, J. Cooke, D. Leaper, and N. T. Georgopoulos. “Reactive oxygen species (ROS) and wound healing: the functional role of ROS and emerging ROS-modulating technologies for augmentation of the healing process.” In: *International Wound Journal* 14.1 (2017), pp. 89–96.
- [12] M. Sheridan, L. Shea, M. Peters, and D. Mooney. “Bioabsorbable polymer scaffolds for tissue engineering capable of sustained growth factor delivery.” In: *Journal of Controlled Release* 64.1-3 (2000), pp. 91–102.
- [13] C. Dwivedi, I. Pandey, H. Pandey, S. Patil, S. B. Mishra, A. C. Pandey, P. Zamboni, P. W. Ramteke, and A. V. Singh. “In vivo diabetic wound healing with nanofibrous scaffolds modified with gentamicin and recombinant human epidermal growth factor.” In: *Journal of Biomedical Materials Research Part A* 106.3 (2018), pp. 641–651.

- [14] M. Sattary, M. T. Khorasani, M. Rafienia, and H. S. Rozve. "Incorporation of nanohydroxyapatite and vitamin D3 into electrospun PCL/Gelatin scaffolds: The influence on the physical and chemical properties and cell behavior for bone tissue engineering." In: *Polymers for Advanced Technologies* 29.1 (2018), pp. 451–462.
- [15] P. Taepaiboon, U. Rungsardthong, and P. Supaphol. "Vitamin-loaded electrospun cellulose acetate nanofiber mats as transdermal and dermal therapeutic agents of vitamin A acid and vitamin E." In: *European Journal of Pharmaceutics and Biopharmaceutics* 67.2 (2007), pp. 387–397.
- [16] K. Kim, Y. K. Luu, C. Chang, D. Fang, B. S. Hsiao, B. Chu, and M. Hadjiargyrou. "Incorporation and controlled release of a hydrophilic antibiotic using poly (lactide-co-glycolide)-based electrospun nanofibrous scaffolds." In: *Journal of Controlled Release* 98.1 (2004), pp. 47–56.
- [17] H.-W. Kim, J. C. Knowles, and H.-E. Kim. "Porous scaffolds of gelatin-hydroxyapatite nanocomposites obtained by biomimetic approach: characterization and antibiotic drug release." In: *Journal of Biomedical Materials Research Part B: Applied Biomaterials* 74.2 (2005), pp. 686–698.
- [18] L. Chen, S. Wang, Q. Yu, P. D. Topham, C.-Z. Chen, and L. Wang. "A comprehensive review of electrospinning block copolymers." In: *Soft Matter* 15.12 (2019), pp. 2490–2510.
- [19] Y. Ding, W. Li, F. Zhang, Z. Liu, N. Zanzanizadeh Ezazi, D. Liu, and H. A. Santos. "Electrospun Fibrous Architectures for Drug Delivery, Tissue Engineering and Cancer Therapy." In: *Advanced Functional Materials* 29.2 (2019), pp. 1802852–1802887.
- [20] Y. Zhang, H. Ouyang, C. T. Lim, S. Ramakrishna, and Z.-M. Huang. "Electrospinning of gelatin fibers and gelatin/PCL composite fibrous scaffolds." In: *Journal of Biomedical Materials Research Part B: Applied Biomaterials*. 72.1 (2005), pp. 156–165.
- [21] S. Gautam, C.-F. Chou, A. K. Dinda, P. D. Potdar, and N. C. Mishra. "Surface modification of nanofibrous polycaprolactone/gelatin composite scaffold by collagen type I grafting for skin tissue engineering." In: *Materials Science and Engineering: C* 34 (2014), pp. 402–409.
- [22] S. Gomes, G. Rodrigues, G. Martins, C. Henriques, and J. C. Silva. "Evaluation of nanofibrous scaffolds obtained from blends of chitosan, gelatin and polycaprolactone for skin tissue engineering." In: *International Journal of Biological Macromolecules* 102 (2017), pp. 1174–1185.

- [23] P. Zadehnajar, B. Akbari, S. Karbasi, and M. H. Mirmusavi. "Preparation and characterization of poly ϵ -caprolactone-gelatin/multi-walled carbon nanotubes electrospun scaffolds for cartilage tissue engineering applications." In: *International Journal of Polymeric Materials and Polymeric Biomaterials* (2019), pp. 1–12.
- [24] R. Ramalingam, C. Dhand, C. M. Leung, H. Ezhilarasu, P. Prasannan, S. T. Ong, S. Subramanian, M. Kamruddin, R. Lakshminarayanan, and S. Ramakrishna. "Poly- ϵ -Caprolactone/Gelatin Hybrid Electrospun Composite Nanofibrous Mats Containing Ultrasound Assisted Herbal Extract: Antimicrobial and Cell Proliferation Study." In: *Nanomaterials* 9.3 (2019), pp. 462–483.
- [25] T. Chinembiri, L. du Plessis, M. Gerber, J. Hamman, and J. Du Plessis. "Review of natural compounds for potential skin cancer treatment." In: *Molecules* 19.8 (2014), pp. 11679–11721.
- [26] S. Shao, L. Li, G. Yang, J. Li, C. Luo, T. Gong, and S. Zhou. "Controlled green tea polyphenols release from electrospun PCL/MWCNTs composite nanofibers." In: *International Journal of Pharmaceutics* 421.2 (2011), pp. 310–320.
- [27] Y.-J. Kim, M. R. Park, M. S. Kim, and O. H. Kwon. "Polyphenol-loaded polycaprolactone nanofibers for effective growth inhibition of human cancer cells." In: *Materials Chemistry and Physics* 133.2-3 (2012), pp. 674–680.
- [28] H.-L. Kim, J.-H. Lee, B. J. Kwon, M. H. Lee, D.-W. Han, S.-H. Hyon, and J.-C. Park. "Promotion of Full-Thickness Wound Healing Using Epigallocatechin-3-O-Gallate/Poly (Lactic-co-Glycolic Acid) Membrane as Temporary Wound Dressing." In: *Artificial Organs* 38.5 (2014), pp. 411–417.
- [29] Y. C. Shin, D.-M. Shin, E. J. Lee, J. H. Lee, J. E. Kim, S. H. Song, D.-Y. Hwang, J. J. Lee, B. Kim, and D. Lim. "Hyaluronic acid/PLGA core/shell fiber matrices loaded with EGCG beneficial to diabetic wound healing." In: *Advanced Healthcare Materials* 5.23 (2016), pp. 3035–3045.
- [30] E. J. Lee, J. H. Lee, L. Jin, O. S. Jin, Y. C. Shin, S. J. Oh, J. Lee, S.-H. Hyon, and D.-W. Han. "Hyaluronic acid/poly (lactic-co-glycolic acid) core/shell fiber meshes loaded with epigallocatechin-3-O-gallate as skin tissue engineering scaffolds." In: *Journal of Nanoscience and Nanotechnology* 14.11 (2014), pp. 8458–8463.

- [31] C. Tan, S. Xia, J. Xue, J. Xie, B. Feng, and X. Zhang. "Liposomes as vehicles for lutein: preparation, stability, liposomal membrane dynamics, and structure." In: *Journal of Agricultural and Food Chemistry* 61.34 (2013), pp. 8175–8184.
- [32] F. Pires, V. P. Geraldo, A. Antunes, A. Marletta, O. N. Oliveira Jr, and M. Raposo. "On the role of epigallocatechin-3-gallate in protecting phospholipid molecules against UV irradiation." In: *Colloids and Surfaces B: Biointerfaces* 173 (2019), pp. 312–319.
- [33] S. Xia, S. Xu, and X. Zhang. "Optimization in the preparation of coenzyme Q10 nanoliposomes." In: *Journal of Agricultural and Food Chemistry* 54.17 (2006), pp. 6358–6366.
- [34] D. Papahadjopoulos, T. M. Allen, A. Gabizon, E. Mayhew, K. Matthay, S.-K. Huang, K. D. Lee, M. C. Woodle, D. D. Lasic, and C. Redemann. "Sterically stabilized liposomes: improvements in pharmacokinetics and antitumor therapeutic efficacy." In: *Proceedings of the National Academy of Sciences* 88.24 (1991), pp. 11460–11464.
- [35] S. Zalipsky. "Synthesis of an end-group functionalized polyethylene glycol-lipid conjugate for preparation of polymer-grafted liposomes." In: *Bioconjugate Chemistry* 4.4 (1993), pp. 296–299.
- [36] A. Akbarzadeh, R. Rezaei-Sadabady, S. Davaran, S. W. Joo, N. Zarghami, Y. Hanifehpour, M. Samiei, M. Kouhi, and K. Nejati-Koshki. "Liposome: classification, preparation, and applications." In: *Nanoscale research letters* 8.102 (2013), pp. 1–9.
- [37] E. Laudadio, C. Minnelli, A. Amici, L. Massaccesi, G. Mobbili, and R. Galeazzi. "Liposomal formulations for an efficient encapsulation of epigallocatechin – 3 – gallate: An in-silico/experimental approach." In: *Molecules* 23.2 (2018), pp. 441–459.
- [38] T. Valente, J. L. Ferreira, C. Henriques, J. P. Borges, and J. C. Silva. "Polymer blending or fiber blending: A comparative study using chitosan and poly (ϵ -caprolactone) electrospun fibers." In: *Journal of Applied Polymer Science* 136.11 (2019), pp. 47191–47202.
- [39] Y. Zhou, D. Yang, X. Chen, Q. Xu, F. Lu, and J. Nie. "Electrospun water-soluble carboxyethyl chitosan/poly (vinyl alcohol) nanofibrous membrane as potential wound dressing for skin regeneration." In: *Biomacromolecules* 9.1 (2007), pp. 349–354.

- [40] E. Vega-Avila and M. K. Pugsley. “An overview of colorimetric assay methods used to assess survival or proliferation of mammalian cells.” In: *Proceedings of the Western Pharmacology Society*. Vol. 54. 2011, pp. 10–14.
- [41] H. Wang and J. A. Joseph. “Quantifying cellular oxidative stress by dichlorofluorescein assay using microplate reader.” In: *Free Radical Biology and Medicine* 27.5-6 (1999), pp. 612–616.
- [42] H. A. Rather, R. Thakore, R. Singh, D. Jhala, S. Singh, and R. Vasita. “Antioxidative study of Cerium Oxide nanoparticle functionalised PCL-Gelatin electrospun fibers for wound healing application.” In: *Bioactive Materials* 3.2 (2018), pp. 201–211.
- [43] C. A. Schneider, W. S. Rasband, and K. W. Eliceiri. “NIH Image to ImageJ: 25 years of image analysis.” In: *Nature Methods* 9.7 (2012), 671–675.
- [44] M. L. Swift. “GraphPad prism, data analysis, and scientific graphing.” In: *Journal of Chemical Information and Computer Sciences* 37.2 (1997), pp. 411–412.
- [45] J. H. Weisburg, D. B. Weissman, T. Sedaghat, and H. Babich. “In vitro cytotoxicity of epigallocatechin gallate and tea extracts to cancerous and normal cells from the human oral cavity.” In: *Basic & Clinical Pharmacology & Toxicology* 95.4 (2004), pp. 191–200.
- [46] J. H. Kim, N. J. Kang, B. K. Lee, K. W. Lee, and H. J. Lee. “Gallic acid, a metabolite of the antioxidant propyl gallate, inhibits gap junctional intercellular communication via phosphorylation of connexin 43 and extracellular – signal – regulated kinase1/2 in rat liver epithelial cells.” In: *Mutation Research/Fundamental and Molecular Mechanisms of Mutagenesis* 638.1-2 (2008), pp. 175–183.
- [47] L.-M. Tasi, D.-Z. Liu, and W.-Y. Chen. “Microcalorimetric investigation of the interaction of polysorbate surfactants with unilamellar phosphatidylcholines liposomes.” In: *Colloids and Surfaces A: Physicochemical and Engineering Aspects* 213.1 (2003), pp. 7–14.
- [48] M. El-Samaligy, N. Afifi, and E. Mahmoud. “Increasing bioavailability of silymarin using a buccal liposomal delivery system: preparation and experimental design investigation.” In: *International Journal of Pharmaceutics* 308.1-2 (2006), pp. 140–148.
- [49] G. Abdelbary and N. El-gendy. “Niosome-encapsulated gentamicin for ophthalmic controlled delivery.” In: *Journal of the American Association of Pharmaceutical Scientists* 9.3 (2008), pp. 740–747.

- [50] H.-Y. Huang, M.-C. Wang, Z.-Y. Chen, W.-Y. Chiu, K.-H. Chen, I.-C. Lin, W.-C. V. Yang, C.-C. Wu, and C.-L. Tseng. “Gelatin–epigallocatechin gallate nanoparticles with hyaluronic acid decoration as eye drops can treat rabbit dry-eye syndrome effectively via inflammatory relief.” In: *International Journal of Nanomedicine* 13 (2018), pp. 7251–7273.
- [51] H. Liu, Z. Jiao, and S. Guo. “Effect of epigallocatechin gallate on the properties of gelatin.” In: *International Journal of Food Properties* 17.10 (2014), pp. 2119–2130.
- [52] F. Pires, V. P. Geraldo, B. Rodrigues, A. d. Granada-Flor, R. F. de Almeida, O. N. Oliveira, B. L. Victor, M. Machuqueiro, and M. Raposo. “Evaluation of EGCG loading capacity in DMPC membranes.” In: *Langmuir* 20 (2019), pp. 6771–6781.
- [53] K. Hashizaki, H. Taguchi, C. Itoh, H. Sakai, M. Abe, Y. Saito, and N. Ogawa. “Effects of poly (ethylene glycol)(PEG) concentration on the permeability of PEG-grafted liposomes.” In: *Chemical and Pharmaceutical Bulletin* 53.1 (2005), pp. 27–31.
- [54] V. Reshetov, D. Kachatkou, T. Shmigol, V. Zorin, M.-A. D’Hallewin, F. Guillemin, and L. Bezdetnaya. “Redistribution of meta-tetra (hydroxyphenyl) chlorin (m-THPC) from conventional and PEGylated liposomes to biological substrates.” In: *Photochemical & Photobiological Sciences* 10.6 (2011), pp. 911–919.
- [55] S. Holzschuh, K. Kaeß, G. V. Bossa, C. Decker, A. Fahr, and S. May. “Investigations of the influence of liposome composition on vesicle stability and drug transfer in human plasma: a transfer study.” In: *Journal of Liposome Research* 28.1 (2018), pp. 22–34.
- [56] F. Pires, V. P. Geraldo, A. Antunes, A. Marletta, O. N. Oliveira Jr, and M. Raposo. “Effect of blue light irradiation on the stability of phospholipid molecules in the presence of epigallocatechin-3-gallate.” In: *Colloids Surf B* 177 (2019), pp. 50–57.
- [57] M Winterhalter, H Bürner, S Marzinka, R Benz, and J. Kasianowicz. “Interaction of poly (ethylene-glycols) with air-water interfaces and lipid monolayers: investigations on surface pressure and surface potential.” In: *Biophysical Journal* 69.4 (1995), pp. 1372–1381.

- [58] C. Decker, H. Schubert, S. May, and A. Fahr. "Pharmacokinetics of temoporfin – loaded liposome formulations: correlation of liposome and temoporfin blood concentration." In: *Journal of Controlled Release* 166.3 (2013), pp. 277–285.
- [59] N. Bhattarai, D. Edmondson, O. Veisoh, F. A. Matsen, and M. Zhang. "Electrospun chitosan-based nanofibers and their cellular compatibility." In: *Biomaterials* 26.31 (2005), pp. 6176–6184.
- [60] H. T. Bui, O. H. Chung, J. D. Cruz, and J. S. Park. "Fabrication and characterization of electrospun curcumin-loaded polycaprolactone-polyethylene glycol nanofibers for enhanced wound healing." In: *Macromolecular Research* 22.12 (2014), pp. 1288–1296.
- [61] R. Scaffaro, F. Lopresti, A. Maio, L. Botta, S. Rigogliuso, and G. Gherzi. "Electrospun PCL/GO – g – PEG structures: Processing – morphology – properties relationships." In: *Composites Part A: Applied Science and Manufacturing* 92 (2017), pp. 97–107.
- [62] E. S. Henle, Z. Han, N. Tang, P. Rai, Y. Luo, and S. Linn. "Sequence-specific DNA cleavage by Fe²⁺-mediated fenton reactions has possible biological implications." In: *Journal of Biological Chemistry* 274.2 (1999), pp. 962–971.
- [63] J. Nakamura, E. R. Purvis, and J. A. Swenberg. "Micromolar concentrations of hydrogen peroxide induce oxidative DNA lesions more efficiently than millimolar concentrations in mammalian cells." In: *Nucleic Acids Research* 31.6 (2003), pp. 1790–1795.
- [64] Y. Shindo, E. Witt, D. Han, and L. Packer. "Dose-response effects of acute ultraviolet irradiation on antioxidants and molecular markers of oxidation in murine epidermis and dermis." In: *Journal of Investigative Dermatology* 102.4 (1994), pp. 470–475.
- [65] A. Bianchi, N. Marchetti, and S. Scalia. "Photodegradation of (-)- epigallocatechin –3–gallate in topical cream formulations and its photostabilization." In: *Journal of Pharmaceutical and Biomedical Analysis* 56.4 (2011), pp. 692–697.
- [66] S. Scalia, N. Marchetti, and A. Bianchi. "Comparative evaluation of different co-antioxidants on the photochemical-and functional-stability of epigallocatechin-3-gallate in topical creams exposed to simulated sunlight." In: *Molecules* 18.1 (2013), pp. 574–587.

- [67] G. J. Fisher, Z. Wang, S. C. Datta, J. Varani, S. Kang, and J. J. Voorhees. "Pathophysiology of premature skin aging induced by ultraviolet light." In: *New England Journal of Medicine* 337.20 (1997), pp. 1419–1429.
- [68] N. B. Menke, K. R. Ward, T. M. Witten, D. G. Bonchev, and R. F. Diegelmann. "Impaired wound healing." In: *Clinics in Dermatology* 25.1 (2007), pp. 19–25.
- [69] S Schreml, R. Szeimies, L Prantl, S Karrer, M Landthaler, and P Babilas. "Oxygen in acute and chronic wound healing." In: *British Journal of Dermatology* 163.2 (2010), pp. 257–268.
- [70] S Suganya, J Venugopal, S. A. Mary, S Ramakrishna, B. Lakshmi, and V. G. Dev. "Aloe vera incorporated biomimetic nanofibrous scaffold: a regenerative approach for skin tissue engineering." In: *Iranian Polymer Journal* 23.3 (2014), pp. 237–248.
- [71] N. Fereydouni, M. Darroudi, J. Movaffagh, A. Shahroodi, A. E. Butler, S. Ganjali, and A. Sahebkar. "Curcumin nanofibers for the purpose of wound healing." In: *Journal of Cellular Physiology* 234.5 (2019), pp. 5537–5554.
- [72] S. Zahid, H. Khalid, F. Ikram, H. Iqbal, M. Samie, L. Shahzadi, A. T. Shah, M. Yar, A. A. Chaudhry, and S. J. Awan. "Bi-layered α -tocopherol acetate loaded membranes for potential wound healing and skin regeneration." In: *Materials Science and Engineering: C* (2019), pp. 438–447.
- [73] G. Ajmal, G. V. Bonde, S. Thokala, P. Mittal, G. Khan, J. Singh, V. K. Pandey, and B. Mishra. "Ciprofloxacin HCl and quercetin functionalized electrospun nanofiber membrane: fabrication and its evaluation in full thickness wound healing." In: *Artificial cells, Nanomedicine, and Biotechnology* 47.1 (2019), pp. 228–240.
- [74] C. Chu, L. Liu, Y. Wang, R. Yang, C. Hu, S. Rung, Y. Man, and Y. Qu. "Evaluation of epigallocatechin-3-gallate (EGCG)-modified scaffold determines macrophage recruitment." In: *Materials Science and Engineering: C* (2019), pp. 505–513.
- [75] H. Kondo, S.-H. Park, K. Watanabe, Y. Yamamoto, and M. Akashi. "Polyphenol (-)-epigallocatechin gallate inhibits apoptosis induced by irradiation in human HaCaT keratinocytes." In: *Biochemical and Biophysical Research Communications* 316.1 (2004), pp. 59–64.

- [76] C. D. Mnich, K. S. Hoek, L. V. Virkki, A. Farkas, C. Dudli, E. Laine, M. Urošević, and R. Dummer. “Green tea extract reduces induction of p53 and apoptosis in UVB-irradiated human skin independent of transcriptional controls.” In: *Experimental Dermatology* 18.1 (2009), pp. 69–77.
- [77] J. H. Chung, J. H. Han, E. J. Hwang, J. Y. Seo, K. H. Cho, K. H. Kim, J. I. Youn, and H. C. Eun. “Dual mechanisms of green tea extract (EGCG)-induced cell survival in human epidermal keratinocytes.” In: *The FASEB Journal* 17.13 (2003), pp. 1913–1915.
- [78] S. K. Katiyar, F. Afaq, A. Perez, and H. Mukhtar. “Green tea polyphenol (–)-epigallocatechin-3-gallate treatment of human skin inhibits ultraviolet radiation-induced oxidative stress.” In: *Carcinogenesis* 22.2 (2001), pp. 287–294.
- [79] C.-C. Huang, J.-Y. Fang, W.-B. Wu, H.-S. Chiang, Y.-J. Wei, and C.-F. Hung. “Protective effects of (–)-epicatechin-3-gallate on UVA-induced damage in HaCaT keratinocytes.” In: *Archives of Dermatological Research* 296.10 (2005), pp. 473–481.

CONCLUDING REMARKS

In this section one intends to summarize the main conclusions of this doctoral thesis.¹

This work thesis focused on the development of a liposome-based carrier for topical/transdermal delivery of EGCG, firstly, to overcome the issue of poor bioavailability of EGCG and, secondly, to offer an adequate skin protection against oxidative stress induced either by blue or UV radiation. Although it was common knowledge the antioxidant/radical scavenging activity of EGCG, the molecular mechanisms underlying its mode of action in cell membrane are not fully understood. Understanding these molecular interactions can reveal the localization of EGCG on cell membrane and lead to a better understanding of the antioxidant action of EGCG, through the analysis of correlation between the structural changes in membrane caused by EGCG and the resistance to radiation damage. Considering this and, to the best of our knowledge, here are encompassed the first Langmuir studies performed to identify the molecular interactions between EGCG and different lipidic monolayers, and as to determine how blue radiation affects these interactions and therefore compromises the monolayer integrity.

Concerning the molecular interactions of EGCG with DPPG monolayer in different molar ratios at the air–water interface, Chapter 5, it was observed that as the amount of EGCG was increased, the surface pressure–area isotherms significantly shifted to lower areas in relation to DPPG monolayer, indicating a

¹The introductory Chapters 1, 2, 3 and the experimental Chapter 4 are excluded from the discussion, because they do not contain new experimental findings.

condensation of the monolayer triggered by EGCG. Furthermore, the accommodation of EGCG in lipidic monolayer induced conformational changes in DPPG headgroups, in particular, significantly reduced the hydration status of phosphate and carbonyl groups of DPPG, which promoted variations in membrane potential. Blue irradiation experiments demonstrated the antioxidant effect of EGCG since the hydration sites of DPPG lipids (carbonyl and phosphate groups) become relatively less vulnerable to radiation damage. The main findings of this study suggest that EGCG displace water molecules at phosphate and carbonyl groups of lipids, triggering a condensing effect in lipid monolayer, which can hamper ROS diffusion across the monolayer and thus, prevent the oxidizing events.

The antioxidant action of EGCG in DPPC and DPPS Langmuir monolayers spread at the air-buffer interface rather than in air-water interface was analyzed to check whether the protonation state of EGCG and the surface charge of lipid modulate the EGCG partitioning to lipidic membrane and, which implications that this entails for the prevention of oxidative damage (Chapter 6). The results indicated that EGCG interacts with both lipids, irrespective of their charge state, perturbing the monolayer structure and morphology. Nonetheless, the affinity and insertion of EGCG was higher for DPPC since the degree of monolayer condensation was larger and the hydrocarbon chains were more ordered in comparison to those obtained in DPPS/EGCG system. So, the results stated that the molecular organization of the lipid (differences in substituents at the headgroup, compaction and hydration regime) dictate EGCG insertion or adsorption in lipid membrane. Moreover, the anionic and neutral forms of EGCG arising from its deprotonation due to subphase pH, efficiently protected both lipid monolayers from blue radiation, indicating that the electron-donating ability was the main mechanism of its radical scavenging action.

The encapsulation rate of the EGCG in DPPG liposomes was investigated as well as the molecular mechanisms underlying the radical scavenging activity of EGCG responsible for conferring liposome-resistance against UV damage (Chapter 7). The liposomal formulation showed good encapsulation efficiency of about ~ 67% indicating that EGCG was well loaded in liposomes and so, certainly, this system has potential to improve the transdermal EGCG bioavailability. The irradiation experiments demonstrated that EGCG and DPPG are co-helpers against oxidative stress-induced by UV radiation, such that the mixed DPPG + EGCG system is significantly less photodegraded than the empty DPPG liposomes and the EGCG in aqueous solution. Additionally, the results also showed that the impairment in the pyrogallol ring of the EGCG caused by UV light significantly reduced the ability of EGCG to protect liposomal lipids against oxidative stress-induced by

UV radiation.

The interactions of EGCG with the DMPC membranes were studied by using MD simulations, Langmuir monolayer film experiments and fluorescence techniques (Chapter 8). The Langmuir monolayer results and the MD simulations indicated that the EGCG penetrates at the lipid ester region and promotes the condensation of the membrane. Also, the steady-state fluorescence results showed that EGCG changes the membrane dipole potential and that 10 % in EGCG-to-lipid molar ratio is the maximum EGCG loading capacity of the DMPC liposomes, which guarantees a better stability since the liposomes do not suffer leakage, aggregation and fusion.

Finally, the idea of encapsulating EGCG inside DPPC liposomes, which are more stable and organized than the obtained DMPC liposomes and embedding them in PCL/Gelatin nanofibers to enhance human fibroblast cells resistance against oxidative stress induced either by H₂O₂ or UV radiation was tested. Also, in this approach Tween 80 and PEG were added to liposomal formulations for enhance elasticity and stability, respectively. The resulting PCL/Gelatin nanofibers containing DPPC + EGCG liposomes showed good biocompatibility, supported human fibroblasts adhesion and delivered EGCG in a controlled and sustained manner, which guaranteed a higher cell survival after oxidative stress to that in raw PCL/Gelatin nanofibers.

In summary, the work presented in this doctoral thesis strengthens the idea that Langmuir monolayer films and liposomes can be used as artificial membrane models that mimic the cell plasma membrane for the understanding of the molecular mechanisms underlying the antioxidant activity of EGCG against blue and UV light. Lastly, DPPC liposomes are suitable and biocompatible nanocarriers for the encapsulation of EGCG that, after being immobilized in PCL/Gelatin nanofibers and applied in human skin cells, efficiently attenuated the UV-induced oxidative stress.

Directions for Future Work

Looking ahead, more studies are needed to fully understand the antioxidant mechanism triggered by EGCG in lipid membranes, since those will ultimately help to further optimize the delivery rate and the therapeutic efficacy of liposomes against skin cancer.

Regarding the Langmuir monolayer film experiments some suggestions for future research are:

- Study the effect of the spreading procedure (co-spread or separately spread at the interface) on the formation of EGCG/lipid monolayer;
- Study the influence of temperature, pH, and physical state of monolayer on the adsorption of EGCG;
- Compare the stability and vulnerability of a monolayer maintained at different surfaces pressures to the radiation damage;
- Incorporate EGCG in mixed monolayer of saturated and polyunsaturated phospholipids and perform irradiation experiments for assessment of antioxidant/prooxidant effect of EGCG in this system;
- Considering that piperine is a natural *bioenhancer* that increases bioavailability and therapeutic index of EGCG, the interaction between both molecules in lipid monolayer should be analyzed to envisage a liposome carrying both molecules for synergistic tumor treatment (experiments currently in progress in our laboratory ²).

Concerning the experiments carried out in liposomes and considering the outcomes of cellular studies some guidelines for future work are:

- Irradiation experiments in DPPG liposomes, the type of by-products photo-generated in presence and absence of EGCG should be identified by high performance liquid chromatography (HPLC) or mass spectrometry;
- The UV–Vis absorption spectra obtained after irradiation should be combined with theoretical calculations (such as density functional theory) for understanding better the photochemical reaction mechanism of the lipid and EGCG molecules (experiments and theoretical studies currently in progress in our laboratory in a collaboration with a Danish and Greek groups)³
- DPPC liposomes composed of different amounts of Tween 80 and PEG should be prepared and characterized by various techniques such as FTIR, differential scanning calorimetry and fluorescence, to better study the influence of the Tween 80 and PEG on the loading efficiency and release behavior of liposomes;

² Publication in preparation for submission: Pires, F., Magalhães-Mota, G., Geraldo, V. P., Ribeiro, P.A., Oliveira Jr, O. N., and Raposo, M. Exploring the effect of co-administration of EGCG and piperine on DPPC monolayer structure: Implications for drug delivery.

³ Publication in preparation for submission: Pires, F., Hoffmann, S., Jones, N. C., Tzeli, D. and Raposo, M. Probing the Electronic States of Epigallocatechin-3-gallate in the 4 to 9 eV Energy Range.

-
- Considering that DPPG is a skin penetration enhancer, a liposomal formulation composed of DPPC:DPPG:EGCG should be designed and tested as another alternative to improve skin resistance against oxidative stress;
 - Co-encapsulation of EGCG with other phytochemicals (such as curcumin, piperine, quercetin) and vitamins (tocopherol and ascorbic acid) in liposomes is another alternative that can provide a synergistic antioxidant effect;
 - Study the antioxidant and prooxidant behavior of EGCG on DNA ⁴ as well as the synergistic interaction between EGCG and lomustine (anticancer drug) to kill the skin cancer cells (experiments currently in progress in our laboratory).

⁴Pivetta, T.P., Pires, F. and Raposo, M. Effect of EGCG on the DNA in presence of UV radiation. Computational Intelligence Methods for Bioinformatics and Biostatistics (CIBB 2018) Proceedings



EFFECT OF BLUE LIGHT ON THE STABILITY OF LIPID MOLECULES IN THE PRESENCE OF EGCG

Since the insertion of EGCG into the phospholipid membrane will occupy a specific area and contribute to the total molecular area, we decided to apply a weighting factor to the experimental isotherms obtained. As the values of A , c and N_A do not change, the weighting factor consisted in the following ratio (equation A.1:

$$\text{Weighting factor} = \frac{MMA \times V_{lipid}}{M_{lipid} \times V_{mixture}} \quad (\text{A.1})$$

where MMA is the average molar mass using the molar fractions of EGCG and DPPG, M_{lipid} is the molecular weight of lipid, $V_{mixture}$ is the solution volume spread and V_{lipid} is the volume of the lipid spread.

When the representation area per lipid is adopted, the isotherms normally shift to the right, to larger areas per lipid as guest molecules are incorporated at the subphase and occupy a given area. The effect is expected to increase with the concentration of guest molecules in case further molecules are incorporated with increasing concentration. Shifts to the left can only happen if the guest molecules induce condensation of the monolayer or disrupts it causing lipid molecules to be removed from the interface.

APPENDIX A. EFFECT OF BLUE LIGHT ON THE STABILITY OF LIPID MOLECULES IN THE PRESENCE OF EGCG

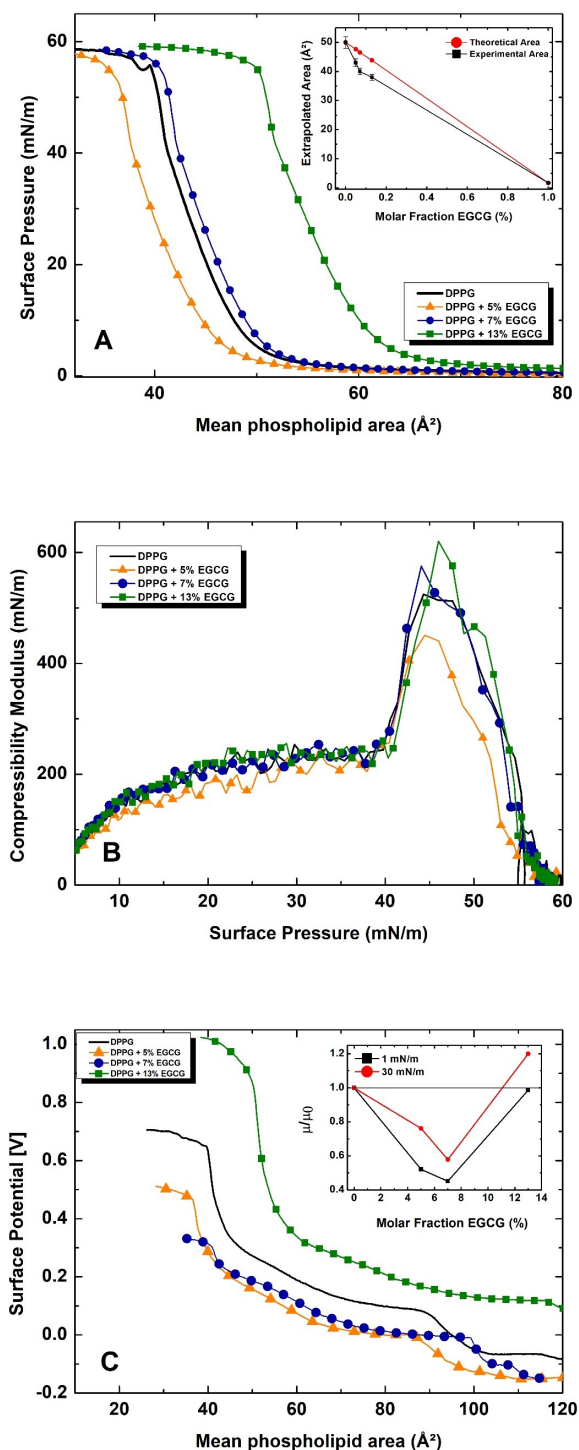


Figure A.1: A) Surface Pressure for DPPG monolayers with different contents of EGCG at water interface. B) Compressional modulus vs surface pressure for DPPG and DPPG + EGCG monolayers at the air/water interface. C) Surface Potential isotherms of DPPG + EGCG monolayers at various concentrations. The top-right inset in Figure 1C shows the ratio between the apparent dipole moment of DPPG + EGCG (μ) and pure DPPG (μ_0) vs. EGCG concentration at 1 mN/m and 30 mN/m. The solid lines in the graph are only to guide the eyes.

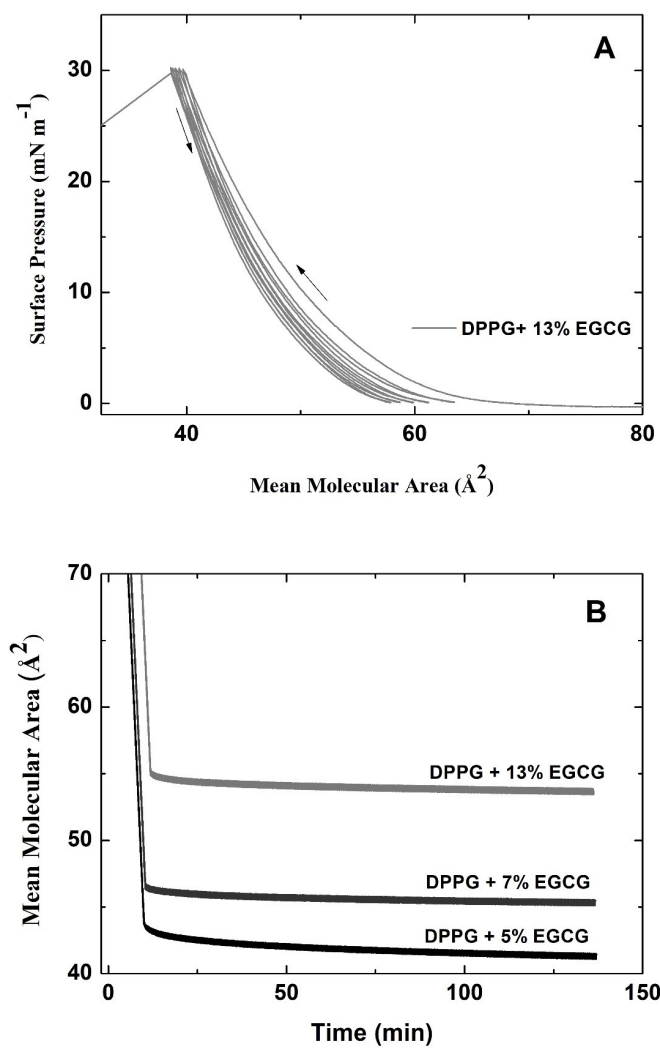


Figure A.2: A. Compression-decompression cycles of DPPG+13% EGCG monolayer irradiated with blue light over 1h at a surface pressure of 30 mN/m. B. Area-time relaxation isotherms of DPPG+EGCG at the three concentrations taken at a constant pressure of 30 mN/m. The almost horizontal lines for the areas after the monolayers were compressed to 30 mN/m do indicate stability.

A P P E N D I X



**T H E I M P A C T O F B L U E L I G H T I N
T U M O R I G E N I C A N D N O N T U M O R I G E N I C
M O N O L A Y E R S C O N T A I N I N G E G C G**

APPENDIX B. THE IMPACT OF BLUE LIGHT IN TUMORIGENIC AND NONTUMORIGENIC MONOLAYERS CONTAINING EGCG

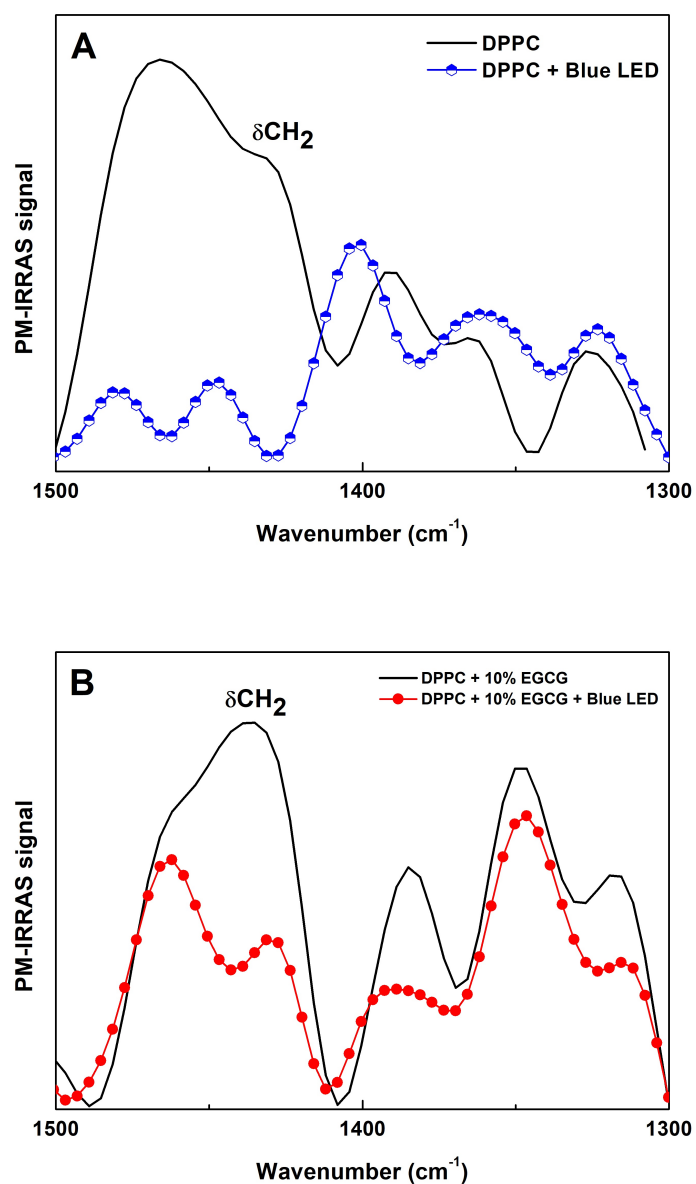


Figure B.1: PM-IRRAS spectra for neat DPPC (A) and mixed EGCG/DPPC monolayer (B) monolayer in the CH_2 methylene deformation region before and after blue light irradiation.

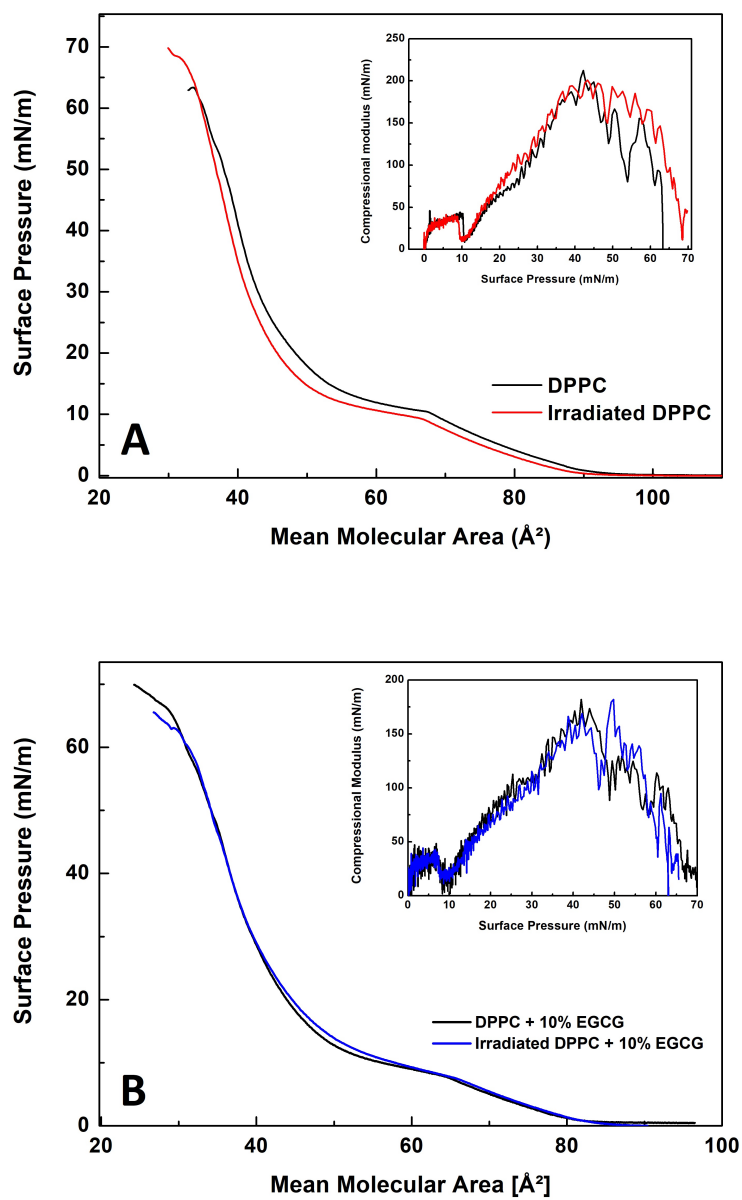


Figure B.2: Surface pressure-area isotherms for neat DPPC (A) and DPPC containing EGCG (B) monolayers before and after blue light irradiation.

APPENDIX B. THE IMPACT OF BLUE LIGHT IN TUMORIGENIC AND NONTUMORIGENIC MONOLAYERS CONTAINING EGCG

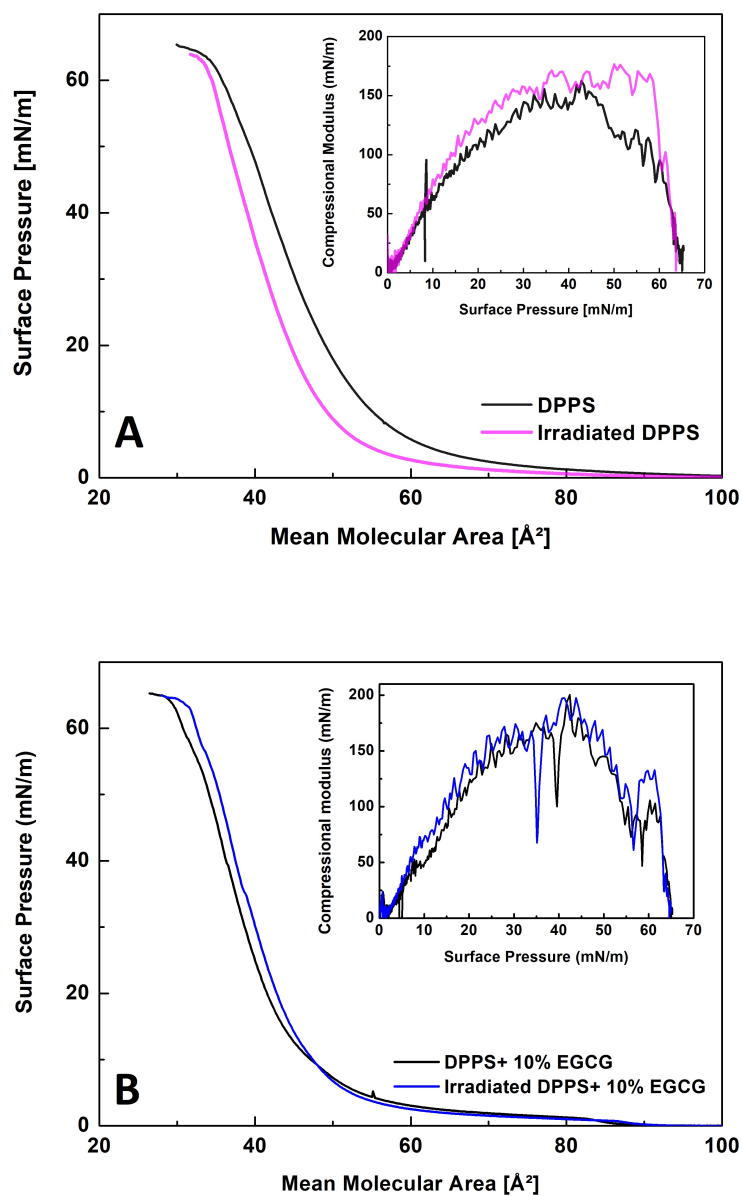


Figure B.3: Surface pressure-area isotherms for neat DPPS (A) and DPPS containing EGCG (B) monolayers before and after blue light irradiation.

APPENDIX



**ON THE ROLE OF EGCG IN PROTECTING
PHOSPHOLIPID MOLECULES AGAINST UV
IRRADIATION**

APPENDIX C. ON THE ROLE OF EGCG IN PROTECTING PHOSPHOLIPID MOLECULES AGAINST UV IRRADIATION

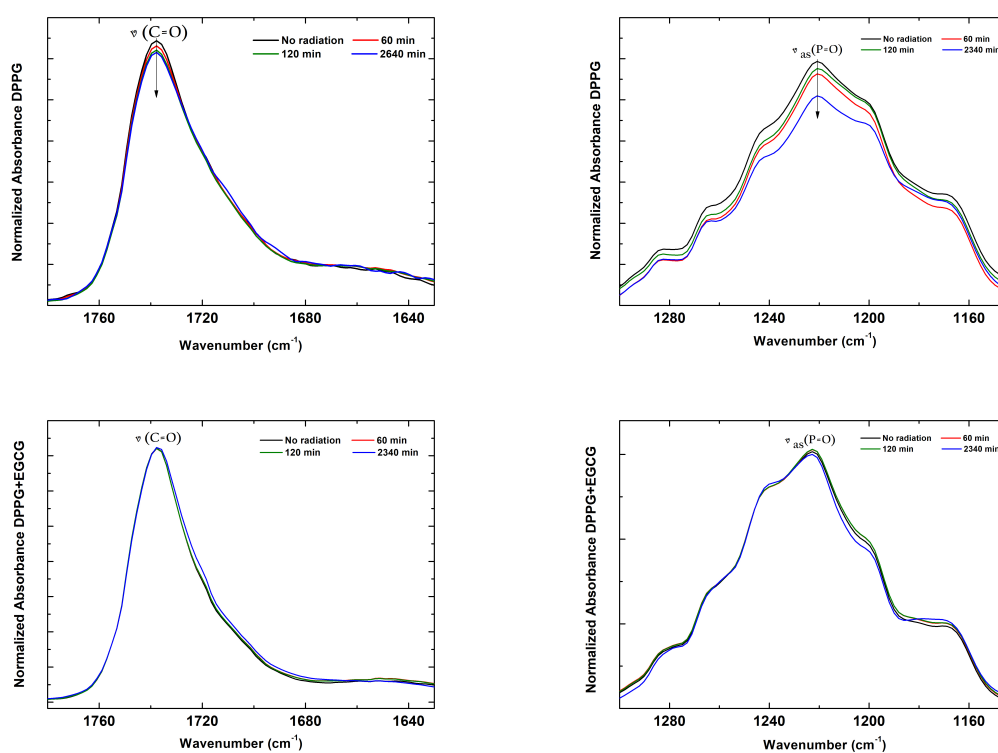


Figure C.1: EGCG seems to protect the phosphate and carbonyl groups of DPPG phospholipids against UV irradiation.

EVALUATION OF EGCG LOADING CAPACITY IN DMPC MEMBRANES

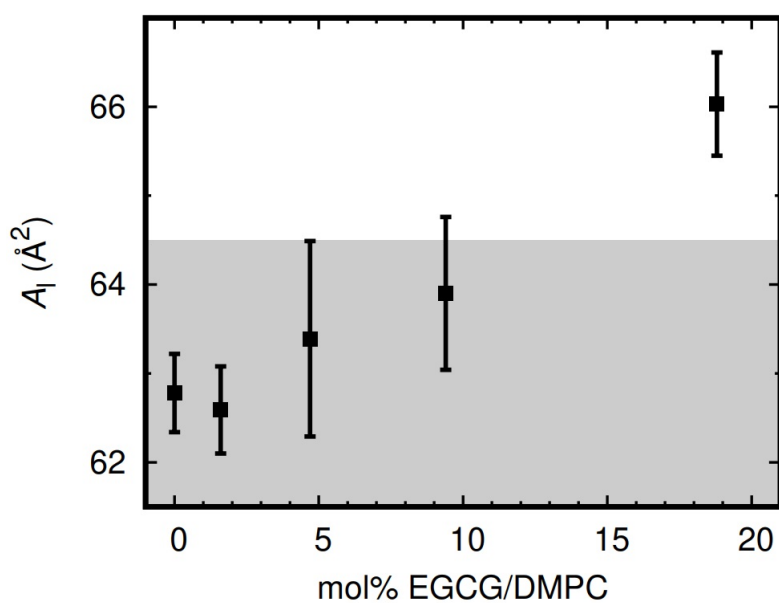


Figure D.1: A_1 values of DMPC head groups calculated in the presence of different amounts of EGCG and assuming that the catechin molecules are in the tails and not in the head group region. These were calculated ignoring the specific area occupied by EGCG. The grey shaded region corresponds to the values measured experimentally for pure DMPC in fluid phase.

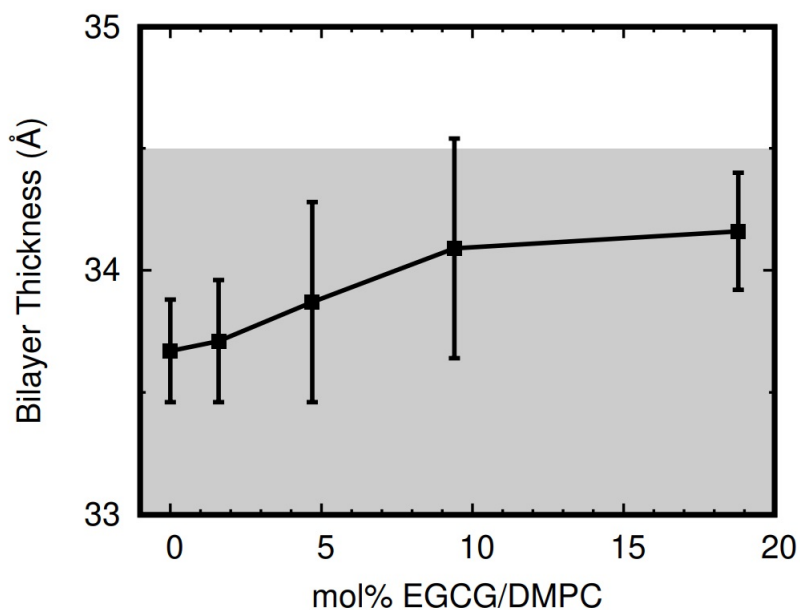


Figure D.2: Membrane thickness values in the presence of different EGCG molar fractions. The thickness is calculated from the distance between the phosphorous atoms average positions in each monolayer. The gray shaded region corresponds to the values measured experimentally for pure DMPC in fluid phase.

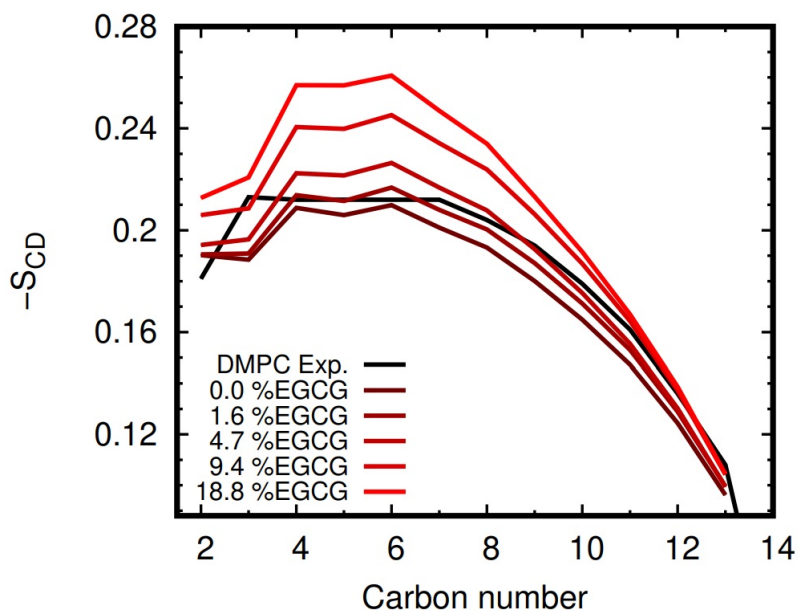


Figure D.3: Deuterium order parameter (S_{CD}) values along the aliphatic chain for the different molar ratios of the EGCG/DMPC systems. The experimental profile presented is for pure DMPC in fluid phase.

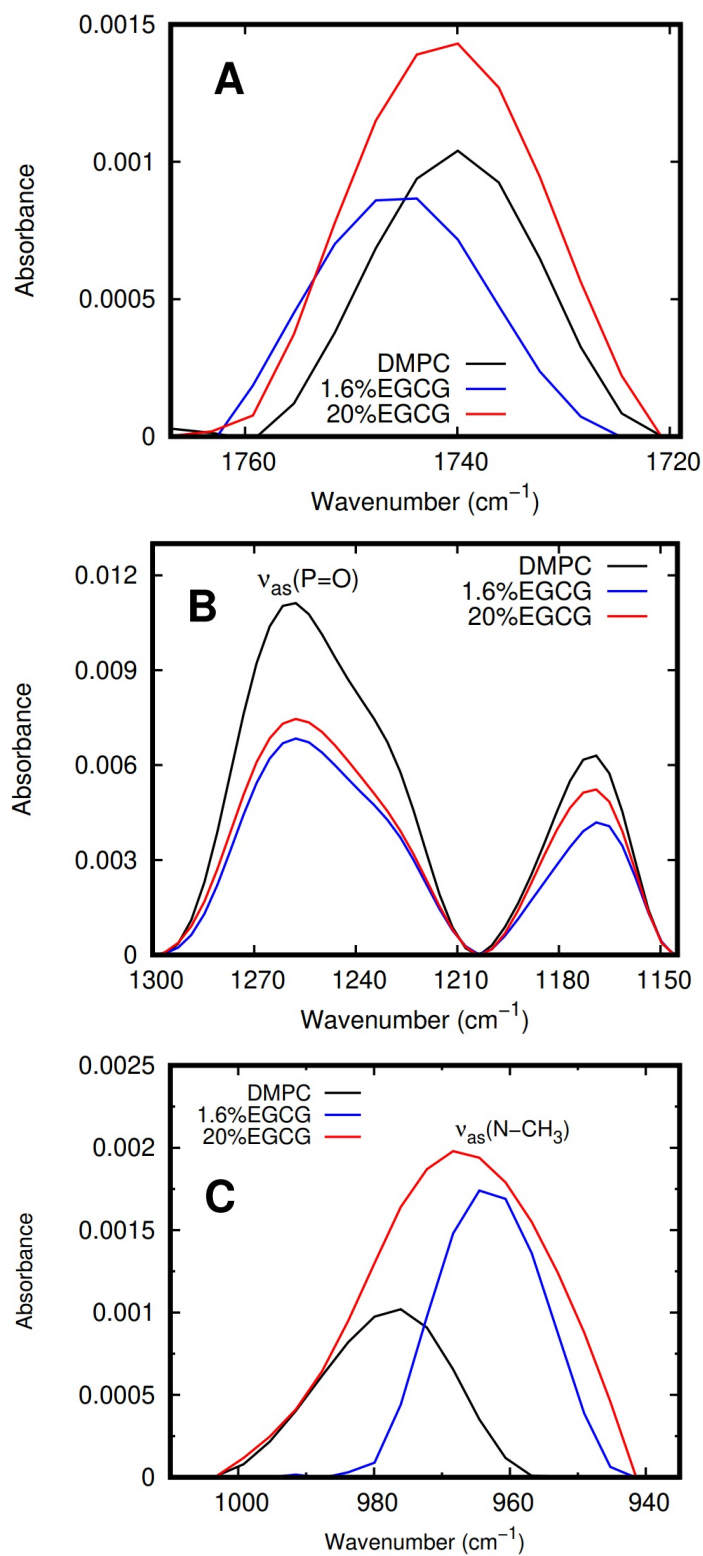


Figure D.4: PM IRRAS measurements for different EGCG molar fractions in DMPC. The PM IRRAS data on DMPC ester C=O (A), phosphate P=O groups (B), and choline N-CH₃ (C) are also shown.

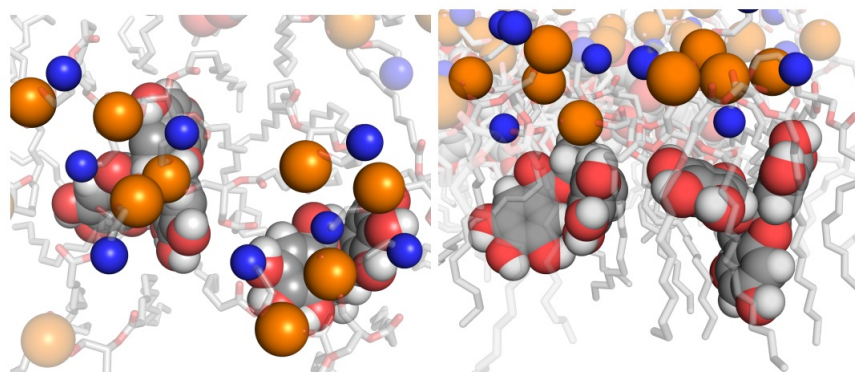


Figure D.5: Top (left) and side-view (right) of DMPC headgroup bending in the presence of EGCG. This figure highlights how the choline (N atom in blue spheres) and phosphate (P atom in orange spheres) groups of DMPC bilayer occupy the space created with EGCG (grey spheres) insertion. The remaining DMPC atoms are shown as transparent grey sticks.